UNIVERSITY OF CALIFORNIA, SAN DIEGO

TAILORED MAGNETIC NANOPARTICLES FOR *IN VITRO, IN VIVO* AND *IN SITU* MAGNETORELAXOMETRY

A dissertation submitted in partial satisfaction of the
requirements for the degree of Doctor of Philosophy

in

Bioengineering

by

Thomas R. Pisanic, II

Committee in charge:

Professor Sungho Jin, Chair
Professor Xiaohua Huang, Co-Chair
Professor Shu Chien
Professor Eduardo Macagno
Professor Gabriel Silva

2006

The dissertation of Thomas R. Pisanic, II is approved, and it is acceptable in quality and form for publication on microfilm.

Co-Chair

Chair

University of California, San Diego

2006

To the Great I am,
to whom much of this is foolishness

"Your manuscript is both good and original; but the part that is good is not original, and the part that is original is not good."

-Samuel Johnson

TABLE OF CONTENTS

LIST OF FIGURES

LIST OF TABLES

LIST OF SYMBOLS

K	Anisotropy energy
$\rho(E^*)$	Anisotropy energy density
K_a	Association constant
U_V	Attractive van der Waals energy
T_B	Blocking temperature
k_B	Boltzmann's constant
τ_B	Brownian rotation time constant
τ_N	Characteristic Néel relaxation time constant
e	Charge of an electron
H_c	Coercivity
C	Concentration
D_c	Critical diameter
K^{-1}	Debye screening length
d	Diameter of the nanoparticle
ε	Dielectric constant
x	Distance between nanoparticles
U_{El}	Electric interaction energy
ϕ	Electric potential
F	Force
R	Gas constant
g	Geometric factor

$\vec{\nabla}$	Gradient operator
A	Hamaker constant
V'	Hydrodynamic volume
U_M	Magnetic attractive energy
H	Magnetic field
Φ	Magnetic flux
B	Magnetic induction
m	Magnetic moment
τ_m	Measurement time
N	Number of bonds
N_I	Number of immobilized particles
Γ	Number of molecules per unit area
μ_0	Permeability of free space
θ	Phase
P	Pressure
λ	Range of binding interaction
k_{off}	Receptor –ligand off rate
k_{on}	Receptor –ligand on rate
ρ_r	Receptor surface density
M_r	Remanent magnetization
r	Sample sensor distance; radius

M_s	Saturation magnetization
γ	Shear stress
U_T	Sum of the interparticle forces
ψ	Superconductor parameter
T	Temperature in Kelvin
δ	Thickness of the outer layer; Superconductor parameter phase difference
η	Viscocity
V	Volume
M	Volume magnetization
χ	Volumetric magnetic susceptibility
U_S	Work due to steric factors

LIST OF ABBREVIATIONS

AC	Alternating current
AMNP	Anionic MNP
Bre	Bt toxin resistant
BSA	Bovine serum albumin
Bt	*Bacillus thuringiensis*
C.I.	Confidence interval
CE	Capillary electrophoresis
CFU	Colony forming units
CPP	Cell penetrating peptide
Cry	Crystal
DC	Direct current
DI	Deionized
DMEM	Dulbecco's modified Eagle's medium
DMSA	Dimercaptosuccinic acid
DNA	Deoxyribonucleic acid
EDTA	Ethylenediaminetetraacetic acid
ELISA	Enzyme linked immunosorbent assay
FBS	Fetal bovine serum
FCS	Fluorescence correlation spectroscopy

FITC	Fluorescein isothiocyanate
FLIP	Fluorescence loss in photobleaching
FLL	Flux locked loop
FRAP	Fluorescence recovery after photobleaching
FRET	Fluorescence resonance energy transfer
GAP	Growth associated protein
GFP	Green fluorescent protein
HBS	HEPES buffered saline
HEPES	Hydroxyethyl piperazineethanesulfonic acid
HIV	Human immunodeficiency virus
HPLC	High performance LC
HSV	Herpes simplex virus
IC	Intercellular
IL	Interleukin
IMDM	Iscove's modified Dulbecco's medium
LC	Liquid chromatography
MARIA	Magnetic relaxometric immunoassay

MCG	Magnetocardiography
MEG	Magnetoencephalography
MES	2-morpholinoethanesulfonic acid
MNP	Magnetic Nanoparticle
MRI	Magnetic resonance imaging
MS	Mass spectrometry
NGF	Nerve growth factor
NHS	*N*-hydroxysuccinimide
NMR	Nuclear magnetic resonance
NSB	Nonspecific binding
PBS	Phosphate buffered saline
PC	Pheochromocytoma
PCR	Polymerase chain reaction
PEG	Polyethylene glycol
PEO	Polyethyleneoxide
PMSF	Phenylmethylsulfonyl fluoride
PVA	Polyvinyl alcohol
PVP	Polyvinylpyrrolidone
RBC	Red blood cell
RF	Radio frequency
S/N	Signal to noise ratio
SA MP	Streptavidin coated Molecular Probes 140nm MNP

SPIO	SPM iron oxide
SPM	Superparamagnetic
SQUID	Superconducting quantum interference device
TAT	Trans-activating transcriptional activator
TAT PTD	TAT Protein transduction domain
TBS	Tris buffered saline
TEM	Transmission electron microscopy
TNF	Tumor necrosis factor- α
TRITC	Tetrarhodamine isothiocyanate
TX	Trition-X 100
USPIO	Ultra small SPIO
UV	Ultraviolet

VITA

1999	Bachelor of Science, Biomedical Engineering Bachelor of Arts, Electrical Engineering The Johns Hopkins University
2000-2003	Teaching Assistant, Department of Bioengineering University of California, San Diego
2001	Master of Science, Bioengineering University of California, San Diego
2004-current	Biomedical Engineer, Magnesensors, Inc.
2006	Doctor of Philosophy, Bioengineering University of California, San Diego

AWARDS

Recipient, National Defense Science and Engineering Graduate Fellowship, 2001-2005
Treasurer, Tau Beta Pi - Maryland Alpha Chapter, 1998
Member, Tau Beta Pi – Maryland Alpha Chapter, 1997-present
Member, Alpha Eta Mu Beta, Biomedical Engineering Honor Society, 1997-present
Recipient, Tau Beta Pi Scholarship, 1998
Recipient, Society of American Military Engineers Scholarship, 1997
Recipient, William Brown Baxley Engineering Scholarship, 1995-1999

PUBLICATIONS

Ozkan M, Pisanic T, Scheel J, Barlow C, Esener S, Bhatia SN. Electro-optical platform for the manipulation of live cells. *Langmuir*, **19** (5): 1532-1538, 2003.

Oh S, Daraio C, Chen LH, Pisanic TR, Fiñones RR, Jin S. Significantly accelerated osteoblast cell growth on aligned TiO2 nanotubes. *Journal of Biomedical Materials Research Part A,* **78A** (1): 97-103, 2006.

Pisanic II TR, Blackwell JD, Shubayev V, Fiñones RR, Jin S. Evaluation of the Effect of Iron Oxide Nanoparticle Internalization upon Cell Response to a Specific Biochemical Cue. *Biomaterials*, 2006 (In submission)

PATENTS

S. Jin and T. R. Pisanic, "Article and Apparatus for Remote Magnetically Induced Treatment of Cancer and Other Diseases, and Method for Operating Such Article", patent application filed in January, 2004.

FIELDS OF STUDY

Major Field: Bioengineering

Studies in Drug Metabolism, Biosensors and Optics

Professors Sangeeta Bhatia and Sadik Esener

Studies in Nanotechnology

Professors Sungho Jin and Xiaohua Huang

ABSTRACT OF THE DISSERTATION

TAILORED MAGNETIC NANOPARTICLES FOR *IN VITRO, IN VIVO* AND *IN SITU* MAGNETORELAXOMETRY

by

Thomas R. Pisanic, II

Doctor of Philosophy in Bioengineering

University of California, San Diego, 2006

Professor Sungho Jin, Chair

Professor Xiaohua Huang, Co-Chair

The development of novel methods of probing biological interactions is critical to the advancement of biomedical science. Recent progress in the synthesis and science of nanoscale structures has engendered a renaissance in the evolution of techniques aimed at the analysis of these interactions. The use of nanomaterials provides the researcher with access to the extended quantum behaviors of these materials and the ability to intimately interact with the fundamental subunits of biology. Magnetic materials on this size scale, such as magnetic nanoparticles (MNPs), also exhibit unique properties not available in larger structures and have likewise become of chief interest in the field of nanotechnology. Through exploitation of

various synthesis techniques and parameters, the physicochemical and magnetic properties of magnetic nanoparticles can be exquisitely controlled.

Magnetorelaxometry is the field of study concerned with the mechanisms of magnetic relaxation and the development of applications that capitalize upon these phenomena. The preferred instrument for the analysis of these magnetic properties is the superconducting quantum interference device (SQUID). This work focuses on the development and chemical modification of MNPs for use with this instrument and the demonstration of novel magnetorelaxometric applications in biomedicine. The basic chemical synthesis of magnetic nanoparticles is first developed and demonstrated, after which the SQUID system and the magnetic properties of a library of synthesis products are analyzed and evaluated for use in magnetorelaxometry. An *in vitro* assay for sepsis diagnostics is then developed based upon the conjugation of anti-*Escherichia coli* O157:H7 antibodies to magnetic nanoparticles and the magnetorelaxometric quantification of binding of these MNPs to the target pathogen in buffer, serum and blood. Next, parameters for the conjugation of insecticidic crystal proteins to MNPs are developed and optimized for an *in vivo* assay for the quantification of toxin binding in the gut of live *Caenorhibditis elegans* nematodes. Lastly, the concentration dependent effects of MNPs upon PC12 cells are evaluated; followed by the development of an antibody based *in situ* assay for the detection of tubulin using the TAT peptide for entry into live cells. The results of these assays underscore the utility of magnetorelaxometry for applications in biomedicine.

CHAPTER 1

INTRODUCTION

1.1 Magnetic Nanoparticles

1.1.1 Definition and Types of

Nanotechnology is the science and application of submicroscopic materials, such as nanoparticles, whose dimensions range from one to hundreds of nanometers. Materials on this scale can be seen both as very large molecules, allowing access to extended quantum behaviors, and as materials so small that they exhibit characteristics and attributes not available to larger structures. Recent advances in chemistry, biology, physics and materials science in this size regime have endowed researchers with the ability to not only create a plethora of nanometer scale materials, but also to precisely tailor their properties for many novel and exciting applications. Still in its infancy, however, nanotechnology has found a natural partner in biomedicine, where the biological entities involved, such as prokaryotic and eukaryotic cells (1-100 μm), proteins (1-10 nm) and viruses (20-450 nm), lie on size scales similar to or larger than the materials concerned. The development of biocompatible nanomaterials allows unprecedented access to and interaction with the fundamental subunits of biology.

One of the foremost areas of nanotechnology is magnetic nanoparticles (MNPs), or the science and development of nanometer regime structures, and the fluids composed of such

structures (i.e., ferrofluids), which possess magnetic properties. In particular, the science of magnetic nanoparticles is concerned with the materials, synthesis, characteristics and applications of nanoscale ferromagnetic and ferrimagnetic materials. Ferromagnetic materials consist of elemental metals such as of iron, nickel and/or cobalt or alloys of these metals and are characterized by the parallel alignment of the magnetic moments of their constituent atoms resulting in large net magnetizations. Ferrimagnetic materials, on the other hand, are composed of ionic compounds, and in particular oxides of the ferromagnetic elements. The magnetism of ferrimagnetic oxides arises from the net magnetic moment of the atoms on different iron oxide sublattices having unequal opposing moments.

1.1.2 Types of Synthesis

Various magnetic nanoparticles and solutions composed thereof have been routinely synthesized over the last forty years. What began as the simple grinding of bulk magnetic materials into irregularly shaped, polydisperse magnetic particles has evolved into the recent development of processes and techniques that can yield highly uniform "monodisperse" magnetic nanoparticles with explicitly tailored sizes and shapes. The development of techniques producing precisely controlled nanoparticle morphologies allows for creation of solutions of nanoparticles with uniform physicochemical properties which capitalize on the sum of the individual properties of the constituent particles. By modifying the properties of the individual nanoparticles, highly controllable and functional ferrofluids can be developed for specific applications.

The goal of the modern synthesis of nanoparticles is the development of nanomaterials with specifically tailored and controlled properties to produce highly functional fluids for special applications. Of particular interest to the materials scientist is the production of nanoparticles of uniform size and shape, thereby allowing tight control of the fluid's bulk

properties. With reference to the synthesis of magnetic nanoparticles, there are two primary categories of synthesis methods, the first, of which all the cases encompassed herein are taken, is a solution based synthesis, which can be further broken into organic and aqueous based techniques. The second primary category of magnetic nanoparticle synthesis is an aerosol or vapor phase synthesis.

Solution based syntheses of magnetic nanoparticles involve the formation of nanoparticles from precursor chemicals in liquid media. Variables such as solute concentration, temperature, the presence and pressure of gases, and solvent characteristics can be modified to precisely determine the properties of the resulting nanoparticles. All forms of solution based synthesis follow a similar paradigm: nucleation, followed by the separation and subsequent maturation of nuclei into uniform nanoparticles. The exact process of maturation is achieved in one of three ways, specifically, homogeneous precipitation, through individual nucleation events and growth by diffusion; Ostwald ripening, through multiple nucleation events and "self sharpening" of the individual particles into monodispersion; and nuclei aggregation, where small, individual subunits aggregate into larger uniform nanoparticles. Figure 1-1 schematically shows the three mechanisms of uniform particle formation in solution.

The most well utilized magnetic nanoparticles in biomedicine are the oxides of iron, magnetite (Fe_3O_4), and the further oxidized and more stable maghemite, or Fe_2O_3. There are five primary types of solution based synthesis of iron oxide nanoparticles, namely: coprecipitation, decomposition of organic precursors, microemulsion, sonochemistry and the polyol process. Several variants of these methods, particularly the first, involve the use of various coatings and surface modifications which engender further biocompatibility and/or stability to the resulting MNPs.

The most oft used method of solution based iron oxide synthesis is coprecipitation. Coprecipitation normally involves one of two processes: the oxidation of a ferrous hydroxide suspension via various oxidizing agents; or the aging of stoichiometric mixtures of ferric and ferrous hydroxides in aqueous media. The various parameters involved in these methods, as described later, can be carefully adjusted to create uniform suspensions of nanoparticles over a wide (2 to 100 nm) range.

A second method of iron based nanoparticle synthesis is the thermal decomposition of organic precursors. In this method, iron precursors are decomposed in the presence of organic surfactants at high temperatures (over 200 °C). This method often allows for exquisite control over particle uniformity and properties, but is primary plagued by the fact that the resulting hydrophobic particles must be further modified to form stable aqueous solutions.

The final three major methods of solution based iron oxide nanoparticle synthesis are microemulsion, sonochemistry and the polyol process. In microemulsion, microdroplets of aqueous phase solutions are contained within assemblies of surfactant molecules and dispersed into an oil phase solution, yielding discrete nanometer regime aqueous “cavities” within the oil solution. These cavities separate and confine particle formation, thus creating well dispersed particles with controlled properties. Sonochemistry utilizes high frequency probes to create highly reactive reaction conditions which can generate free radicals, and, in the presence of an iron precursor, result in free radical mediated generation of iron oxide nanoparticles. The polyol process, on the other hand, involves the use of a liquid polyol which acts as a solvent and reducing agent of a metallic precursor. While normally used for the production of iron alloy as opposed to iron oxide nanoparticles, in the polyol process, the metal precursor is dissolved in the polyol and the solution is heated to a specified temperature at which point the metal precipitates. By carefully controlling the precipitation

kinetics and/or by seeding the solution with foreign particles, well defined nanoparticle shapes and sizes can be obtained.

1.1.3 Magnetic Properties

What separates magnetic nanoparticles from other types of nanostructures and particles is their innate ability to be readily manipulated via an external magnetic field. The interaction of magnetic fields with magnetic nanoparticles can be used to move, heat, detect, track, and generate forces upon the nanoparticles for use in numerous applications. Additionally, the permeability of biological tissues to magnetic fields makes magnetic nanoparticles particularly attractive in biomedicine and allows for the easy external/noninvasive manipulation of the nanoparticles in biological samples or specimens. The properties of magnetic nanoparticles and their solutions are directly dependent upon the particles' size, shape and chemical structure, which can all be manipulated through exploitation of the synthesis parameters.

When placed in a magnetic field, **H**, magnetic nanoparticles respond, as other materials do, according to the relation:

$$\mathbf{B} = \mu_0(\mathbf{H} + \mathbf{M}) \qquad (1.1)$$

where **B** is the magnetic induction, μ_0 is the permeability of free space, and **M=m**/V is the volume magnetization, where **m** is the magnetic moment on a volume, V, of the material. While all materials respond to magnetic fields, it is only certain materials, designated ferromagnetic, ferrimagnetic and antiferromagnetic which respond strongly to magnetic fields and exhibit magnetic states even in the absence of a magnetic field. The response of a typical material to a magnetic field is described by the relation:

$$\mathbf{M} = \chi\mathbf{H} \tag{1.2}$$

where χ is the volumetric magnetic susceptibility. The value of χ varies with the type of material, ranging from 10^{-6} to 10^{-1} for paramagnetic materials and -10^{-3} to -10^{-6} for diamagnetic materials. The response of ferro, ferri and antiferromagnetic materials, however, cannot be described by the linear relation in (1.2). In these materials, electron exchange forces produce parallel and/or antiparallel alignment of atomic moments within the material itself and give rise to an innate magnetization, even in the absence of an external field. The susceptibility of these materials is not a constant, but rather a function of the external field itself, as well as the temperature and current state of the material's magnetic domains. This relationship is most readily described by the material's characteristic sigmoidal M-H (or B-H) curve, which illustrates the increasing alignment of the atomic moments within the material upon increasing **H**, eventually leading to the complete alignment of the spins, viz. the saturation magnetization, M_s, of the material.

Ferromagnetic and ferrimagnetic materials typically exhibit hysteresis, or irreversibility, in response to magnetic fields, attributable to impurities, grain boundaries and magnetic anisotropies. The magnetism that remains in a magnetic material following removal of an external field is known as the remanent magnetization, M_r. It is possible, however, for the magnetization of these materials to be lowered back to zero by the application of an external magnetic field in the opposite direction. The magnitude of negative direction external magnetic field required to bring the material magnetization back to zero is known as the coercive field or coercivity, H_c. An M-H loop of a given hypothetical magnetic material, showing the saturation magnetization, M_s, the remanent magnetization, M_r, and the coercivity, H_c, is schematically shown in Figure 1-2.

Magnetic materials consist of spatially distinct domains, or groups of spins pointing in the same direction and acting in a cooperative manner. The boundaries between these domains are known as domain walls and are typified by a characteristic width and energy. It is the generation and motion of these domains which is the primary means of controlling demagnetization. In larger particles (> several hundred nanometers), it becomes energetically favorable for the formation of multiple domains and domain walls. The M-H loop of multi-domain particles is typically characteristically narrow, due to the small field energy required to move domain walls. However, as the magnitude of the external magnetic field is decreased, magnetic domain walls within the materials can become pinned at impurities and grain boundaries within the material itself, so that, even at zero external field, the material remains magnetized (thus contributing to the remanent magnetization). As the size of magnetic materials decreases and reaches a critical diameter, D_c, the formation of domain walls becomes unfavorable and the particle as a whole acts as a single domain, viz., a single domain particle. The single domain particles become magnetized through the coherent rotation of spins, which is more demanding energetically than domain wall movement and thus results in larger coercivities (wider M-H curves).

As one decreases magnetic particle size even farther, typically under 100 nm, the spins start to become affected by random thermal fluctuations to the point where at a certain size the particle becomes superparamagnetic (SPM) and the magnetization itself fluctuates in response to thermal energy. The time variation of the magnetization of a magnetic material is called Néel relaxation (Neel 1949; Neel 1951) and can be given by:

$$\frac{dM}{dt} = -\frac{M(t) - M(t=\infty)}{\tau_N} \tag{1.3}$$

where $M(t=\infty)$ is the equilibrium magnetization and τ_N is the characteristic relaxation time constant for relaxation over an energy barrier described by:

$$\tau_N = t_0 e^{\Delta E / k_B T} \quad (1.4)$$

where ΔE is the energy barrier to moment reversal, $k_B T$ is the thermal energy and t_0 is typically assumed to be a constant value of roughly 10^{-9} s. The energy barrier is determined by several factors such as magnetocrystalline and shape anisotropies, but in the simplest form, assuming uniaxial anisotropy, $\Delta E = KV$, where K is the anisotropy energy density and V is the particle volume. The direct proportionality between ΔE and V becomes particularly significant for smaller particles, as now ΔE becomes comparable to the thermal energy, $k_B T$, for example, at room temperature (~293K). While strictly speaking the superparamagnetic transition at a given temperature and material is defined as the volume at which $KV = 25 k_B T$ (Cullity 1972), an important principle arises in determining the definition of superparamagnetism, as the term becomes nebulous without a statement of the measurement time, τ_m, and temperature, T. Depending on the measurement time following exposure to an external magnetic field, a magnetic nanoparticle can appear paramagnetic if $\tau_N << \tau_m$ or ferro/ferrimagnetic if $\tau_N >> \tau_m$. This becomes particularly relevant in some of the systems described in this dissertation, where, following field exposure, a net magnetic moment is measured on particles commercially described as superparamagnetic. Similarly, given a particular measurement time, the temperature at which $\tau_m = \tau_N$ is called the blocking temperature, T_B, and moment measurements taken at $T < T_B$ will yield a quasi static remanent moment, while measurements at $T > T_B$ will yield a paramagnetic or 0 moment measurement. This principle is schematically shown in Figure 1-3.

The intrinsic response of magnetic systems and nanoparticles also results in alteration and modulation of their extrinsic behavior. For example, energy is required for both domain wall

motion in multi-domain particles and for moment alignment and saturation in SPM particles and is characterized by the area enclosed by the M-H curve. If this energy is supplied from an external time varying magnetic field, a constant flow of energy into the material results in the transference of that energy into thermal energy and the generation of heat. This is the characteristic principle underlying hyperthermia, which is a biomedical application that capitalizes upon this phenomenon and is discussed further in Section 1.2.4.

MNPs can also be physically manipulated by an external magnetic field gradient. The magnetic force acting on a point-like magnetic dipole with magnetization, **M**, is given by:

$$\vec{F} = (\vec{M} \cdot \vec{\nabla})\vec{H} \tag{1.5}$$

where $\vec{\nabla}$ is the gradient operator and $\vec{H}$ is the [external] magnetic field vector. The value of $\vec{M}$ is determined by the M-H curve and the direction which the moment is pointing. It is important to note that a magnetic field **gradient** is required to exert a force, F, upon an MNP, as a uniform field can only give rise to a torque upon the particle. In the presence of an external magnetic field gradient, a force and, when free to move a velocity, is generated upon MNPs and the entities to which they are attached. It is upon these principles that several biomedical applications of MNPs have been developed, for example magnetic cell separation (Section 1.2.2) and drug/gene delivery (Section 1.2.3).

1.1.4 Thermodynamics in Solution

While many of the magnetic properties are calculated and determined on stationary or dried magnetic nanoparticles, it is liquid solutions, i.e., suspensions, of MNPs which are primarily used in biomedical applications. The unique properties of magnetic fluids or ferrofluids are normally predicated upon the ability of the MNPs to remain separate, at least prior to and normally even after exposure to a magnetic field. As a colloidal solution of solid

particles with large surface to volume ratios, MNPs have characteristically large free surface energies. Processes which result in lower surface energies, such as particle agglomeration, can readily occur in magnetic fluids, thus dramatically affecting their properties and undermining their utility.

In order to maintain colloidal stability, i.e., to prevent agglomeration, the thermal energy, $k_B T$, must be greater than the sum of interparticle energies. There are basically four distinct interparticle forces which are relevant to the stability of magnetic suspensions: electric and steric repulsion and van der Waals and magnetic attraction. Note that sedimentation due to gravitational forces is not considered here, as the time scale at which this occurs is normally not relevant in dispersed nanoparticle suspensions. Sedimentation/precipitation can, however, readily occur following agglomeration of the particles into larger aggregates.

Electric Repulsion

A uniform magnetic colloidal suspension contains nanoparticles with similar or identical net charges. Coulombic forces between the particles result in a repulsion between the particle surfaces. Additionally, in many applications, particularly in biomedicine, the particles are immersed a physiological saline or electrolyte solution which acts to shield and mitigate the repulsive forces. The electric interaction between particles in an electrolyte solution has been well characterized and can readily be described by the Poisson-Boltzmann equation:

$$\nabla^2 \phi^* = \kappa^2 \sinh \phi^* \tag{1.6}$$

where ϕ^* = $\beta e\ \phi$ is the dimensionless potential and κ^{-1} is the Debye screening length given by:

$$\kappa = (8\pi n e^2 \beta / \varepsilon)^{1/2} \tag{1.7}$$

where e is the charge of an electron, n is the total concentration of anions and cations in the electrolyte solution, $\beta = 1/k_B T$ and ε is the dielectric constant of the solvent. A detailed analysis of the electric interaction energy is beyond the current scope, but ϕ^* and the electrostatic repulsion energy, U_{El}, are basically dependent on the surface potential due to the magnetic and surface molecular charges which are increasingly screened as the salt concentration is increased, thus decreasing the screening length, κ^{-1}. Likewise, by coating the surface of MNPs with highly charged molecules one can form an electrically stabilized MNP suspension. An electrically stabilized MNP suspension will remain stable to typical thermal fluctuations and aggregation if the energy barrier to particle collision is roughly greater than $5\ k_B T$.

Steric Repulsion

Most magnetic nanoparticle constructs consist of relatively thick adsorbed or specifically chemically bound surface layers or surfactants which act to physically prevent close interaction between suspended nanoparticles. As two or more particles approach each other and the surface layers intersect, the surface molecules require energy to physically distort, preventing the particles from coming together. Additionally, and more significantly, as the local concentration of surface molecules between the particles increases, the osmotic pressure also necessarily increases, resulting in further energy being expended. Assuming P=RTC (where C= n/V=concentration), i.e., the ideal gas law applies, the work due to steric factors, U_S, created is given by:

$$U_S = PV = \frac{2}{3}\pi\Gamma k_B T\left(\delta - \frac{x}{2}\right)^2\left(\frac{3}{2}d + 2\delta + \frac{x}{2}\right)/\delta \qquad (1.8)$$

where P is the osmotic pressure, V is the volume of overlapping molecules, Γ is the number of molecules per unit area of nanoparticle surface, δ is the thickness of the outer layer, d is the diameter of the particles and x is the distance between the particles. Similarly to the electrically stabilized case, the surface layer can be modified or thickened to increase U_S and form a sterically stabilized MNP suspension.

Van der Waals Attraction

When the particles do come in close proximity to one another, the orbiting electrons of the particles induce and interact with electric dipoles in the other particles resulting in the attractive so-called van der Waals force. The van der Waals interaction between two spherical particles can be readily described by the well-known expression:

$$U_V = -\frac{A}{6}\left(\frac{2}{l^2+4l}+\frac{2}{(l+2)^2}+\ln\frac{l^2+4l}{(l+2)^2}\right) \tag{1.9}$$

where U_V is the attractive van der Waals energy, A is the Hamaker constant [which specifies the dispersive forces involved in the system and is calculated from the optical dielectric properties of the particles and medium, A~4x10^{-20} J for iron oxides in an aqueous solution (Chan, Henderson et al. 1985)], and l =2(x/d) +2.

Magnetic Attraction

The last major force which exists between MNPs in suspension is the magnetic interaction between the moments of the individual particles. Assuming ferrimagnetic, single domain particles, with magnetic moments m_1 and m_2, where $m=(\pi/6)Md^3$, the magnetic attractive energy, U_M, between two point dipoles is given by:

$$U_M = \frac{\mu_0 m_1 m_2}{4\pi x^3}\left[\hat{m}_1\cdot\hat{m}_2 - 3(\hat{m}_1\cdot\hat{x}_{12})(\hat{m}_2\cdot\hat{x}_{12})\right] \tag{1.10}$$

thus particles with larger susceptibilities (or are physically larger) or which are placed in stronger magnetic fields will have stronger moments and be more likely to aggregate.

As previously stated, in order to maintain stability in the magnetic suspension, the sum of the interparticle forces, U_T, must be less than the thermal energy, that is:

$$\kappa_B T > U_T = U_{El} + U_S + U_V + U_M \tag{1.11}$$

A plot of the theoretical normalized interaction energy versus x of sterically and electrically [only] stabilized Fe_2O_3 suspensions with and without a saturating applied external field are shown in Figure 1-4. Figure 1-5 shows a schematic of oleic acid stabilized magnetic nanoparticles and its interaction energies as a function of the distance between them.

1.2 Magnetic Nanoparticles in Biomedicine

1.2.1 Overview and Special Considerations

The unique properties of magnetic nanoparticles and solutions composed thereof combined with the increasing number of techniques allowing for control of their size as well as their ability to be coated or functionalized with biomolecules makes them an attractive tool for use in current and next generation biomedical applications (Berry and Curtis 2003; Pankhurst, Connolly et al. 2003; Tartaj, del Puerto Morales et al. 2003; Ito, Shinkai et al. 2005). Indeed, MNPs are currently used in several biomedical applications, for example, cell labeling with magnetic nanoparticles is now a widely used means of *in vitro* cell separation, where a high gradient magnetic field is used to isolate cells of interest, tagged with magnetic particles, from a heterogeneous population (Molday and Molday 1984; Radbruch, Mechtold

et al. 1994). Targeted drug/gene delivery is used to deliver drugs or genes regio-specifically by attaching them to magnetic nanoparticles and locally concentrating the resulting complexes *in vivo* to the desired locale (Scherer, Anton et al. 2002; Krotz, Sohn et al. 2003; Vasir and Labhasetwar 2005; Dobson 2006). Similarly, magnetic hyperthermia, the local concentration of magnetic nanoparticles and subsequent heating via AC magnetic fields, has shown promise as a potentially viable cancer therapy (Jordan, Scholz et al. 1999; Moroz, Jones et al. 2002). MNPs are also readily utilized as MRI contrast agents, where, once injected into the bloodstream, they are taken up differentially and act to modulate relaxation times (Bonnemain 1998; Wang, Hussain et al. 2001; Josephson, Kircher et al. 2002). And it has additionally been shown that if cells are labeled with large enough numbers of magnetic nanoparticles, that these cells can be located, tracked and recovered using high resolution imaging techniques, such as high-resolution magnetic resonance imaging (MRI) (Hsu, Dodd et al. 2000; Lewin, Carlesso et al. 2000). Lastly, another application, magnetorelaxometry, or the measurement of magnetic viscosity or the net magnetic moment of a system of magnetic nanoparticle after removal of a magnetic field (Rheinlander, Kotitz et al. 2000; Lange, Kotitz et al.), has recently been developed and is covered in depth in subsequent sections.

Each biomedical application, however, poses additional constraints and concerns for their production and use. As an obvious example, a MNP solution normally should be "biocompatible," i.e., nontoxic to biological systems, particularly if it is intended for use *in vivo*. For this reason, it is the oxides of iron, Fe_2O_3 and Fe_3O_4, which are generally considered physiologically biocompatible, that are almost exclusively used for both *in vitro* and *in vivo* biomedical applications, (Lacava, Azevedo et al. 1999; Kim, Yoon et al. 2006). Conversely, most ferromagnetic materials such as pure iron, nickel and cobalt are biotoxic, highly susceptible to oxidation and not considered safe for most biomedical purposes (Wormuth 2001). Additionally, MNPs designed for biomedical uses must be stable in aqueous solution at

neutral pH and isotonicity (330 mOsm). This constraint, while seemingly not stringent, can, based on the previously mentioned thermodynamic considerations, actually act as a significant hurdle in many MNP preparations. Furthermore, MNPs must be coated in such a way as to not only prevent agglomeration, but also biodegradation, nonspecific interactions and in *in vivo* applications, unwanted clearance from the body.

1.2.2 Cell Separation

The most obvious attribute of MNPs is their ability to be preferentially pulled or manipulated by an external gradient magnetic field. This property led to the one of the first widely used biomedical applications for MNPs: cell separation. In many cases in biomedicine and biomedical research, it is desirable to isolate or remove biological entities, such as cells, from a heterogeneous population. Thirty years ago, Molday, et. al. showed that magnetic microspheres could be conjugated to antibodies and used to separate and isolate specific cells using permanent magnets or electromagnets (Molday, Yen et al. 1977). This was followed, 5 years later, with Molday's seminal paper on the preparation of Protein A conjugated magnetic **nano**particles for labeling and separating antibody conjugated cells (Molday and MacKenzie 1982). Since then, an entire industry has developed around this concept: the tagging of a biological entity with magnetic material and the subsequent removal of the entities via a fluid based magnetic separation device. Much of the work that has gone into MNP research for biomedical purposes centers on the development of methods of specifically tagging entities of interest with magnetic material and is of prima facie relevance to this dissertation. This is made feasible through the development of biocompatible and chemically modifiable nanoparticle coatings, such as dextran, polyvinyl alcohol, and phospholipids (Sangregorio, Wiemann et al. 1999; Pardoe, Chua-anusorn et al. 2001) to which antibodies or

other binding entities can be attached, either prior to or following attachment to the entity of interest. A schematic of a basic antibody based magnetic separation is shown in Figure 1-6.

1.2.3 Targeted *In Vivo* Drug/Biomolecule Delivery

Another longstanding biomedical application that utilizes the action at a distance manipulation of magnetic nanoparticles is targeted drug/gene delivery. One of the primary problems in the delivery of chemotherapeutics is the lack of specificity of their delivery. Once a drug enters the bloodstream, via oral, intravenous, or other, it is systemically distributed throughout the body, resulting in, not only reduced efficacy, but potentially dangerous side effects to other tissues. In an ideal case, drugs would act on and be directly targeted to the tissue of interest. This desire naturally lent itself to the proposition of using magnetic nanoparticles (or microparticles) as carriers of drugs to locally target and concentrate the agents to specific regions using magnetic forces. Specific targeting of the drugs accomplishes two tasks: first, reduction in the systemic distribution of the agent and the subsequent deleterious side effects and second, reduction in the required dosage of the agent by increasing the local concentration of the agent to the area of interest. In targeted delivery, the drug or chemotherapeutic is transiently attached to biocompatible MNPs in suspension and injected into the bloodstream of the subject. Once the particle solution has entered the bloodstream, it is concentrated using a strong, typically permanent, magnet fixed outside the body over the region of interest. After the drug has been sufficiently concentrated at the region of interest, the drug or agent is released via enzymatic reaction or by changing the local physiological conditions, such as pH, osmolality or temperature (Alexiou, Arnold et al. 2000). These techniques have been primarily applied to tumors in animal subjects such as rat (Widder, Morris et al. 1983; Pulfer and Gallo 1998), rabbit (Alexiou, Arnold et al. 2000) and swine (Goodwin, Bittner et al. 2001), but have recently entered clinical trials in humans

(Lubbe, Bergemann et al. 1996; Gallo and Hafeli 1997; Lubbe, Alexiou et al. 2001). Using the same principles, magnetofection involves the attachment of viral vectors containing genes of interest to magnetic carriers and then locally concentrating them for *in vitro* and *in vivo* gene transfection (Scherer, Anton et al. 2002; Plank, Scherer et al. 2003; Plank, Schillinger et al. 2003; Xenariou, Griesenbach et al. 2006).

1.2.4 Magnetic Hyperthermia

As mentioned in previous sections, MNPs undergo heating in the presence of an external alternating magnetic field. This has been known for quite some time and, given the fact that cells can be necrotically destroyed via heat, was the impetus behind the crude demonstration of their use as *in vivo* heating/ablating agents a half century ago (Gilchrist, Medal et al. 1957). Since then, mainly in the last twenty years, much research has gone into developing a variety of schemes of delivering and heating MNP solutions for the treatment of tumors (Gordon, Hines et al. 1979; Rand, Snow et al. 1982; Borrelli, Luderer et al. 1984; Mitsumori, Hiraoka et al. 1994; Jordan, Scholz et al. 1997; Jones, Winter et al. 2002; Moroz, Jones et al. 2002). Additionally, it was discovered that many cancers are even more susceptible to heat than healthy tissue, in particular temperatures between 41°C and 46°C (Jordan, Scholz et al. 1999). A variety of techniques have been proposed and developed in order to capitalize on this phenomenon and have given rise to the field of hyperthermia. Further heating of the tissue, to temperatures greater than 46°C and up to 56°C, causes necrosis, coagulation and carbonization, is called thermo-ablation and encompasses an entirely separate field of study. Despite great efforts towards the development of other hyperthermic systems such as radiofrequency (RF), local and interstitial hyperthermia, there are several problems that typically impede their widespread use, most notably the shielding of deep tissues by bone structures such as the pelvis and skull resulting in thermal underdosage and regrowth of the

tumor. The transparency of biological tissue to magnetic fields and the use of guided magnetic hyperthermia can potentially circumvent this problem. A formal analysis of magnetic hyperthermia is beyond the current scope, but the basic principle involves the dispersion of a biocompatible MNP solution to the target [cancerous] tissue followed by the application of an external alternating magnetic field at specific amplitudes and frequencies, which are well tolerated by the surrounding tissues, resulting in conduction of heat from the MNP solution to the diseased tissue and thermal inactivation of cellular processes (Jordan, Wust et al.).

1.2.5 MRI Contrast Enhancement

Magnetic resonance imaging (MRI) is based on the nuclear magnetic resonance (NMR) or resonant absorption of magnetic field of hydrogen protons in water molecules within the body. A signal is produced by the relaxation of magnetic moments in the hydrogen atoms. This relaxation is characterized by the longitudinal and transverse relaxation times, denoted T_1 and T_2, respectively. Various paramagnetic and SPM MNP solutions, called magnetic contrast agents, have been developed to shorten both the T_1 and T_2 relaxation times. The most commonly used [paramagnetic] agents are composed of gadolinium ion complexes and act to shorten T_1 times(Johnston, Liu et al. 1987), but several iron oxide based solutions that shorten T_2 times are also commercially available (Weissleder, Elizondo et al. 1990; Weissleder, Elizondo et al. 1990; Bonnemain 1998; Choi, Choi et al. 2004; Muldoon, Sandor et al. 2005). These MNPs are coated with dextran or starch and rely on the selective uptake by the reticuloendothelial system of various tissues and structures at different rates, particularly the liver and spleen, resulting in an increased contrast in the detected signal between the tissues (Fahlvik, Holtz et al. 1990; Kubaska, Sahani et al. 2001; Halavaara, Tervahartiala et al. 2002). By adjusting the size of the nanoparticles, these rates can also be varied. Indeed, two classes

of SPM MRI contrast agents exist: superparamagnetic iron oxides (SPIOs) consisting of nanoparticles greater than 50nm that are rapidly taken up ($t_{1/2}$~10 min.) and typically used for liver and spleen imaging (Fahlvik, Holtz et al. 1990) and ultra-small superparamagnetic iron oxides (USPIOs) with dimensions less than 50nm which exhibit much longer half lives ($t_{1/2}$> 2 hrs.) are used for angiography (Wacker, Wendt et al. 2002; Wacker, Reither et al. 2003) and visualization of the central nervous system (Dousset, Delalande et al. 1999).

1.2.6 Cell Tracking and Intracellular Delivery

Recently, much attention has been given to the possibility of tagging or labeling cells of interest and tracking their movements or interactions *in vivo* (Lok 2001). This so-called "cellular imaging" has proved feasible with the use of high resolution MRI techniques, capable of tracking magnetically labeled cells at near microscopic resolutions (Lewin, Carlesso et al. 2000; Bulte, Douglas et al. 2001; Bulte, Duncan et al. 2002). Cell tracking is a particularly attractive solution in progenitor and stem cell research, as it is highly desirable to have a means of monitoring their location, fate and biodistribution (Miyoshi, Smith et al. 1999). While cellular imaging was proposed and attempted over ten years ago, early attempts were frustrated by poor cellular uptake via endocytosis (Bulte, Ma et al. 1993; Jacobs and Fraser 1994; Yeh, Zhang et al. 1995; Schoepf, Marecos et al. 1998; Dodd, Williams et al. 1999). To this end, many groups have investigated the use of various organic coatings as a means of optimizing the delivery of MNPs to or into cells. In some instances, MNPs have been coated with ligands to cell surface receptors in order to utilize a receptor mediated endocytotic pathway versus the slower passive internalization via fluid phase endocytosis (Kohler, Sun et al. 2005; Sonvico, Mornet et al. 2005). More notably, MNPs have been modified to allow their free passage into cells using lipophilic coatings such as polyethylene glycol (PEG) (Gupta and Curtis 2004; Zhang, Sun et al. 2004) or dendrimers (Bulte, Douglas et al. 2001), or with well-

known transfection agents such as the HIV derived TAT protein (Josephson, Tung et al. 1999; Lewin, Carlesso et al. 2000; Josephson, Kircher et al. 2002; Kircher, Allport et al. 2002). In several cases it has been shown that even a simple dimercaptosuccinic acid (DMSA) coating can vastly improve uptake efficiency, presumably by endowing the MNPs with an anionic charge, resulting in nonspecific adsorption to the cell surface followed by endocytosis into the cell (Wilhelm, Gazeau et al. 2002; Billotey, Wilhelm et al. 2003).

1.2.7 Other Miscellaneous Applications

There are a wide range of other biomedical applications not discussed here to which MNPs are currently being investigated and employed. Examples of these diverse applications include: intraocular repair, where magnetic nanoparticles are being investigated as a means of physically correcting retinal detachment (Dailey, Li et al. 1997); magnetic twisting cytometry, where nanoparticles and microparticles are attached to surface receptors in order to exert a force via external field and measure the biomechanical properties of the cytoskeleton (Wang, Butler et al. 1993); rotational magnetic endosome microrheology, where a magnetic force is applied to endocytosed MNPs to probe the viscoelastic properties of live cells (Wilhelm, Gazeau et al. 2003); as well as *in situ* gene expression (Weissleder, Moore et al. 2000) and other tissue engineering applications such as mechanical conditioning (Cartmell, Dobson et al. 2002) and cell patterning (Ito, Takizawa et al. 2004), to name only a few.

1.3 SQUID Magnetorelaxometry

1.3.1 Principles of SQUID Magnetometry

The superconducting quantum interference device (SQUID) is the most sensitive detector of magnetic flux currently known. In simple terms, SQUIDs act as extremely sensitive

magnetic flux to voltage transducers, theoretically capable of detecting a single quantum of magnetic flux. Their detailed operation, while beyond the current scope, is based on the Josephson junction, the interruption of two superconductors by a thin insulating layer, as shown in Figure 1-7. Briefly, each superconductor has a parameter, ψ (such as current), and corresponding phase, θ, associated with it and the difference in these phases $\delta = \theta_1 - \theta_2$ affects the electrical properties of the junction, namely, in a direct current (DC) SQUID, the voltage, V, across two parallel Josephson junctions, according to the relation:

$$V = \frac{\pi}{2e}\left(\frac{d\delta}{dt}\right) \tag{1.12}$$

A change in an applied magnetic flux, Φ_A, typically generated in a pickup coil connected to an input coil inductively linked to the SQUID, generates a current in the superconductors and results in a phase difference, δ, which is then measured as the output voltage. Each quantum of flux, Φ_0, equivalent to 2.07×10^{-15}Wb, changes the output phase of V, which oscillates between V_{min} andV_{max}, by 2π, thus the V- Φ_A curve is roughly sinusoidal, and acts as a non-linear flux to voltage transducer. In order to be useful, a typical DC SQUID system utilizes a flux locked loop (FLL), where a modulating flux, Φ_M, is applied to the SQUID at an oscillator controlled frequency ω and amplitude $\leq \Phi_0/2$, and holds the SQUID voltage at one of the maxima of the V- Φ_A curve. Now when a there is a change in external flux, $\Delta\Phi$, it contains a voltage component at frequency ω (instead of 2ω) and is detected by a lock-in amplifier which then adjusts Φ_M to return the output voltage back to its maximum. The magnetic field/flux, then, is detected as an "error signal" in the difference in the amplitude of V at frequency ω. A schematic of a typical DC SQUID system, including the FLL, oscillator and lock in amplifier is shown in Figure 1-8. Figure 1-9 shows a picture of a high temperature

(HT) DC SQUID instrument and sensor chip, developed by DiIorio et. al. (Dilorio, Yoshizumi et al. 1991), that is used for the experiments described in the current work.

1.3.2 Principles of Magnetorelaxometry

As previously stated, the magnetic moment of MNPs following application of an external magnetic field decays over time due to thermal fluctuations. Such magnetic decay is called Néel relaxation after its founder Louis Néel. The study of MNP systems which undergo this phenomenon in a liquid medium is known as magnetorelaxometry and was first proposed and developed a decade ago by Kötitz et. al. (Kotitz, Fannin et al. 1995; Kotitz, Matz et al. 1997). Magnetorelaxometry is based on the fact that the magnetic moments of MNPs in solution randomize and effectively relax in two ways: through Néel relaxation, the kinetics of which are given in (1.3), and Brownian rotation whose time constant, τ_B, is characterized by the equation:

$$\tau_B = \frac{3V'\eta}{k_B T} \tag{1.13}$$

where V' is the hydrodynamic volume and η is the viscosity of the solution (Debye 1929; Bogardus, Scranton et al. 1975; Kotitz, Fannin et al. 1995). Given these equations a magnetic particle solution, based on the size of the particles and viscosity of the solution, can be developed/chosen such that $\tau_B << \tau_N$ and Brownian relaxation occurs much more rapidly than Néel relaxation. If one measures the remanent magnetization, M_r, of an MNP suspension in a saturating field at $\tau_B < t_M < \tau_N$ the particles in solution will have randomized and give no net signal. However, if any of the MNPs in the solution are attached to a large or solid support, they will give a net magnetic signal, m_{net}, according to:

$$m_{net} = N_I MV \tag{1.14}$$

where N_I is the number of immobilized MNPs contained within the solution and M is the magnetic moment determined by the M-H loop of the magnetic nanoparticles. This magnetic moment, which decays via Néel relaxation once the magnetizing field is removed, can result in an induction, B, in a SQUID sensor located at distance r from the particles of:

$$B = \frac{\mu_0}{4\pi}\left[\frac{3(m_{net}\cdot r)}{r^5} - \frac{m_{net}}{r^3}\right] \tag{1.15}$$

and likewise cause a phase shift, δ, between the superconductors that is detected as a voltage within the SQUID system. So, then, the SQUID sensor detects the net magnetic flux from immobilized or "bound" magnetized MNPs. A schematic of showing the magnetization and measurement process used in current experiments is shown in Figure 1-10.

1.3.3 Magnetorelaxometry for Bioassays

In biomedicine and biomedical research, it is often desirable to detect and quantify the binding of one biochemical entity to another. For example, in a typical enzyme linked immunosorbent assay (ELISA), samples containing an unknown quantity of a particular antigen are added to containers, such as wells in a microtiter plate, containing "capture" antibodies to that antigen that have been immobilized onto its base and/or walls. Following an appropriate incubation time (usually ~ 1 hour), the sample is washed away and a second antibody to the antigen, conjugated to a reactive enzyme, is added and allowed to bind (usually ~1 hour). After washing this "detection" antibody away, a substrate which reacts with the enzyme by forming a colored or fluorescent product is added. After the reaction has been allowed to proceed for a sufficient amount of time (>15 minutes), the resulting solution

is analyzed by a spectrophotometer or fluorimeter, resulting in a signal that has been shown to be proportional to the amount of antigen originally present in the solution, which can be determined with an appropriate standard curve. Assays such as these, while common in biomedicine, are often tedious, costly and time-consuming. The prospect of increased speed, sensitivity and simplification are obviously attractive. This led researchers to first propose the use of magnetorelaxometry for use in bioassays, as an alternative method of binding quantification (Kotitz, Bunte et al. 1997; Kotitz, Matz et al. 1997).

In contrast to ELISAs, the recently developed magnetorelaxometric bioassay, or magnetic relaxometric immunoassay (MARIA) (Kotitz, Bunte et al. 1997; Kotitz, Matz et al. 1997), consists of labeling the detection antibody with a magnetic nanoparticle, rather than an enzyme. In a typical assay preparation, a mixture of both the magnetically labeled detection antibody and the sample can then be added to a microwell to which the capture antibody has been adsorbed and allowed to form immunocomplexes consisting of antigen, immobilized by the capture antibody, linked to MNPs via the detect antibody. Following brief application of a magnetic field, the m_{net} described in (1.14) is detected by the SQUID system and can be directly correlated with the signal from a standard set of conditions to determine the level of antigen in the samples. Figure 1-11 shows a schematic of a typical magnetorelaxometric immunoassay and a plot of the results compared with an ELISA. Note that the binding and, hence the magnetic signal are directly correlated *in time*. This scheme offers several key advantages over traditional type assays, including ultra high sensitivity (attomolar), a homogeneous format, viz. no need to wash/remove unbound labels, and the ability to do live cell assays and study molecular binding kinetics in real time.

Several other biomedical applications of magnetorelaxometry have recently been proposed and developed and are the basis of majority of the present work. While most of the work on magnetorelaxometry has centered around its use in ELISA type assays (Chemla,

Crossman et al. 2000; Enpuku, Hotta et al. 2001; Enpuku, Kuroda et al. 2003; Horng, Yang et al. 2005; Ludwig 2006), some groups have also investigated its use in other applications as well, such as the detection of bacteria in solution (Grossman, Myers et al. 2004), liquid phase biochemical assays (Chung, Hoffmann et al. 2005; Hong, Wu et al. 2006) and assessments of GI tract motility (Cora, Romeiro et al. 2005; Klein, Stein et al. 2005; Cora, Romeiro et al. 2006).

1.4 Scope of the Dissertation

The overall objective of the dissertation is to develop tailored magnetic nanoparticles, optimize their use in novel magnetorelaxometric bioassays and to demonstrate the scientific and clinical utility of such assays.

This dissertation is divided into four experimental chapters. Chapter Two deals with a preliminary demonstration of the synthesis of magnetic nanoparticles and their stabilization, analysis of various MNPs for magnetorelaxometry, general optimization of magnetorelaxometric assay conditions and calibration of the SQUID system. These set the basis for the magnetorelaxometric assays developed in subsequent chapters. Potential improvements to MNP characteristics and the SQUID system are also proposed and discussed.

Chapter Three demonstrates a rapid *in vitro* MARIA assay for sepsis diagnostics using a known bacterial pathogen, *E. coli* O157:H7, with very high sensitivity and specificity. MNPs are conjugated to modified anti-*E. coli* O157:H7 antibodies and a pseudo-homogeneous and fully homogeneous MARIA assay are demonstrated in a buffer solution. The clinical sensitivity and specificity of the homogeneous assay is then demonstrated. This is followed by the inoculation and quantitative detection of the target pathogen in human serum and blood samples. Future work and the potential of MARIA for use in sepsis diagnostics are discussed.

Chapter Four demonstrates the ability of magnetorelaxometry to be used for *in vivo* applications. *C. elegans* is used as a model organism and MNPs are conjugated and developed for a scientifically relevant bioassay – the binding of toxins to the gut of wild type nematodes versus mutant nematodes lacking polysaccharides necessary for binding of the toxin. The results of the assay and limitations of the model system are discussed and alternatives are proposed.

Chapter Five is concerned first with the synthesis and development of MNPs which can readily penetrate the plasma membrane and pass into the cytoplasm of the cell. The cytotoxicity of one such MNP solution, anionic magnetic nanoparticles (AMNPs), is examined in a PC12 model cell system, followed by the demonstration of an intracellular protein magnetorelaxometric immunoassay (MARIA), viz., an *in situ* magnetorelaxometric assay, using TAT and anti-tubulin conjugated MNPs. Practical issues in the development of intracellular magnetorelaxometric assays are discussed, as well planned improvements.

Lastly, Chapter Six contains a brief discussion of the contribution of this work to nanotechnology and biomedical diagnostics, followed by future considerations of magnetorelaxometry in bioassays.

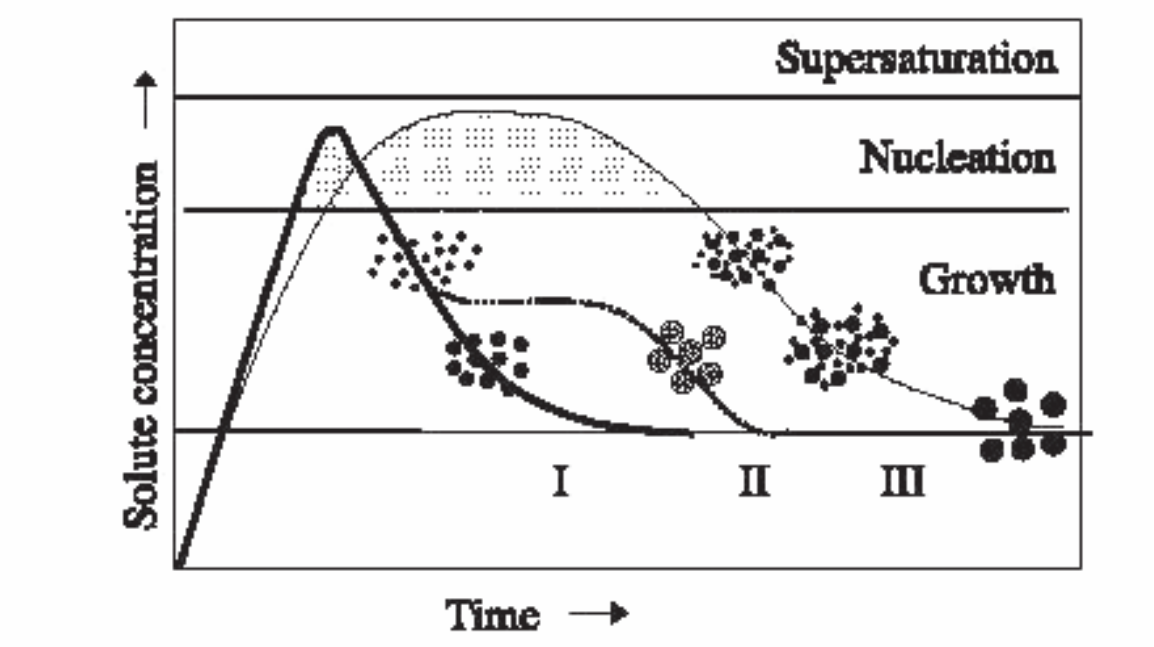

Figure 1-1. Various mechanisms of magnetic nanoparticle formation in solution: curve I: individual nucleation and uniform growth by diffusion; curve II: nucleation, growth and aggregation of smaller subunits; curve III: multiple nucleation events and Ostwald ripening. Taken from (Tartaj, del Puerto Morales et al. 2003).

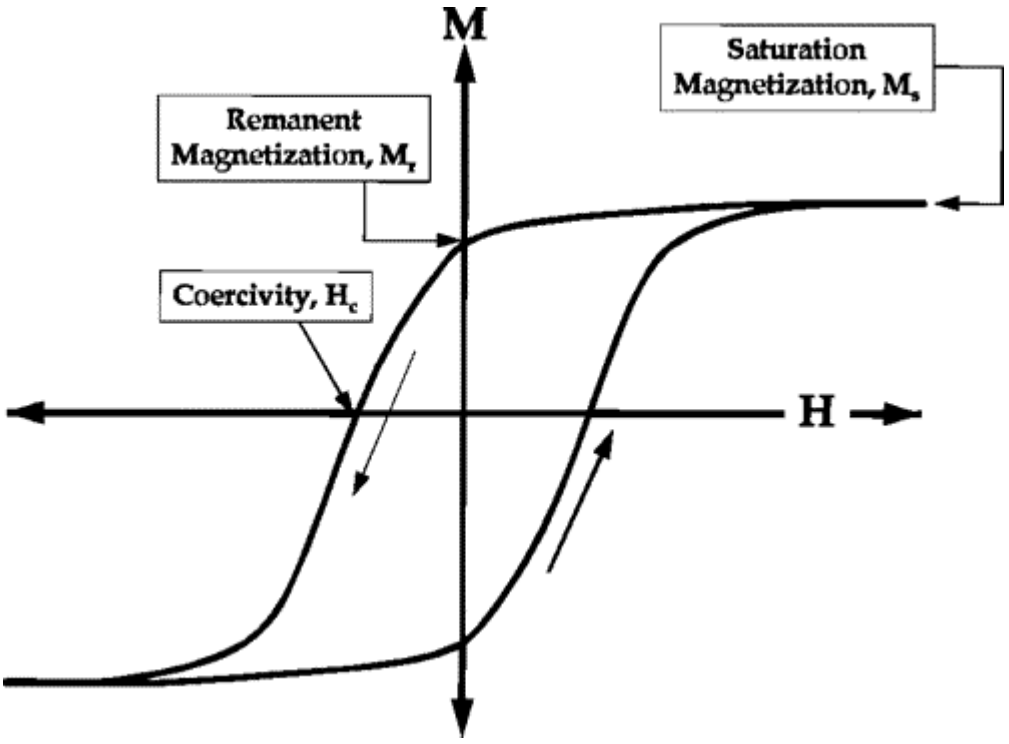

Figure 1-2. Representative M-H loop or curve from a hypothetical magnetic material, showing the saturation magnetization, M_s, remanent magnetization, M_r, and coercivity, H_c. Taken from (Leslie-Pelecky and Rieke 1996).

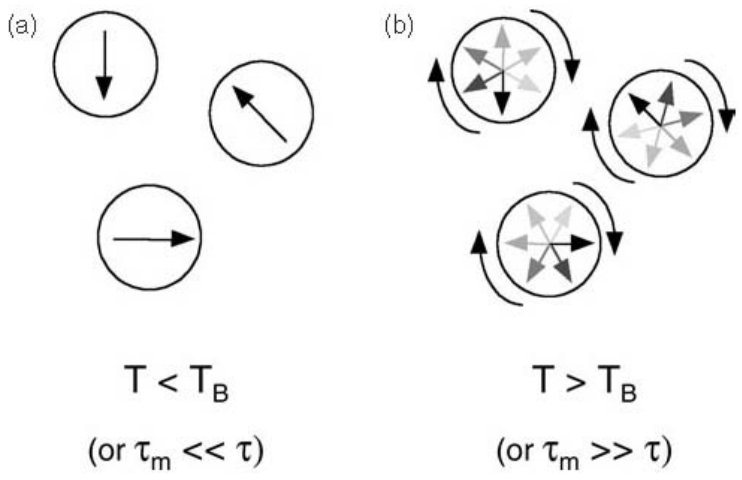

Figure 1-3. Illustration of the principle of superparamagnetism and the effect of measurement time and/or temperature on the observation and measurement of magnetic moments (shown as arrows). Case (a) depicts the case where the measurement temperature, T, is significantly lower the blocking temperature T_B or the measurement time, τ_m is much lower than the relaxation time constant, resulting in the measurement of a quasi-static moment. Alternatively, case (b) shows the opposite case, where $T_B << T$ and $\tau << \tau_m$, resulting in the measurement of [super]paramagnetism. Taken from (Pankhurst, Connolly et al. 2003).

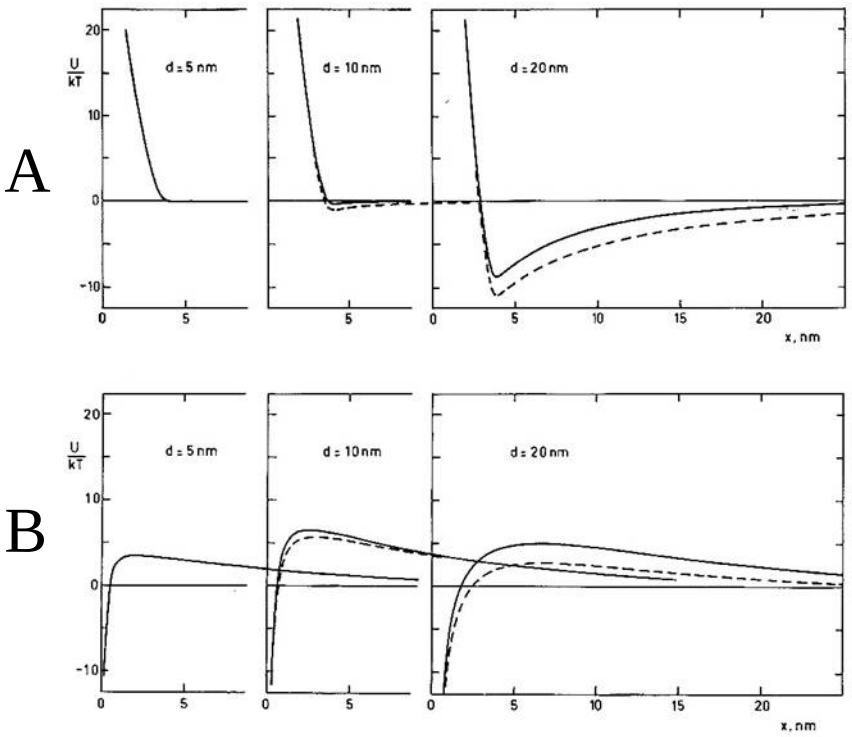

Figure 1-4. Normalized energies versus distance between magnetic nanoparticles for a (A) hypothetical oleic acid sterically stabilized and (B) electrically stabilized 5, 10 and 20nm Fe_2O_3 suspension in a 10^{-3} monovalent electrolyte solution with and without an applied saturating magnetic field. Taken from (Berkovsky 1978).

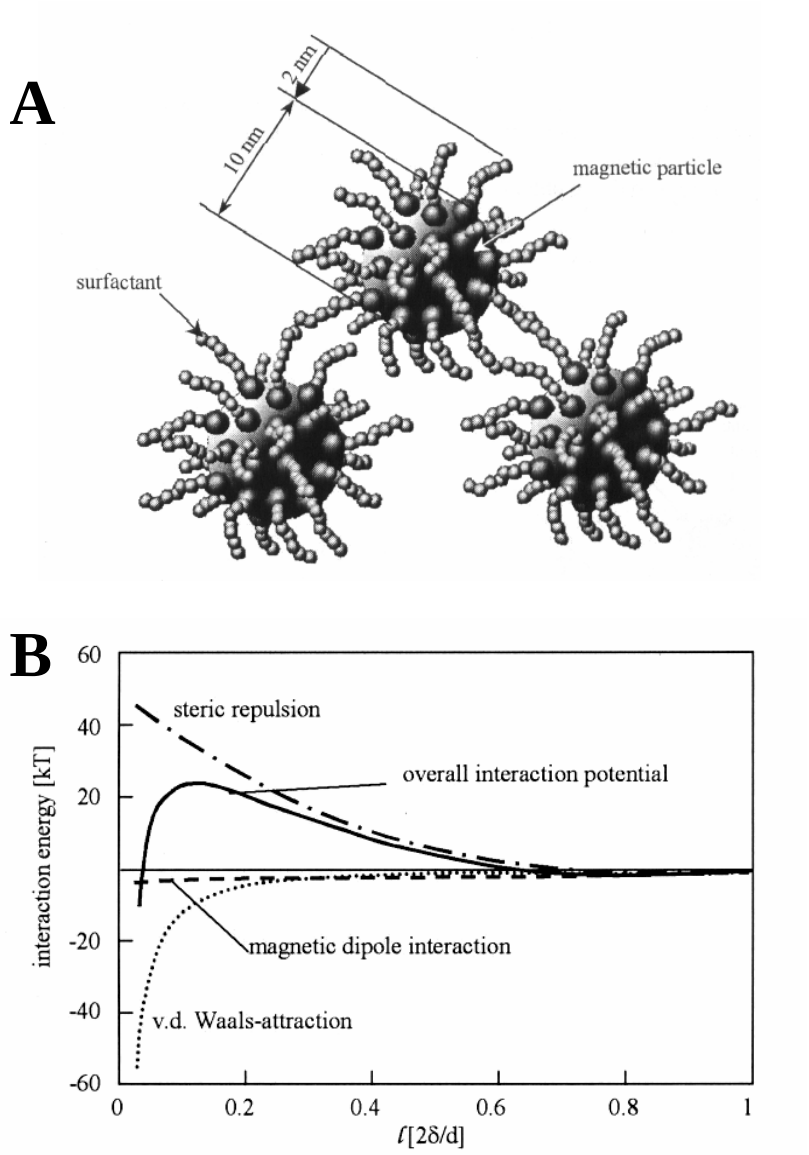

Figure 1-5. (A) Schematic of a surfactant/oleic acid sterically stabilized MNP suspension. Particles and surfactant are not shown to scale for reasons of clarity. (B) Interaction energies of sterically stabilized MNPs as a function of interparticle distance, *l*, where δ is the steric coating and d is the diameter of the nanoparticles. Adapted from (Odenbach 2002).

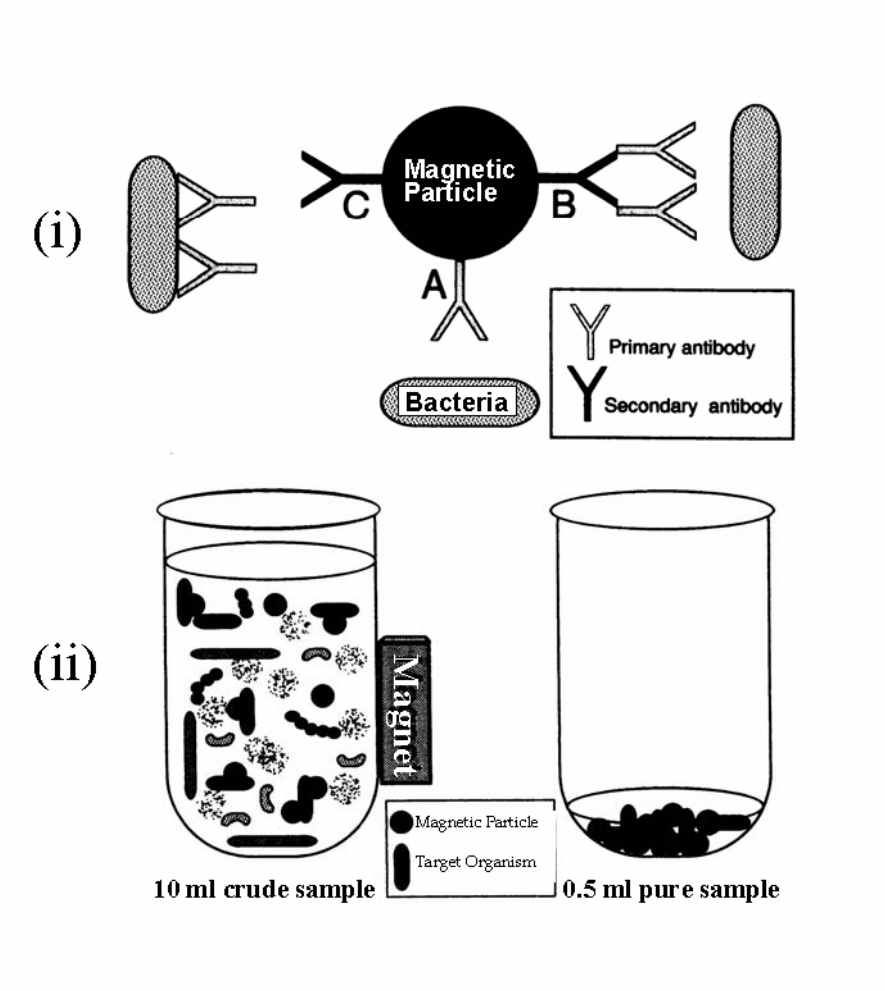

Figure 1-6. Immunomagnetic separation of bacteria. (i) Labeling of bacteria can occur through (A) direct attachment of the primary antibody to the MNPs, (B) direct attachment of a secondary antibody to the primary antibody or (C) tagging of bacteria with primary antibody, followed by attachment of a secondary antibody directly attached to the MNPs. (ii) Basic immunospecific magnetic separation of bacteria from a heterogeneous mixture. Adapted from (Olsvik, Popovic et al. 1994).

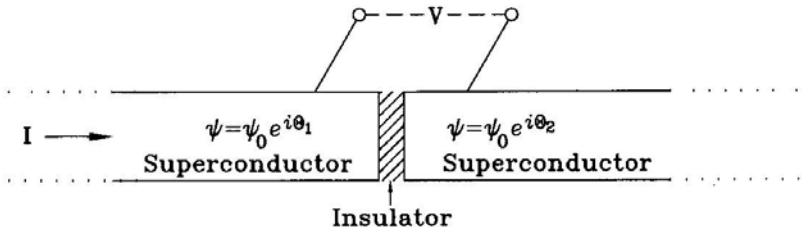

Josephson Equations

$$I = I_0 \sin\delta \quad \text{(dc)}$$

$$V = \frac{\hbar}{2e}\left(\frac{d\delta}{dt}\right) \quad \text{(ac)}$$

$$\delta = \Theta_1 - \Theta_2$$

Figure 1-7. The Josephson junction. Two superconductors are separated by a thin insulating layer. The phase of the superconducting order parameter, ψ, is a function of the current flow through the junction and gives rise to the unique electrical properties described by the Josephson equations. Adapted from (Jenks, Thomas et al. 1997).

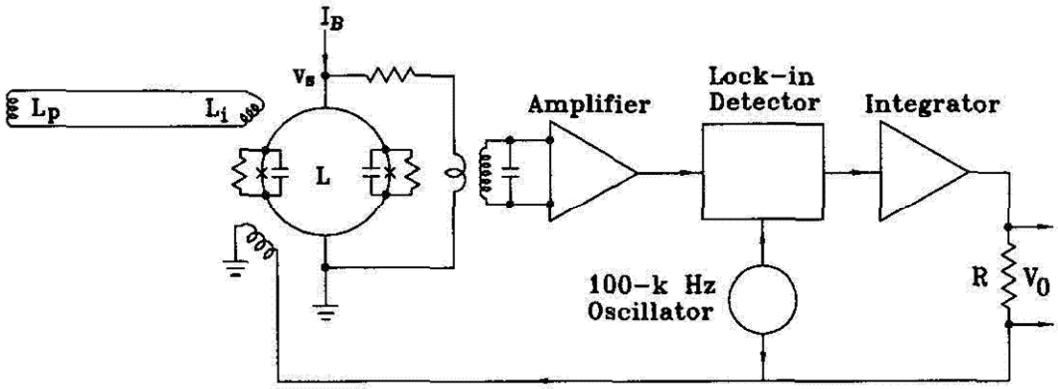

Figure 1-8. Schematic of a basic SQUID system, showing the pickup coil, SQUID and FLL. A change in magnetic field/flux at the pickup coil with inductance, L_P, and coupled to the input coil with inductance, L_I, is detected by the inductively coupled SQUID which results in a phase difference, δ, and voltage output from the SQUID. The voltage is amplified, detected and fed back to the SQUID as a modulating flux to maintain the voltage at an extremum on the V-Φ curve. Adapted from (Clarke 1966).

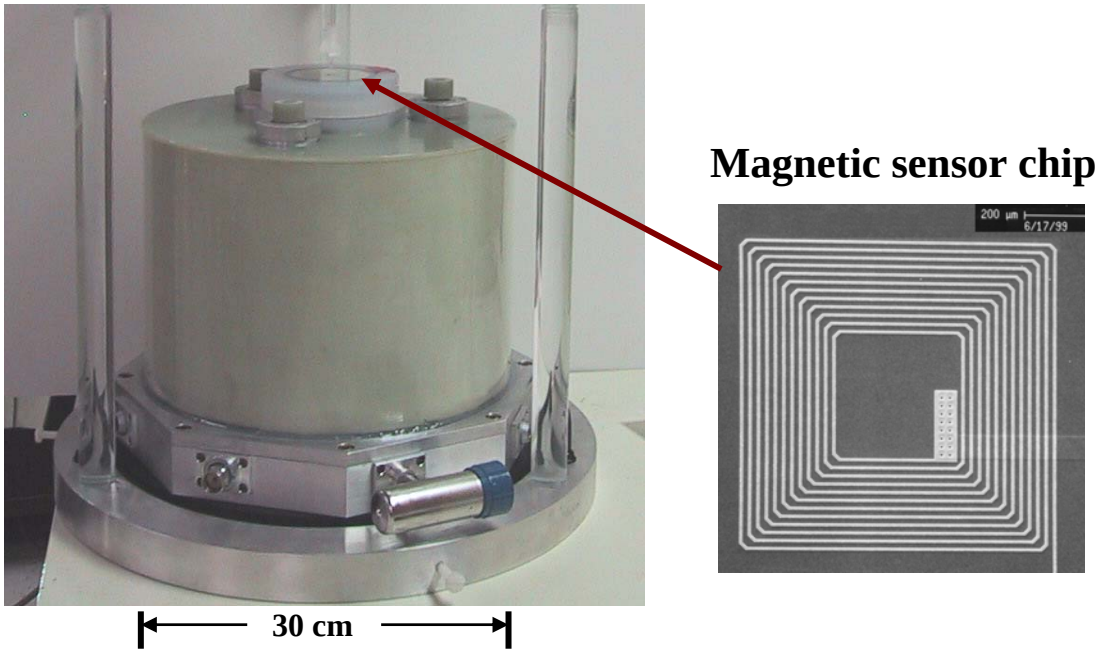

Figure 1-9. DC SQUID system used in current work, showing instrument and sensor chip. Adapted from (Dilorio, Yoshizumi et al. 1991).

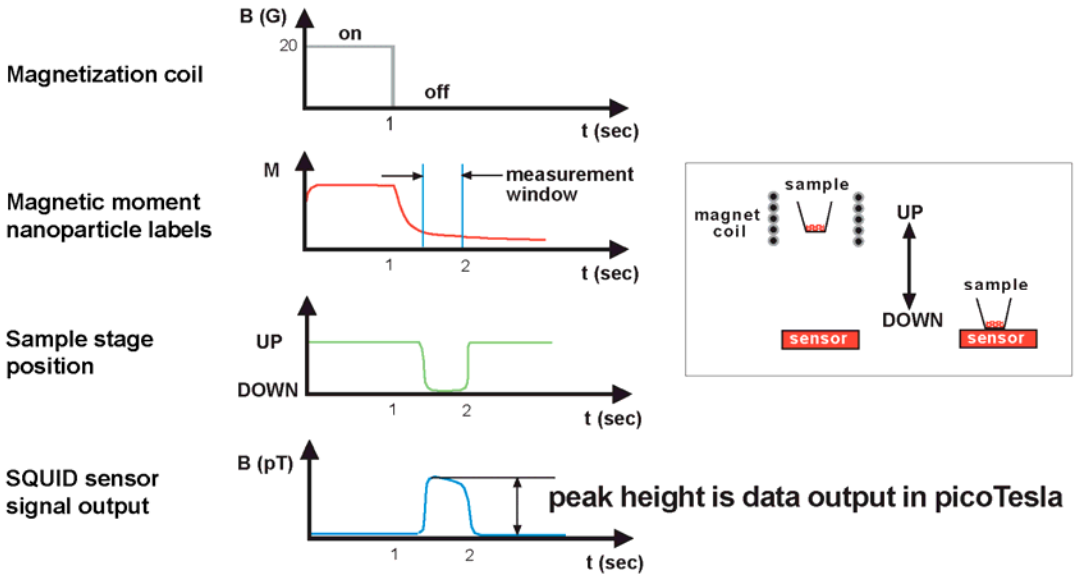

Figure 1-10. A typical magnetorelaxometric measurement. A fluid sample containing MNPs is magnetized and, after removal of the magnetizing field, immediately begins to undergo Néel relaxation. The sample is rapidly brought into proximity of a SQUID sensor, where the remanent magnetization of the immobilized MNPs is detected.

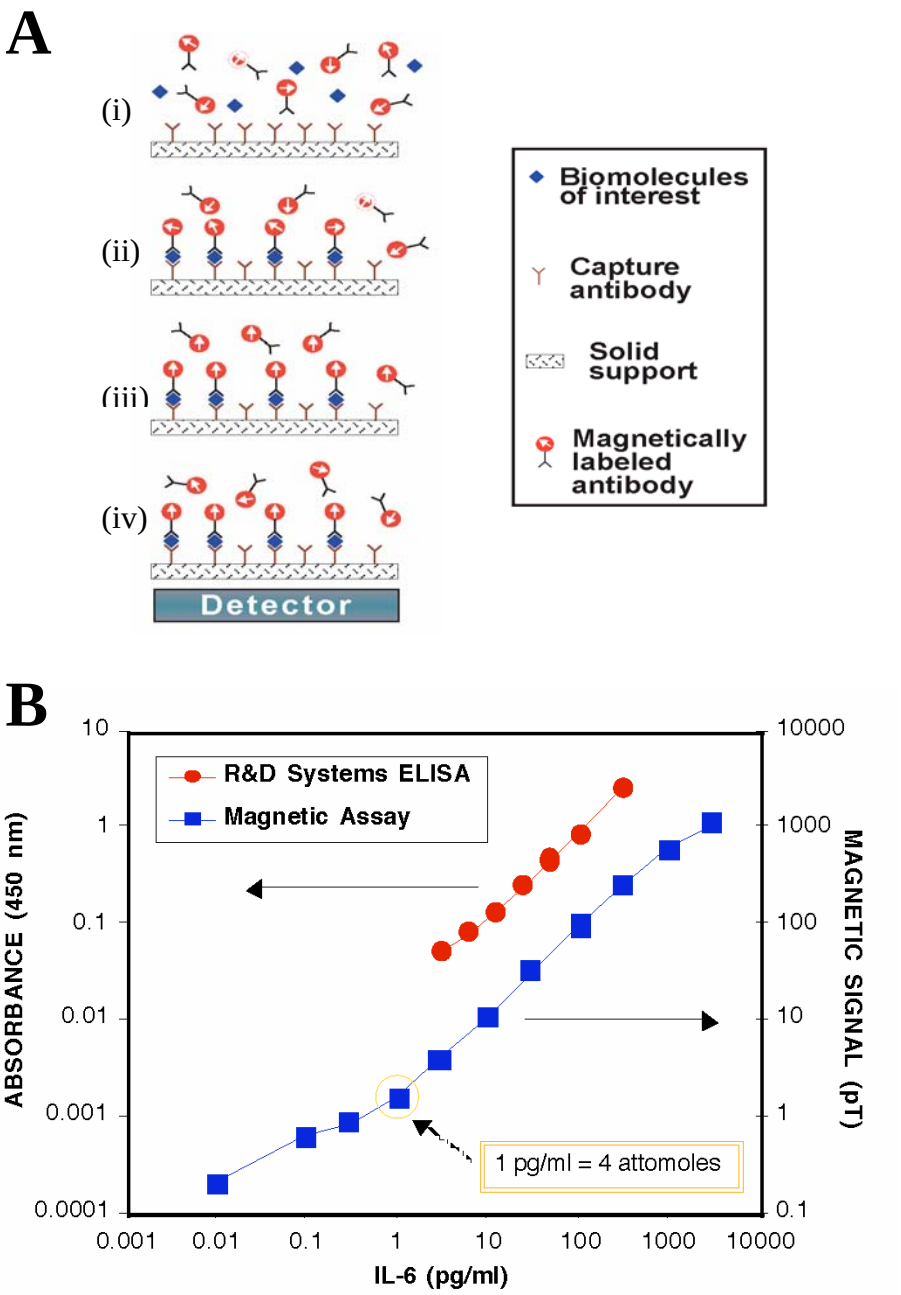

Figure 1-11. A typical MARIA. (A) (i) A sample containing an unknown amount of an antigen of interest and MNP labeled detection antibodies is added to a microwell coated with a capture antibody, (ii) immune complexes are formed on a solid support, (iii) a 20G external field is applied to magnetize and align the moments of the MNPs, (iv) the field is removed, allowing the unbound labels to rotate via Brownian relaxation, and the net magnetization of the [bound] labels is measured in the SQUID instrument. (B) Data from a typical MARIA assay, as compared with a typical ELISA, plotted as magnetic signal vs. concentration of antigen.

CHAPTER 2

MAGNETIC NANOPARTICLE SYNTHESIS AND MAGNETORELAXOMETRIC CALIBRATION

2.1 Abstract

Magnetic nanoparticles are currently being used in a wide array of biomedical applications. Each application, however, requires MNPs with unique and specialized magnetic and colloidal properties, particular to the desired function. Through careful control of various synthesis parameters, the size, structure and physical characteristics of MNPs can often be exquisitely controlled. The ability to synthesize iron oxide MNPs of various shapes and sizes is demonstrated, as well as the synthesis of both ionically and sterically stabilized MNPs suitable for use in biomedical applications. Additionally the remanent magnetizations of numerous biological ferrofluids are analyzed in order to screen them for use in magnetorelaxometric assays. Lastly, the sensitivity of the SQUID measurement system is demonstrated and reagent and assay conditions are optimized for magnetorelaxometric assays.

2.2 Introduction

Routine methods of magnetic nanoparticle synthesis have existed for over 40 years, beginning with the grinding of bulk magnetic materials into rough, irregular polydisperse suspensions (Papell 1965); much effort has been given to the development of alternative, chemical means of creating homogeneous, monodisperse MNP solutions with controllable physical characteristics. The primary impetus behind the first aqueous synthesis of iron oxide ferrofluids (Khalafalla and Reimers 1973) was advances in magnetic recording media, where control over MNP characteristics dramatically affects the properties and utility of the media. Since then, particularly in the last twenty years, many groups have developed a variety of chemical schemes to create and modulate the characteristics of magnetic fluids (Leslie-Pelecky and Rieke 1996; Vayssieres, Chaneac et al. 1998; Hyeon 2003; Tartaj, del Puerto Morales et al. 2003). In the realm of biomedicine, control over these characteristics can be particularly important, as the particles interact with complex, nonlinear systems, capable of modifying and reacting with the particles.

In general, the first requirement of any magnetic fluid intended for biomedical use is that it be stable in aqueous solution under normal physiological pH and salinity. As previously demonstrated, the stability of ferrofluids involves the balance of interparticle forces which are drastically affected by the dispersion medium. In particular, increased salinity shields and weakens electrostatic repulsions, while changes in pH can, depending on the surface chemistry, eliminate them altogether. This implies that many preparations of MNPs, regardless of toxicity issues, are rendered unsuitable for use in the majority of biomedical applications. Additionally, most biomedical applications, particularly those *in vivo*, require that the ferrofluid obey the Hippocratic Oath to "First, do no harm," viz., they must be biocompatible. With this in mind, the last ten years have witnessed a tremendous effort toward the development of an abundance of methods for the production of MNP solutions,

intended for biomedical use, that meet both criteria. In general, the methods employed are used to produce MNPs of iron oxides, namely magnetite, Fe_3O_4, and maghemite, Fe_2O_3. While ferromagnetic materials such as pure iron, cobalt and nickel possess strongly magnetic behavior, they are toxic and highly susceptible to oxidation and are of lesser interest to the biomedical community. As such, the work described herein is limited to the use and discussion of iron oxide MNP solutions.

Ideally, an MNP fabrication process allows for control over the size, shape and purity of the MNPs and maintains a narrow size distribution, i.e., it results in a monodisperse solution. A wide range of solution based techniques for the production of biocompatible iron oxide ferrofluids have been proposed and developed to accomplish this end (Leslie-Pelecky and Rieke 1996). While a thorough analysis of these techniques is beyond the current scope, they can be broken down into basic groups including: coprecipitation, sonochemistry, microemulsions, polyols, and high-temperature decomposition of organic precursors. Examples of methods of coprecipitation and sonochemical synthesis are demonstrated below.

Much of the effort that has gone into the development of biocompatible ferrofluids has focused on various means of coating MNPs with biologically inert coatings which minimize both interparticle interactions and allow for further modification and specific control over interactions with biological entities. These coatings include, but are not limited to: dimercaptosuccinic acid (DMSA) (Fauconnier, Pons et al. 1997), EDTA (Blesa, Borghi et al. 1984), citric acid (Massart and Cabuil 1987), dextran (Molday and MacKenzie 1982; Weissleder, Elizondo et al. 1990; Wang, Hussain et al. 2001), polyvinyl alcohol (PVA) (Lee, Isobe et al. 1996; Lin, Watanabe et al. 2003; Albornoz, Sileo et al. 2004), bovine serum albumin (BSA) (Liberti and Pino 1997; Mikhaylova, Kim et al. 2004), polyethylene glycol (PEG) (Butterworth, Illum et al. 2001; Zhang, Kohler et al. 2002; Gupta and Curtis 2004), starch (Kim, Mikhaylova et al. 2003), dendrimers/triblock copolymers (Strable, Bulte et al. 2001;

Harris, Goff et al. 2003) and silica (Ennas, Musinu et al. 1998; Huang and Chen 2005). In some techniques, these coatings are present in and part of the actual MNP synthesis procedure, while in others the MNPs are created first and then coated with the substance. The common goal of creating reliably controllable, functional, biocompatible ferrofluids, however, is shared among all of these techniques.

As the stated objective in this work is the production of tailored MNPs for use in magnetorelaxometric assays, toward this end the syntheses of MNPs of various physicochemical properties are described, and the stability and magnetic properties of which are discussed. These properties are then screened along with a large library of commercially available MNPs for use in magnetorelaxometric assays. From this library, those MNP solutions which display the best properties, such as chemical functionality, high M_r, low nonspecific binding (NSB) and high colloidal stability are chosen for use in magnetorelaxometric assays. The sensitivity and linearity of the SQUID measurement system is demonstrated as the signal levels are determined while the number of immobilized MNPs and their distance from the sensor is varied. Lastly, means of reducing nonspecific binding are researched and optimized.

2.3 Syntheses of Magnetic Nanoparticles

2.3.1 Basic Aqueous Synthesis of Iron Oxide Nanoparticles

There are basically two primary methods of synthesis via coprecipitation of MNPs in aqueous solution: the aging of stoichiometric mixtures of ferrous and ferric hydroxides and the less commonly used method of oxidizing ferrous hydroxide solutions with various agents (Tartaj, del Puerto Morales et al. 2003). An example of each is described in this section. The

method described for ferrous hydroxide oxidation was modified in order to produce magnetite particles with high values of M_r and M_s while maintaining superparamagnetic properties. The superparamagnetic size limit at room temperature for spherical magnetite MNPs (K=-1.1x10^{5}ergs/cm^3), as described in Section 1.1.3, yields a critical particle diameter, $D_{c,}$ of 26nm (Gee, Hong et al. 2003). It is just above this size that magnetite will start to [undesirably] maintain its remanent magnetization for extremely long periods of time (minutes or more).

2.3.1.1 Materials and Methods

Aging of Stoichiometric Mixtures. Fe_3O_4 magnetic nanoparticles were prepared according to the so-called Massart method (Massart 1981; Massart 1982). Two starting solutions were made by adding 5.406 g of $FeCl_3$ (Sigma-Aldrich, St. Louis, MO) to 20ml of deionized (DI) water and, separately, adding 1.988g of $FeCl_2$ (Sigma-Aldrich, St. Louis, MO) to 5ml of a 2N solution of HCl (Sigma-Aldrich, St. Louis, MO). These solutions were then added to 100ml of DI water under vigorous stirring, to which 120ml of a 2M ammonia solution was added and remained under vigorous stirring for 5 minutes, during which, a black precipitate formed, indicating the synthesis of Fe_3O_4.

Oxidation of Ferrous Hydroxide Solutions. Magnetite nanoparticles were prepared through a modification of the method described in (Sugimoto and Matijevic 1980). Three starting solutions were prepared by adding .69505g of $FeSO_4$ (Sigma-Aldrich, St. Louis, MO) to 10 ml of DI water which had been degassed by bubbling nitrogen for >2 hours; adding .84165g of KOH (Sigma-Aldrich, St. Louis, MO) to 10 ml of degassed water; and adding 2.0222g of KNO_3 to 10ml of degassed water. 1ml of the KOH solution, 1ml of the KNO_3 and 7ml of degassed water were mixed together in a test tube and further degassed with nitrogen for 2

hours. To this solution, 1ml of the $FeSO_4$ solution was added and the resulting solution was degassed for 1 minute at room temperature. The test tube was then immersed into an oil bath preheated to 90°C and was continued to be degassed for 5 minutes, at which point the tube was sealed and the mixture allowed to age at 90°C for 3 hours resulting in the formation of a black precipitate.

TEM Analysis. The MNP solutions were dried onto a carbon TEM grid and were observed using a transmission electron microscope (TEM) (JEOL 200CX operated at 200 KV).

2.3.1.2 Results

Both syntheses were successful in creating a dark opaque black precipitate, a well known characteristic of magnetite (The further oxidized, maghemite, is known to be brown or reddish brown). These precipitates were dried and analyzed via TEM to confirm the synthesis of MNPs. Figure 2-1 shows TEM images indicating the size and shape of the synthesized particles.

The chemical reaction which preceded the formation of magnetite in the case of stoichiometric aging case can be given by:

$$2FeCl_3 + FeCl_2 + 4H_2O + 8NH_3 \rightarrow Fe_3O_4 + 8NH_4Cl \quad (2.1)$$

and for the case of ferrous hydroxide oxidation:

$$3Fe^{2+} + NO_3^- + 3H_2O \rightarrow Fe_3O_4 + 3NO_2^- + 6H^+ \quad (2.2)$$

Both of these products responded strongly to the presence of an external NdFeB magnet by rapidly migrating toward it, indicating a strong magnetic behavior. Additionally, both

products were unstable in water due to the absence of little to no ionic repulsion energy, U_e, as well as the absence of any coating layers required for steric repulsion, U_s.

2.3.2 Tuning the Size and Shape of Iron Oxide Nanoparticles

As previously mentioned, the magnetic behavior of MNPs is highly dependent upon, not only their chemical composition, but also their size and shape. These parameters can often be exquisitely controlled through both the means of synthesis and the reaction conditions within those means. Examples of both reaction condition controlled and method controlled MNP synthesis are presented and demonstrated. Once again, the goal of these syntheses is to produce SPM MNPs with strong magnetic properties such as high values of M_r and M_s, as would be desirable in magnetorelaxometric assays. As an example of reaction condition controlled synthesis, the method of coprecipitation by aging of stoichiometric ratios of ferric and ferrous hydroxides is repeated, but this time with tight control over the reaction parameters and modification of the noncomplexing salt. The method used is modified from (Vayssieres, Chaneac et al. 1998), who showed that the size of the coprecipitated magnetite could be adjusted and controlled through the management and use of different concentrations of noncomplexing salts as well as the pH. The method described herein is intended to produce monodisperse magnetite particles of a larger 12nm diameter than Massart's method (6-10nm), the largest previously demonstrated with the stoichiometric aging of ferrous and ferric hydroxide gels method. As an example of method controlled synthesis, a sonochemical synthesis procedure is demonstrated. Sonochemistry involves the excitation of fluids by a high frequency (kHz to MHz) vibrating probe. The energy of the probe causes a process called acoustic cavitation, the rapid formation, growth and collapse of bubbles in a liquid medium from acoustic energy. Cavitation sites can reach temperatures over 5000K, pressures over 20MPa and extraordinarily high cooling rates (10^{10}K/s) (Suslick 1988) resulting in highly

reactive local environments. The method described here is for the production of 50x18nm magnetite nanorods and is taken from (Kumar, Koltypin et al. 2001). Not only is the magnetic particle volume an important determinant in the magnetic properties of MNPs, but also their geometric shape. Elongated magnetic nanoparticles normally magnetize along their long axes, which results in a higher anisotropy energy density, *K,* which, in turn, yields higher τ_N and M_r values, according to (1.4).

2.3.2.1 Materials and Methods

Parameter Controlled Aging of Stoichiometric Mixtures. The method for the formation of 12nm magnetite is modified from (Vayssieres, Chaneac et al. 1998) to produce particles with the desired characteristics. A precursor solution was prepared by adding 4.04g of iron nitrate, $Fe(NO)_3$ (Sigma-Aldrich, St. Louis, MO), and .994g of $FeCl_2$ (Sigma-Aldrich, St. Louis, MO), to 5ml of a 0.5M solution of tetramethylammonium nitrate., $N(CH_3)_4NO_3$, (TMAN) (Sigma-Aldrich, St. Louis, MO). The reaction solution was made by adding 7ml of a 25% tetramethylammonium hydroxide (TMAH) solution (Sigma-Aldrich, St. Louis, MO) to 25ml of 0.5M TMAN which remained vigorously stirred throughout the procedure. Both solutions were preliminarily deoxygenated by bubbling N_2 for 45 minutes, which continued throughout the reaction. To initiate the reaction, 2.5ml of the iron solution was added to the pH monitored (Corning 442 pH Conductivity Meter, Corning, NY) vigorous stirred, deoxygenated reaction solution, at which point the pH of the solution immediately dropped to 6.5 and was raised to 9.5-10.5 with TMAH within 15 seconds and maintained in this range for 30 minutes. The product was centrifuged at 1500g for 5 minutes, yielding a very black, precipitated centrifugate. The supernatant was removed and the MNPs were resuspended in 1M HNO_3 and centrifuged again. The wash process was repeated an additional 3 times, followed by a

final resuspension in DI water, resulting in a stable ferrofluid which was degassed and aged under argon for 15 days.

Sonochemical Synthesis of Magnetite Nanorods. Magnetite nanorods were synthesized according to (Kumar, Koltypin et al. 2001). 100ml of DI water was deoxygenated by bubbling N_2 for 40 minutes, to which 1g of Iron Acetate, $Fe(CH_2COO)_2$ (Sigma-Aldrich, St. Louis, MO), and 20mg of γ-cyclodextran (Fluka, Seelze, Switzerland) were added and the resulting solution was sealed and transferred into a sealed glovebox under Argon. The solution was then irradiated with a sonochemical probe (Sonics and Materials Model V-750, Ti horn, 20kHz) for 40 minutes at 11% amplitude followed by 1.5 hr at 6% amplitude resulting in a concentrated (due to evaporation) solution with a black precipitate. 15ml of DI water was added to the final product to yield a volume of 28ml. The product was concentrated and the excess reactants were removed by centrifugation for 20 minutes at 3200g in Centricon filters (Millipore, Billerica, MA). The resulting retentate was resuspended in 50ml of DI water.

TEM Analysis. The MNP solutions were dried onto a carbon TEM grid and were observed using a transmission electron microscope (TEM) (JEOL 200CX operated at 180-200 KV).

2.3.2.2 Results

Both syntheses resulted in the formation of a magnetically responsive opaque black precipitate, indicative of magnetite. The physical dimensions of the products were analyzed via TEM analysis, both revealing the formation of nanoparticles. Figure 2-2 shows the resulting micrographs of the MNP products. The parameter controlled coprecipitation method, shown in Figure 2-2(A) yielded roughly spherical particles, larger and more

polydispersed than expected, with a size range between 10nm-22nm, and an average diameter of approximately 15-17nm. These MNPs presumably formed through the chemical reaction:

$$2Fe(NO_3)_3 + FeCl_2 + 8N(CH_3)_4OH \rightarrow Fe_3O_4 + 6N(CH_3)_4NO_3 + 2N(CH_3)_4Cl + 4H_2O \quad (2.3)$$

These particles, having been stabilized by the coordination of nitrate ions (Massart 1982), were stably dispersed in DI water at pH values >8.5.

The sonochemical synthesis, shown in Figure 2-2(B) produced a somewhat more monodisperse solution, but also of larger than anticipated MNPs, with dimensions on the order of 30x80nm to 30x300nm, with the vast majority lying between 30x180nm and 30x220nm. The discrepancy between the previously published results (Kumar, Koltypin et al. 2001) and those shown here is most likely due to the extremely volatile and reactive nature of sonochemical synthesis, which is notorious for its fickle and irreproducible results (Suslick and Price 1999). Nonetheless, it can be assumed that the extreme conditions surrounding cavitation result in the formation of free radicals, through a series of reactions, yielding the products:

$$\begin{aligned} &H_2O))))))H + OH \\ &H + H \rightarrow H_2 \\ &OH + OH \rightarrow H_2O_2 \\ &Fe(CH_3COO)_2 \rightarrow Fe^{2+} + 2(CH_3COO)^- \end{aligned} \quad (2.4)$$

and the resulting, magnetite forming, reaction:

$$3Fe^{2+} + 2H_2O_2 \rightarrow Fe_3O_4 + 2H_2 \quad (2.5)$$

The product was not stable in water and quickly settled to the bottom under the force of gravity. The larger size and magnetic moments resulted in large values of U_M and the subsequent formation of large aggregates, observable with the naked eye.

2.4 Ionic and Steric Surface Coatings for Use in Biomedical Applications

The purpose of the syntheses described thus far has been the generation of highly magnetically responsive MNPs with desirably large remanent and saturation magnetizations. Such particle characteristics are preferred for applications requiring the generation of large magnetic forces, such as cell separation, and those where high M_r values result in better signal characteristics, such as magnetorelaxometry. Minimal considerations for use in biomedical applications, such as stability at neutral pH and millimolar ionic strengths, have not been addressed thus far and are considered here.

As stated previously, there are two methods of ferrofluid stabilization: ionic, through the adsorption or coordination of highly charged species to the surface of the MNPs and steric, through the attachment or coating of the surface with thick layers of extended molecules such as polymers/crosslinked polysaccharides, bulky proteins or silica. Ionic and steric stabilization both act to increase the repulsive forces, U_e and U_s respectively, between the MNPs, making agglomeration energetically unfavorable. Also of importance in the development of particle coatings for biomedical applications is their ability to be modified or functionalized with bioactive molecules for control over specific interactions with biological entities. While many techniques, as described above, have been developed for the stabilization and functionalization of MNP suspensions intended for biomedical applications, two techniques, one of each methodology, were chosen, attempted and are demonstrated here. The first method ionically stabilizes the MNPs via thiolation of the surface with dimercaptosuccinic acid (DMSA), resulting in anionic magnetic nanoparticles (AMNPs) which

are stable in select biological buffers between pH 3 and 11 (Fauconnier, Pons et al. 1997). Additionally, DMSA coatings can intrinsically be functionalized, containing disulfides which can, in principle, be reduced and reacted to biomolecules of interest (Halbreich, Sabolovic et al. 2000). As an example of steric stabilization, the ubiquitously utilized dextran is reacted with and immobilized onto the surface of maghemite MNPs. The resulting ferrofluid is stable or quasi- stable in all biological buffers between pH 4-11. Dextran coated MNPs can also be functionalized with biomolecules through oxidation and amination, as has been extensively demonstrated (Molday and Molday 1984; Weissleder, Lee et al. 1991; Lewin, Carlesso et al. 2000; Josephson, Kircher et al. 2002).

2.4.1 Materials and Methods

Synthesis of AMNPs. Maghemite nanoparticles were synthesized, as previously described above and in (Massart 1982). Two starting solutions were made by adding 5.406 g of $FeCl_3$ (Sigma-Aldrich, St. Louis, MO) to 20ml of deionized (DI) water and, separately, adding 1.988g of $FeCl_2$ (Sigma-Aldrich, St. Louis, MO) to 5ml of a 2N solution of HCl (Sigma-Aldrich, St. Louis, MO). These solutions were then added to 100ml of DI water under vigorous stirring, to which 120ml of a 2M ammonia solution was added and remained under vigorous stirring for 5 minutes, during which, a black precipitate formed, indicating the synthesis of Fe_3O_4. This solution was centrifuged at 900g for 5 minutes, the supernatant was removed and the nanoparticle solution was redispersed in DI water. This solution was centrifuged at 900g for 5 minutes and resuspended in DI water. This washing process was repeated 4 additional times and the centrifugate was finally resuspended in 35 ml of DI water, resulting in an opaque black solution. This solution was heated to 80°C and the MNPs were oxidized to Fe_2O_3 by bubbling oxygen for 2 hours. The mass of resulting maghemite was determined (through drying and weighing) to be 1.68g of Fe_2O_3 in 50ml of DI water. DMSA coating was

performed as previously described (Fauconnier, Pons et al. 1997). Separately, 0.26g of DMSA (Sigma-Aldrich, St. Louis, MO) was added to 313ml of deoxygenated DI water (via 1 hour of nitrogen bubbling) and 205ml of deoxygenated DI water was added to the maghemite solution. These solutions were deoxygenated for an additional 2 hours at room temperature. The maghemite solution was then vigorously stirred while bubbling nitrogen and the pH of both solutions was adjusted to 3.0 with HNO_3 prior to mixing the solutions under vigorous stirring with constant nitrogen bubbling. The reaction was allowed to proceed for 30 minutes and the resulting mixture was spun down at 800g for 5 minutes and resuspended in 200ml of DI water. Under constant stirring, the pH of this solution was adjusted with NaOH to 9.25-9.5 and maintained for 30 minutes before lowering the pH to 7.4 with HCl. The resulting solution was centrifuged at 1000g for 10 minutes to remove any precipitated aggregates and the resulting opaque dark brown supernatant was deoxygenated with nitrogen and stored under nitrogen at 4°C. The final concentration of Fe_2O_3 was adjusted with DI water to 75mM or 150mM Fe concentration.

Synthesis of Dextran Coated Maghemite. Dextran coated maghemite was synthesized through modification of a process previously described in (Palmacci and Josephson 1993). 67.5g of dextran T-10 (Fluka, Switzerland) and 4.734g of $FeCl_3$ (Sigma-Aldrich, St. Louis, MO) was added to 100 ml of DI water. This solution was sterile filtered and deoxygenated by bubbling nitrogen overnight. This solution was put into a sealed 3 neck flask under N_2 with constant stirring. The flask and a solution of ammonium hydroxide (Sigma-Aldrich, St. Louis, MO) were then put on ice. 1.569g of $FeCl_2$ (Sigma-Aldrich, St. Louis, MO) was directly added to the mixture under nitrogen and constant vigorous stirring. To this solution, 5.625ml of ice cold ammonium hydroxide was added dropwise to the mixture, resulting in a greenish suspension, which was slowly heated to 80°C over the course of an hour and maintained at

this temperature for 75 minutes under nitrogen and constant stirring. The resulting, reddish brown slurry was then dialyzed against DI water for a period of 3 days with constant water changes, sterile filtered with a 0.22µm filter to remove larger aggregates and then concentrated with Centricon filters (Millipore, Billerica, MA). The resulting ferrofluid was deoxygenated with nitrogen and stored under nitrogen at 4°C.

TEM Analysis. The MNP solutions were dried onto a carbon TEM grid and were observed using a transmission electron microscope (TEM) (JEOL 200CX operated at 180-200 KV).

2.4.2 Results

The AMNP synthesis procedure resulted in a highly stable magnetically responsive MNP suspension with physical characteristics identical to those shown in Figure 2-1. The reaction procedure is schematically represented and summarized in Figure 2-3. The resulting ferrofluid, while stable in a pH range from 3 to 11, becomes unstable and undergoes heavy aggregation in the presence of phosphates and/or proteins, presumably due to charge interactions and shielding with the highly negative phosphate groups. The solution was stored indefinitely in water at 4°C and remained colloidally stable for >2 years. It should be additionally noted that the 25nm magnetite cubes synthesized in 2.3.1.1 and the large magnetite nanorods synthesized in 2.3.2.1 cannot be stabilized ionically, as shown in Figure 1-4, due to strong interparticle magnetic attractions, viz. high U_m values.

The product of the dextran coated maghemite was also strongly magnetically responsive and, being sterically stabilized, at least marginally stable in all physiological buffers. The marginal stability arose from particle-particle interactions which steadily increased during storage. After several days in storage, a significant proportion of the particles had settled to the bottom of the container under the influence of gravity. Subsequent TEM analysis, shown

in Figure 2-4, revealed the formation of large aggregates, >400nm, of polydisperse dextran MNP complexes. Because the original ferrofluid had previously easily passed through a 0.22 μm filter and now, on subsequent filtration attempts, immediately clogged the filter, it is clear that these aggregates formed post synthesis. The "shelf-life" of this MNP preparation is significantly shorter than the already short shelf life of 4 months of commercially prepared dextran coated ferrofluids. It seems that while this preparation is capable of creating a stable MNP suspension, it is not optimized for extended use; in fact earlier works using similar preparations reported the use of lyophilization for storage (Shen, Weissleder et al. 1993).

2.5 Physicochemical and Magnetorelaxometric Characteristization of Synthesized and Commercially Available Iron Oxide Magnetic Nanoparticles

2.5.1 General Requirements of MNPs for Use in Magnetorelaxometric Assays

For applications as highly particular as magnetorelaxometry, the constraints placed upon MNP characteristics are quite stringent, as compared with most other biomedical applications. In addition to the necessity of ferrofluidic stability in physiological buffers and pH ranges, the magnetic characteristics play a fundamental role in generation of signal in magnetorelaxometric assays. As stated in previous sections, in order for immobilized MNPs to be readily distinguished from those in solution τ_B must be significantly less than τ_N, both of which are dependent on the magnetic particle volume. Additionally, the interparticle magnetic attraction described in (1.10) increases by the square of the magnetic volume and thus, for a given material, MNPs with larger τ_N (and M_r) are also normally increasingly likely to aggregate; in fact MNPs with solid magnetic diameters greater than 20nm that are stable in physiological buffers have yet to be produced. The combination of these constraints gives only a narrow range within which the parameters of the synthesized MNPs must lie,

although there does exist some alternative synthesis strategies capable of producing MNPs with desirable characteristics that will be described herein. Figure 2-5 shows the Brownian and Néel relaxation times, as given by equation (1.4) and (1.13), of magnetite MNPs as a function of particle diameter. As can be seen from this figure, particles of diameter <15nm, where $\tau_N<\tau_B$ are all but immediately excluded for use in magnetorelaxometric assays.

2.5.2 Magnetorelaxometric Screening of a Library of Magnetic Nanoparticles

As the stated objective of this dissertation is the development and optimization of MNPs for magnetorelaxometric assays, it is imperative to begin with MNPs of adequate magnetic characteristics. While it is technically feasible to estimate the magnetic characteristics, such as M_r, M_s and τ_N, of a given nanoparticle from fundamental equations, this normally proves impractical in practice, as these characteristics can be highly affected by many parameters such as the crystal purity, synthesis route, and type of stabilizing coating employed (Goya, Berquo et al. 2003), not to mention the specific requirements of the system itself (e.g., the measurement time). In light of this, it becomes necessary and easier to test MNP preparations manually, using the magnetorelaxometry SQUID sensor. Additional considerations for the use of MNPs in magnetorelaxometric assays include the presence and amount of any particle-particle aggregates, gravitational settling and the nonspecific binding (NSB) characteristics of the particles, all of which produce false signal and can significantly increase the background signal. These values can be easily tested in the SQUID system by taking measurements of the remanent magnetization of the particles in solution. Particles with high M_r values in solution are unsuitable for magnetorelaxometric assays as they undermine the sensitivity of the instrument by producing signal in the absence of specific binding. These characteristics will be more specifically addressed in the results section following the

screening of the magnetic characteristics of a large library of dried MNP preparations given below.

2.5.2.1 Materials and Methods

AMNP and dextran MNP solutions were synthesized as described in Section 2.4.1 Commercially prepared MNP suspensions were obtained from: Quantum Magnetics (QM) (San Diego, CA), Immunicon (Huntingdon Valley, PA), Bangs Labs (Fishers, IN), Micromod (Rostock, Germany), Kisker Biotech (Steinfurt, Germany), ChemiCell (Berlin, Germany), Molecular Probes (Eugene, OR), Dynal (Lake Success, NY), Miltenyi Biotec (Auburn, CA), BD Pharmingen (San Diego, CA), R&D Systems (Minneapolis, MN), StemCell Technologies (Tuckwila, WA) and Ademtech (Pessac, FR), as well as the academic institution, Advanced Materials Research Institute (New Orleans, LA). The MNP suspensions were diluted in phosphate buffered saline to concentrations between $1x10^7$ to $6x10^{13}$ particles per 5 µl, depending upon the stated magnetic material concentration per MNP. 5µl of each diluted particle solution were allowed to dry at the base of a microwell (Greiner Bio-One, Monroe, NC) at 37°C for 2 hours. Each microwell was cut out and sealed before measurement in the SQUID system. The samples were analyzed individually in quadruplicate in the SQUID system, where, after various incubation times, they were briefly magnetized in a 20G field and immediately brought into close proximity to the SQUID sensor via pneumatically controlled actuator, as shown in Figure 1-10. The SQUID sensor recorded the magnetic field strength in picotesla due to the remanent magnetization of each sample.

2.5.2.2 Results

The M_r values for each of the dried MNP samples were obtained and are given in Table 2-1. Each MNP preparation is characterized by the overall particle dimensions, the size of the

magnetic core(s) and the type of stabilizing coating. The data is given in terms of overall remanent signal, signal per 10^9 MNPs, signal per µg of iron, and is sorted by signal per hydrodynamic volume of MNP (including coating) which will yield the greatest number of MNPs per unit area of binding. The colloidal stabilities of the suspensions are also given, as determined by the overall signal of the particles in solution. MNP suspensions with backgrounds <20pT per 5000pT of total possible signal per sample after 1 hour in solution are considered colloidally stable and potentially useful in magnetorelaxometric assays.

Overall, the Molecular Probes 140nm, streptavidin-coated MNPs, whose core MNP is developed and licensed by Immunicon, was determined to be the best suited preparation for magnetorelaxometric assays due to its high signal to volume ratio of 0.064 pT/nm^3, direct functionality (streptavidin coated), and high colloidal stability, with little to no detectable background signal when suspended in a PBS with 1% BSA solution. These properties arise from the [unpublished] proprietary method of particle synthesis, as described in (Liberti and Pino 1997). In brief, magnetite MNPs are synthesized according to Massart's method, yielding, as previously described, a colloidally unstable MNP suspension, due to the formation of magnetically mediated agglomerates within the solution. These agglomerates can apparently be temporarily disrupted by irradiating the sample with an ultrasonic probe and, if disrupted in the presence of a coating agent, such as BSA, the individual MNPs can be coated with the agent before reagglomerating into smaller, colloidally stable aggregates. These aggregates can then be separated according to size through the use of high gradient magnetic separation to form a stable, monodisperse solution of ~90nm MNP aggregates with an additional ~50nm coating of the agent. These MNPs have significantly higher M_r values than other preparations, presumably due to the intimate contact between the subparticles in the core of the MNPs. This intimate contact poses 2 advantages: first it increases the overall magnetization of the parent MNP, through the sum of the individual subparticles, secondly,

it allows for magnetizing interaction of the individual moments of the subparticles and thus extends the Néel relaxation time of the overall particle. It should be additionally noted that the previously observed colloidal instability of the dextran coated MNP solution and the inability of the coprecipitated MNPs and the sonochemically synthesized magnetite nanorods to be readily biofunctionalized immediately precludes them, as prepared, for use in magnetorelaxometric assays. Additionally, the size of the AMNPs in the DMSA stabilized ferrofluid and its instability in the presence of phosphates and proteins also prevents them from use in magnetorelaxometric assays. This does not necessarily prevent them from use in other types of assays, as will be shown in Chapter 5.

2.6 SQUID Calibration and Preliminary Magnetorelaxometric Assays

2.6.1 Calibration of SQUID signal vs. Number of MNPs and Distance from Sensor

As previously illustrated, the SQUID system is capable of detecting the remanent magnetization signal from magnetized immobilized MNPs. However, to yield a useful quantitative assay, this signal should scale, in theory, to the total number of immobilized MNPs, N_I, in the sample. This allows for an easy calculation of the total number of bound species of *any* sample in *any* assay, where the sample is equidistant from the SQUID sensor. As a sample is moved away from the sensor, the magnetic field/induction falls off according to (1.15), while still maintaining its proportionality to N_I. In this section, the signal level is analyzed as a function of the total number of dried/immobilized Molecular Probes 140nm MNPs in the sample and distance from the sensor itself, allowing for direct calibration of the number of bound MNPs at a given distance from the sensor.

2.6.1.1 Materials and Methods

A microtiter plate (Nalgee-Nunc International, Rochester, NY) was thoroughly washed with DI water and 100µl of a 2µg/ml biotinylated BSA solution (Sigma-Aldrich, St. Louis, MO) was added to each well, after which the plate was incubated at 37°C for 90 minutes. The plate was then thoroughly washed 4 times in a PBS/Tween 20 solution (Sigma-Aldrich, St. Louis, MO). After washing, 10µl of 140nm MNPs (Molecular Probes, Eugene, OR) at various concentrations was added to the wells in quadruplicate and allowed to dry at room temperature overnight. The SQUID system was outfitted with a modified sample holder containing a threaded attachment. The distance from the SQUID sensor was varied by rotating the sample holder along the threaded attachment, effectively raising the sample from the SQUID sensor. Each microwell was cut out and sealed before measurement in the SQUID system. The samples were analyzed individually in quadruplicate in the SQUID system, where, after various incubation times, they were briefly magnetized in a 20G field and immediately brought into various proximities to the SQUID sensor via pneumatically controlled actuator, as shown in Figure 1-10. The SQUID sensor recorded the magnetic field strength in picotesla due to the remanent magnetization of each sample.

2.6.1.2 Results

The results of the calibration experiments are plotted in Figure 2-6 and Figure 2-7. Figure 2-6 shows a plot of the magnetic signal in pT as a function of the number of 140nm MNPs immobilized onto the well. Each trace on the plot represents the remanent signal vs. N_I at a different distance from the sensor; the minimum distance is 0.5mm and is set by the distance between the SQUID sensor chip and the measurement window to the outside world. As can be seen from the plot, the chip maintains a largely linear relationship between N_I and the distance to the sensor above the sensitivity threshold of the instrument, near 1-2 pT, with

increasing standard deviations as this threshold is approached. With the experimental conditions and reagents used in this assay, the detection limit for the SQUID system lies in the vicinity of $1x10^4$ to $1x10^5$ MNPs at the closest sample to sensor distance, although values as low as 5000 MNPs have been detected with this instrument with modifications in the microwell geometry (data not shown).

If one plots the signal as a function of distance from the sensor for a set N_I, a plot as shown in Figure 2-7 is obtained. Near the sensor, at distances less than 7mm, the signal level is a complex function, as it can be shown (Berkov and Kotitz 1996) that the flux generated at the sensors for small magnetizing fields can be given by:

$$\Phi_A = N_I \frac{\mu_0 m}{4\pi} \cdot \frac{mB_{mag}}{3k_B T} \cdot g \cdot k_B T \rho(E^*) \ln 10 \qquad (2.6)$$

Where B_{mag} is the magnetizing field (20G), g is a geometric factor dependent upon the magnetic coupling between the sample and the SQUID which is a function of the distance away, the sample size and the sensor geometry, and $\rho(E^*)$ is the anisotropy energy density distribution, evaluated at a mean anisotropy energy E^*. Alternatively, at distances >7mm, the sample behaves as a point dipole whose signal drops roughly according to the cube of the separation distance as shown in the plot and given in (1.15).

2.6.2 Reduction of Nonspecific Binding

The relevance of any quantitative assay is ultimately determined not by the signal generated from a given sample, but the signal generated from a sample as compared to a control or set of controls. The signal generated by the assay reagents and measuring system itself is referred to as the system noise and it is the ratio of the detectable signal of interest to this noise (i.e, S/N) that ultimately determines the sensitivity of the measuring instrument

and the significance of the data. In magnetorelaxometry, SQUID instrumental considerations aside, this noise is generated by undesirable magnetic background signals, most notably from any MNP aggregation which results in larger τ_B, and NSB of the magnetic labels to sample and the sample container, all of which are indistinguishable from specifically bound MNPs. The phenomena responsible for these interactions are largely similar to those responsible for NSB in ELISAs, namely van der Waals, ionic and hydrogen binding. Various chemical schemes have been employed to reduce these interactions and the subsequent NSB associated with them. The primary difference in magnetorelaxometric assays is the potential background signal generated from interactions with the labels themselves. In this section, the use of various blocking agents are attempted and analyzed for their ability to effectively lower the background noise and thus increase the S/N.

2.6.2.1 Materials and Methods

A solution of 1% BSA (Sigma-Aldrich, St. Louis, MO), 5% sucrose (Sigma-Aldrich, St. Louis, MO) and 0.05% sodium azide (Sigma-Aldrich, St. Louis, MO) in 10mM PBS was created. Additionally, solutions yielding final concentrations of 1% polyvinylpyrrolidone (PVP; Sigma-Aldrich, St. Louis, MO) or 1% polyethylene glycol (PEG; Sigma-Aldrich, St. Louis, MO) were made in 10mM PBS or in the BSA sucrose solution. In the first experiment, the BSA, PVP, PEG solutions, including the base BSA-sucrose solution, were dispensed into micotiter wells (Greiner Bio-One, Monroe, NC) and incubated at 37°C for 1 hour. The plates were washed 5 times in PBS-Tween 20 (Sigma-Aldrich, St. Louis, MO) before the experiment. After washing, 15µl of Molecular Probes 140nm streptavidin coated MNPs (SA-MP) at a concentration of $1x10^8$ MNPs/15µl was added to the wells. In a second, separate experiment, premade solutions of Starting Block (Pierce Biotechnology, Rockford, IL) and Super Block (Pierce Biotechnology, Rockford, IL) and the BSA sucrose solution were dispensed into the

micotiter wells and incubated for 5 minutes, before being patted dry with no wash; after which, each microwell was cut out and sealed before measurement in the SQUID system. The samples were analyzed individually in quadruplicate in the SQUID system, where, after various incubation times, they were briefly magnetized in a 20G field and immediately brought into close proximity to the SQUID sensor via pneumatically controlled actuator, as shown in Figure 1-10. The SQUID sensor recorded the magnetic field strength in picotesla due to the remanent magnetization of each sample.

2.6.2.2 Results

The results of the experiments to evaluate the efficacy of various blocking agents are summarized in Figure 2-8. An initial experiment comparing entirely different blocking methodologies, using PVP and PEG, along with mixtures of BSA with the two, were compared with a traditional BSA block, is shown in Figure 2-8(A). As can be seen from the data, the BSA block alone was more successful at preventing the immobilization of MNPs onto the well surface, with only an average 1.35pT background signal at 30 minutes, as compared to 21.2pT and 460pT for the PVP and PEG blocks, respectively. At later timepoints, the BSA block also outperformed the other two, giving a background signal of 64pT as compared to 3723pT and 184pT for PEG and PVP at 1195 minutes. The data indicate that the BSA, protein based, block is much superior to the extended hydrophilic polymer, PEG, and extended semi-hydrophobic polymer, PVP, for the reduction of NSB to the polycarbonate well surface.

In addition to the traditionally "in-house" created protein based blocking agents such as PBS BSA solutions, there exist several proprietary "improved" blocking agents that are commercially available for use. However, when two of these blocking agents, namely Starting Block and Super Block, were compared with a simple BSA block, as shown in Figure 2-8(B),

the BSA block still proved superior at reducing nonspecific binding in both short incubation times (30 minutes) and long incubation times (1148 minutes), giving background signals of only 0.85pT and 1.48pT, respectively. The difference in blocking effectiveness is most apparent at the latter timepoint, where the use Starting Block and Super Block resulted in background signals of 10pT and 4.3pT, respectively. Based upon this data it was concluded that the standard BSA block was equivalent or better than the other methods tested and this block was used for all subsequent magnetorelaxometric assays described in this work.

2.7 Discussion

2.7.1 Summary

In this chapter, the syntheses of iron oxide MNPs with various geometries and physicochemistries were successfully demonstrated. Additionally it was shown that these geometries could be tailored based on control over the synthesis parameters and the synthesis methodology employed. Examples of both ionic and steric stabilization techniques were also demonstrated and evaluated for their effect on the short term and long term colloidal stability of the MNP suspensions under various buffer conditions. The minimal requirements and desirable magnetic characteristics for MNPs intended for use in magnetorelaxometric assays were presented and discussed. It was then reasoned that the determinants of these characteristics were sufficiently complex and nonlinear as to warrant experimental evaluation of a large library of MNP preparations. These preparations were evaluated and ranked based upon their remanent signal per unit volume as measured by the SQUID system. Based on this data and further considerations such as the colloidal stability and functionalizability of the MNP preparations, one preparation was selected as optimal for magnetorelaxometric assays. Once selected, the SQUID system was calibrated and the detected magnetic field was shown

to scale with the number of immobilized MNPs in the sample. The magnetic signal, for samples in proximity to the sensor, was also shown to be a complex function, less sensitive to sample sensor spacing than at larger separations, which behave as a point dipole source, dropping off with the cube of the separation distance. Finally, magnetorelaxometric assay conditions were further optimized through evaluation of various blocking agents aimed at reducing the NSB of the MNPs, and thereby reducing the overall system noise in the SQUID system.

2.7.2 Implications for Magnetorelaxometric Assays

The results of this chapter have significant implications for the use of MNPs in magnetorelaxometric assays and the subsequent work presented in this dissertation. While a specific MNP preparation was chosen as optimal for use in these assays through the screening of a large library of MNPs it was also shown that the magnetic characteristics of MNPs, even of similar magnetic, chemical and physical characteristics, are highly variable and dependent upon the synthesis chemistry, technique and conditions employed. This highlights the inherent technical difficulty in determining and developing specific MNP synthesis strategies for highly specialized magnetic applications such as magnetorelaxometry.

The further demonstration of a linear relationship between the sensed magnetic field, B, and N_I acts to validate the use of the SQUID system for quantitative magnetorelaxometric assays. It additionally allows for, background signal aside, precise quantification of N_I in any sample/assay preparation. The magnitude of the sensed magnetic field was also shown to be much less sensitive to sample sensor spacing when in proximity to the sensor chip itself than at larger distances. This further validates the employment of micotiter wells of reasonable dimensions for use in magnetorelaxometric assays, as the sensitivity of the instrument will not be significantly undermined by moderate changes in the volume and dimensions of the

sample. Finally, the demonstration of blocking agents that can reduce the background noise near the sensitivity limit of the system reinforces the choice of specific MNP preparations for use in magnetorelaxometric assays.

2.7.3 Potential for Improvements in Magnetic Nanoparticle Preparations and SQUID Instrumentation for Magnetorelaxometric Assays

While the most suitable MNP preparation has been chosen and the conditions for its use in magnetorelaxometric assays has been further optimized, significant improvements to both the MNP magnetic characteristics and instrumentation are undoubtedly feasible. To begin with, as discussed in Chapter 1, the values of M_r and M_s are highly dependent upon the volume of the magnetic core of the MNPs. While not exhaustive, the colloidally stable dispersions presented in this chapter all consisted of MNPs with magnetic cores or subparticles <20nm, which is nominally below the size of 26nm required for transition of magnetite to extended ferrimagnetic behaviors such as significantly larger values of τ_N. Despite this, it was shown that through innovative synthesis methods that these smaller cores could be brought into close proximity and coated to form stable aggregates, somewhat mimicking the magnetic response of a larger solid magnetic core with higher M_r and τ_N, but at the cost of significantly greater MNP dimensions (and thus fewer bound MNPs per unit binding area). An ideal MNP preparation, however, would incorporate a solid magnetic core of dimensions near or above the 26nm limit thereby yielding higher values of both M_r and τ_N *without* sacrificing loss in binding area upon immobilization due to large hydrodynamic radii. As previously mentioned, however, creating a stable aqueous dispersion of particles on this scale has not only yet to be demonstrated, it is extremely technically challenging due to the huge interparticle magnetic attractions present at this size scale. In the meantime, there are specific improvements that can be made in this or any SQUID detection system intended for

magnetorelaxometry. Most notably, the quicker the sample can be brought into proximity with the sensor following magnetization, the less Néel relaxation that will have occurred and the larger the magnetizing field, the larger the moment that will be induced in the sample, both resulting in a greater value of *B* sensed by the SQUID system. These improvements also pose some technical difficulties, however, as the sample holder and instrumentation, while paramagnetic or diamagnetic in nature, still undergo magnetization and produce a background signal, albeit at a much lower level and for a much shorter time period. Optimization of these parameters must be determined for each system individually, as these characteristics are dependent on many factors such as the instrument design, material makeup and geometry.

2.7.4 Conclusions

The current SQUID instrument setup has been calibrated and evaluated for its use in magnetorelaxometric assays. The most suitable MNP preparation, based on colloidal stability, chemical functionality and magnetic characteristics was chosen by manually screening a large library of commercially prepared MNPs. Using a standard magnetorelaxometric setup, a detection threshold of $<10^4$-10^5 immobilized MNPs was demonstrated. Additionally it was shown that, through the use of appropriate blocking agents, the background signal for assays at <1hr. could be reduced to near the SQUID sensitivity limit. These calibrations and optimizations establish the basis for the magnetorelaxometric assays developed in subsequent chapters.

2.8 Acknowledgements

The MNP synthesis work was funded by the NDSEG fellowship. The incalculable previous hard work that went into the design and creation of the High T_c SQUID system by Mark

DiIorio, Kai Yang and the others who I am not aware of, is greatly appreciated and makes all of this work feasible. Additional thanks go to Kai Yang for his work on the measurement of these samples and to both Kai and Mark DiIorio for their help in data analysis.

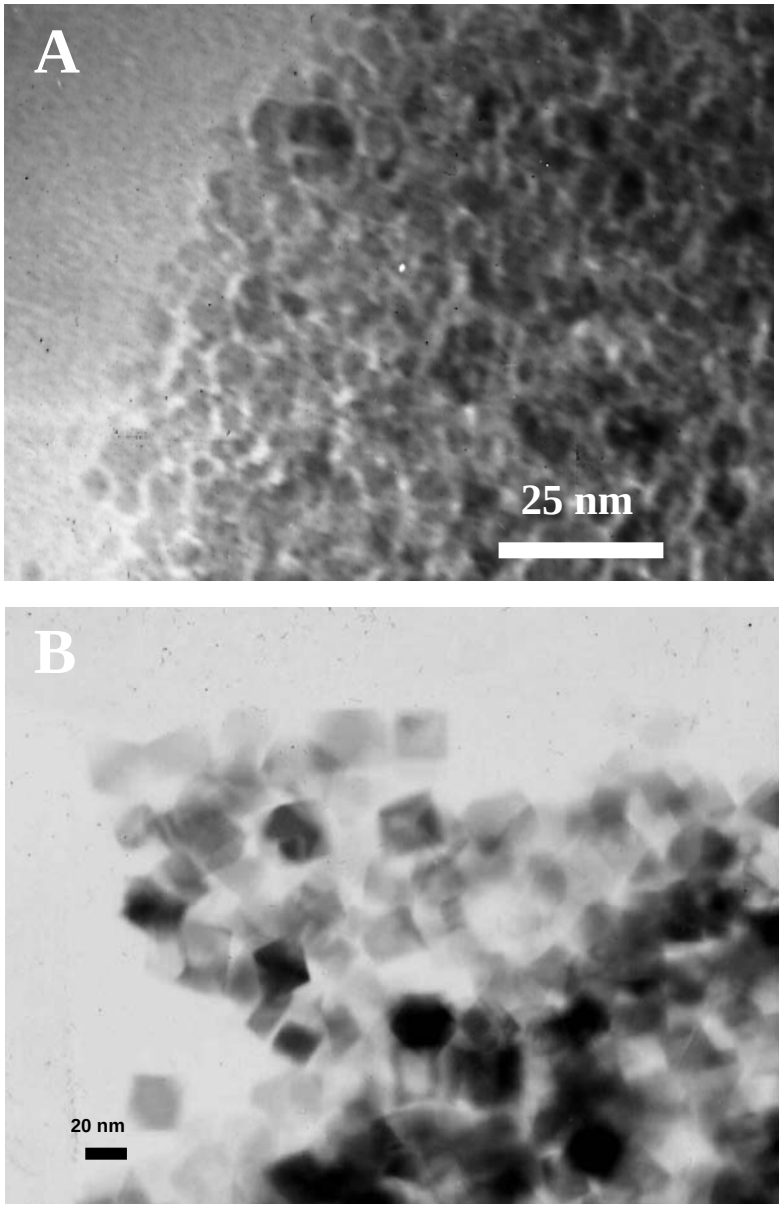

Figure 2-1. Transmission electron micrographs of magnetite nanoparticles created by (A) aging of stoichiometric mixtures of ferrous and ferric hydroxide gels in the presence of ammonia and (B) oxidation of a ferrous hydroxide solution by potassium nitrate.

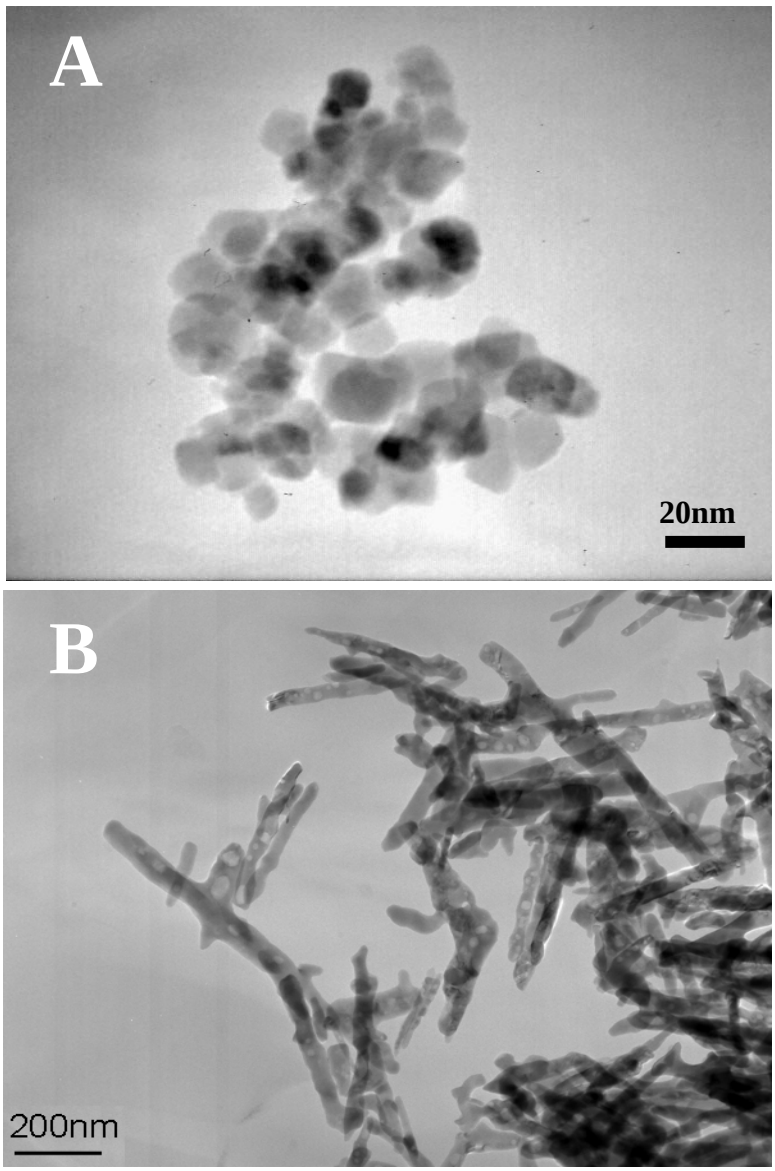

Figure 2-2. Geometric modulation of iron oxide nanoparticles. (A) Size modulation by variance of reaction conditions in stoichiometric aging. Larger nanoparticles are produced through the addition of a noncomplexing salt, in this case tetramethylammonium nitrate and lower reaction pH (~9). (B) Synthesis of specific MNP geometries through alternative synthesis methods. Magnetite nanorods are synthesized through sonochemical irradiation of an aqueous solution of iron acetate in the presence of γ-cyclodextran.

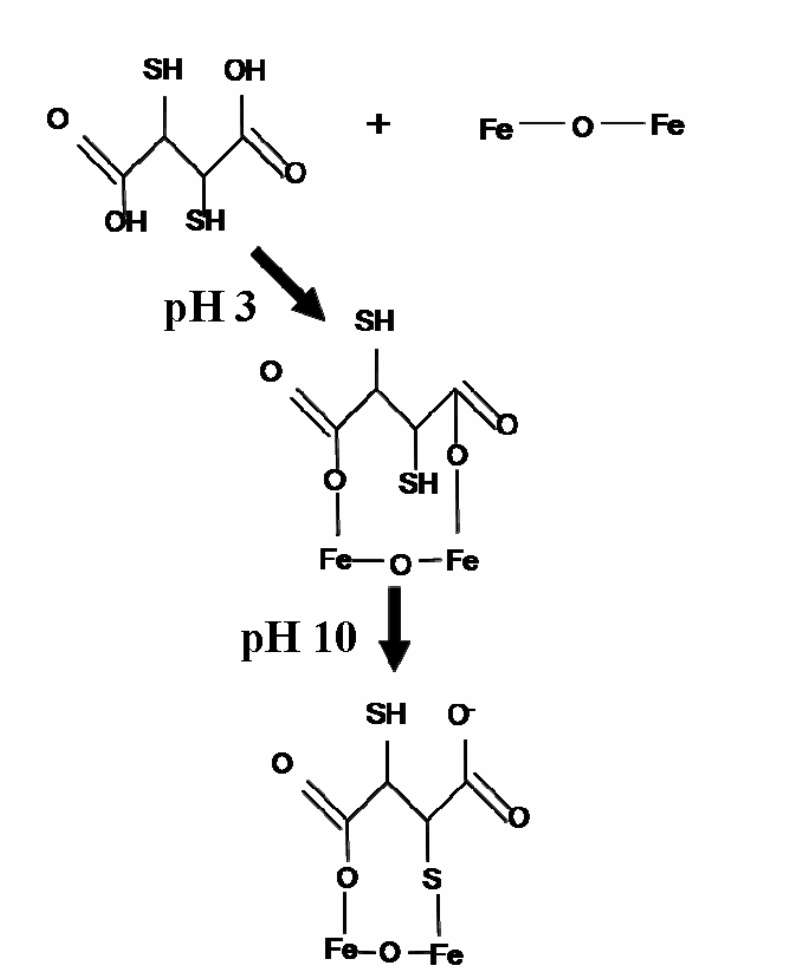

Figure 2-3. Ionic coordination and stabilization of iron oxide nanoparticles. Dimercaptosuccinic acid is added and coordinated to the surface of an iron oxide MNP via iron carboxylic acid bonds at pH 3. Subsequently raising the pH to 10 preferentially creates bonds between the thiol and iron groups and releases the carboxylic acid groups. The MNPs remain stable in solution due to ionic repulsion between the negatively charged carboxylic acid groups.

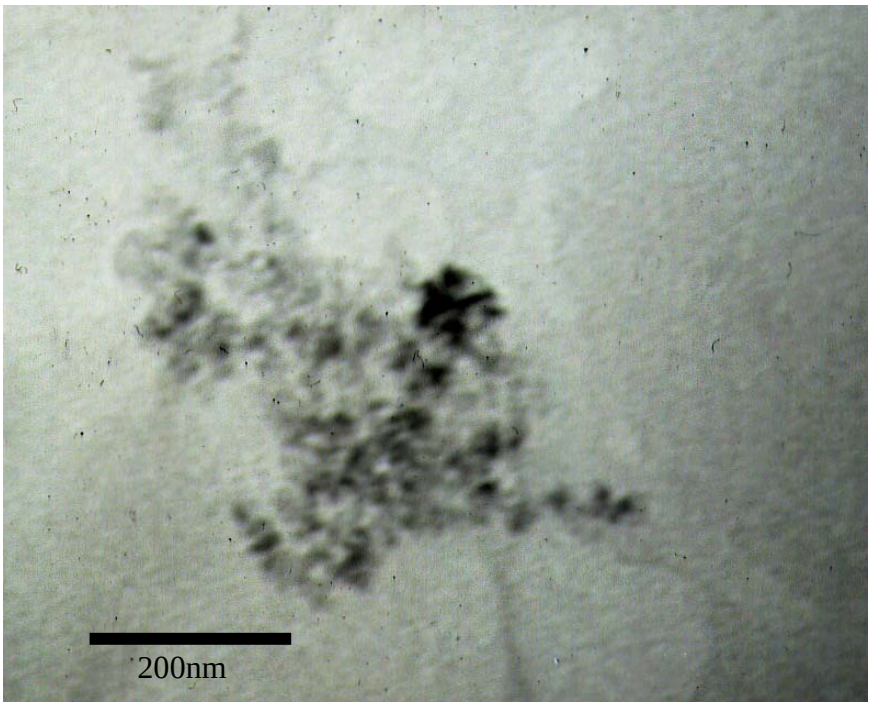

Figure 2-4. Electron micrograph of sterically stabilized iron oxide nanoparticles Sterically stabilized iron oxide nanoparticles. Transmission electron micrograph of iron oxide synthesized in the presence of and coated with dextran. Image shows aggregates of the dextran MNP complexes in excess of 400nm.

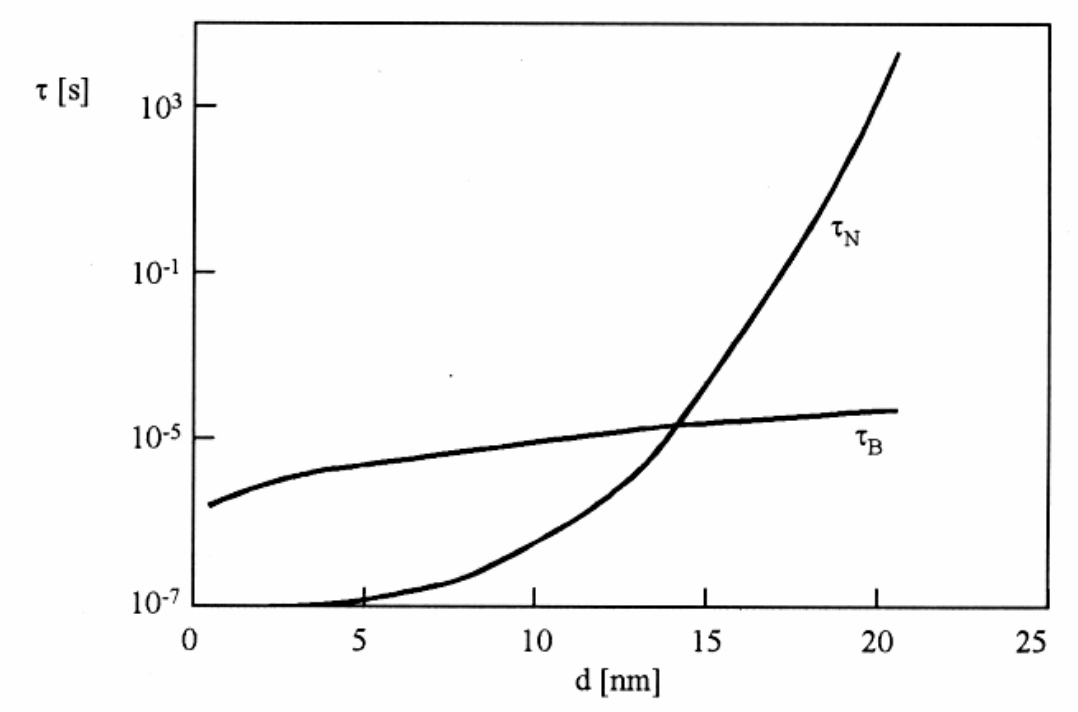

Figure 2-5. Relationship between Brown and Néel relaxation time constants, τ_B and τ_N, versus nanoparticle diameter for magnetite. To be useful for liquid phase magnetorelaxometry, τ_N should be significantly greater than τ_B. Taken from (Odenbach 2002).

Table 2-1. Magnetorelaxometric evaluation of various magnetic nanoparticles, sorted by remanent magnetic signal (pT) per unit MNP volume. MNPs were dried into wells, magnetized and their M_r values were evaluated in the SQUID system. The MNP solutions were additionally evaluated for colloidal stability in aqueous phosphate buffer, if possible. MNPs used in Chapters 3-5 are highlighted in yellow; MNPs synthesized in this chapter are in bold.

Manufacturer	Hydrodynamic particle size (nm)	Core size (nm)	Crystal size (nm)	Coating	# of particles	Remanent Signal (pT)	Signal(pT) normalized to 1E9	signal/vol (pT/nm^3)	signal / ug(Fe)	Colloidally Stable?	notes
QM	50	35	12	protein	3.0E+08	4140	13800.0	0.211	117537	N	Unstable
Immunicon	100	80		BSA	1.0E+09	59600	59600.0	0.114	42509	Y	Limited quantity; exploratory synthesis, unfunctionalized
AMRI	12	12			1.05E+12	73118	69.6	0.077	14716	N/A	Uncoated, in organic solvent
QM WH250	250	230			4.0E+06	2374	601012.7	0.073	18038	N	Unstable
Micromod (2280113G)	250	220	15-25	streptavidin	1.0E+08	57600	576000.0	0.070	19754	N	Unstable
Molecular Probes	140	108		streptavidin	6.5E+08	59436.0	91440.0	0.064	26507	Y	Highly Consistent
Micromod (0080209G)	250	220	15-25	streptavidin	1.0E+08	51600	516000.0	0.063	17696	N	Unstable
Chemicell (Mn ferrite)	150	90		poly-saccharide	1.0E+08	10900	109000.0	0.062	54601	N/A	Exploratory synthesis, did not test stability
Micromod (0070209G) Germany	130	116	15-25	streptavidin	1.0E+09	63701.3	63701.3	0.055	14903	N	Unstable
AMRI (magnetite)		8		ligand	1.00E+12	12961	13.0	0.048	9244	N/A	In organic solvent
QM P250	250	230			4.0E+06	1506	381265.8	0.047	11443	N	Unstable
QM 50	50	40		dextran	1.0E+09	2914	2914.0	0.045	16627	Y/N	Short shelf life
R&D Systems	140	105		streptavidin	1.65E+07	945	57272.7	0.040	18067	Y	*Same structure* as Molecular Probes
Immunicon conjugated (anti-dig) lot#2641	140	108		streptavidin	1.0E+08	5080	50800.0	0.035	14726	Y	Same structure as Molecular Probes
StemCell EasySep	150	110		dextran	1.00E+08	6115	61150.0	0.035	16777	Y	Medium signal, stable in blood, unfunctionalized
Kisker (Germany)	PMC-130	116	15-25	streptavidin	1.0E+09	38606.1	38606.1	0.034	9032	N/A	Short shelf life
Immunicon	140	108		BSA	2.70E+07	1215	45000.0	0.031	13045	Y	Base Molecular Probes MNP
Micromod (1820109T) Germany	130	116	15-25	plain	1.0E+09	35444.5	35444.5	0.031	8292	N/A	Unfunctionalized
R&D Systems	140	105		streptavidin	1.65E+07	681	41272.7	0.029	13020	Y	Same structure as Molecular Probes
Chemicell (Germany)	150	80-100		poly-saccharide	1.0E+09	48300	48300.0	0.027	24	Y	Unfunctionalized
Chemicell (MAG-SA 100 Fe3O4)	100	65		streptavidin	1.00E+09	1.38E+04	13846.0	0.026	18411	N	Unstable
QM 150 x-link	150	130		anti-h HLA-I	1.00E+07	360	36000.0	0.020	5984	N	Unstable
Chemicell (MAG-SA 150 Fe3O4)	150	100		streptavidin	1.00E+09	3.29E+04	32866.0	0.019	12002	N	Unstable
Chemicell (Co ferrite)	150	90		poly-saccharide	1.0E+08	3150	31500.0	0.018	15779	N/A	Exploratory synthesis, did not test stability
Kisker (Harvard)	250	210		dextran	2.60E+08	35258	135607.7	0.017	5347	N	Unfunctionalized
QM 150	150	130		plain	3.0E+07	862	28733.3	0.016	4776	N/A	Short shelf life, unfunctionalized
Micromod (1260109G)	250	220	15-25	dextran	1.0E+08	12942.8	129428.0	0.016	4439	N/A	Unstable
Chemicell (MAG-CMX 150 Fe2O3)	150	100		dextran	1.00E+08	2.72E+03	27220.0	0.015	9940	N	Unstable
BD Pharmingen	170 - 300	200		CD19	5.00E+06	547	109400.0	0.013	4994	N	Unstable
Chemicell (MAG-CMX 150 Fe3O4)	150	100		plain	1.00E+09	2.13E+04	21275.0	0.012	7769	N	Large background
QM 250	250	230		dextran	9.0E+06	885	98333.3	0.012	2951	N	Unstable
BD Pharmingen	170 - 300	200		CD19	1.00E+08	9392	93920.0	0.011	4287	Y	Large Backgournd in solution
Chemicell fluidMAG-BC-SA	100	65		streptavidin	5.00E+09	27444	5488.8	0.010	7299	Y	Lower signal than similar particles
BD Pharmingen	100 - 450	300		dextran	1.0E+07	2199	219900.0	0.010	2974	Y	medium signal, stable
Kisker	250	210		streptavidin	1.05E+08	7962	75828.6	0.009	2990	N	Unstable
Chemicell fluidMAG-BC-SA	100	65		streptavidin	5.00E+07	237	4740.0	0.009	6303	Y	Batch to batch variation
Kisker	130	100		amine-dextran	1.10E+09	11441	10400.9	0.009	3798	N	Unstable
Micromod Nanomag-D 250	250	200		streptavidin	1.00E+08	6528	65280.0	0.008	2980	N	Unstable
Micromod Nanomag-silica 250	250	200		silica	1.00E+08	6215	62150.0	0.008	2837	N	Unstable
Micromod Nanomag-BNF	100	65		PEG-COOH	1.00E+09	3681	3681.0	0.007	4895	N	Unstable
Micromod Nanomag-BNF	100	65		Nh2	1.00E+09	3133	3133.0	0.006	4166	N	Unstable
Liquids Research	12	9		polyethylenimine	1.00E+11	496	5.0	0.005	2485	Y	Unfuntionalized
Micromod Nanomag-D 130	130	95		streptavidin	1.00E+08	604	6040.0	0.005	2573	N/A	Lower signal than similar particles
Chemicell (lot#011/03)	150	90		streptavidin	1.0E+08	919	9190.0	0.005	4603	N	Unstable
QM	50	50		protein	1.0E+09	338	338.0	0.005	987	N	Unstable
Micromod Nanomag-D 130	130	95		PEG-COOH	1.00E+08	594	5940.0	0.005	2530	N/A	Lower signal than similar particles
Chemicell beadMAG-SA	100	65		streptavidin	5.00E+09	10339	2067.8	0.004	2750	N	Unstable
Micromod Nanomag-D 130	130	95		PEG-NH2	1.00E+08	347	3470.0	0.003	1478	N/A	low signal
Chemicell (MAG-CMX 100 Fe3O4))	100	65		dextran	1.00E+10	13825	1382.5	0.003	1838	N	Unstable
QM SA150	150	130		anti-h HLA-I	1.7E+08	653	3841.2	0.002	638	N	Unstable
AMRI (permalloy)	10	10		Au	5.00E+12	5623	1.1	0.002	411	N/A	In organic solvent
QM 150	150	130		anti-h HLA-I	9.0E+07	337	3744.4	0.002	622	N	Unstable
Chemicell (MAG-CMX 100 Fe2O3)	100	65		dextran	1.00E+08	1.02E+02	1020.0	0.002	1356	N	Unstable
QM 150	150	110		dextran	1.0E+07	26	2600.0	0.001	713	N	Unstable
QM	50 - 100	50		BSA	1.0E+09	220	220.0	0.001	643	N	Unstable

Table 2-1. (cont…)

AMRI	12	12		silica	1.0E+11	69.4	0.7	0.001	147	N/A	Lower signal than similar particles
Micromod (0040209G)	100	52	5-15	streptavidin	1.0E+09	294	294.0	0.001	764	N	Unstable
Chemicell (MAG-PAS 100	100	65		carboxydextran	1.00E+09	2.92E+02	292.0	0.001	388	N	Unstable
StemCell EasySep	250	120		dextran	3.50E+08	1124	3211.4	0.000	679	Y	Low signal
Miltenyi	50	30	10	streptavidin	1.00E+11	1502	15.0	0.000	203	Y	Small size, very stable, highly consistent
AMNP	**6-14**	**8**	**8**	**DMSA**	**1.00E+12**	**43**	**0.0**	**0.000**	**31**	**Y/N**	**Synthesized in house; not stable with protein or phosphates**
QM	50	35	12	streptavidin	8.00E+09	80.2	10.0	0.000	85	N	Unstable
QM	50	35	12	protein	1.0E+09	9.8	9.8	0.000	83	N/A	Lower signal than similar particles
Merck (France)	203	133		streptavidin	1.0E+09	471	471.0	0.000	73	N	Unstable
Merck (France)	410	210		polystyrene	1.0E+09	3170	3170.0	0.000	125	N	Unstable
Bangs Lab	350	190	1-20	polystyrene	1.0E+09	1516.6	1516.6	0.000	81		Low signal
Dextran-Maghemite	**100-400**	**100-400**	**10**	**Dextran**	**4.60E+09**	**4071**	**885.0**	**0.000**	**12**	**Y/N**	**Synthesized in house; very short shelf life**
Bangs Lab	350	190	1-20	plain	1.0E+08	119.8	1198.0	0.000	64	Y	Low signal
Ademtech Bio	213	150		streptavidin	1.00E+08	22.4	224.0	0.000	24	Y	Low signal
Kisker	50	35		dextran	2.00E+11	230	1.2	0.000	10	Y	Low signal
Stemcell StemSep	90	70		dextran	1.00E+09	6	6.0	0.000	6	N/A	Low signal
AMRI (permalloy)	10	10		Au	5.00E+12	34	0.0	0.000	2	Y	Low signal
Micromod (2100109R)	100	52	5-15	plain	1.0E+09	6.2	6.2	0.000	16	Y	Low signal
Chemicell (Germany)	50	15	10-20	carboxy-dextran	1.0E+10	6.9	0.7	0.000	75	Y	Low signal
Micromod Nanomag-D 100	100	65		NH2	1.00E+09	2.6	2.6	0.000	3	N	Low signal
AMRI (permalloy)	10	10		Au	5.00E+12	13	0.0	0.000	1	N/A	Low signal
Micromod Nanomag-D 100	100	65		streptavidin	1.00E+09	1.6	1.6	0.000	2	N	Low signal
Kisker (Germany)	100	52	5-15	streptavidin	1.0E+10	3.8	0.4	0.000	1	Y	Low signal

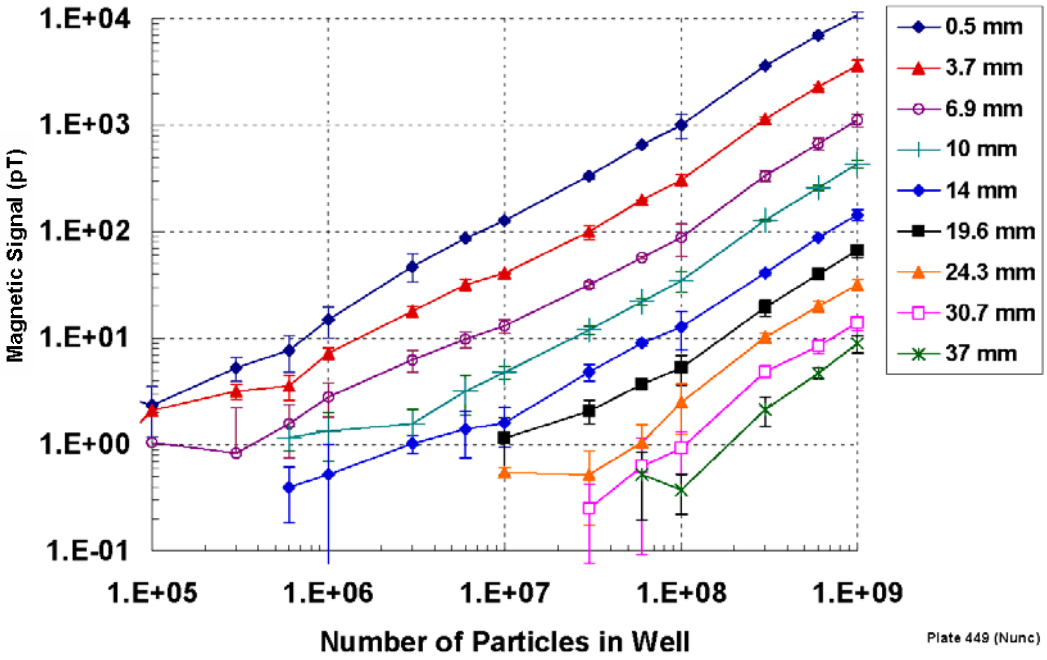

Figure 2-6. SQUID system measured magnetic signal in picotesla at various sample to sensor spacings as a function of number of 140nm MNPs (Molecular Probes) immobilized onto a microtiter well bottom.

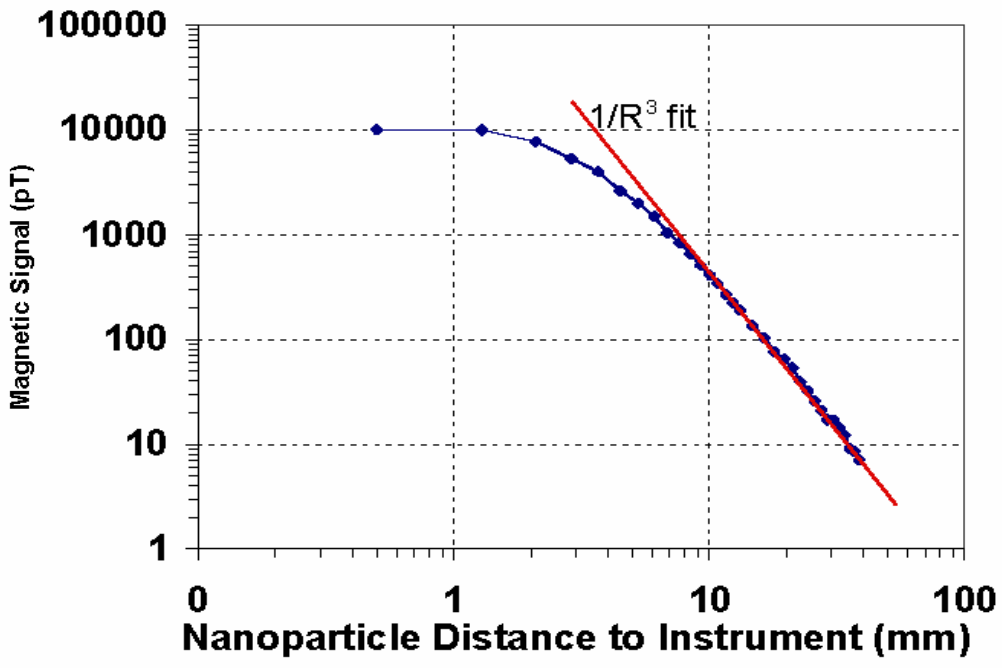

Figure 2-7. SQUID system measured magnetic signal as a function of distance from the SQUID sensor for 10^9 140nm Molecular Probes MNPs.

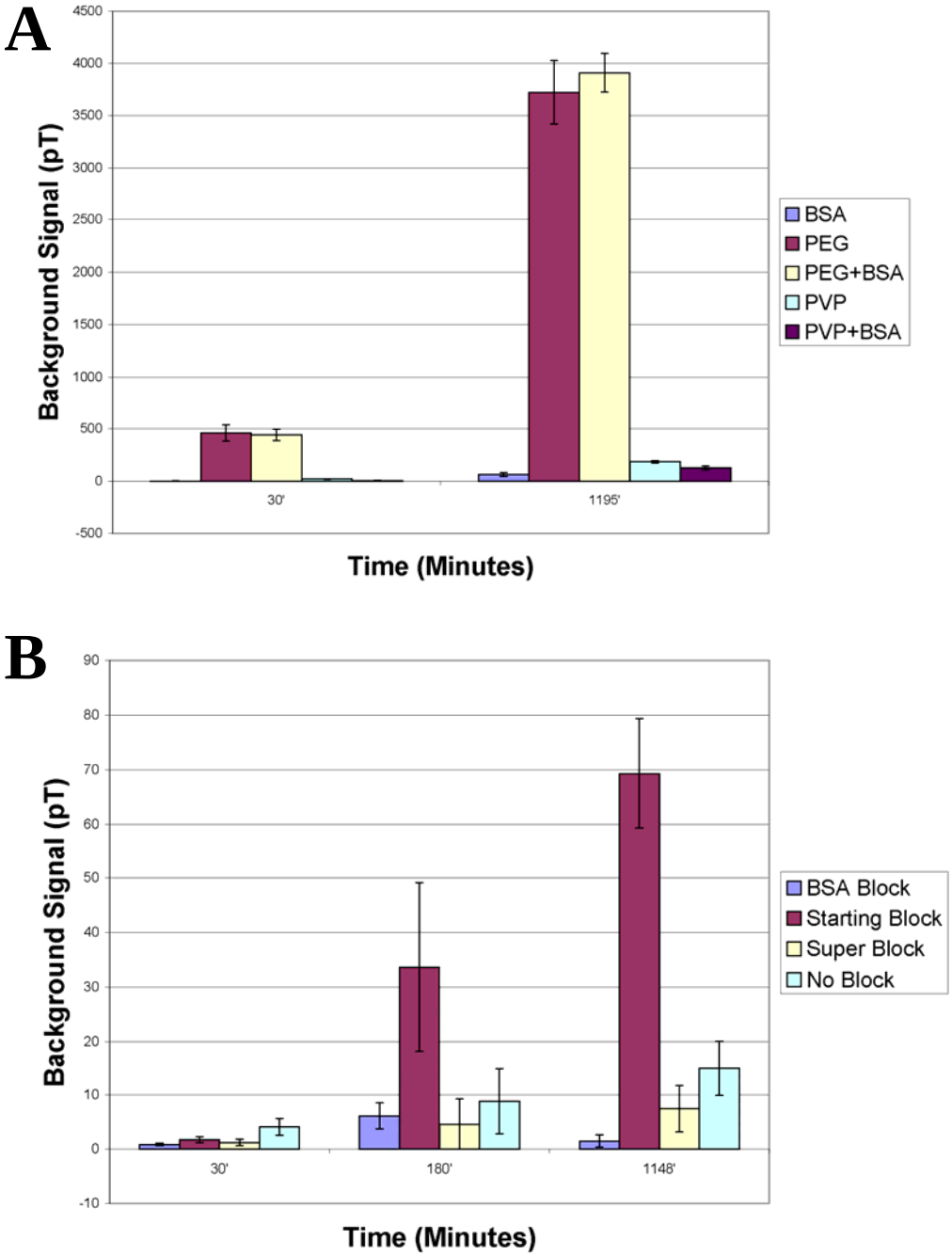

Figure 2-8. Comparison of various blocking agents, as a function of background signal/nonspecific immobilization of MNPs versus time in a micotiter well. (A) Comparison between different blocking methodologies: protein Based (BSA), hydrophilic Spacer based (PEG) and semi-hydrophobic spacer based (PVP). (B) Comparison between various protein based blocking agents: in house BSA block versus commercially prepared blocks "Starting Block" and "Super Block." In all cases, the in-house prepared protein based BSA block performs as well or better than the other blocks.

CHAPTER 3

IN VITRO SEPSIS DIAGNOSTICS USING MAGNETORELAXOMETRY

3.1 Abstract

Rapid and sensitive diagnosis is critical to the effective treatment of infectious diseases and can significantly increase the number of positive outcomes in many aggressive, life threatening illnesses. The primary goal of this chapter is the demonstration of a rapid magnetorelaxometric assay for *in vitro* diagnostics, namely sepsis diagnostics. Starting in physiological buffer, human serum or human blood, a pathogen of interest, *Escherichia coli* O157:H7, is specifically labeled with magnetic nanoparticles and detected using SQUID magnetometry using *S. aureus* and *E. coli* O138 as negative controls. The processes of biotinylation and conjugation of anti-*E. coli* O157:H7 antibodies to streptavidin coated magnetic nanoparticles are developed and optimized, resulting in a novel conjugation method and the development of a true mix and measure assay for sepsis diagnostics. The clinical sensitivity and specificity of the assay is then demonstrated with *E. coli* O138 as a negative control. A total assay time, including preparation, of less than 45 minutes in PBS is also demonstrated. Such an assay paradigm is readily amenable to many other clinically and scientifically useful detection assays and providaes several key advantages over current methodologies.

3.2 Introduction

The rapid, sensitive and specific detection of cells in a heterogeneous population or matrix is of vital interest to many biomedical applications. Methods of rapid cell detection are particularly important in the area of diagnostic assays, where they are critical to the effective treatment of infectious diseases and can significantly increase the proportion of positive outcomes in many aggressive, life threatening illnesses including sepsis/septicemia. Despite these considerations, clinical sepsis diagnosis typically requires several days to weeks before an identification of a given bacterial pathogen can be achieved. Furthermore, current methodologies are often inaccurate, resulting in inappropriate antimicrobial treatment in 25% of sepsis cases in the U.S (Harbarth, Garbino et al. 2003). These issues are responsible for making sepsis the second leading cause of death in non-coronary ICUs, the 10th leading cause of death overall in the U.S. and the number one cause of death in neonatal intensive care units for low birth-weight children (NIH 2004). Sepsis mortality rates are estimated to be 18-29% and sepsis results in annual health care costs in excess of $17 billion. Autopsies have revealed that failure to accurately diagnose and provide efficient and specific antimicrobial therapies is the most common avoidable error in sepsis mortalities (Hotchkiss and Karl 2003).

Most clinical microbiological diagnostics are performed through culture of the etiologic agent using appropriate substrates and analysis of the resulting amplified bacteria. This process, while typically considered the "gold standard" of microbial analysis normally requires days or weeks to complete and can often be inaccurate due to sample contamination. This often results, not only in significant delays in treatment, but also in suboptimal treatments with reduced efficacy, unnecessary side effects or even death. While there are *no* adequately rapid and sensitive methods for sepsis diagnostics currently being clinically utilized, these issues have prompted the proposal and demonstration of several novel methods of bacterial pathogen detection. One promising method of bacterial detection and

identification is the use of polymerase chain reaction (PCR). PCR involves the amplification and identification of bacterial DNA from a clinical sample and is capable of detecting down to a few copies of DNA. This technique, however, is tedious, time consuming, normally in excess of 24 hours, and requires extremely pure samples and highly trained personnel (Malins, Fielden et al. 2004). Another proposed technique for sepsis diagnostics is flow cytometry, the detection of specifically fluorescently labeled cells by their passage in a fluid and subsequent detection of their emission of light upon excitation. Normally used for the detection and enumeration of eukaryotic cells, several problems, however, exist in its application to prokaryotes. In particular, the smaller size and lower DNA content (~1000 fold less than eukaryotes) of bacteria, both of which can significantly vary based on growth conditions, makes them particularly difficult to analyze with this method (Ivnitski, Abdel-Hamid et al. 1999). Traditional ELISA techniques have also been applied to the area of sepsis diagnostics, but suffer from the need for labor and time intensive preenrichment steps, as well as the typical sample prep and washing steps required in traditional ELISAs (Ivnitski, Abdel-Hamid et al. 1999). Other techniques aimed at quantifying the host response through detection of various biomarkers, such as tumor necrosis factor α (TNF-α), interleukin-6 (IL-6), IL-1 receptor antagonist (IL-1ra), IL-8, C-reactive protein and procalcitonin have been investigated, but have all proven to be too nonspecific and insensitive to be considered for clinical use thus far (Carrigan, Scott et al. 2004)

Several biosensor based approaches to bacterial detection have also been recently developed, including: impedimetric (Suehiro, Hamada et al. 2003), amperometric (Shah and Wilkins 2003), piezoelectric (Vaughan, Carter et al. 2003; Su and Li 2004), acoustic (Deng, Bao et al. 1996), optical (Schneider, Edwards et al. 1997; Ferreira, Werneck et al. 2001; Horvath, Pedersen et al. 2003) including bioconjugated fluorescent nanoparticles (Zhao, Hilliard et al. 2004), surface plasmon resonance (Bokken, Corbee et al. 2003), and bioluminescence (Hobson,

Tothill et al. 1996). A detailed analysis of these techniques, many of which are described and critiqued by Ivnitski, et. al. (Ivnitski, Abdel-Hamid et al. 1999), is beyond the current scope. Table 3-1 lists some of the commercially produced devices intended for the identification of bacteria. In general, however, these and other biosensor based methodologies suffer from one or more of several key issues: insensitivity (amperometric, piezoelectric, acoustic, surface plasmon resonance), extended prep and/or measurement times (PCR, fluorescent nanoparticles, bioluminescence), interference from other biochemicals and biological entities (bioluminescence, impedimetric, amperometric, piezoelectric, acoustic, optical) and lack of physical robustness (piezoelectric, acoustic).

Of particular note to the current work is the recent introduction of the idea of utilizing magnetorelaxometry for the detection of bacteria (Grossman, Myers et al. 2004). While directly comparable to the techniques proposed in this chapter, this preliminary demonstration is far from being clinically useful. In particular, the authors cite a minimum detection limit of over $5x10^6$ bacteria in a 20µl sample volume, corresponding to a drastically unrealistic $2.8x10^8$ bacteria/ml. Additionally, the manuscript failed to demonstrate the detection of bacteria in a clinically relevant setting, using only PBS instead of blood or serum as a suspension buffer. Nonetheless, this proof of concept research demonstrates the potential utility of magnetorelaxometry for sepsis diagnostics.

The previous two chapters have outlined the principles and provided the fundamental basis for SQUID based magnetorelaxometric assays. In this chapter those principles are applied to the development of a biomedical assay for real-world clinical applications and sepsis diagnostics in particular. *Escherichia coli* (*E. coli)* O157:H7 is an enterohemorrhagic pathogen which is responsible for one of the most dangerous foodborne illnesses (Pickering, Obrig et al. 1994; Nataro and Kaper 1998; Phillips 1999). Upon infection of an individual, *E. coli* O157:H7 releases potent toxins into the host organism causing severe damage to the lining

of the intestine and typically resulting in hemorrhagic colitis and hemolytic-uremic syndrome, occasionally leading to death, particularly in children and the elderly (Pickering, Obrig et al. 1994). These issues have led to many attempts of late toward methods of detection and identification of this pathogen in particular (Phillips 1999; Su and Li 2004; Zhao, Hilliard et al. 2004). These efforts have been hampered, however, by the common drawbacks previously described and thus there is a continued and pressing need for the rapid and *ultra*sensitive detection of *E. coli* O157:H7, particularly in clinical specimens (NIH 2004).

In this chapter a rapid, highly sensitive antibody based magnetorelaxometric assay for the detection of *E. coli* O157:H7 in physiological buffer, human serum and human blood is developed and demonstrated. The assay, based upon the previously delineated principles of magnetorelaxometry, requires no separation of unbound labels from the bacteria prior to measurement in the SQUID system. The unique fundamentals of magnetorelaxometry allow for the detection of cells in suspension in a manner similar to the solid phase, ELISA type assays previously described in Section 1.3.4. In this case, however, the "solid support" is not the microtiter well surface, but the surface of the cell itself. As shown in (1.13), the Brownian rotation/relaxation time constant, τ_B, of an object in solution is directly proportional to the volume of the object. Thus a cell, in this case a bacterium, such as *E. coli* of dimensions near 1-2μm will rotate almost 1000 times slower (~10^6 times slower for mammalian cells) than a ~140nm unbound MNP, effectively resulting in immobilization of the MNPs attached to the bacterium at the preset measurement time, τ_M, of the SQUID system (3 seconds) which lies above the τ_B of the MNP (0.95 milliseconds for a 140nm sphere) and the right near the τ_B of the cell (2.76 seconds for the long axis of a tablet shaped *E. coli* with dimensions 0.8μm x 2μm). Figure 3-1 shows a schematic depicting a hypothetical suspended cell magnetorelaxometric assay. Similar to the solid phase assay described in Chapter One, the detection antibody and SA MP MNPs are mixed with the antigen, only this time it is immobilized as a surface antigen

on the cell instead of to an adsorbed capture antibody. After a brief magnetizing field, the sample is brought into proximity of the SQUID sensor for measurement, during which time the unbound MNPs randomize in solution, producing no net magnetic moment. However, the MNPs that are bound to the cells through the detection antibodies remain "immobilized" before detection and thus produce a net magnetic moment equal to the sum of the moments of the bound MNPs, which is directly proportional to the total number of cells in the solution.

After a pseudo homogeneous version of the suspended cell magnetorelaxometric assay is initially developed, the conjugation and assay methods are optimized and developed to produce a true homogeneous, mix and measure assay, with a total measurement time near 10 minutes and total assay time less than 45 minutes. The linearity, clinical sensitivity and specificity of the assay are also demonstrated. The implications of and potential improvements on the assay are then discussed.

3.3 **Materials and Methods**

3.3.1 Microbiological Cell Culture

Bacterial strains of *Escherichia coli* O157:H7, *E. coli* O138, and *Staphylococcus aureus* were obtained from the American Type Culture Collection (ATCC) and cultured using standard methods. Bacteria were grown in Trypticase Soy Broth and on Trypticase Soy Agar plates (BD Biosciences, San Diego, CA). Bacterial concentrations for use in the assays were determined by either cell counting, counts of colony forming units (CFU), or both.

3.3.2 Antibody Biotinylation Procedures

3.3.2.1 Amine Biotinylation Procedure

Anti-*E. coli* O157:H7 antibody (Maine Biotechnology Services, Portland, ME) was suspended in 10mM PBS (Sigma-Aldrich, St. Louis, MO) at a concentration of 1mg/ml. 1 mg of NHS-PEO_4-Biotin (Pierce Biotechnology, Rockford, IL) was dissolved in to 100µl DI water and this solution was added to the antibody solution at 10µl per ml of antibody solution. The reaction was allowed to proceed under constant rocking for 1 hour at room temperature. The resulting solution was purified twice via gel filtration (Pierce Biotechnology, Rockford, IL) and suspended in 10mM PBS at a concentration of 0.5mg/ml.

3.3.2.2 Sulfhydryl Biotinylation Procedure

Anti-*E. coli* antibody (Maine Biotechnology Services, Portland, ME) was suspended at a concentration of 1mg/ml in a solution containing 100mM Sodium Phosphate (Sigma-Aldrich, St. Louis, MO), 150mM NaCl (Sigma-Aldrich, St. Louis, MO), 10mM EDTA (Sigma-Aldrich, St. Louis, MO) dissolved in DI water. 6mg of 2-mercaptoethanolamine (Pierce Biotechnology, Rockford, IL) was dissolved in 100µl of the 100mM PBS with EDTA solution and added to the antibody solution at 10µl per 100µl of antibody solution and allowed to react for 90 minutes at 37°C. The reduced antibody solution was then twice purified via gel filtration (Pierce Biotechnology, Rockford, IL). 2mg of Maleimide-PEO_2-Biotin (Pierce Biotechnology, Rockford, IL) was then dissolved in 200µl of the PBS/EDTA buffer and added to the purified reduced antibody at a ratio between 1:1 and 4:1 biotin:full antibody molecules. This mixture was reacted for two hours at room temperature before being twice purified via gel filtration and suspended in 10mM PBS (Sigma-Aldrich, St. Louis, MO) at a concentration of 0.5-0.75mg/ml.

3.3.3 Assay Protocols

3.3.3.1 Pseudo-Homogeneous Assay in PBS

5µl of an ice cold 0.5mg/ml solution of the amine biotinylated anti-*E. coli* O157:H7 antibody was added to a 45µl solution of ice cold 10mM PBS containing $2x10^6$ *E. coli* O157:H7. The mixture was kept on ice and allowed to react for 1 hr with rocking. After incubation, the bacteria were diluted to 2ml with ice cold 10mM PBS and centrifuged at 8000g for 5 minutes. The supernatant was discarded and the bacteria were washed 3 additional times in ice cold 10mM PBS with centrifugation for 5 minutes at 8000g, being finally resuspended in 100µl of ice cold 10mM PBS containing 1% BSA (Proliant Inc., Ankeny, IA). The remaining bacterial concentration was determined by optical counting and the resulting solution was diluted into vials with a PBS/BSA solution to various numbers of bacteria per 3µl. SA MP MNPs were spun at 1000g for 2 minutes and the supernatant was retained. 1µl of this solution was added per 3µl to each of the prepared bacteria samples and allowed to bind for 1 hour at room temperature while rocking. 11µl of the PBS/BSA solution was then added per 4µl of each of the mixed samples. 15µl of the resulting solutions were pipetted into individual BSA blocked microtiter wells (Greiner Bio-One, Monroe, NC). Each microwell was then cut out and sealed before measurement in the SQUID system. The samples were analyzed individually in quadruplicate in the SQUID system, where, after various incubation times, they were briefly magnetized in a 20G field and immediately brought into close proximity to the SQUID sensor via pneumatically controlled actuator, as shown in Figure 1-10. The SQUID sensor recorded the magnetic field strength in picotesla due to the remanent magnetization of each sample.

3.3.3.2 Pseudo-Homogeneous Assay in Blood

20µl of an ice cold 0.5mg/ml solution of the amine biotinylated anti-*E. coli* O157:H7 antibody was added to an 80µl solution of ice cold normal human blood (San Diego Blood Bank, San Diego, CA). containing $2x10^6$ *E. coli* O157:H7. The mixture was kept on ice and allowed to react for 1 hr with rocking. After incubation, the bacteria were diluted to 2ml with ice cold 10mM PBS and centrifuged at 8000g for 5 minutes. The supernatant was discarded and the bacteria were washed 3 additional times in ice cold 10mM PBS with centrifugation for 5 minutes at 8000g, being finally resuspended in 100µl of ice cold 10mM PBS containing 1% BSA. The remaining bacterial concentration was determined by optical counting and the resulting solution was diluted into vials with a PBS/BSA solution to various numbers of bacteria per 3µl. 5µl of a solution containing $2x10^{11}$ 50nm SA MP MNPs per µl of 10mM PBS (Miltenyi Biotec, Auburn, CA) was added per 3µl to each of the prepared bacteria samples and allowed to bind for 1 hour at room temperature while rocking. 7µl of the PBS/BSA solution was then added per 8µl of each of the mixed samples. 15µl of the resulting solutions were pipetted into individual BSA blocked microtiter wells (Greiner Bio-One, Monroe, NC). Each microwell was then cut out and sealed before measurement in the SQUID system. The samples were analyzed individually in quadruplicate in the SQUID system, where, after various incubation times, they were briefly magnetized in a 20G field and immediately brought into close proximity to the SQUID sensor via pneumatically controlled actuator, as shown in Figure 1-10. The SQUID sensor recorded the magnetic field strength in picotesla due to the remanent magnetization of each sample.

3.3.3.3 Homogeneous Assay Protocols

Preparation of Magnetically Labeled Antibody: Magnetically labeled antibody was prepared in one of two manners. The first method involved the use of 100nm streptavidin coated MNPs

(ChemiCell, Berlin, Germany) which were mixed with the amine biotinylated antibody at a ratio of 200 antibody per MNP. The MNPs were allowed to react for 30 minutes before a separate solution of D-biotin at 8.4µg/ml in DI water was added at a ratio of 2000 biotin/MNP. In the second and preferred method of preparation, SA MP MNPs were spun at 1000g for two minutes and the supernatant retained. These particles were then mixed with the sulfhydryl biotinylated antibody at a ratio of 15,000 antibody per MNP at $1x10^8$ MNPs per 5µl in 10mM PBS with 1%BSA and allowed to react for 30 minutes at room temperature.

Homogeneous Assay for Signal vs. Total Bacteria: Using either the ChemiCell or MP magnetically labeled antibody preparation, dilutions of *E. coli* O157:H7, *E.coli* O138, or *S. aureus* at various concentrations in bacteria/µl were mixed with either $1x10^8$ SA MP MNPs or $5x10^8$ ChemiCell MNPs to yield a total of 5µl per well per sample and allowed to react for 30 minutes at room temperature. The samples were then pipetted into individual BSA blocked microtiter wells (Greiner Bio-One, Monroe, NC). Each microwell was then cut out and sealed before measurement in the SQUID system.

Homogeneous Assay for CFU/ml of PBS: E. coli O157:H7 and *E. coli* O138 were suspended in 10mM PBS at various bacterial concentrations per ml of buffer. These solutions were then preconcentrated with Centricon filters (Millipore, Billerica, MA) from a volume of 19ml and resuspended in 111µl of 10mM PBS with 1% BSA. To this solution, 22.5µl of the MP magnetically labeled antibody preparation was added and allowed to react for 20-30 minutes. The samples were then pipetted into individual BSA blocked microtiter wells (Greiner Bio-One, Monroe, NC). Each microwell was then cut out and sealed before measurement in the SQUID system. Colony forming units (CFU) were determined by dilutional plating and colony counts the following day.

Homogeneous Assay for CFU/ml of Human Serum: E. coli O157:H7 and *E. coli* O138 were suspended in normal human serum (Chemicon, Temecula, CA) at various bacterial concentrations per ml of serum. The serum was then centrifuged at 3200g for 15 minutes and the supernatant discarded. The bacteria were resuspended in 10mM PBS with 1% BSA and respun for 15 minutes at 3200g and the supernatant was discarded. 111µl of the remaining centrifugate was mixed with 22.5µl of the MP magnetically labeled antibody preparation and allowed to react for 20-30 minutes. The samples were then pipetted into individual BSA blocked microtiter wells (Greiner Bio-One, Monroe, NC). Each microwell was then cut out and sealed before measurement in the SQUID system. Colony forming units (CFU) were determined by dilutional plating and colony counts the following day.

Homogeneous Assay for CFU/ml of Human Blood: E. coli O157:H7 and *E. coli* O138 were suspended in drawn human blood (San Diego Blood Bank, San Diego, CA) at various bacterial concentrations per ml of blood. To these solutions an anti-CD45 immunorosette forming solution (StemCell Technologies, Tuckwila, WA) was added at 50µl per ml of blood and allowed to react for 20 minutes at room temperature with constant rocking. The blood was then centrifuged at 200g for 15 minutes and the plasma was retained. The plasma was diluted 1:1 in 10mM PBS and respun for 15 minutes at 3200g and the supernatant was discarded. The centrifugate was then washed again in 10mM PBS and centrifuged for 15 minutes at 3200g and the supernatant was discarded. 111µl of the remaining centrifugate was mixed with 22.5µl of the MP magnetically labeled antibody preparation and allowed to react for 20-30 minutes. The samples were then pipetted into individual BSA blocked microtiter wells (Greiner Bio-One, Monroe, NC). Each microwell was then cut out and sealed before measurement in the

SQUID system. Colony forming units (CFU) were determined by dilutional plating and colony counts the following day.

Magnetic Detection by SQUID Magnetometer: The samples were analyzed individually in quadruplicate in the SQUID system, where, after various incubation times, they were briefly magnetized in a 20G field and immediately brought into close proximity to the SQUID sensor via pneumatically controlled actuator, as shown in Figure 1-10. The SQUID sensor recorded the magnetic field strength in picotesla due to the remanent magnetization of each sample.

3.4 Results and Discussion

3.4.1 Antibody Biotinylation and Conjugation

The colloidal stability of a conjugated streptavidin coated MNP solution is highly dependent upon the method and extent of biotinylation of the conjugate itself. For instance, if a solution of conjugate that contains more than one biotin per molecule is added to a streptavidin MNP solution, it will invariably act as a crosslink between the individual MNPs. This poses a particular problem in magnetorelaxometric applications, as the crosslinking causes the formation of large agglomerates with much larger Brownian rotation times and ultimately results in a large background signal, rendering magnetic detection all but impossible. On the other hand, if a solution of conjugate that contains less than one biotin per molecule is added to the streptavidin MNP solution, the unbiotinylated antibodies will act to block binding sites on the target of interest and thus effectively undermine the detection sensitivity of the assay.

With these considerations in mind, two methods of anti-*E. coli* O157:H7 antibody biotinylation were performed: *N*-hydroxysuccinimide (NHS) mediated biotinylation of

primary and secondary amines and the "site directed" conjugation via reduction and biotinylation of select disulfide/sulfhydryl groups on the antibody molecules. NHS modification of primary and secondary amines involves the nucleophilic attack on amines in the antibody molecules by the carbonyl group of the NHS biotinylation reagent resulting in a stable amide linkage, as shown in Figure 3-2. The primary drawback of this method of biotinylation is the fact that amine groups are more or less homogeneously distributed throughout the antibody molecules. This poses several potential problems. First, since the site of biotinylation is *de facto* random, the orientation of the resulting antibody MNP conjugates cannot be controlled and often result in the blocking of the antigen binding sites and reduced binding efficiency. The second problem this method poses is that the NHS group is readily susceptible to hydrolysis and thus the reaction is difficult to accurately control and the NHS biotinylation agent must be added in excess, producing multibiotinylated antibodies. These multibiotinylated antibodies will, as previously described, readily crosslink most streptavidin MNPs and are thus only usable in a pseudo homogeneous assay format, where they are added to the sample, allowed to bind to the target and the excess antibodies are washed away prior to the addition of streptavidin coated MNPs.

The primary impetus behind the second method of antibody biotinylation was not the generation of conjugated MNPs with properly oriented binding sites, but rather the biotinylation of the antibody at specific, discrete sites resulting in tighter control over the stoichiometry of the procedure. Toward this end, the disulfide bridges between the antibody heavy chains were selectively reduced to expose only the sulfhydryl groups in the hinge region of the antibody molecule and effectively split the antibody molecule in half. These sulfhydryl groups can then be discretely targeted for biotinylation through an alkylation reaction by a maleimide activated biotinylation agent resulting in a stable thioether linkage. Indeed, this methodology, shown in Figure 3-3, was successful at creating a discretely

biotinylated highly reactive antibody that does not appreciably crosslink streptavidin coated MNPs. Using appropriate biotinylation ratios, there was little to no detectable crosslinking between the MNPs, The presumable reason for this is derived from the innate instability of free sulfhydryl groups in the presence of atmospheric oxygen. Following reduction of the disulfides, if the antibodies are biotinylated at a ratio between 1 and 2 biotin per full antibody molecule, the reduced sulfhydryl groups will reoxidize and preferentially form disulfide bridges between the few unbiotinylated antibody halves and those with only one biotin, ultimately resulting in antibodies and antibody halves with only one biotin per molecule. The use of higher ratios of maleimide-biotin:antibody typically resulted in multibiotinylated half antibodies as evidenced from the rapid observable crosslinking of streptavidin coated MNPs.

3.4.2 Pseudo-Homogeneous Assays

Pseudo-homogeneous assays are so-named due to their need for sample washing after addition of a detection antibody, prior to addition of the MNP detection agent which does not require a wash step. Thus, the simplicity of a pseudo homogeneous assay lies in between a heterogeneous, ELISA type, assay that requires several wash steps and a homogeneous assay which requires only the mixing of reagents with the sample and no wash steps. The differences in the assay types are schematically compared in Figure 3-4. Thus, a pseudo homogeneous assay for the given system involves labeling *E. coli* O157:H7 in solution with a biotinylated detection antibody, followed by a wash step to remove unbound antibody. The antibody conjugated bacteria are then combined with streptavidin coated MNPs before measurement in the SQUID system

3.4.2.1 Pseudo-Homogeneous Assay in PBS

A pseudo-homogeneous magnetorelaxometric assay was performed using phosphate buffered saline (PBS) as a suspension buffer. Various numbers of *E. coli* O157:H7 versus *S. aureus* as a control were labeled with biotinylated antibody and incubated with 140nm SA MP MNPs; these were also compared with *E. coli* O157:H7 without antibody labeling, before measurement in the SQUID system. The results of the pseudo-homogeneous assay are shown in Figure 3-5 as magnetic signal versus total number of bacteria in the sample. The assay was successful at detecting as few as 400 *E. coli* O157:H7 with a signal to noise ratio >2 in a 15µl sample volume. Note that this is a drastic improvement of over 4 orders of magnitude better than previously published reports by Grossman, et. al. (Grossman, Myers et al. 2004). The plot shows decent linearity and a background signal for all controls near the instrument noise level (1pT).

3.4.2.2 Pseudo-Homogeneous Assay in Blood

In a first demonstration of its kind, a pseudo-homogeneous magnetorelaxometric assay was also performed using human blood as the suspension buffer. In this assay, the use of different, smaller, 50nm streptavidin coated MNPs was required as these were the only MNPs found to be colloidally stable and give a moderate background in blood in the SQUID system (data not shown). These particles utilize a dextran coating and better resist interaction with blood constituents, but are also much more weakly magnetic than the preferred Molecular Probes particles. This effectively resulted in a much lower magnetic signal per bacterium in solution and a minimum detection limit of 50,000 bacteria in a 15µl sample volume with a signal to noise ratio between 1.5 to 2 over an incubation time in blood between 90 and 1110 minutes. Figure 3-6 (A) shows a plot of the magnetic signal versus the number of bacteria at various measurement times. While the magnetic signal is not directly proportional

to the number of bacteria in solution, this is most likely due to the very large number of MNPs and bacteria in the solution (1000 fold more MNPs than assays using SA MP MNPs) acting to crosslink the bacteria, resulting in incomplete surface coverage of the individual bacteria and a nonlinear relationship between the two parameters. Figure 3-6 (B) shows a plot of the magnetic signal as a function of incubation time of various numbers of bacteria with the MNPs. It is evident from the data that while once again there is not direct scaling, the binding of the MNPs to the bacteria follows a similar, nearly directly proportional time course in each of the samples.

3.4.3 Homogeneous Assays

Homogeneous assays, as opposed to the previously described heterogeneous assays, are true "mix and measure" assays and do not require any wash steps prior to detection in a prepared sample. One of the primary goals of this magnetorelaxometric assay development is the demonstration of the assay under clinically relevant conditions. As such, samples were created in terms of more realistic colony forming units (CFU) per ml. In order to use clinically realistic bacterial concentrations, however, brief "preconcentration" steps were required during sample preparation for the magnetorelaxometric assay in order to achieve detectable numbers of bacteria in a standard 35µl sample. With the incorporation of these steps, homogeneous assays with high linearity, sensitivity and specificity are demonstrated.

3.4.3.1 Homogeneous Assay in PBS

The results of a homogeneous assay using phosphate buffered saline as a suspension buffer, plotted as magnetic signal versus CFU/ml, are shown in Figure 3-7 (A). The results show a high degree of linearity, with a detection limit below 2000 CFU/ml with a signal to noise ratio >2 compared to the negative control of over 750,000 *E. coli* O138. In comparison to

the pseudo-homogeneous assay results, the homogeneous assay resulted in over an order of magnitude greater sensitivity (2K versus >26.5K CFU/ml, respectively) and, as plotted as signal vs. time in Figure 3-7 (B), could be performed in less than 45 minutes with a S/N>10 versus 1500 *E. coli* O138 as compared to the >3 hours assay time required in the case of the pseudo-homogeneous assay.

The utility of a given diagnostic test is normally measured by its clinical sensitivity and specificity. The sensitivity of a clinical test is defined as the number of samples that test positive divided by the total number of samples that are truly positive. Likewise, the clinical specificity is defined as the number of samples that test negative divided by the number that are truly negative. In order to evaluate the sensitivity and specificity of this homogeneous magnetorelaxometric assay for sepsis diagnostics, criteria for positive and negative tests were determined with reference to negative controls of no bacteria and 1500 *E. coli* O138 CFU per ml. 20 individual "positive" samples of 2000 *E. coli* O157:H7 CFU per ml were then created and tested against these criteria in order to evaluate the test sensitivity. Based on the chosen criteria for a positive test of any signal greater than the signal given by zero bacteria plus two standard deviations (as determined by 8 measurements), the specificity of the homogeneous assay was determined to be 90% (95% Confidence Interval (C.I.), 67 and 96%), as shown in Figure 3-8. In a separate evaluation, negative criteria were also determined in order to test the clinical specificity of the assay. The negative samples containing 1500 *E. coli* O138 CFU per ml which gave an average signal of 4.5pT with an SD of 3.3pT were used as standards. Similar to the sensitivity assay, the criteria for a negative test was defined as a sample measurement below the average negative value plus two standard deviations (<4.5pT + 2*3.3pT = 11.1pT). Based upon these criteria the specificity in the 20 samples was determined to be 100% (95% C.I., 91 and 100%), as shown in Figure 3-9. The overall sensitivity and specificity evaluation results are shown in Table 3-1.

3.4.3.2 Homogeneous Assay in Serum

As mentioned previously, proper evaluation of a clinical test requires its demonstration in clinically relevant settings and fluids. Toward these ends, the homogeneous magnetorelaxometric assay was further amended for use in biologically relevant fluids such as serum and blood. Biological fluids, however, can pose significant problems in many, if not all, diagnostic/detection assays. For example, the opacity of blood and the autofluorescence of biomolecules all but eliminate the potential for fluorescent based assays in pure blood and serum. Additionally, the heterogeneity and complexity of these fluids typically interferes with many detection schemes. Initially, this was also true in this case and proved challenging as the SA MP MNPs are not stable in pure biological samples, showing significant aggregation and background signal. This problem was circumvented through slight modification of the wash/concentration steps. With these adjustments, beginning with various bacterial CFU loads per ml of serum, a homogeneous assay was developed and tested. In Figure 3-10 the results of the homogeneous assay in serum are plotted showing excellent linearity of signal to CFU/ml. As few as 2700 *E. coli* O157:H7 CFU/ml were detected with a signal to noise ratio of ~3 against a negative control of 130,000 *E. coli* O138 CFU/ml.

3.4.3.3 Homogeneous Assay in Blood

The last and most difficult challenge in clinical diagnostics is analysis of and detection in blood samples. Blood is a complex medium, consisting largely of red and white blood cells, serum proteins, clotting factors, antibodies and many other potentially interfering substances. And since the SA MP MNPs are not stable in blood, the significant volume (~45%) taken up by the red blood cells (RBCs) and white blood cells poses additionally challenges for dilution

and concentration of the bacteria in the sample. Through the use of immunorosette forming agents and differential centrifugation, however, these cells can be almost entirely removed, leaving only the plasma and bacteria. Utilizing such a process, various CFU counts of *E. coli* O157:H7 and O138 were spiked into blood samples and a homogeneous assay was performed. The data from this experiment is shown in Figure 3-11. As can be immediately seen from the data, there is a large background/negative signal, high standard deviations and although the positive samples give higher signal than the negatives, they do not scale, at least at the first timepoint. The extreme heterogeneity of blood makes the cause of these issues is difficult to specifically diagnose, but at the very least has to do with inconsistencies and inefficiencies in the washing/concentration steps. Potential improvements to the whole blood homogeneous and other assays are discussed below.

3.5 Sepsis Assay Development Conclusions

In this chapter, a prototype magnetorelaxometric assay for *E. coli* O157:H7 sepsis diagnostics was proposed, developed and demonstrated. The homogeneous assay proved to be significantly more rapid and sensitive than most current sepsis diagnostic methodologies, with a detection limit below 2000 CFU per ml in PBS. Furthermore, this detection limit was also demonstrated in a clinically relevant biofluid, viz. human serum. The developed assay is applicable to almost any bacterial pathogen and provides significant advantages over previous techniques, with a sensitivity improvement of over 5 orders of magnitude compared with previously published magnetorelaxometric assay data for bacterial detection (2.8×10^8 compared to 2×10^3 CFU/ml) and one order of magnitude better than the pseudo homogeneous assay (26×10^3 CFU/ml). A clinical sensitivity of 90% and a clinical specificity of 100% were also each demonstrated on pools of 20 samples. Additionally, a pseudo-homogeneous assay, with reduced sensitivity of 50,000 total bacteria, was successfully

performed in human blood, as was a homogeneous version that detected 20,000 *E. coli* O157:H7 CFU per ml of blood. This last assay, while successful in detecting the presence of the target pathogen, showed little to no linearity in signal and needs further improvement.

3.6 Considerations for Further Development

Despite the success of the prototype diagnostic assay, there are still several critical improvements that can be made to significantly increase its potential clinical utility. The first and most obvious is the further development of methods of sensitive and quantitative detection of pathogens in *blood*. The primary hurdle to this is difficulty in synthesizing an MNP with adequate colloidal stability in blood and serum. None of the MNPs tested, with the exception of the weakly magnetic Miltenyi MNPs, were as stable in blood or serum as they were in simple buffer solutions. This problem, however, appears to be readily tractable, as current investigations continue to be undertaken on the conjugation of antibodies to MNPs from StemCell Technologies. As can be seen in Table 2-1, the remanent magnetization signal of the StemCell MNPs is more than half the measured M_r value of the SA MP MNPs, yet these MNPs are relatively stable, even in whole blood. The current challenge with these MNPs lies in the lack of readily conjugatable reactive groups on these dextran coated MNPs. Preliminary attempts were made to oxidize and conjugate reduced antibodies to the created aldehyde groups through a hydrazide-maleimide heterobifunctional linker. While successful, the resulting stability of the MNPs was severely undermined, and this process will require further optimization.

The second area of optimization involves the measuring system itself, and, in particular, the measurement time. As previously shown, the Brownian time constant of an *E. coli* bacterium is roughly 2.76 seconds along the long axis. This time is actually less than the system measurement time of 3 seconds which implies that much of the signal should be lost

due to rotation. The equation used to calculate this time, however, does not take into account the long cilia and flagella, as shown in Figure 3-12, which extend outward from the soma of the bacterium and, due to both their length and surface area, increase drag and act as a significant stabilizing factor against rotation. Nonetheless, at the typical size of a given bacterial pathogen, some of the measured signal may be lost at a measurement time of 3 seconds. This measurement time, however, is fixed by constraints imposed in the current instrument embodiment and can be readily shortened in future implementations. The current limiting step that sets τ_m at 3 seconds involves the sample stage movement. Other factors which prevent the use of extremely rapid measurement times include mechanical vibration and eddy current which act on time scales of hundreds of milliseconds. These problems can also be overcome to a great extent through instrument design and simple signal processing algorithms. Shortening the measurement time should also increase the magnetic signal, as less Néel relaxation will have occurred as well, effectively boosting the measured signal per MNP. Incidentally, it additionally opens the door the use of smaller nanoparticles with lower τ_B times that were previously disqualified from use in the current system due to Néel relaxation and would potentially allow for a greater amount of magnetic material to be bound per bacterium. At present, these considerations are being addressed in the development of a next generation of the SQUID measurement system.

3.7 Acknowledgements

This work was supported by NIH grant 5 U01 AI066578-02, (NIAID) "Ultra-sensitive magnetic assays for sepsis diagnostics". We are sincerely grateful to Aline Grigorian, who aided in the instruction of proper microbiological techniques.

Table 3-1. Commercial manufacturers of devices for the detection of bacteria, showing the type of detection technique used, reported detection limit, and approximate analysis times. Taken from (Ivnitski, Abdel-Hamid et al. 1999)

Manufactures and/or developers of the commercial instruments for detection of bacteria[a]

Commercial instrument	Detection technique	Detection limit (cells/ml)	Analysis time (min, h)
Midas Pro (Biosensori SpA., Milan, Italy)	Amperometry	10^6	20 min
The PZ 106 Immuno-biosensor System (Universal Sensors, New Orleans, USA)	Piezoelectric	10^6	40 min
Bactometer (Bactomatic, Princeton, NJ, USA)	Impedimetry	10^5	3–8 h
Integrated Genetics, MA, USA	DNA probe for *Salmonella*	1 cell/g	2 days
Enzo Biochem, NY, USA	DNA probe for the bacterium *Chlamydia*	–	–
Hybritech, CA, USA	DNA probe for bacteria	–	–
Malthus 2000 (Malthus Instruments, Stoke-on-Trent, England, UK)	Conductance	10^5	8–24 h
Unilite (Biotrace, Bridgend, UK)	Bioluminescence	10^3	15 min
Lumac Biocounter (Lumac B.V., Schesberg, Netherlands)	Bioluminescence	10^3	20 min
Coulter counter (Coulter Electronics, Canada)	Coulter counter	5×10^4	30 min
Thermal activity monitor (Thermometric, Northwich, Cheshire, UK)	Microcalorimetry	10^5	3 h
BIA-core (Pharmacia, Uppsala, Sweden)	Surface plasmon resonance	10^5	1 h
Vitek AutoMicrobic System (BioMerieux Vitek, Hazelwood, MO)	Optical	10^4	4 h

[a] Nelson, 1985; Feng, 1992; Tietjen and Fung, 1995; Hobson et al., 1996.

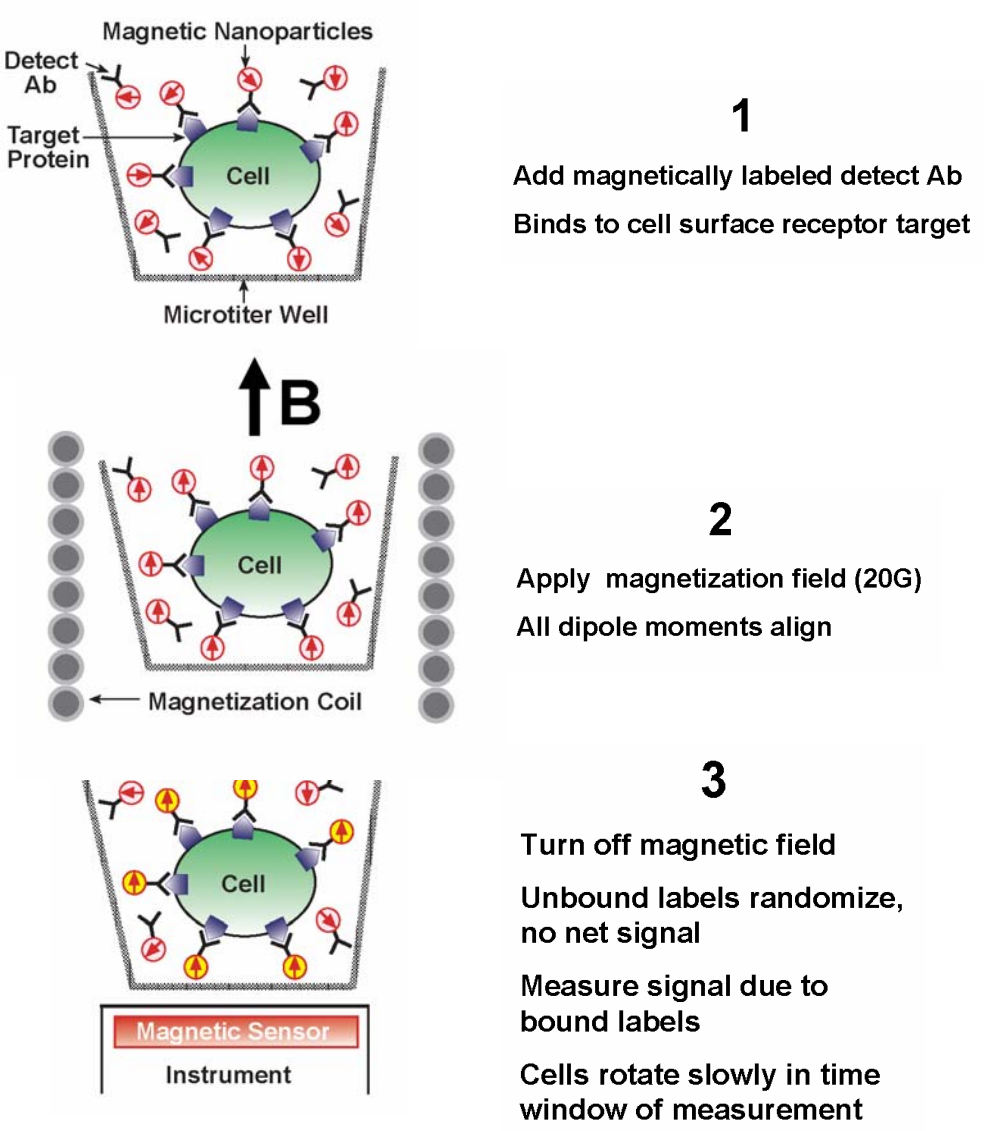

Figure 3-1. Magnetic relaxometric detection of suspended cells. Magnetic signal is given in picotesla and is proportional to the number of MNPs bound to the target cells/antigens.

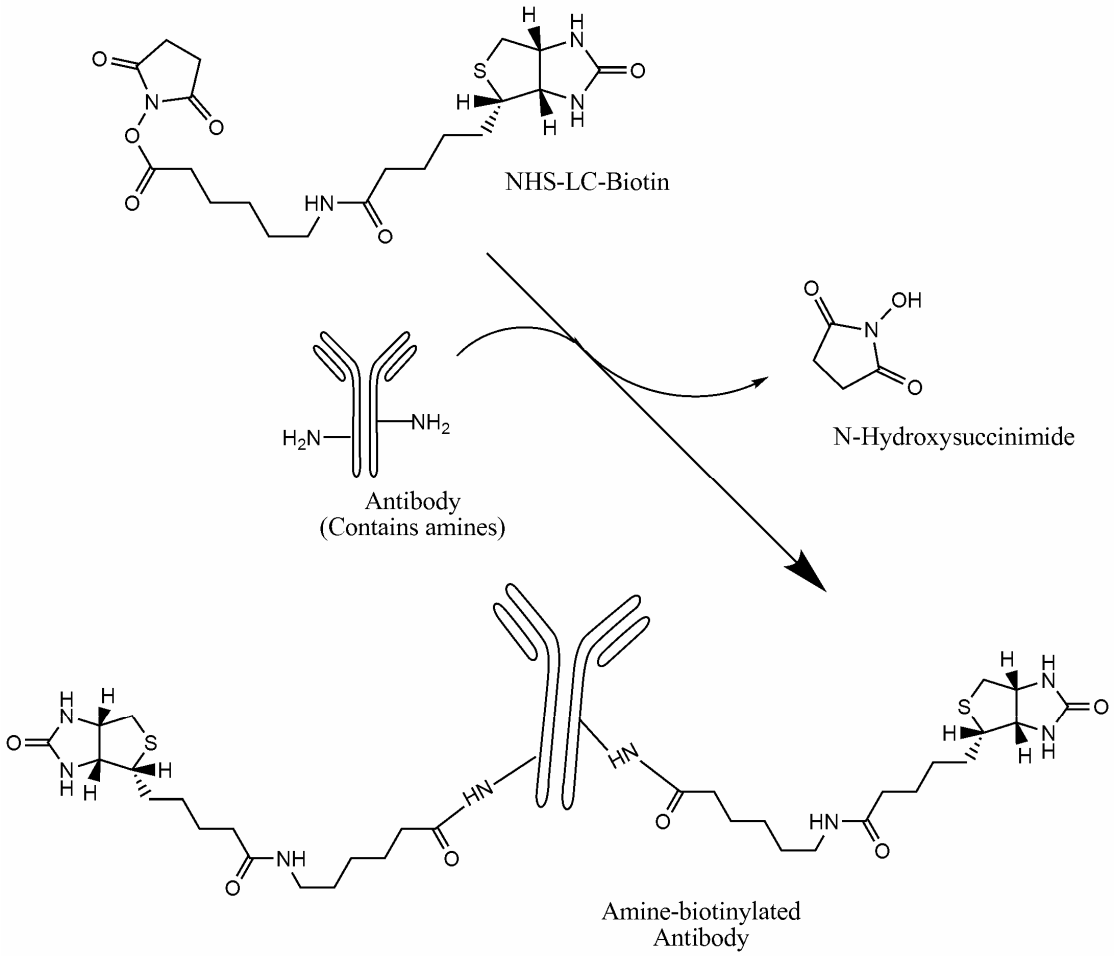

Figure 3-2. NHS biotinylation procedure to antibody amines. The NHS group of the NHS-LC-biotin reacts with nucleophilic amines on the antibody molecule to form stable amide linkages through a long chain to the biotin molecule.

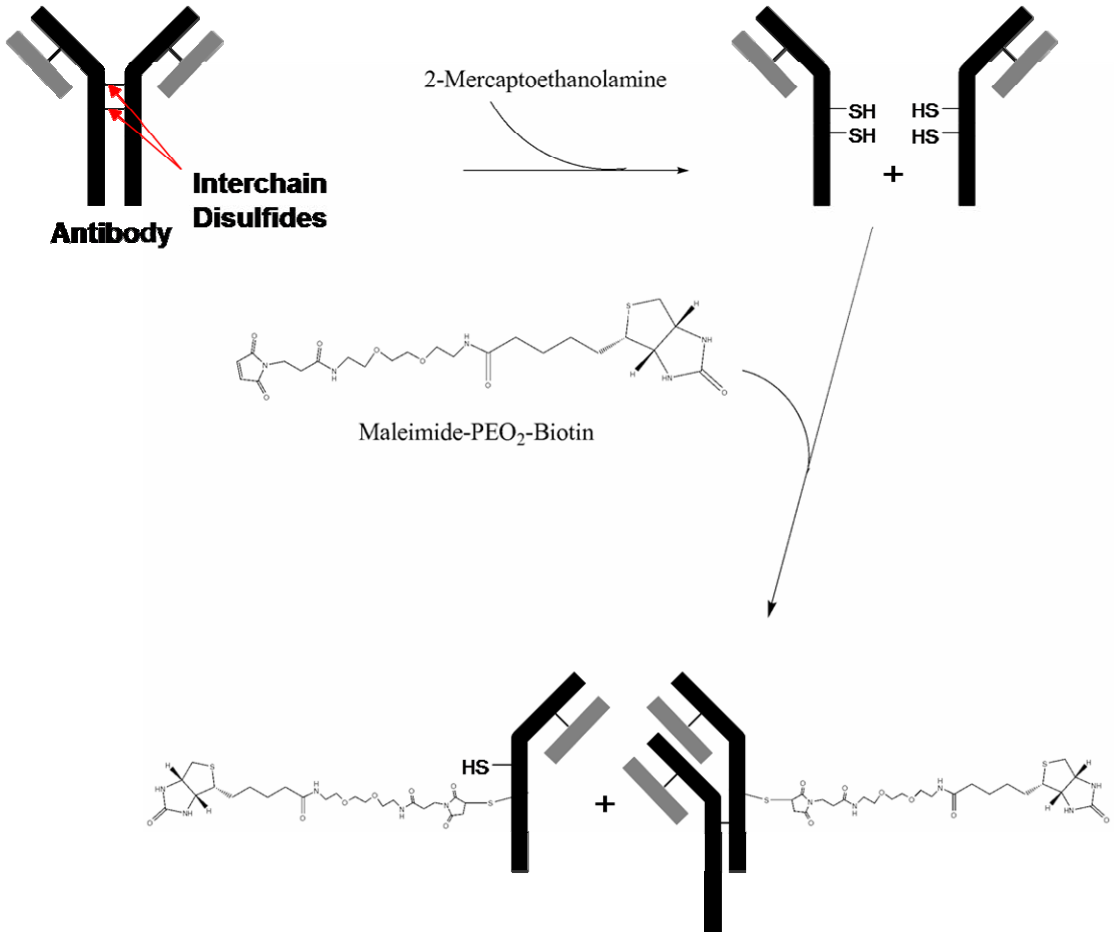

Figure 3-3. Reduction and sulfhydryl antibody biotinylation procedure. The disulfide bonds between the heavy chains of the antibody molecule are selectively reduced by 2-mercaptoethanolamine resulting in two half antibody molecules. The resulting sulfhydryl groups can be reacted with the maleimide group of maleimide-PEO_2-biotin at low concentrations to form stable thioether bonds between biotin and some of the half antibody molecules. Once removed from the reducing agent, the unreacted sulfhydryl groups can reoxidize with sulfhydryl groups from other antibodies, thus allowing better control over discrete low biotinylation ratios while reducing free unbiotinylated antibody.

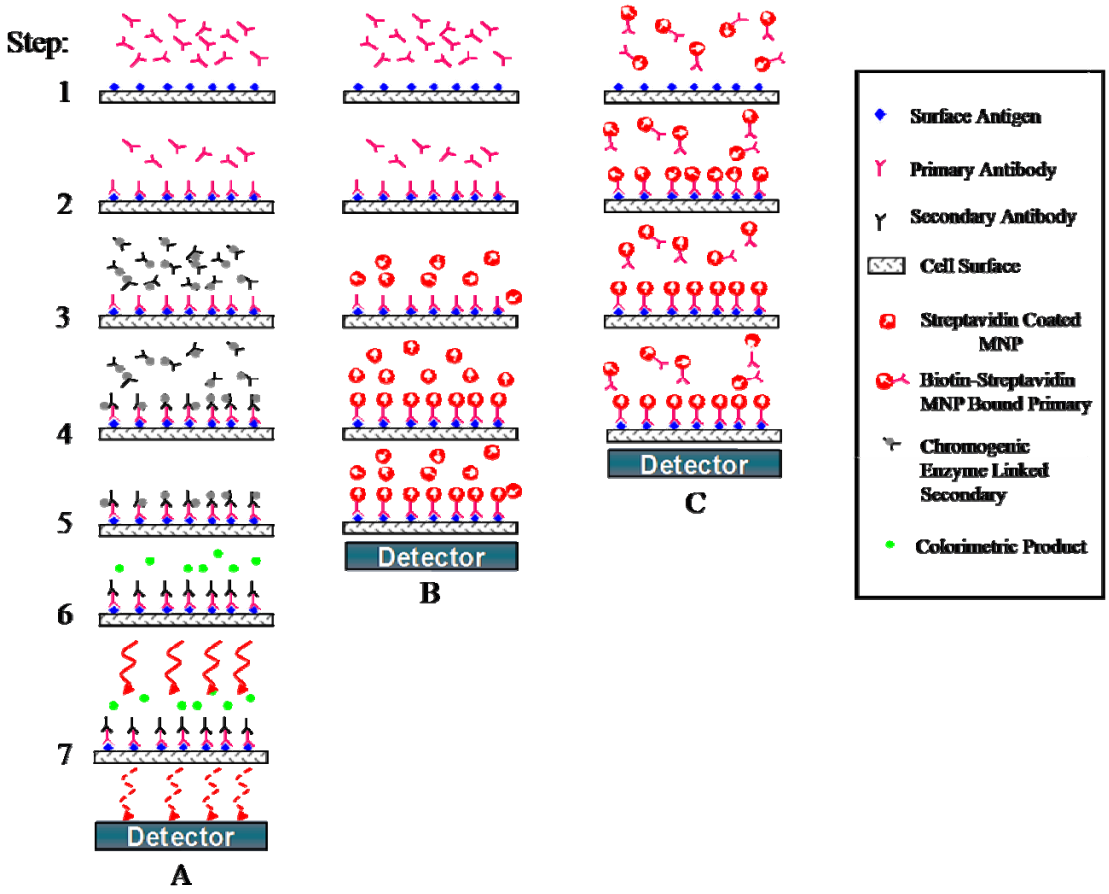

Figure 3-4. Comparison between various immunoassay paradigms for cell detection/quantification: (A) standard ELISA based, (B) Pseudo-homogeneous magnetorelaxometry and (C) Homogeneous magnetorelaxometry. In (A) a detect antibody is added to the cells, incubated, washed away and followed with an enzyme linked secondary antibody which also must be washed away. An agent which reacts with the chromogenic enzyme is added and, after incubation, the absorbance at a specified wavelength is measured. In (B), a biotinylated primary antibody is incubated with the cells and washed away. A streptavidin coupled MNP solution is then added and the sample undergoes magnetorelaxometric measurement. In (C), a magnetically labeled primary antibody is mixed with the cells and, after incubation, undergoes magnetorelaxometric measurement.

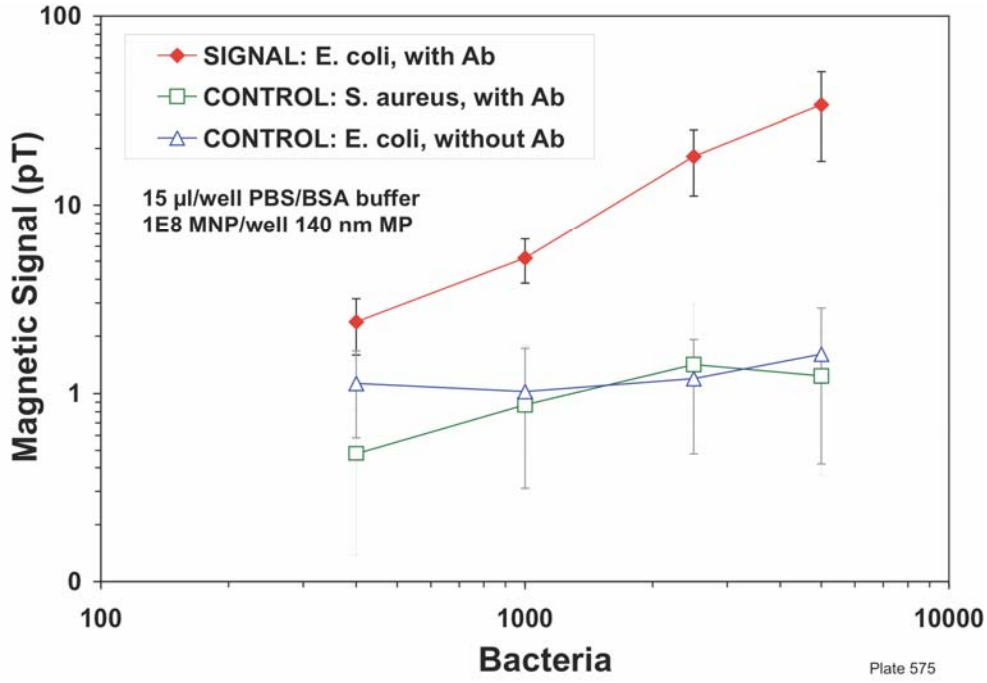

Figure 3-5. Pseudo-homogeneous quantitative magnetorelaxometric detection of absolute number of *E. coli* O157:H7 suspended in PBS; plotted as magnetic signal versus number of bacteria as compared with the negative controls of *Staphylococcus aureus* and *E. coli* O157:H7 not incubated with antibody.

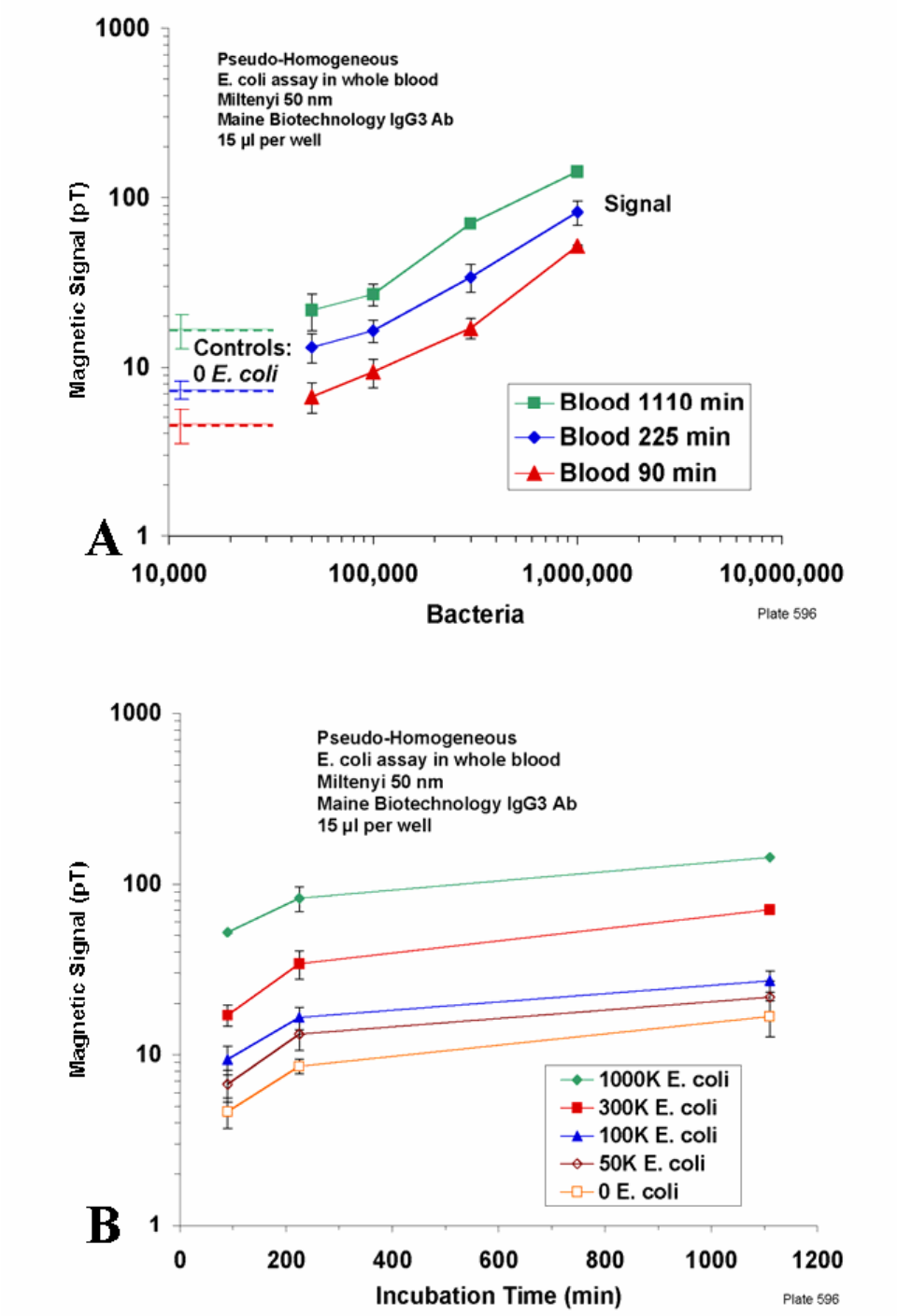

Figure 3-6. Pseudo-homogenous magnetorelaxometric detection of *E. coli* O157:H7 in whole blood. (A) Magnetic signal as a function of number of bacteria at various timepoints. (B) Magnetic signal as a function of time for various numbers of bacteria.

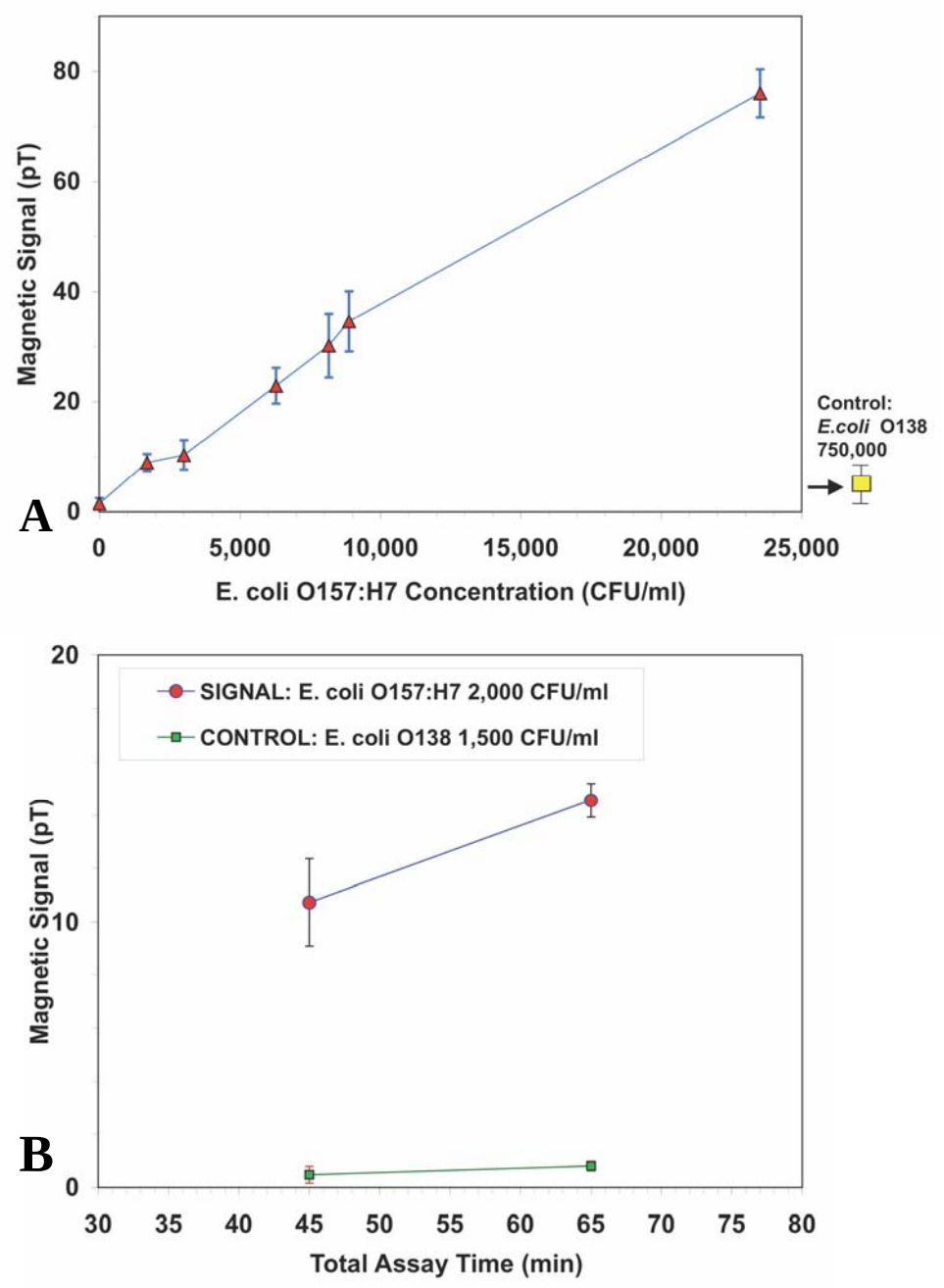

Figure 3-7. Homogeneous quantitative magnetorelaxometric detection of *E. coli* O157:H7 CFU suspended in PBS. (A) Magnetic signal versus number of CFU. (B) Magnetic signal versus total assay time for 2000 *E. coli* O157:H7 CFU/ml, showing detection in less than 45 minutes including sample preparation.

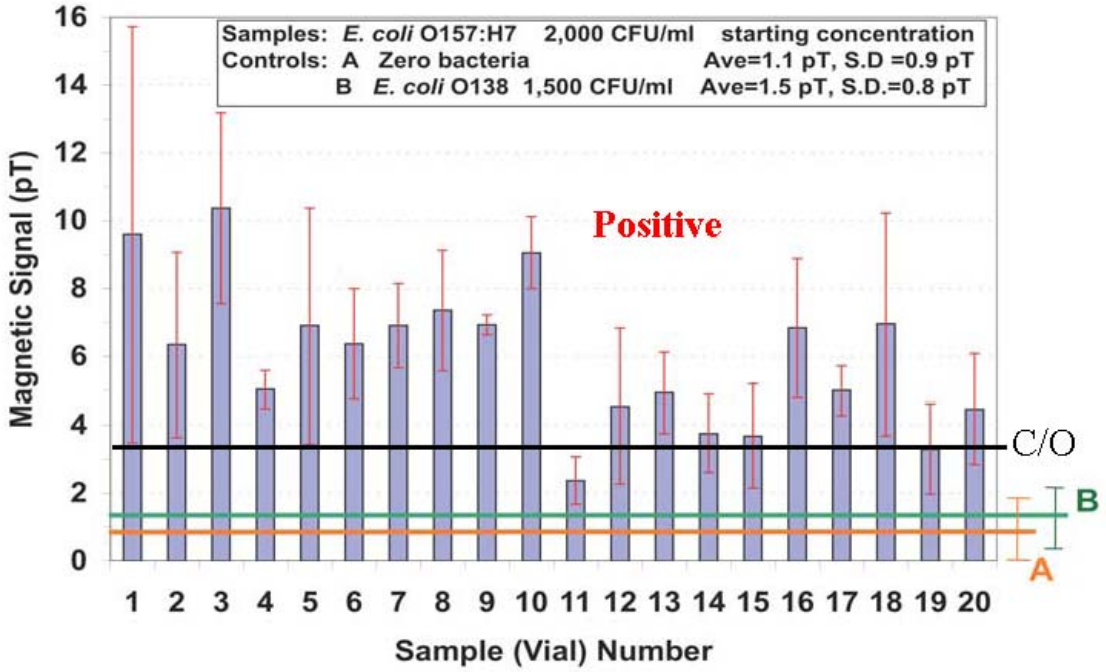

Figure 3-8. Clinical sensitivity of the homogeneous magnetorelaxometric assay for 2000 *E. coli* O157:H7 CFU suspended in PBS. The two controls are (A) 0 bacteria and (B) 1500 *E. coli* O138 CFU/ml (shown by horizontal lines). Positive/negative cutoff (C/O) is shown in black. Samples 11 and 19 tested negative by the criteria, thus resulting in a sensitivity of 18/20 or 90%.

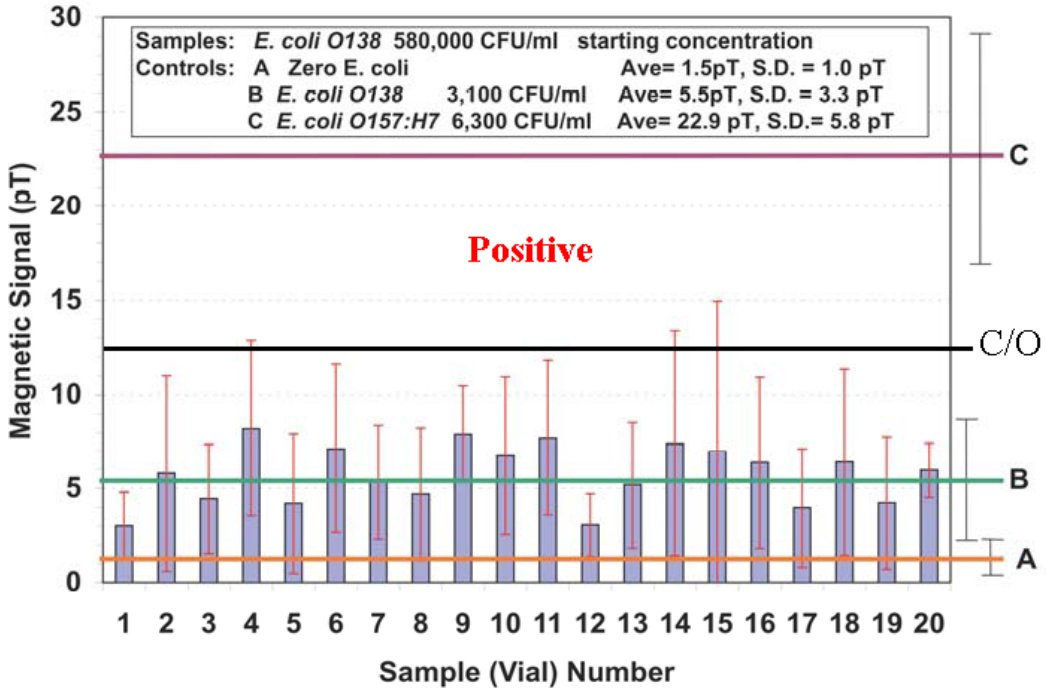

Figure 3-9. Clinical specificity of the homogeneous magnetorelaxometric assay using 580,000 *E. coli* O138 CFU suspended in PBS. Controls are shown by horizontal lines: (A) 0 bacteria negative control; (B) 3100 *E. coli* O138 CFU/ml; (C) Positive control of 6300 *E. coli* O157:H7 CFU/ml. Positive/negative cutoff (C/O) is shown in black Assay demonstrated a specificity of 100% .

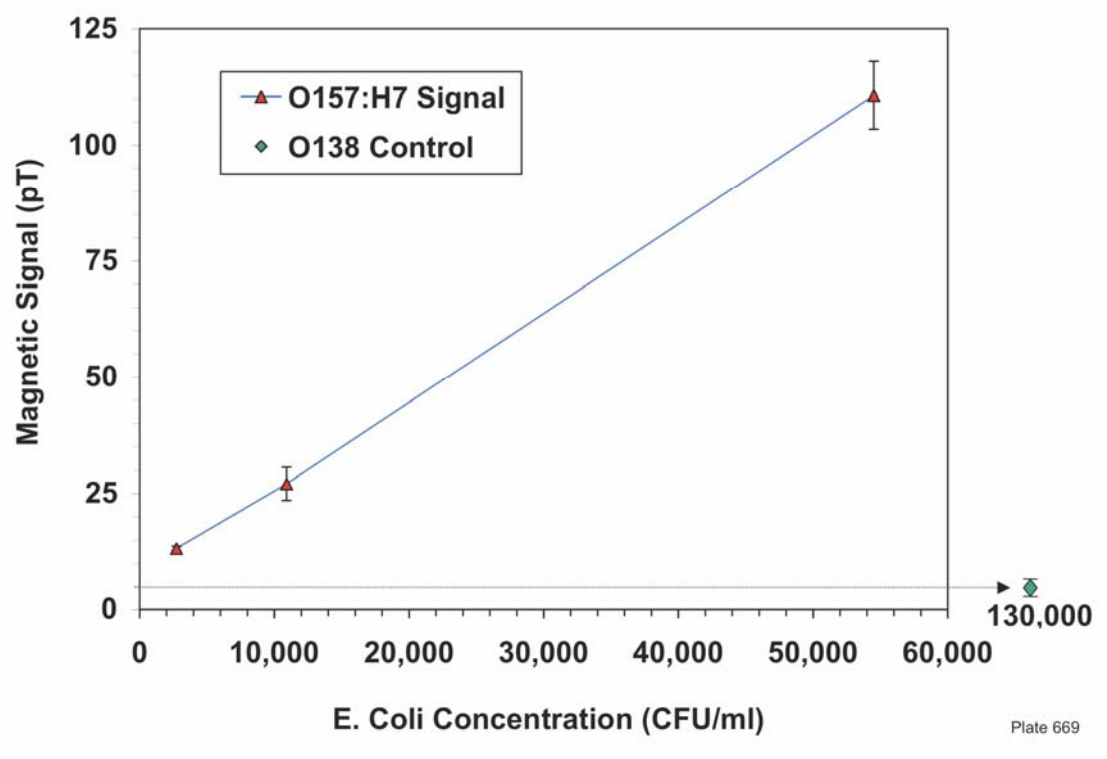

Figure 3-10. Homogeneous quantitative magnetorelaxometric detection of *E. coli* O157:H7 CFU suspended in human serum, showing a detection limit below 2700 CFU/ml. with 130,000 *E. coli* O138 CFU as a negative control.

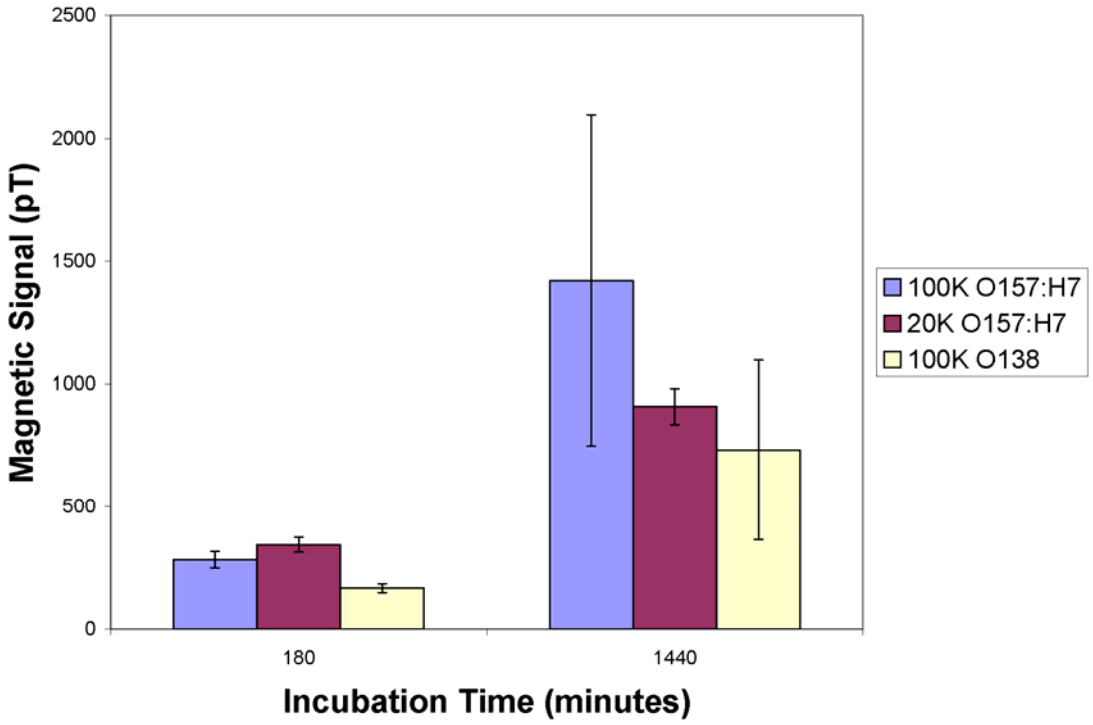

Figure 3-11. Preliminary homogeneous quantitative magnetorelaxometric detection of *E. coli* O157:H7 CFU suspended in human blood. The signal does not scale at earlier timepoints and shows large variabilities and high background levels at the later timepoint. Negative control is 100,000 *E. coli* O138 CFU/ml.

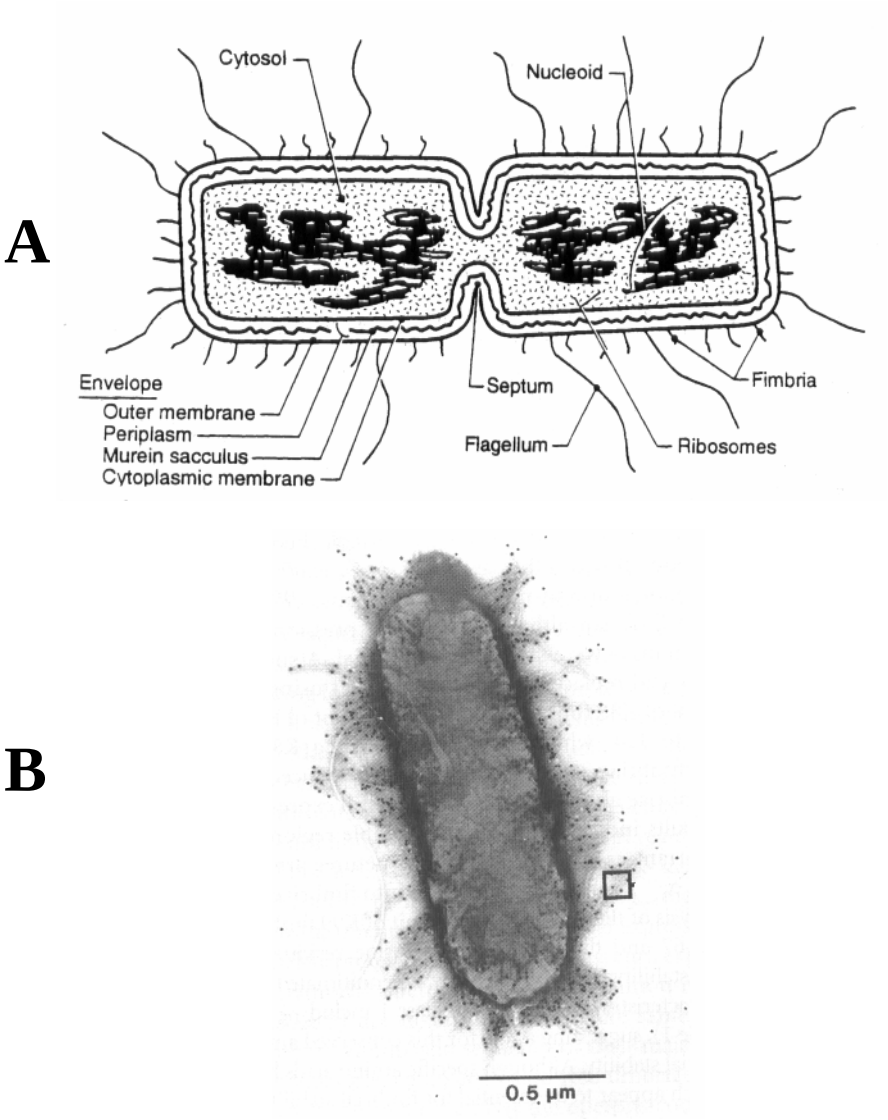

Figure 3-12. Structure of a typical *E. coli* bacterium. (A) Schematic representation, with labeling of major cellular structures, including flagella and fimbriae. (B) Electron micrograph of *E. coli*, with colloidal gold labeled antibodies against fimbriae. Adapted from (Neidhardt 1996).

CHAPTER 4

IN VIVO MAGNETORELAXOMETRIC QUANTITATIVE BINDING ASSAY

4.1 Abstract

In this chapter, the potential use of rapid, non-invasive magnetorelaxometric assays for *in vivo* applications is demonstrated. *Caenorhabditis elegans* is used as a simple living organism model system and a scientifically important binding interaction within the system is chosen, namely the binding of insecticide *Bacillus thuringiensis* crystal (Cry) proteins to carbohydrates expressed on the surface of gut cells in *C. elegans*. A specific Cry protein, Cry5B toxin, is purified, and a biotinylation and streptavidin coated magnetic nanoparticle labeling procedure for the toxin was developed and optimized. The resulting labeled toxin is then fed independently to two different *C. elegans* strains, one wild type (strain N2) that is susceptible to Cry5B and another, *bre-5* mutants, that do not produce the surface carbohydrates required for toxin binding. The difference in the binding kinetics of the magnetically labeled Cry5B between the two strains is monitored in real time and analyzed via magnetorelaxometry using the SQUID system. The results of the assay show a statistical difference between the binding of the toxin in the two strains. The results and sensitivity of SQUID magnetorelaxometry are then discussed in relation to the chosen binding paradigm and alternatives and improvements are proposed.

4.2 Introduction

The use and evaluation of living subjects is critical to almost every area of biomedical research. Throughout the history of modern mankind, the use of animals in this research has paralleled the development of biology and medicine. The lives of some 75-100 million vertebrate animals are dedicated annually in the name of bioresearch, representing not only a tremendous monetary investment, but also an untold sacrifice on the part of the animals themselves (Baumans 2004). In light of the continuous demand for, yet increasing public opposition to, animal studies, analysis techniques which can provide scientific advantages and significantly increase the welfare of laboratory animals are of valuable interest to the scientific community.

In Chapter 3 it was demonstrated that magnetorelaxometry can be used for the diagnostic quantification of extracellular binding events in a controlled medium. Such assays provide significant temporal and sensitivity advantages when compared to conventional quantification approaches such as optical techniques and bacterial culture. Another potential advantage of the use of magnetorelaxometry and other magnetic techniques is the innate "transparency" of biological tissue to magnetic fields. This magnetic transparency shared by all biological tissues, from cells to entire organisms including humans, serves as the basis for several non-invasive medical diagnostic techniques, including MRI (Lauenstein and Semelka 2005), magnetoencephalography (MEG) (Wheless, Castillo et al. 2004) and magnetocardiography (MCG) (Steinberg, Roguin et al. 2005). This property allows for the ability to magnetically "see" into the body, that is, to potentially non-invasively magnetically investigate biological tissue. With this in mind, the expansion of magnetorelaxometry to *in vivo* systems is not only a theoretical possibility, but in principle, a technically tractable one. In fact, the principles underlying *in vivo* magnetorelaxometry are identical to those of *in vitro*

systems, except that instead of probing cells within an artificially created matrix, the matrix is native and predetermined, viz., the organism itself.

In this chapter, the feasibility of noninvasively detecting and monitoring real time binding events in viable living organisms is proposed and developed. The use of living organisms, however, poses several additional challenges. First, as previously mentioned, control over the detection matrix and its chemical composition is all but eliminated. Second is the problem of delivery of the magnetic detection labels to the region of interest within the organism, which can be significantly hampered by the organism's anatomy. Lastly, the physiology of every living organism is unique and independently interacts with and responds, often specifically, to physical and chemical entities which it encounters or to which it is exposed. This can prove extremely problematic in the use of *in vivo* agents (here, MNPs), particularly if the organism is designed to actively remove such agents. In light of these concerns, it is important to choose an appropriate preliminary model system and target within that system which minimizes these potential impediments to a proof of concept demonstration.

The soil nematode *Caenorhabditis elegans* (*C. elegans*) is a widely used model system in biological research, mainly due to its simplicity (only 1mm long with 959 somatic cells). Despite this simplicity, *C. elegans* possesses a wide range of differentiated tissues and shares many biological functions with vertebrates, including humans (Cranfield, Dawe et al. 2004). With both its cell lineages delineated (Sulston, Schierenberg et al. 1983) and its genome sequenced (Anonymous 1998), *C. elegans* is an extremely well-characterized system. This combined with its manageable size and simple care makes it an excellent model system for *in vivo* magnetorelaxometry. Figure 4-1 shows a micrograph of a typical *C. elegans* nematode along with a schematic depicting its anatomy.

Crystal (Cry) proteins made by the bacterium *Bacillus thuringiensis* (Bt) are pore-forming toxins which target insects, are innocuous to vertebrates and have thus been used for more

than 50 years throughout the world as an organic means of pest control (Gilbert 2002). Once ingested, Cry proteins are protealytically activated and bind to receptors on the gut cells. The efficacy of Cry proteins as a means of controlling insects, however, is undermined by the previously observed development and adaptation of resistant insect populations (Gould 1998). Similar to insects, along with other nematodes, *C. elegans* has also been shown to be susceptible to Bt Cry proteins through a similar route (Marroquin, Elyassnia et al. 2000). Plant parasitic nematodes are extremely destructive and cause approximately $80 billion in damage per year worldwide (Griffitts, Whitacre et al. 2001). Bt toxin binding to the nematode gut thus serves as an appropriate, scientifically important model receptor-ligand binding system for *in vivo* magnetorelaxometric measurements. Recently it has additionally been shown that mutations in specific *C. elegans* genes, called *bre* (for Bt resistance), which encode for a putative β-1,3-galactosyltransferase, confer resistance to the Cry protein Cry5B (Marroquin, Elyassnia et al. 2000) and led to the discovery that the binding partner of activated Cry toxins are surface carbohydrates on the gut cells. *C. elegans* strains that lack the *bre* gene, such as *bre-5*, are resistant to Bt toxins such as Cry5B and their binding and hence act as an appropriate control. Figure 4-2 shows phase and fluorescent micrographs showing binding of fluorescently labeled Cry5B to wild type *C. elegans*, but not to the mutant *bre-5(ye17)* strain.

Given the model system, *C. elegans*, and the binding paradigm, Cry5B to the surface of its gut cells, the objectives of this chapter are to: (1) Develop and optimize a method of conjugation of the Cry5B toxin to MNP labels; (2) Demonstrate a magnetorelaxometric assay on the binding of magnetically labeled Cry5B to surface receptors on the gut of the nematode, *C. elegans*; (3) Demonstrate specificity of the binding by comparing this binding to a genetic mutant, *bre-5*, lacking the binding receptor. Toward these ends, methods of semi-quantitative biotinylation and attachment of the resulting modified Cry5B toxin to magnetic nanoparticles and removal of excess toxin are developed and optimized. Initially, bare SA MP MNPs are fed

to live *C. elegans* to evaluate the level of NSB of the MNPs to the nematodes. Different methods of Cry5B conjugation to the MNPs are then evaluated based upon both their ability to prevent particle aggregation and the ability of the resulting product to bind to the gut of the wild type nematodes versus the *bre-5* mutants. The resulting assay data is then plotted, evaluated and discussed. A schematic illustrating the *in vivo C. elegans* binding assay is shown in Figure 4-3.

4.3 Materials and Methods

4.3.1 *C. elegans* Culture

C. elegans strains wild type Bristol N2 and the negative mutant *bre-5(ye17)* were propagated using standard techniques (Brenner 1974). The nematodes were maintained separately on NG plates and fed with *Escherichia coli* strain OP50.

4.3.2 Toxin Preparation and Biotinylation

Cry5B protoxin was purified as described in (Griffitts, Whitacre et al. 2001) by Raffi Aroian and Brad Barrows (UCSD). Cry5B crude spore lysate pellets were resuspended with 3.8ml of water and the toxin crystals were solubilized with a 30ml solution of 8.7mM tripotassium citrate, 43.4mM citric acid and 10mM dithiothreitol. The resulting solution was spun at 8000RPM for >5 minutes and the supernatant was kept. Toxin was precipitated by adding 0.75ml of 1M tripotassium citrate to the resulting solution. The toxin was resuspended in 20mM HEPES buffer (Sigma-Aldrich, St. Louis, MO) at a concentration of 4mg/ml. The protoxin was then trypsinized at a 200:1 toxin:trypsin mass ratio and allowed to react for 2 hours at 25°C, before undergoing gel filtration (Bio-Rad, Hercules, CA).

Purified active Cry5B in 20mMHEPES pH 8 buffer at a concentration of 0.5-1.5mg was reacted with biotinamidocaproate-N-hydroxy-succinimide (Sigma-Aldrich, St. Louis, MO) at a ratio of 1:0, 1:0.25, 1:0.5, 1:0.75 or 1:1 toxin:biotin for 2 hours at room temperature before being purified with gel filtration (Bio-Rad, Hercules, CA). The resulting protein concentration was determined via BCA protein quantification.

4.3.3 Toxin Conjugation and Nanoparticle Purification

SA MP MNPs (Molecular Probes, Eugene, OR) were spun at 300g for 2 minutes to remove any agglomerates and the supernatant was retained. Biotinylated toxin was incubated with these SA MP MNPs for 1.5-2 hours in either water with or without 0.3% BSA or 30mM HEPES buffered saline (HBS) with or without 0.3% BSA at various toxin:MNP ratios between 20,000:1 and 500,000:1. Following incubation, the coated MPs were magnetically decanted 3-4 times in 2ml microcentrifuge tubes by placing a NdFeB magnet on the side of the tube and allowing the MNPs to accumulate on the side of the tubes for 10-20 minutes and resuspended in ~1.5ml of buffer. After the final decantation, the MNPs were suspended in buffer to a concentration of roughly $4x10^9$-$2x10^{10}$ MNP/ml. In some instances, the final MNP product was exposed to an AC degausser (60 Hz, McMaster-Carr, Atlanta GA). The degausser was manually brought into proximity of the MNPs and rapidly withdrawn.

4.3.4 General Assay Protocol

Bare MNPs or magnetically labeled toxin was added to 150-1000 live or dead nematodes at $1x10^7$-$5x10^8$ MNPs in 35µl of M9 buffer (Sigma-Aldrich, St. Louis, MO) alone or with 0.3% BSA, *E.coli* OP50, or both. The nematodes were mixed directly into BSA blocked microtiter wells (Greiner Bio-One, Monroe, NC; Nalgene-Nunc International, Rochester, NY), as described previously, or dispensed into wells immediately prior to measurement with the

SQUID system. Each microwell was cut out and sealed before measurement in the SQUID system. The samples were analyzed individually in quadruplicate in the SQUID system, where, after various incubation times, they were briefly magnetized in a 20G field and immediately brought into close proximity to the SQUID sensor via pneumatically controlled actuator, as shown in Figure 1-10. The SQUID sensor recorded the magnetic field strength in picotesla due to the remanent magnetization of each sample.

4.4 Results and Discussion

4.4.1 Nonspecific Binding of MNPs to *C. elegans*

Of primary initial concern in the development of any assay is the level of nonspecific binding and/or background of the sample. To address this issue, the NSB of bare streptavidin coated MNPs to live and dead wild type *C. elegans* was evaluated. 200 live or dead nematodes were incubated with MNPs at different ratios and compared with MNPs with no nematodes. These initial results are shown in Figure 4-4. As is evident from the plot, there is actually less background signal in the case with dead nematodes and even less with the live ones, when compared to MNPs alone. The background does increase with higher numbers of MNPs, as is to be expected. The lower background in the case with nematodes is most likely due to their physical blocking of the microtiter well surfaces, where apparently almost all of the NSB takes place. This NSB level is relatively high (25-175 pT, ~2.5×10^6-1.75×10^7 MNPs) and was significantly improved on subsequent assays through the addition of BSA to the MNP solutions. Additionally, the lower NSB in the case of the live nematodes may be accounted for by the agitation they provide within the well, effectively "sweeping" nonspecifically bound MNPs from the surface of the microplate.

4.4.2 Effects of Toxin Preparation and Purification Conditions on Particle Stability

As previously shown in Chapter 3, the streptavidin surface, while providing a simple scaffold for the attachment of biotinylated binding agents, also poses a potentially significant problem in its use in magnetorelaxometric assays. In order to attach the Bt toxin to the MNPs it must first be biotinylated. This can prove more difficult in the case of Cry5B, where sulfhydryl groups are not discretely located, as in the case of immunoglobulins, and thus controlling the stoichiometry of the biotinylation procedure proves to be somewhat more delicate. If the Cry5B toxin is biotinylated at more than one biotin per molecule, it will act to effectively crosslink the MNPs, resulting in larger τ_B and colloidal instability. On the other hand, if the toxin is biotinylated at less than one biotin per molecule, there exists excess unbiotinylated toxin left over from the conjugation procedure which could potentially interfere and saturate the binding sites within the nematodes. In an attempt to address both of these issues, the toxin was amine biotinylated using a reaction scheme similar to Figure 3-2, at various ratios and the toxin was added to the SA MP MNPs at an excess in an attempt to saturate the streptavidin binding sites on the MNPs (>10,000 sites)and prevent MNP crosslinking. Following coordination of the toxin to the MNPs, the MNPs were magnetically pulled out of solution and washed to remove the unbound toxin and prevent its interference with the assay.

The basic assay protocol involves the feeding of the toxin conjugated MNPs to the wild type and the mutant nematodes in the measurement well itself. The initial assay data of binding to wild type *C. elegans* for various biotinylation ratios is shown in Figure 4-5. Note that the signal increases as the ratio of biotinylation reagent to toxin is increased to 1:1, initially indicating increased binding to the nematodes. However, if the 1:1 ratio MNPs are fed in an assay to the wild type nematodes, but this time with mutants and no nematodes as controls, as in Figure 4-6, we see that, while there does exist a differential binding between

the strains, a significant portion of the signal is due to background from aggregation and NSB of the MNPs. In order to address this issue, the ratio of 1:1 biotinylated toxin to MNPs was adjusted in order to see the effect of increasing binding site saturation ratios on the aggregation of the MNPs. As can be seen in Figure 4-7, increasing saturation ratios does reduce the background significantly, going from 473 pT for 2:1 toxin:binding site ratio down to 42.9 for a 50:1 ratio for $1x10^{8}$ MNPs at 16 minutes incubation in the microplate well. The 50:1 ratio, however, wastes a significant amount of the tediously produced Cry5B toxin. In light of this, a biotinylation ratio of 1:0.75 or 1:0.5 toxin:biotin and 18:1 toxin:binding site was used on most of the remaining assays in an attempt to conserve the toxin yet maintain a reasonably low background signal.

The last parameter that was adjusted in order to reduce aggregation and the subsequent background signal was the magnetic separation/washing of the particles. Following magnetic separation, the MNPs are in very close proximity to each other and retain a magnetic moment following removal of the field and thus magnetically attract one another according to (1.10). It stands to reason, then, that by reducing the time the MNPs are exposed to the magnetic field during the wash steps, the less physically close and magnetized they will become. Given time, the magnetic moments of the individual SPM MNPs will relax and become less attracted to another, potentially redispersing into the solution. Additionally, one method of rapidly reducing the level of magnetization in a magnetic material is AC degaussing. In this method an alternating, positive and negative, magnetic field is brought into proximity of the magnetic sample and then withdrawn, effectively tracing the B-H loop to a lower level of magnetization. The effect of total magnetic separation time, relaxation time and AC degaussing on background signal was investigated, as shown in Figure 4-8. Toxin conjugated MNPs and bare SA MP MNPs were exposed to either 0 minute (stock MNP) or 3x12 minute≈35 minute magnetic separations/washes and compared with stock MNPs

exposed to 4x20 minute=80 minutes of magnetic washes. The samples were then split and half were set aside and the other half were AC degaussed as described. The data show the highest background signal from the 35 minute separations with no AC demagnetization. Following AC demagnetization, these backgrounds can both be significantly reduced. The lowest background levels came from the particles that remained unexposed to any field (including demagnetizing) and the particles exposed to 80 minutes of magnetic washing, but were allowed to relax over a 24 hour period and not demagnetized. This implies that AC degaussing is only effective on particles that have been exposed to high magnetizing fields and have not yet relaxed. Exposing unmagnetized or relaxed MNPs to an AC degaussing field acts to effectively raise the magnetic moments of the particles and increase interparticle attractions. Based on the data, the preferred method for magnetic washing, which balanced particle recovery, toxin reactivity and maintained a low level of background, became a 4x10 minute wash with 24 hours of relaxation time and no AC demagnetization.

4.4.3 Effect of Parameter Optimization on *In Vivo* Binding Data

In a typical assay involving a detection label, optimization involves steps of increasing the specific binding of the label and reduction of its nonspecific binding. Given a specific set of binding partners, only the second of these two options remains. Adjustments to reagent preparation, however, can have drastic effects on the specificity and sensitivity of a given assay. This principle also holds in the case of the *in vivo* magnetorelaxometric assay. For example, as in Figure 4-9, if an *in vivo* assay is run utilizing a lower magnetic separation time (35 min. vs. 80 min.) and toxin:biotin ratio (1:0.75 vs. 1:1), as compared to the assay in Figure 4-6, both the background signal and the overall signal are reduced due to a reduction in aggregation on the MNPs, yet the plots show similar a similar signal:noise ratio of 2. If the toxin:biotin ratio is lowered even further to 1:0.5 with an identical magnetic separation

method, as in Figure 4-10, the aggregation is even further reduced resulting in a proportional decrease in both the signal and background. Finally, taking this into account and seeking to optimize the signal:noise ratio, the toxin:biotin ratio was maintained at 1:0.5, but the toxin conjugated MNPs were incubated in separate vials and dispensed into the microwells immediately prior to each measurement time by the SQUID system. This method resulted in the lowest background (~5 pT) and highest signal to noise ratio (~3), as is shown in Figure 4-11.

4.5 Conclusions

4.5.1 *In Vivo* Assay Development Summary and Conclusions

In this chapter, an *in vivo* magnetorelaxometric assay was proposed, developed and demonstrated using Cry5B toxin binding to wild type *C. elegans* as a model system. This is the first time an *in vivo* magnetorelaxometric assay has been successfully demonstrated. Through various means of modifying the MNP labeled toxin preparation parameters, an increasingly colloidally stable toxin conjugated MNP solution was developed resulting in a lower background signal and an increase in the quantitative signal to noise ratio of toxin binding to wild type nematodes versus mutants lacking the required binding receptor. The overall background was reduced by over a factor of 60 (318 to ~5pT at 100 minutes assay time) and the signal to noise increased from ~2.2 to over 3 (wild type/mutant; 142 minutes assay time).

The signal:noise ratio is somewhat less than anticipated and may be due to several peculiarities inherent in the chosen system, the first of which is uncertainties in the mechanism of binding of the Bt toxin to the gut cells. While it is known that these toxins form pores within the membranes of the gut cells it, the stability of the binding of the toxin to

surface carbohydrates prior to pore formation is unknown. Given a typical receptor-ligand kinetic reaction of:

$$R + L \underset{k_{off}}{\overset{k_{on}}{\rightleftarrows}} RL \tag{3.1}$$

and since the signal detected by the SQUID system is the gross number of immobilized MNPs, if the "off-rate," k_{off}, of the reaction is significantly large as compared to the on rate, k_{on}, that is $k_{on}>k_{off}$ not $k_{on}>>k_{off}$, then k_{on}/k_{off} and the association constant, K_a, will be small and at any given time the number of intact bonds will be small. An additional unknown is the number of Bt toxin receptors on each midgut cell, which, if small, proportionally lowers the number of bonds at a given time. These problems are additionally exacerbated by the presence of the magnetic label whose physical mass undergoes a shear stress when attached within a fluid such as the gut of the nematode, and thus requires more bonds to form within a given time in order to form a stable complex. Indeed, the number of bonds between a magnetically labeled toxin and a given cell, N, can be described by:

$$N = (160\lambda / k_B T)\left[\gamma / \ln(K_a \rho_r)\right](r^3{}_b / r_c) \tag{3.2}$$

where λ is the range/length of interaction between the toxin and the receptors, γ is the shear stress on the particle, K_a is the association constant, ρ_r is the receptor surface density, r_b is the radius of the particle, and r_c is the radius of the midgut cell (Cozensroberts, Quinn et al. 1990; Sarda, Pointu et al. 2004). From this equation, it is additionally important to note that if λ is small, viz. the binding length between the toxin and the surface carbohydrates involved in binding is small, the number of active bonds is proportionally affected and less MNPs will be immobilized at any given time. The second problem inherent in the system is related to the previously raised concern of the response of the organism, in that following ingestion the Bt toxin at a sufficient concentration, a wild type nematode will stop feeding within roughly 10

minutes, while the mutant nematode will continue to feed. This ultimately results in a limitation in the number of MNPs that can reach and bind to the midgut cells, and an increase in NSB to the mutant nematodes. This also precludes the possibility of a pseudo-homogeneous type assay of feeding the biotinylated toxin to the nematodes, followed by a chase with SA MP MNPs, as the concentration required for binding of the toxin would cease the feeding of the wild type nematodes.

4.5.2 Proposed Alternatives and Model Systems

While many of the issues encountered are peculiar to the *C. elegans* Bt toxin binding system, they act to emphasize the importance of choosing an appropriate model system. By simply choosing an alternative binding scheme, many of these problems could be circumvented. For example, in the case of antibody:antigen binding, λ is extended by the [known] length of antibodies and while K_a is not normally known exactly, it is typically quite high as opposed to the K_a of toxin:carbohydrate binding which is not known. The problem of the ceasing of feeding behavior would also not be an issue in the case of an antibody based detection scheme and allow for the binding to steady state based upon the above considerations. In light of these considerations, an alternative antibody based, scientifically important, binding scheme for *C. elegans* is being investigated and pursued.

This work serves as a model for the use of magnetorelaxometry in *in vivo* assays, including the use of other organisms. The aforementioned concerns act as general guidelines when choosing appropriate binding partners in any animal. While the experiments in this chapter were performed in microtiter wells, the exquisite sensitivity of the SQUID system, even at larger sample to sensor spacings (as shown in Figures 2-6 and 2-7), does not preclude the use of larger animals, including vertebrates, even humans. The ability to detect as few as 10^9

MNPs in a sample up to roughly 4cm from the sensor opens up a wide range of possibilities for its use in *in vivo* binding assays.

4.6 Acknowledgements

This work was supported by the NIH grant 1 R43 HL80655-01A1 NIH SBIR Phase I NHLBI "Ultra-sensitive assays using SQUID magnetic sensors". The work of Brad Barrows in isolation and purification of the Cry5B toxin, and culture of the nematodes was greatly appreciated and was critical to the conduction of this research.

A

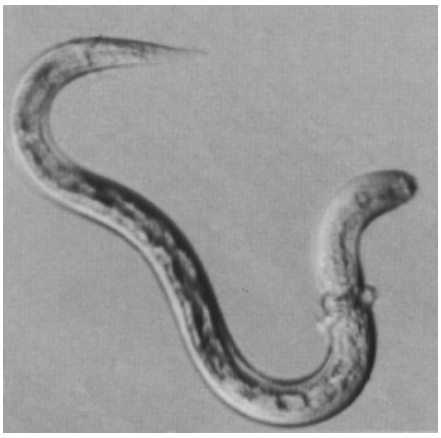

B

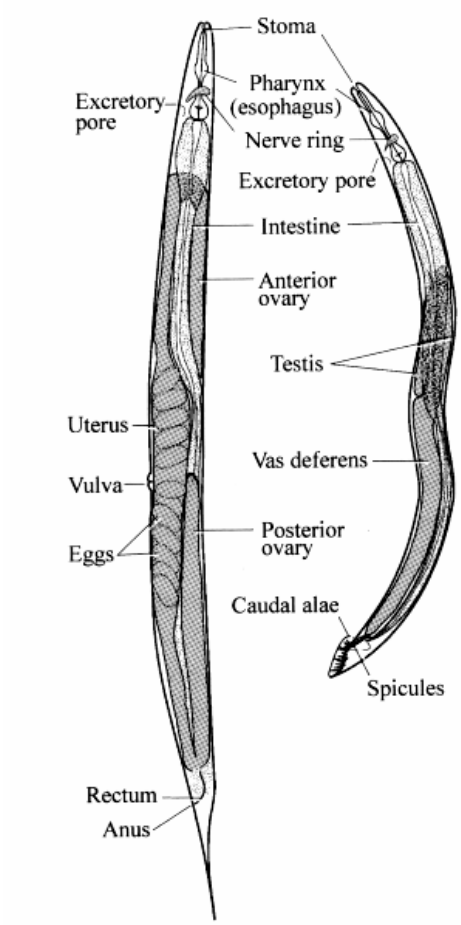

Figure 4-1. *Caenorhabditis Elegans* nematode anatomy. (A) Phase contrast image of a typical nematode. (B) Schematic of *C. elegans* full body anatomy with labeling of major structures. Adapted from (Chen, Chen et al. 2004).

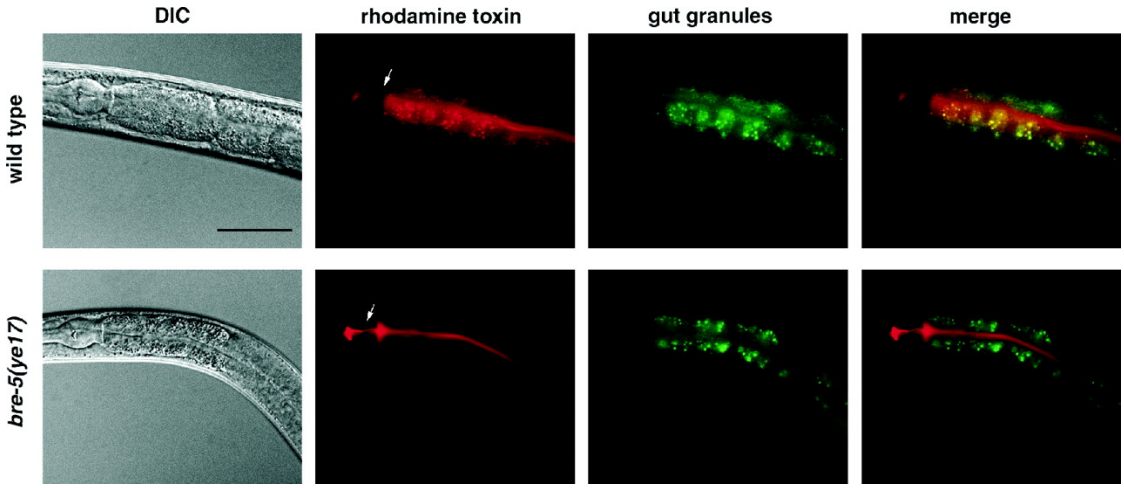

Figure 4-2. Binding of rhodamine labeled Cry5b toxin to wild-type *C. elegans* versus *bre-5* mutants. The toxin binds to and enters the wild-type gut cells and colocalizes with gut granules, but is confined to the lumen and does not bind to the gut cells in the mutant. Taken from (Griffitts, Whitacre et al. 2001).

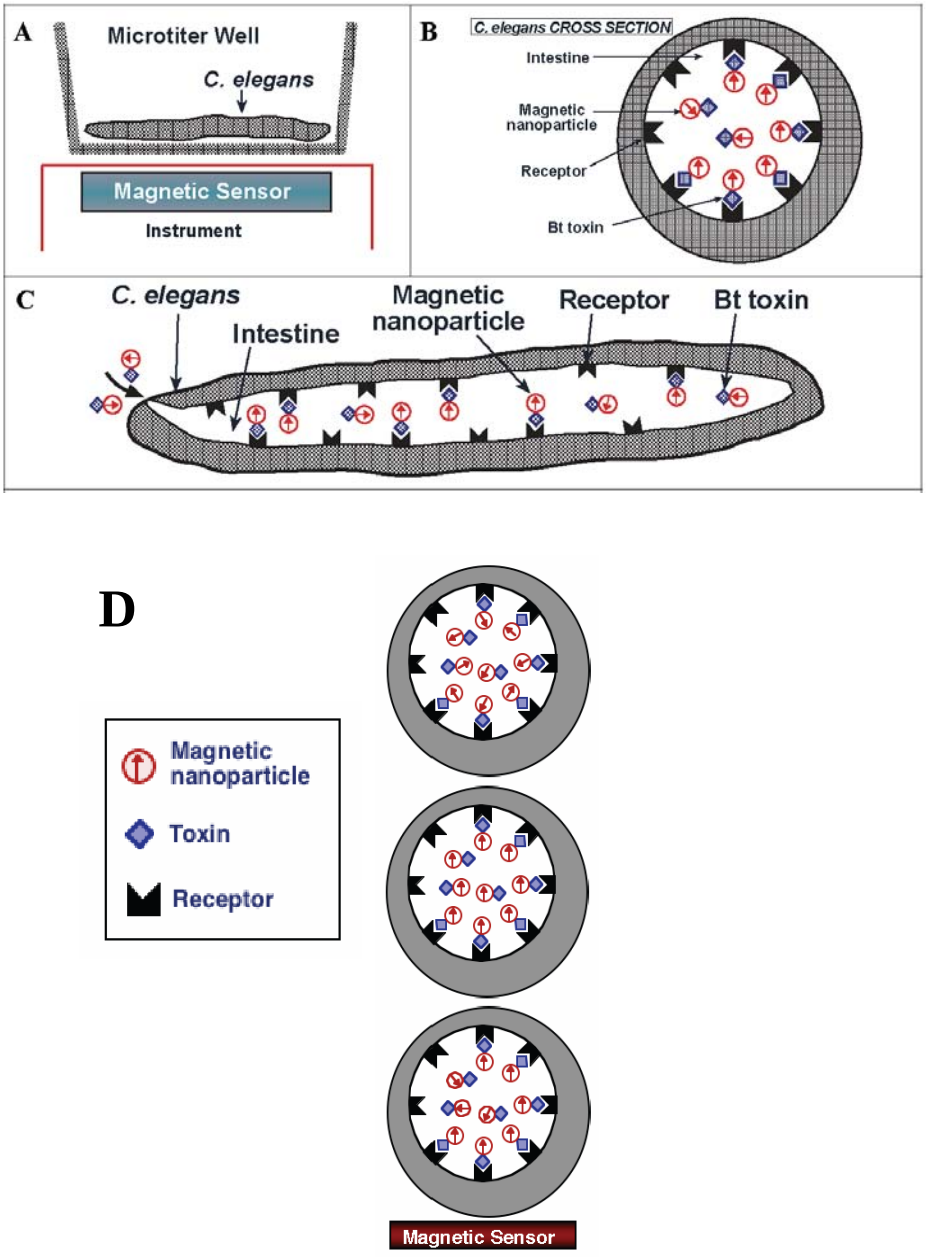

Figure 4-3. Schematic of the *in vivo* receptor assay in *C. elegans*. (A) Measurements are conducted by the SQUID system with the nematodes in microtiter wells. (B) Cross sectional view of MNP labeled Cry5B toxin inside the lumen of the nematode. (C) Side view of *C. elegans*, showing binding of the Cry5B toxin to the gut cell surface receptors. (D) Magnetorelaxometric measurements do not require removal of unbound labels, as, following magnetization, the labels quickly randomize and only the bound labels contribute to the net magnetic moment, as detected by the SQUID system

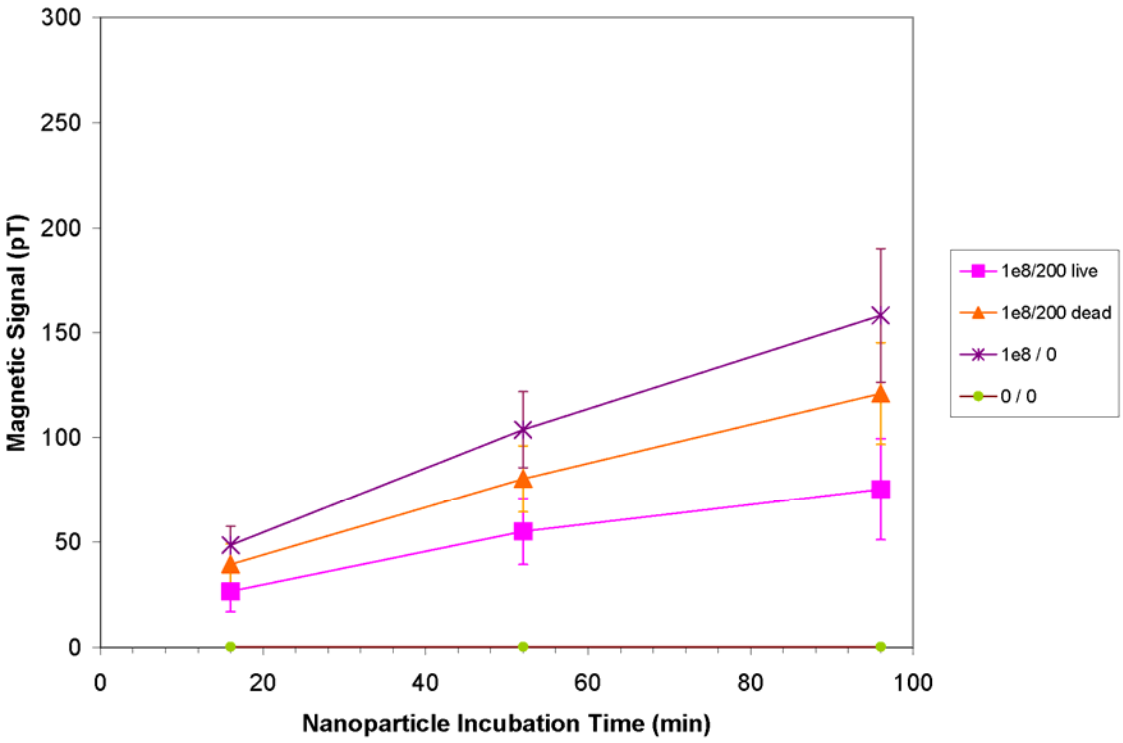

Figure 4-4. Nonspecific binding experiment of bare 140nm MNPs to live and dead wild-type *C. elegans* and to the well surface as compared to the system background (0/0).

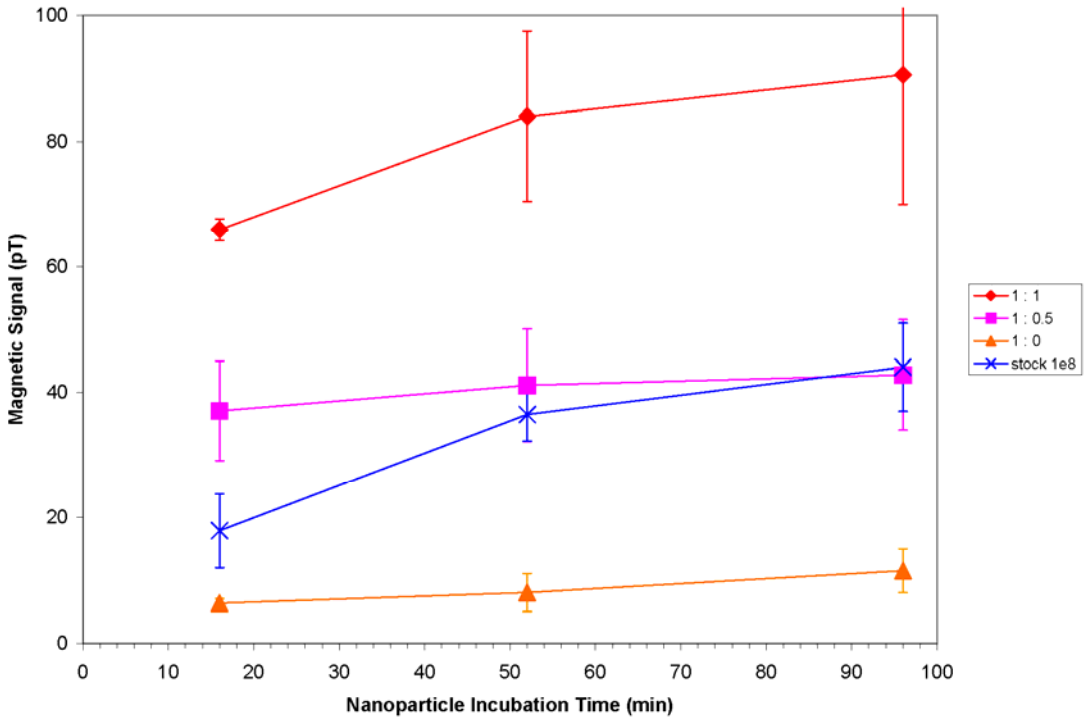

Figure 4-5. Effect of various toxin to biotin ratios on binding to wild-type *C. elegans*, as compared to bare 140nm MNPs.

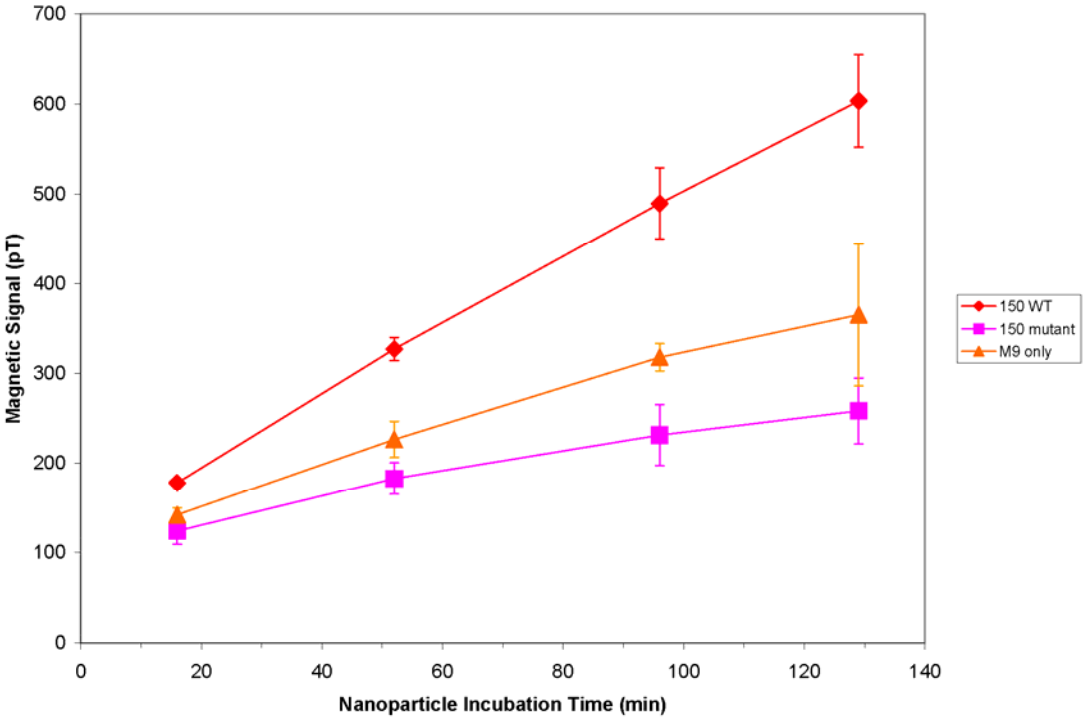

Figure 4-6. *In vivo* magnetorelaxometric assay showing differential binding of 1:1 biotinylated Cry5B toxin conjugated to 140nm MNPs to wild-type *C. elegans* versus *bre-5* mutants over time.

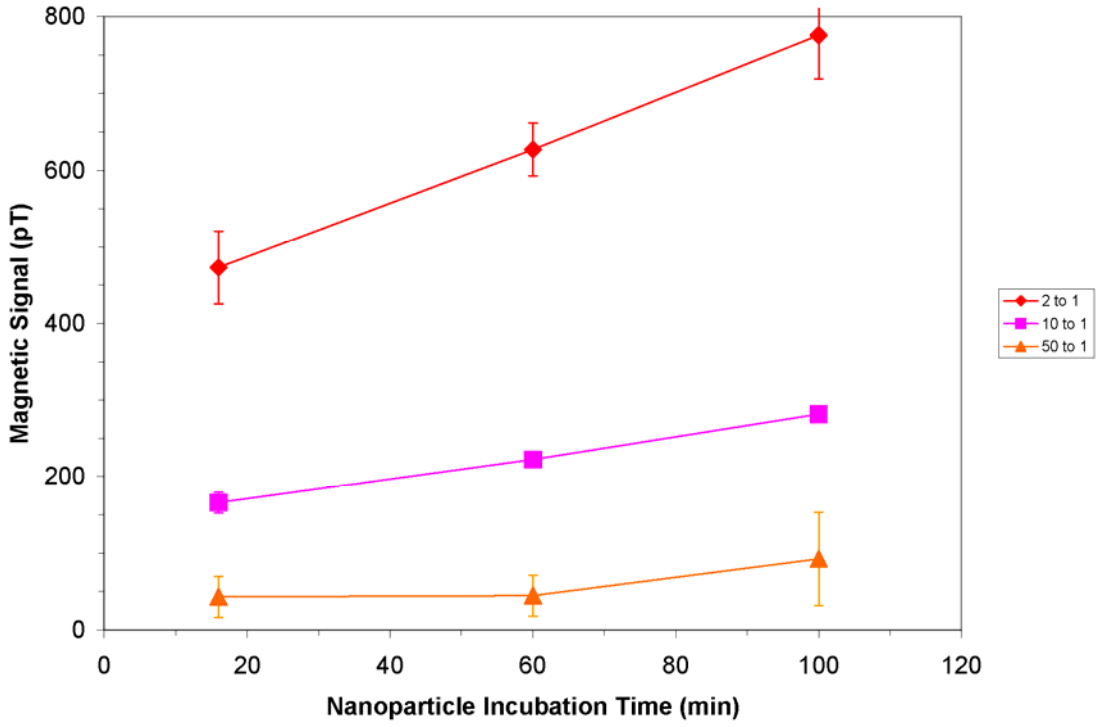

Figure 4-7. Magnetorelaxometric background signal versus time for various 1:1 biotinylated toxin to MNP binding site conjugation ratios. Higher ratios saturate the streptavidin sites on the MNPs and prevent crosslinking of the MNPs.

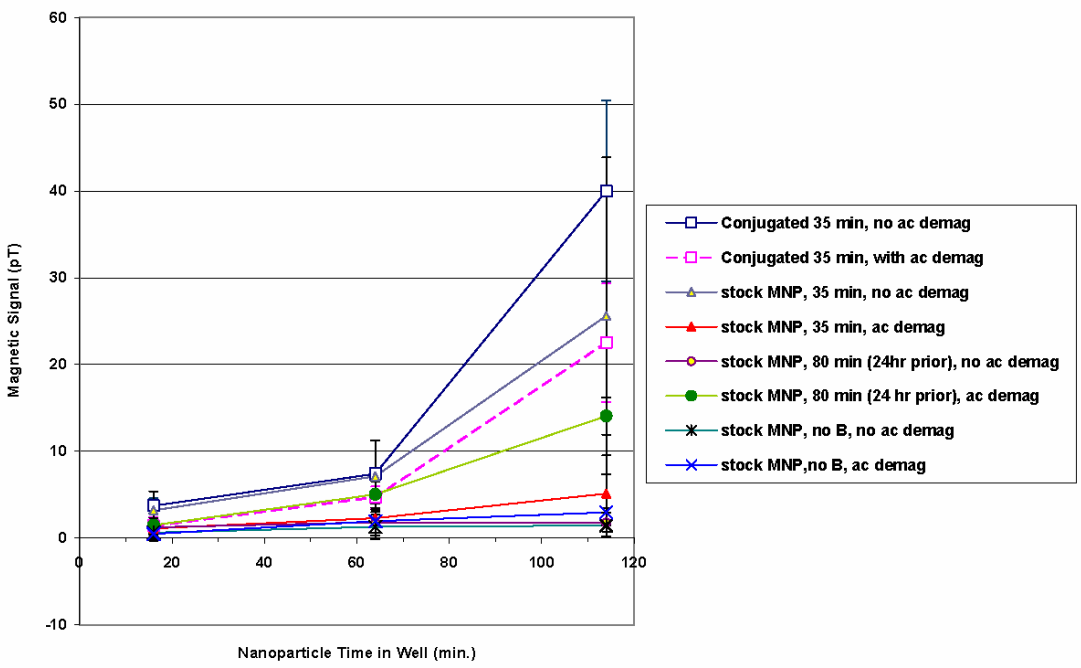

Figure 4-8. Effect of various magnetic decantation procedures and AC demagnetization upon magnetorelaxometric background signals over time. Lowest background levels were achieved by allowing the MNPs to relax over a 24 hour time period prior to measurement.

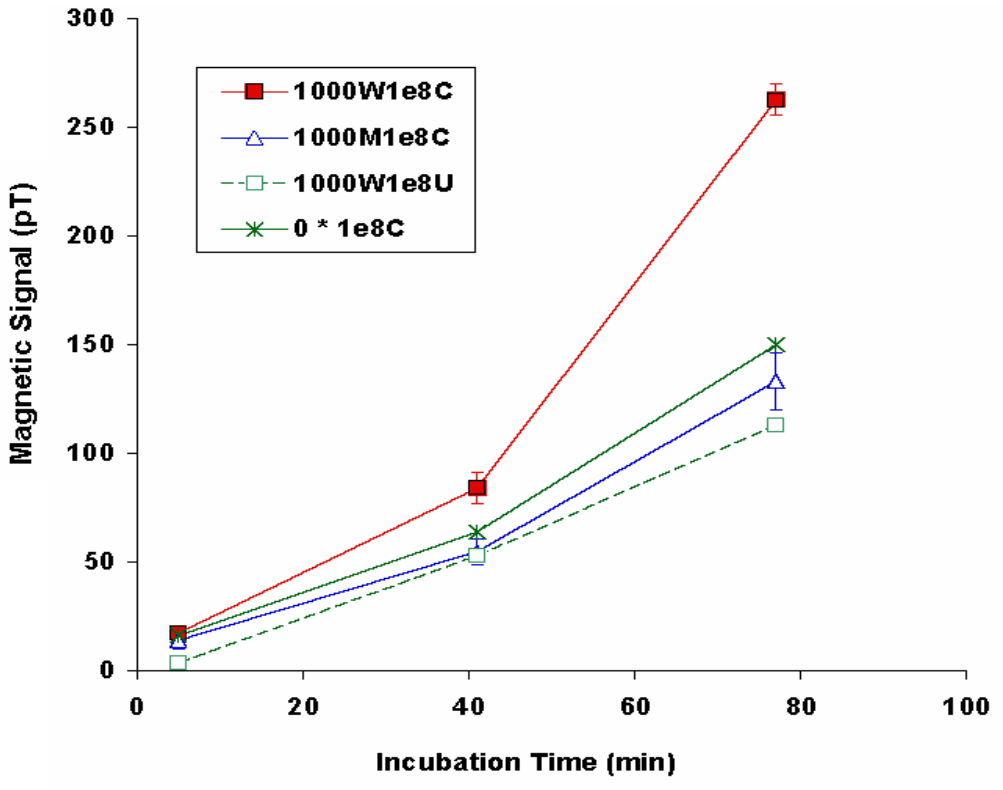

Figure 4-9. Magnetorelaxometric assay on *C. elegans* using 1:0.75 biotinylated toxin. Wild-type nematodes show greater binding of MNP labeled toxin than mutants or when wild-type nematodes are incubated with bare MNPs.

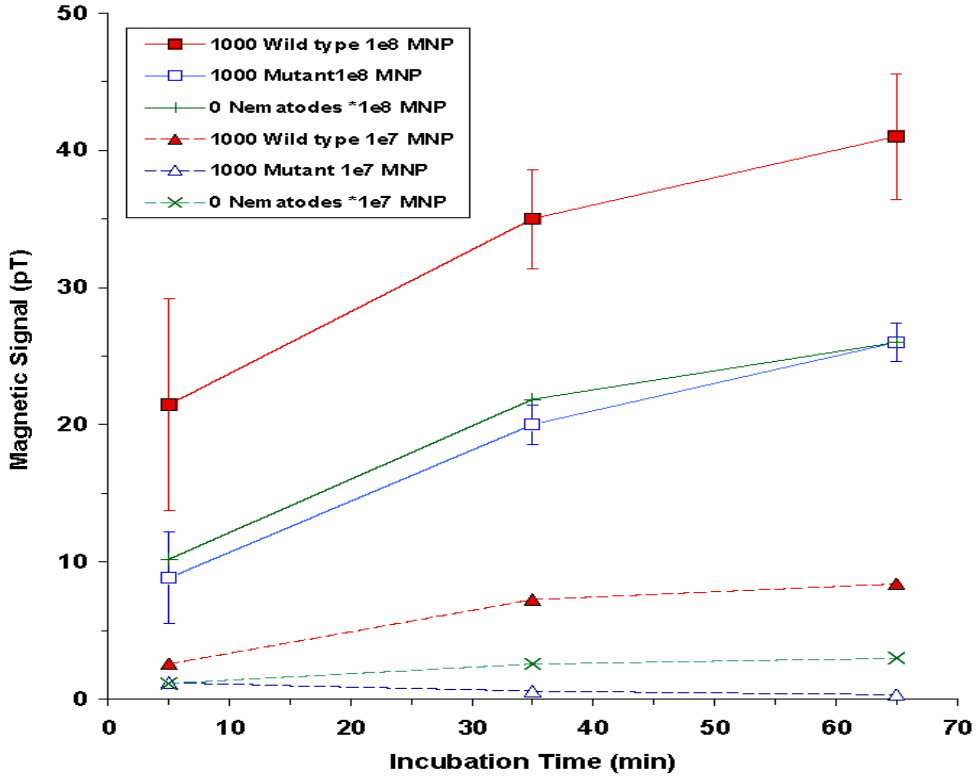

Figure 4-10. Magnetorelaxometric assay data on *C. elegans* using 1:0.5 biotinylated toxin, showing differential binding of wild-type nematodes over mutants. Top three traces show data using 10^8 MNPs per sample, while the bottom three used 10^7 per sample. Lower biotinylation ratio reduces background and signal.

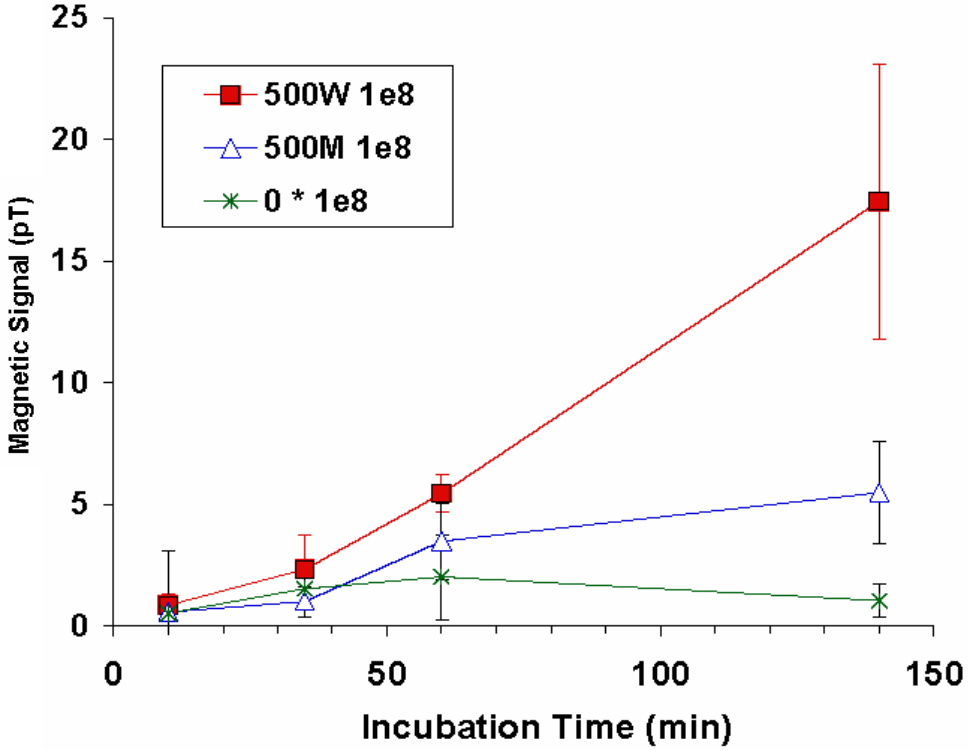

Figure 4-11. Magnetorelaxometric assay on *C. elegans* using 1:0.5 biotinylated toxin and background reducing conjugation procedures. Optimization of conjugation resulted in a signal to noise of >3.

CHAPTER 5

IN SITU-INTRACELLULAR DELIVERY OF MAGNETIC NANOPARTICLES AND INTRACELLULAR MAGNETORELAXOMETRY

5.1 Abstract

In the previous chapters, magnetorelaxometric assays were demonstrated for the detection of cells in solution and for binding interactions in a model organism, i.e., for *in vitro* and *in vivo* assays. Both of these paradigms utilized extracellular binding targets to magnetically quantify the total number of cells or binding interactions in the chosen systems. In this chapter, the utility of magnetorelaxometric assays is further developed and demonstrated to include the detection of intracellular proteins in livings cells in real time, viz. *in situ* detection of intracellular protein. Initial experiments are carried out to evaluate the long term cytotoxicity and the effect that the delivery of synthesized anionic magnetic nanoparticles into the intracellular space of a model cell system (PC12 cells) has upon the ability of those cells to respond to a specific biochemical cue, namely nerve growth factor. General conclusions as to the use of magnetic nanoparticles in *in vivo* and phenotypic dependent *in vitro* applications are then drawn. Using separate synthesis and delivery mechanisms, magnetic nanoparticles are then conjugated with a cell penetrating peptide, TAT, alone or with an antibody to the intracellular protein tubulin and delivered into the intracellular space

of living cells. Several issues specifically pertaining to the effect that TAT conjugation has upon the colloidal stability, nonspecific binding and intracellular delivery efficiency of the magnetic nanoparticles are addressed and resolved by adjusting various conjugation and assay parameters. Following delivery of the magnetic nanoparticles into the intracellular space, magnetorelaxometric measurements are taken to determine the extent of both nonspecific and tubulin specific nanoparticle binding within the cells. These results are discussed and the limitations of and future considerations for intracellular magnetorelaxometry are then proposed and discussed.

5.2 Introduction

The delivery of magnetic nanoparticles (MNPs) to or into various cell types has become an area of increasing interest in the biomedical sciences (Berry and Curtis 2003; Pankhurst, Connolly et al. 2003; Tartaj, del Puerto Morales et al. 2003; Ito, Shinkai et al. 2005). Targeted drug/gene delivery is used to deliver drugs or genes regio-specifically by attaching them to magnetic nanoparticles and locally concentrating the resulting complexes *in vivo* to the desired locale (Scherer, Anton et al. 2002; Krotz, Sohn et al. 2003; Vasir and Labhasetwar 2005; Dobson 2006). Similarly, magnetic hyperthermia, the local concentration of magnetic nanoparticles and subsequent heating via AC magnetic fields, has shown promise as a potentially viable cancer therapy (Jordan, Scholz et al. 1999; Moroz, Jones et al. 2002). And it has additionally been shown that if cells are labeled with large enough numbers of magnetic nanoparticles, that these cells can be located, tracked and recovered using high resolution imaging techniques, such as high-resolution magnetic resonance imaging (MRI) (Hsu, Dodd et al. 2000; Lewin, Carlesso et al. 2000; Kircher, Allport et al. 2002). The "action at a distance" properties of MNPs and the lack of interference of biological entities make the use of MNPs an attractive option for the manipulation of and interaction with living cells.

The delivery of MNPs into and interaction with living cells, however, poses several technical challenges and naturally raises concern over the effects of their intimate contact with cellular machinery. In light of these considerations, the potential utility of MNP mediated cellular applications should stimulate interest in both the development of these applications, as well as careful evaluation of the limitations and risks, particularly for *in vivo* uses, inherent in such uses of MNPs. This chapter addresses and evaluates both general cytotoxicological issues of MNPs and the use of a construct for a specific biomedical application, namely the detection and quantification of intracellular protein in living cells via magnetorelaxometry.

5.3 Intracellular Delivery and Cellular Toxicity of Anionic Magnetic Nanoparticles

In numerous applications, much effort has been dedicated to the development of efficient mechanisms of both passive and active delivery of MNPs into cells of interest. For example in cell tracking via high resolution MRI, cells of interest must be labeled with relatively large amounts of magnetic material in order to be readily detected. Moreover, both targeted drug delivery and hyperthermia require very large amounts of MNPs to be injected or targeted to the area of interest. While there is obvious reason for concern over the containment of drug treatment or hyperthermic damage to the region of interest, the surrounding healthy tissue must also necessarily be exposed to high concentrations of MNPs. Iron oxide is normally considered to be safe for *in vivo* use, but the effects of moderate to high concentrations of iron oxide upon cell function remain to be adequately elucidated. Although a few studies have been performed investigating the acute cytotoxicity of magnetic nanoparticles and their qualitative effects upon cellular morphology, little work has focused on quantifying the effects

that iron oxide internalization has upon cell behavior and, in particular, the ability of cells to appropriately respond to biological cues.

Many groups have investigated the use of various organic coatings as a means of optimizing the delivery of MNPs to or into cells. In some instances, MNPs have been coated with ligands to cell surface receptors in order to utilize a receptor mediated endocytotic pathway versus the slower passive internalization via fluid phase endocytosis (Kohler, Sun et al. 2005; Sonvico, Mornet et al. 2005). More notably, MNPs have been modified to allow their free passage into cells using lipophilic coatings such as polyethylene glycol (PEG) (Gupta and Curtis 2004; Zhang, Sun et al. 2004) or dendrimers (Bulte, Douglas et al. 2001), or with well-known transfection agents such as the HIV derived TAT protein (Josephson, Tung et al. 1999; Lewin, Carlesso et al. 2000; Kircher, Allport et al. 2002; Zhao, Kircher et al. 2002). In several cases it has been shown that even a simple dimercaptosuccinic acid (DMSA) coating, as performed in Section 2.4, can vastly improve uptake efficiency (Wilhelm, Gazeau et al. 2002; Billotey, Wilhelm et al. 2003; Wilhelm, Billotey et al. 2003), presumably by endowing the MNPs with an anionic charge, resulting in nonspecific adsorption to the cell surface followed by endocytosis into the cell. Indeed these techniques succeed in delivering large numbers of MNPs into the cells (up to 3-4 orders of magnitude over fluid phase endocytosis), but a valid concern arises over the effects that large intracellular concentrations of iron oxide might have upon normal cell behavior. While it is currently generally accepted that magnetic nanoparticles produce little to no *in vivo* toxicity (Lacava, Azevedo et al. 1999; Kim, Yoon et al. 2006), very little research has been presented on the effects that magnetic nanoparticles have upon normal cellular function and phenotype. The literature that does exist has either mainly investigated only the viabilities of cells exposed to MNPs for extended periods of time (several days) or presents mainly qualitative data such as scanning electron micrographs or immunostaining of exposed cells. In particular, several groups, such as Hilger et al. have

shown that the nanoparticle coatings themselves can have significant effects upon cell viability (Hilger, Fruhauf et al. 2003). In a series of papers, Curtis and Wells studied the effects that various nanoparticle surface coatings had on cellular morphology, uptake efficiency, cytotoxicity and, in one case, cell mobility (Berry, Wells et al. 2003; Berry, Wells et al. 2004; Gupta and Curtis 2004). Indeed, these papers have shown that nanoparticles and the surface coatings employed can have a dramatic effect upon the *relative* cell behavior and morphology. More quantitatively, Hussain et. al. presented data on the effects that various metal/metal oxide nanomaterials had upon liver cell function *in vitro* (Hussain, Hess et al. 2005). Here we demonstrate with a given nanoparticle that these changes in cell behavior and phenotype can be quantified and directly correlated with the level of AMNP exposure.

In order to clearly evaluate the effects that iron oxide nanoparticle internalization might have upon cell behavior, phenotype and response to biological cues, a readily quantifiable model cell system was chosen. The PC12 pheochromocytoma line is a clonal cell line originally derived from a rat adrenal medullary tumor and established by Greene and Tischler in 1976 as paradigm for neurobiological and neurochemical studies. The most notable characteristic of PC12 cells is their well-characterized rapid and reversible response to nerve growth factor (NGF), resulting in the extension of neurite-like processes typical of sympathetic neurons (Tischler and Greene 1975). Under normal culture conditions, these processes can reach several hundred microns to up to 1 cm in length. This profound and easily observable response makes PC12 cells an ideal model system for the study of neural stem cell development and differentiation, neurite regulation and outgrowth, and as a general model of cell response to biochemical cues. In addition to general cell morphology, there exist previously reported specific quantifiable criteria when evaluating the response of PC12 cells to NGF, including: neurite length, number of neurites or “sprouts” extending from cell body,

number of branches per neurite, number of intercellular processes and quantification of NGF-induced expression of specific proteins.

Enhanced endocytosis via [anionic] DMSA coating is a simple, efficient and well-characterized method of intracellular delivery of iron oxide (Fe_2O_3) nanoparticles. While several studies have clearly shown little to no *in vivo* toxicity of either of these components individually (Aposhian and Aposhian 1990; Lacava, Azevedo et al. 1999; Kim, Yoon et al. 2006), only recently have they been combined to deliver large numbers of nanoparticles into cells. Although the precise mechanism by which DMSA coatings enhance internalization remains to be elucidated, these coatings have been purported to deliver upwards of three orders of magnitude more iron oxide into cells as compared to nanoparticles lacking coatings (Wilhelm, Billotey et al. 2003). Here, the specific effects that DMSA coated MNPs have upon cultured PC12 cells are examined and the ability of these cells to respond to NGF as compared to control cells is evaluated. More specifically, the effects that various DMSA coated MNP concentrations have upon: cellular cytoskeletal structure, cell viability, ability of cells to generate neurite processes, the lengths of these neurites, the average number of sub-branches from each neurite, the average number of intercellular contacts per-cell, and the expression of the growth-associated protein GAP-43 are compared and contrasted.

5.3.1 Materials and Methods

5.3.1.1 Anionic Magnetic Nanoparticle Synthesis

Maghemite nanoparticles were synthesized, as previously described above and in (Massart 1981; Massart 1982). Two starting solutions were made by adding 5.406 g of $FeCl_3$ (Sigma-Aldrich, St. Louis, MO) to 20ml of deionized (DI) water and, separately, adding 1.988g of $FeCl_2$ (Sigma-Aldrich, St. Louis, MO) to 5ml of a 2N solution of HCl (Sigma-Aldrich, St. Louis,

MO). These solutions were then added to 100ml of DI water under vigorous stirring, to which 120ml of a 2M ammonia solution was added and remained under vigorous stirring for 5 minutes, during which, a black precipitate formed, indicating the synthesis of Fe_3O_4. This solution was centrifuged at 900g for 5 minutes, the supernatant was removed and the nanoparticle solution was redispersed in DI water. This solution was centrifuged at 900g for 5 minutes and resuspended in DI water. This washing process was repeated 4 additional times and the centrifugate was finally resuspended in 35 ml of DI water, resulting in an opaque black solution. This solution was heated to 80°C and the MNPs were oxidized to Fe_2O_3 by bubbling oxygen for 2 hours. The mass of resulting maghemite was determined (through drying and weighing) to be 1.68g of Fe_2O_3 in 50ml of DI water. DMSA coating was performed as previously described (Fauconnier, Pons et al. 1997). Separately, 0.26g of DMSA (Sigma-Aldrich, St. Louis, MO) was added to 313ml of deoxygenated DI water (via 1 hour of nitrogen bubbling) and 205ml of deoxygenated DI water was added to the maghemite solution. These solutions were deoxygenated for an additional 2 hours at room temperature. The maghemite solution was then vigorously stirred while bubbling nitrogen and the pH of both solutions was adjusted to 3.0 with HNO_3 prior to mixing the solutions under vigorous stirring with constant nitrogen bubbling. The reaction was allowed to proceed for 30 minutes and the resulting mixture was spun down at 800g for 5 minutes and resuspended in 200ml of DI water. Under constant stirring, the pH of this solution was adjusted with NaOH to 9.25-9.5 and maintained for 30 minutes before lowering the pH to 7.4 with HCl. The resulting solution was centrifuged at 1000g for 10 minutes to remove any precipitated aggregates and the resulting opaque dark brown supernatant was deoxygenated and stored with nitrogen at 4°C. The final concentration of Fe_2O_3 was adjusted with DI water to 75mM or 150mM Fe concentration.

5.3.1.2 PC12 Cell Culture

The rat pheochromocytoma cell line PC12 was grown in high-glucose Dulbecco's Modified Eagles Medium (DMEM) (Gibco, Grand Island, NY) containing 10% fetal bovine serum (FBS) (Invitrogen, Carlsbad, CA), 5% heat-inactivated horse serum (Omega Scientific Inc., Tarzana, CA), 100 U/ml penicillin and 100 mg/ml streptomycin (Gibco, Grand Island, NY) at 37°C in 5% CO_2 until reaching 70% confluence.

5.3.1.3 Delivery of Anionic Magnetic Nanoparticles into PC12 Cells

PC12 cells were plated from culture at a concentration of approximately 20,000 cells/ml into 6 or 24 wells in high-glucose Dulbecco's Modified Eagles Medium (DMEM) (Gibco, Grand Island, NY) containing 10% fetal bovine serum (FBS) (Invitrogen, Carlsbad, CA), 5% heat-inactivated horse serum (Omega Scientific Inc., Tarzana, CA), 100 U/ml penicillin and 100 mg/ml streptomycin (Gibco, Grand Island, NY) at 37°C and allowed to adhere for 2 days. The following day, the cells were washed and the media was replaced with serum and phosphate free HEPES buffered DMEM (Invitrogen, Carlsbad, CA) in order to prevent particle agglomeration. To this solution a concentrated stock solution of AMNPs was added, yielding final iron concentrations of 15mM, 1.5mM and 150μM, as well as a phosphate-free DMEM control. After overnight incubation, the cells were washed and the modified DMEM was replaced with media containing 1% FBS, 5% heat inactivated horse serum, 1% penicillin-streptomycin and nerve growth factor (NGF) (Sigma-Aldrich, St. Louis, MO), was added to a working concentration of 100ng/ml to induce sprouting. The cells were cultured with this media, including changes every other day, for the remainder of each experiment.

5.3.1.4 Transmission Electron Microscopy

Cells were fixed in an aqueous solution of 100mM sodium cacodylate (Sigma-Aldrich, St. Louis, MO) containing 2% paraformaldehyde (Sigma-Aldrich, St. Louis, MO) and 2% glutaraldehyde (Sigma-Aldrich, St. Louis, MO) at 37°C for 2 minutes and then allowed to cool to room temperature for 25 minutes. The cells were then washed 3 times in ice cold 100mM cacodylate buffer and kept on ice. Cells were then post-fixed in ice cold 100mM sodium cacodylate containing 1% osmium tetroxide (Sigma-Aldrich, St. Louis, MO) for 30 minutes on ice and then washed 3 times with ice cold DI water followed by a 30 minute post fixation in 2% uranyl acetate (Fluka, Seelze, Switzerland) and another three washes with ice cold DI water. The samples were then serially dehydrated in ethanol at room temperature and finally embedded in Durcupan (Fluka, Seelze, Switzerland), which was sectioned prior to TEM analysis. The samples were then placed onto a carbon TEM grid and were observed using a transmission electron microscope (TEM) (JEOL 200CX operated at 180-200 KV).

5.3.1.5 Live/Dead Cell Staining

Prior to, 2, 4 and 6 days following AMNP exposure, the cells were first washed in PBS at 37°C and left in 1ml of PBS/well. Calcein AM and ethidium homodimer-1 (Ethyl-D) were used from a LIVE/DEAD Viability/Cytotoxicity Kit (Invitrogen, Carlsbad, CA) and diluted with PBS to a final concentration of 10μM each. Each well was aspirated and 20μl of both stain solutions was added to each well and incubated at 37°C for 20 minutes. The samples were analyzed via fluorescent microscopy with appropriate fluorescent filter cubes (FITC cube for calcein, TRITC cube for Ethyl-D). A total of at least 300 cells were counted per condition per sample per timepoint, with green fluorescence (emission 515nm) indicating living cells and red fluorescence (emission 635nm) indicating dead cells.

5.3.1.6 Fluorescent Microscopy

The PC12 cells were plated as described above into wells containing sterile glass coverslips. 2 days, 4 days and 6 days following AMNP exposure the coverslips from particular wells of each exposure condition were removed and extracted in a solution of 10mM 2-morpholinoethanesulfonic acid (MES) buffer (Sigma-Aldrich, St. Louis, MO), 138mM KCl, 3mM $MgCl_2$, 2mM EDTA, 320mM sucrose for 45 seconds, followed by fixation in the same buffer containing 4% formaldehyde for 15 minutes. The coverslips were then washed once in Tris buffered saline (TBS) (150mM NaCl, 20mM Tris-HCl, pH 7.4) and stored in TBS at 4°C until staining. At the time of staining, the samples were permeabilized in a solution of TBS containing 0.5% Triton-X 100 (TX) for 10 minutes and then rinsed 3 times in TBS containing 0.1% TX for 4 minutes each rinse. The samples were then blocked in a solution of TBS-0.1% TX with 2% BSA (Sigma-Aldrich, St. Louis, MO), and 0.1% sodium azide (Sigma-Aldrich, St. Louis, MO) for 10 minutes, followed by incubation for 20 minutes with mouse anti-tubulin (Molecular Probes, Eugene, OR) diluted to 1 µg/ml in the blocking buffer. The samples were then washed four times in TBS-0.1% TX and fluorescein conjugated anti-mouse secondary antibody was then added at 5µg/ml of blocking buffer and incubated for 20 minutes. The samples were washed 4 times in TBS-0.1% TX and then incubated with rhodamine-phalloidin diluted in blocking buffer to 1µg/ml for 20 minutes and then washed twice in TBS-0.1% TX. Finally the samples were rinsed once in TBS, once in DI water, drained and mounted onto glass slides. The samples were then analyzed by standard fluorescent microscopy at 100X with fluorescein and rhodamine filter cubes, for microtubules and actin, respectively.

5.3.1.7 Neurite Analysis

Six days following exposure to AMNPs, the samples were analyzed via phase contrast microscopy at a magnification of 10X. Micrographs of random areas of the culture plates were

taken and subsequently analyzed with ImageJ (NIH, Bethesda, MD) for number of neurites per cell, length per neurite and number of intercellular processes per cell. Depending on the growth characteristics, 30-50 cells were analyzed for each parameter for each experimental condition.

5.3.1.8 Western Blot

Six days following exposure to AMNPs, cells were lysed in a 50mM Tris-HCl buffer containing 10% glycerol, 0.1% sodium dodecyl sulfate (SDS) (Sigma-Aldrich, St. Louis, MO), 1% Triton X-100, 150mM NaCl, 1.5mM $MgCl_2$, and protease inhibitors [2μg/ml aprotinin, 50μM leupeptin, 1μM pepstatin, 10mM phenylmethylsulfonyl fluoride (PMSF) and 5mM EDTA]. The samples were then reduced in 10% β-mercaptoethanol and centrifuged at 13,000 RPM for 5 minutes. 30μg of protein was added to each lane of 10% SDS-polyacrylamide gel and underwent electrophoresis at 160V for 90 minutes. The separated protein was then transferred to nitrocellulose membrane at 50V for 1 hour in a Tris-glycine transfer buffer (Invitrogen, Carlsbad, CA) containing 12mM Tris base, 95mM glycine, and 20% methanol. The gels were then blocked in 5% nonfat dry milk (Bio-Rad, Hercules, CA) for 1 hour and incubated overnight at 4°C with anti-GAP-43 antibody diluted 1:1000 in a 1% BSA solution. Horseradish peroxidase conjugated goat anti-mouse IgG (ECL Kit; Amersham, Arlington Heights, IL) was then applied for 1 hour at room temperature. The blots were developed in luminal and exposed to Hyperfilm ECL (Amersham, Arlington Heights, IL). The molecular weights were compared with prestained low-range standards (Bio-Rad).

5.3.2 Results

As previously stated, AMNPs have been shown to be readily taken up by a variety of cells via an endocytotic mechanism. The internalization of AMNPs by PC12 cells was verified

using transmission electron microscopy (TEM). Figure 5-1 shows large numbers of AMNPs free within the cytoplasm and contained inside numerous endosomes within the cells. It was additionally noted that the intracellular levels of AMNPs were qualitatively proportionate to the added concentrations of the particles (data not shown).

5.3.2.1 Acute Cytotoxicity

In the initial assessment into the effects of AMNP internalization, standard cytotoxicological evaluations of acute toxicity to the cells were performed using a fluorescent live/dead stain. Fluorescent images of cells stained with a live (green) and dead (red) stain 6 days after AMNP exposure are shown in Figures 5-2A (15 mM iron concentration) and 2B (Control cells). Assessment of cell viability (n=300 per timepoint) through a series of experiments demonstrates statistically significant reductions in PC12 cell viability after exposure to the particles (Figure 5-2C). Almost all observed cell death occurs within the first 48 hours following incubation with the particles and the total observed cell death increases as a function of AMNP exposure concentration. Additionally, significant cell detachment was observed and quantified as a function of the concentration of added AMNPs, as shown in Figure 5-2D.

5.3.2.2 Alterations in Cytoskeletal Structure

In addition to PC12 cell viability, their phenotype and ability to respond to NGF were also affected by medium to high concentrations of AMNPs. In order to quantify phenotypic changes of PC12 cells in response to NGF, previously published methods of evaluation were employed (Shubayev and Myers 2004). Initially, prior to NGF exposure, the cells are undifferentiated, spherical in shape and do not produce neurites , as seen in Figure 5-3A -NGF. Following exposure to NGF, as shown in Figure 5-3A +NGF, PC12 cells differentiate

into neuronal type cells and begin to extend neurites into the periphery. Cellular morphology and cytoskeletal structure at various timepoints were investigated using immunofluorescence for tubulin (fluorescein, green) and rhodamine (TRITC labeled phalloidin, red) (Figures 5-3B-D). Figures 5-3B-D clearly indicate the dramatic reduction in PC12 cell ability to generate neurites following NGF induction with increasing concentrations of AMNPs. Upon increasing AMNP concentrations, the cells assume an increasingly spheroidal shape, thus minimizing cell surface area and contact with the media. While the perinuclear cytoskeletal structure of cells exposed to an iron concentration of 15mM (Figure 5-3D) appear intact relative to control, the cells exhibit little to no axonal sprouting and fail to form neurites. At [Fe] = 1.5mM, the cells have a diminished ability to form mature neurites, while at 0.15mM and below there are no qualitatively visible morphological differences when compared to control cells.

5.3.2.3 Diminished Cellular Response to a Specific Biochemical Cue

While previous reports have also shown qualitative disruption of the cytoskeleton due to exposure to high concentrations of magnetic nanoparticles (Zhang, Kohler et al. 2002; Berry, Wells et al. 2003; Berry, Wells et al. 2004; Gupta and Curtis 2004), this study investigates methods of quantifying phenotypic changes in cells as a function of nanoparticle concentration. Based on previous literature (Shubayev and Myers 2004), the following parameters were used to evaluate these phenotypic changes: frequency of neurite lengths, the number of neurites or "sprouts" extending from cell body, the number of branches per neurite, the number of intercellular processes and quantification of NGF-induced expression of specific proteins.

The most obvious effect that exposure to the AMNPs has upon the cells is their ability to generate mature neurites. The average number of neurites which sprouted from each [remaining] live cell (dead cells were not included) was measured at each of the three

concentrations and compared with media only control (Figure 5-4). Figure 5-4A shows a typical NGF-stimulated PC12 cell in culture with arrows showing the location of its neurites (N) and a line delineating the length of an extended neurite. The data from this evaluation, plotted in Figure 5-4B, shows the effect of AMNPs on the generation of neurites. Of the live cells evaluated, those exposed to 0.15mM, 1.5 mM, and 15mM AMNP iron concentrations on average produced 2.67, 1.9, 0.97 neurites per cell (n=30 cells/condition), respectively, as compared with 2.79 in the control cells. The lengths of the neurites which did extend were further evaluated, as shown in Figure 5-4A. Of those cells which did sprout neurites (nonsprouting cells were not included), not only were there fewer neurites per cell, but the lengths of the neurites which did extend, were dramatically affected by exposure to AMNPs. In Figure 5-4C, an inverse correlation between the level of AMNP exposure and the ability of the cells to respond normally to NGF and extend neurites into the periphery is seen. The histogram shows the frequency of neurite lengths of cells exposed to AMNP concentrations. Notice the increasing inability of PC12 cells exposed to higher AMNP concentrations (≥1.5 mM iron) to develop mature extended neurites, once again clearly indicating a negative feedback mechanism between AMNP exposure and the production of neurites.

Similar to most neuronal type cells, the neurites of PC12 cells typically branch out in order to establish intercellular contacts. Such branching is vital to the formation of neuromuscular connections, synaptogenesis, neurite extension, regeneration and signal transduction associated with these processes. As such, formation of intercellular contacts is considered a metric of PC12 cell and neuronal morphology. Additionally, it has been readily verified that disruption of these abilities results in diminished *in vivo* function and utility of neuronal type cells. Typical intercellular contacts (IC) for control cells (0 mM Fe) are shown in figured 5-5A. Figure 5-5B shows that nanoparticle exposure reduces the ability of neurites to develop intercellular contacts and thus physically interact with one another. When plated at a standard

density, the cells exposed to AMNPs fail to develop intercellular contacts at the same frequency as control cells. For each condition, the contacts (as indicated in Figure 5-5A) of over 250 cells were tallied and divided by the total number of cells. Even exposure to the most moderate of AMNP concentrations results in an over 30% reduction in intercellular contacts per cell (1.01 contacts/cell for control compared with 0.67 contacts/cell in 0.15 mM treated cells), likewise, higher concentrations further diminish intercellular communication (1.5mM:0.31 contacts/cell; 15mM:0.09 contacts/cell).

Lastly considered were the effects of AMNP exposure on the expression of protein related to axonal sprouting and neuronal function in order to determine whether the effects of exposure were strictly morphological or phenotypic as well. Growth Associated Protein – 43 (GAP-43) is a neuronal protein associated with axonal growth, neuronal plasticity and learning and is necessary for the development and function of a variety of neuronal systems. GAP-43 has also been shown to be an efficient marker for the presence of neuronal growth cones. Figure 5-6 (A, B) demonstrates a western blot of PC12 cell lysates using a monoclonal mouse anti-GAP-43 antibody, 6 days following exposure to various concentrations of AMNPs. HRP-tagged SDS-PAGE standards were used as molecular weight markers and β-actin blots were used as loading controls. Notice the decline in GAP-43 protein expression following exposure to increasing concentrations of AMNPs. Specifically, 0.15 mM AMNP iron concentration showed a GAP-43 band intensity comparable to the untreated control (C) and at [Fe]=1.5mM band intensity was significantly diminished, whereas GAP-43 levels were virtually undetectable in cells exposed to AMNPs at [Fe]=15mM.

It should be noted that, consistent with earlier literature (Aposhian and Aposhian 1990), it was independently verified that DMSA concentrations (7.5, 75 and 750 μM) that are equivalent to or higher than the net concentrations of DMSA in experiments have little to no measurable effect on the parameters tested in these studies. While this certainly does not

exclude the possibility that DMSA might have an effect upon these parameters when carried intracellularly into the cell, it does confirm that the effects seen here are not the result of DMSA exposure alone.

5.3.3 Conclusion

In summary, these results indicate that even temporary exposure to iron oxide/AMNPs results in a dose dependent reduced ability of PC12 cells to appropriately respond to nerve growth factor. This may have significant implications for *in vivo* and phenotypic dependent *in vitro* uses of AMNPs and iron oxide magnetic nanoparticles in general. In particular it was shown that the exposure of cells to locally high concentrations of magnetic nanoparticles can adversely affect cell function, phenotype and viability. These findings also indicate and confirm previous reports that the presence of intracellular iron oxide can result in significant changes in cell behavior and viability. Furthermore, taking into account the results of other investigators, it seems that nanoparticle surface coatings, while perhaps innocuous themselves, can drastically affect the behavior of cells exposed to nanostructures coated with these agents. It seems that there are three plausible explanations for this discrepancy: first, that coordination of the coating agent with the nanostructure facilitates entry into or interaction with cells of both the nanostructure and surface chemicals, thereby magnifying any interactions (positive or negative) with cellular components; a second, alternative explanation is the variance in the effectiveness of the coatings to shield the nanostructures from [potentially adverse] interactions with cellular components; thirdly, there may also be a combination of these effects. The underlying causes of certain biological effects and interactions may be easier to diagnose than others, such as cytotoxic effects from known toxic nanostructures like cadmium selenide (CdSe) based quantum dots, where toxicity differences between various coatings can almost certainly be explained through the second posited

explanation (Derfus, Chan et al. 2004; Hoshino, Fujioka et al. 2004; Kirchner, Liedl et al. 2005). In certain cases, however, such as exhibited here, the combination of two materials/chemicals, normally considered safe and nontoxic, results in a more toxic material than either of the individual components themselves. This implies the notion that biocompatibility and toxicity of nanomaterials need to be treated and evaluated as complete structures and not simply as the superposition of their individual constituents. It should be noted that in the case of ferrofluid cytotoxicological studies, the implementation of a bare MNP control, while desirable, often raises more questions than it answers. Firstly, an MNP coating is required for colloidal MNP stability in aqueous biological solutions making it unsuitable as an accurate comparison. Bare MNPs are highly unstable in saline solutions; form optically visible aggregates, and produce an interaction of such disparate physical characteristics so as to be irrelevant as a proper control against a stably dispersed ferrofluid. On the other hand, the implementation of a different stabilizing coating would beg the question of which coating to utilize and what effect the other coating itself would have upon the cells.

In conclusion, the results of this work further bolster recent calls for increased attention and interest into the toxicity of nanomaterials (Service 2005; Nel, Xia et al. 2006), and, in particular, emphasize the importance of evaluating manifestations of nanostructures and likewise any associated chemical modifications on an individual case by case, basis. Failure to fully evaluate these structures along with their coatings as a whole, may lead to lack of parameter control in *in vitro* experiments, as well as incorrect conclusions concerning their biocompatibility and the biosafety of their *in vivo* use.

5.4 Quantitative Intracellular Magnetorelaxometry

In the previous section it was shown that the delivery of moderate to large quantities of iron oxide, or, more specifically, anionic iron oxide magnetic nanoparticles into neuronal type cells can significantly affect the cell phenotype and viability over time. It was ultimately reasoned that such effects are most relevant to *in vivo* applications, where improper evaluation of toxicity issues can have more drastic or serious consequences. These conclusions, however, do not eliminate the potential use of MNPs for intracellular biomedical purposes, but rather act as a caveat for its proper use in such applications, particularly those involving living subjects. With this in mind, the delivery of remotely controllable functional entities, such as MNPs, into living cells remains of intrinsic utility in the development of novel biomedical applications. In this section it is shown that this is indeed the case, as MNPs are modified and delivered into living cells as a means of detecting the presence of specific intracellular proteins through magnetorelaxometry.

The capability of detecting intracellular binding events in live cells can benefit a wide range of applications, including therapeutics, clinical diagnostics and basic science. As an example, in drug delivery, a tool that can accurately determine the rate of release of a therapeutic delivered inside a cell would be especially valuable, as the delivery plays a major role in the effectiveness and time course of the therapeutic. Similarly, for drug development, intracellular assays that quantitatively measure protein expression in response to a drug would also be very useful. For example, assays to determine the xenobiotic induction cytochrome P450 (CYP) enzyme expression can help determine potentially harmful interactions between drugs. Adverse drug reactions are one of the top six causes of death in the U.S. (Lazarou, Pomeranz et al. 1998). Ultimately, the ability to quantify the expression and dynamics of proteins in live cells on a time scale of seconds could improve understanding of protein and second

messenger pathways, leading to the elucidation of key cellular processes in biomedicine and disease.

The extensive utility of so-called "proteomics" has engendered the development of various useful techniques aimed at probing the intracellular protein environment. However, there are important limitations either with making *quantitative* measurements, using *live* cells, or both. In particular, with the inception of green fluorescent protein (GFP) and related technologies has come the advent of several powerful fluorescent-based techniques that have revolutionized the study of live cells (Lippincott-Schwartz and Patterson 2003). One drawback is that a gene construct must be made and transfected into cells for each protein to be studied, requiring significant expertise and impacting ease of use. As with all fluorescent-based techniques, any form of protein quantification is hampered by variations in optical setups, background fluorescence, autofluorescence, quenching, and photobleaching. These factors limit most current fluorescence based strategies to "semi" quantitative or to relative comparisons of protein expression. Several fluorescence based techniques such as fluorescence recovery after photobleaching (FRAP), fluorescence loss in photobleaching (FLIP), and fluorescence resonance energy transfer (FRET) have proved invaluable in elucidating the diffusion constants, mobilities, and protein-protein interactions of various proteins, respectively. These techniques, however, do not readily determine absolute protein concentrations. Fluorescence correlation spectroscopy (FCS) is comparably more quantitative in determining intracellular protein levels on live cells than other fluorescence based techniques (Elson 2004). Based on several assumptions, FCS data yields an auto-correlation function, the amplitude of which can be used to determine the concentration of the fluorescent species. The drawbacks of FCS include: can only readily determine the concentration of proteins within a relatively narrow range of concentrations (nanomolar regime), requires somewhat elaborate setup and a high level of computation, and needs relatively high levels of

fluorophore photostability. While FCS can provide real-time data, it is limited to single cell measurements and not amenable to study larger (or heterogeneous) cell populations.

There are other techniques better suited to quantitative analysis but they cannot perform *live* cell assays. In mass spectrometry (MS) and capillary electrophoresis (CE), proteins from lysed cells are protealytically digested and separated based on charge to mass ratios. Relative protein concentrations can be obtained by integrating mass spectrometric peak areas or fluorescent readouts (Ong and Mann 2005; Stutz 2005). MS and CE also suffer from extensive sample prep times, protein proteolysis requirements, only give relative protein levels and are not applicable to many larger proteins. Chromatographic techniques, such as affinity chromatography, liquid chromatography (LC) and high performance LC (HPLC) are often used to separate and purify proteins from cell lysates (Washburn, Wolters et al. 2001). Once purified, the proteins can then be quantified by standard techniques. These techniques, however, require cell lysis, protein solubilization, and are normally very tedious. Gel electrophoresis techniques, such as Western blotting and 2-dimensional electrophoresis, separate proteins based on the charge and size of the molecules using a gradient electric field. Electrophoresis also requires extensive sample prep and assay time, and suffers from background variability, saturation effects, nonlinear relationships between spot size and protein levels, and the inability to readily quantify absolute protein levels (Moritz and Meyer 2003).

One of the intrinsic advantages of magnetorelaxometry is the ability of making quantitative measurements without the need to remove excess labels, thus eliminating the need for wash steps. This advantage could prove particularly useful in intracellular assays, where "washing" of the cell typically requires cell lysis, introduces artifacts and makes accurate quantification of proteins difficult, particularly in living cells. The use of magnetorelaxometry in live intracellular assays, however, is critically dependent upon,

among other things, the ability of MNPs to be reliably delivered into the cytoplasm of the cells. As stated in previous sections, a tremendous amount of effort has been given toward the development of techniques aimed at delivering MNPs into the intracellular space of living cells. Many of these techniques, including DMSA coating, however, follow normal endocytotic mechanisms and effectively sequester the MNPs in endosomes, which all but precludes access to the cytoplasm and, consequently, intracellular proteins.

One demonstrated method of MNP modification for intracellular delivery which does not utilize typical endocytotic pathways is the use of HIV derived, trans-activating transcriptional activator (TAT) protein (Schwarze, Ho et al. 1999). TAT is a member of a larger family of cell penetrating peptides (CPPs) including others such as antennapedia, polyarginine, transportan and HSV-1 VP22 which have also been utilized in the delivery of bioactive agents across the plasma membrane (Zhao and Weissleder 2004). Of these CPPs, however, only TAT, or more specifically the TAT protein transduction domain (PTD) has been successfully conjugated to MNPs and shown to be an efficient method of intracellular delivery into the cytoplasm of living cells. The TAT PTD is derived from a basic region, residues 47-57, of the TAT protein and is required for HIV entry into the cell (Kaplan, Wadia et al. 2005). Since its discovery in 1988 (Frankel and Pabo 1988; Green and Loewenstein 1988), the exact mechanism of TAT mediated transduction across the plasma membrane eluded researchers until it was recently demonstrated that the process occurs via a specialized form of endocytosis called macropinocytosis which all cells perform (Wadia, Stan et al. 2004). Macropinocytosis is receptor independent and characterized by membrane "ruffling." In this process, the highly positively charged TAT peptide binds the cargo to the surface of the cell, presumably to negatively charged surface proteoglycans, and actin membrane protrusions envelope the cargo into vesicles called macropinosomes. These macropinosomes are much

"leakier" than typical endosomes and allow release of some of the cargo into the cytoplasm of the cell where it has access to intracellular constituents.

In the previous two chapters, it was shown that MNPs could be tailored to bind to extracellular protein targets and that these binding events were readily quantifiable via magnetorelaxometry. In this chapter, this paradigm is extended to the detection of intracellular proteins in living cells. MNPs are conjugated to TAT (or, more specifically, TAT PTD) as a means of penetrating the plasma membrane without disrupting its integrity. These MNPs are then further modified through conjugation with anti-tubulin antibodies, endowing the particles with a means of immobilization once inside the cytoplasm by attaching to the "solid support" of the cytoskeleton. Similar to the *in vitro* assays demonstrated in Chapter 3, MNPs which bind to the cells' cytoskeletons are effectively immobilized by the larger τ_B values of the cells as compared with τ_m. Using TAT/anti-tubulin conjugated MNPs, magnetorelaxometric assays are performed on live cells in solution and compared with MNPs conjugated to TAT alone. Figure 5-7 shows a schematic of a typical intracellular magnetorelaxometric assay, where TAT/anti-tubulin antibody conjugated MNPs are delivered into living cells, a brief magnetic field is applied to align the MNP moments and the net magnetic moment from the MNPs bound to microtubules is measured in the SQUID system. In order to confirm that the signal derived from TAT conjugated MNPs is indeed due to their entry in to the intracellular space and not to the significant ionic interactions which initially act to bind the TAT conjugated MNPs to the outside of the cells, these MNPs are also modified with fluorophores and their delivery is confirmed through confocal microscopy. The various issues which arise in the attachment of highly positively charged TAT peptides to negatively charged MNPs are discussed and novel methods are employed to minimize charge induced MNP aggregation. Finally, the key limitations in the model system are

discussed, solutions to which are proposed for future experiments, and prospects for intracellular protein quantification via magnetorelaxometry are considered.

5.4.1 Materials and Methods

5.4.1.1 Basic Preparation of TAT Coated Magnetic Nanoparticles

Preparation Using 50nm Miltenyi Magnetic Nanoparticles. A 1 mg/ml stock solution of biotinylated TAT PTD with sequence YGRKKRRQRRR-aminohexanoic acid-biotin (SynPep, Dublin, CA) was added to a 10mM PBS solution containing 10^{11} 50nm streptavidin coated MNPs/µl (Miltenyi Biotec, Auburn, CA) to yield a final ratio of 0, 4, 10, 20, or 100 TAT/MNP and incubated at room temperature for 30 minutes. To create antibody conjugated MNPs, a 10mM PBS solution of anti-human tubulin antibody (Molecular Probes, Eugene, OR) biotinylated at a ratio of 0.5 to 0.75 biotin per antibody (by Solulink, San Diego, CA) was added to this solution to yield a final ratio of 6 total antibody molecules per MNP. A solution of 10mM PBS with BSA was then added to yield a final prepared MNP solution concentration was $1x10^{12}$ MNP per 5µl of 10mM PBS containing 1% BSA.

Preparation Using 140nm Molecular Probes Magnetic Nanoparticles. A solution of 10% BSA (Sigma-Aldrich, St. Louis, MO) in DI water was added to a stock 10mg/ml solution of 50nm polystyrene spheres (Kisker Biotech, Germany) to yield final BSA concentration of 1%. A 1 mg/ml stock solution of biotinylated TAT PTD with sequence YGRKKRRQRRR-aminohexanoic acid-biotin (SynPep, Dublin, CA) was added to a 10mM PBS solution containing a mixture of 140nm streptavidin coated MNPs/ml (Molecular Probes, Eugene, OR) and the polystyrene sphere solution at a ratio of 1000 polystyrene spheres per MNP, to yield a final TAT-MNP ratio of 0 or 1000 TAT/MNP and incubated at room temperature for

30 minutes. To create antibody conjugated MNPs, a 10mM PBS solution of anti-human tubulin antibody (Molecular Probes, Eugene, OR) biotinylated at a ratio of 0.5 to 0.75 biotin per antibody (by Solulink, San Diego, CA) was added to this solution to yield a final ratio of 100 total antibody molecules per MNP. A solution of 10mM PBS with BSA was then added to yield final prepared solution concentrations of $1x10^8$ MNP and $1x10^{11}$ polystyrene spheres per 5µl of 10mM PBS containing 1% BSA.

Fluorescent Modification of MNPs. For confocal microscopy experiments, a 1mg/ml stock solution of fluorescein conjugated mouse anti-streptavidin antibody (Vector Labs, Burlingame, CA) was added to the MNP solutions at a ratio of 200 antibodies per MNP and incubated for at least 30 minutes at room temperature prior to further modification.

5.4.1.2 Cell Culture

The human B cell line Ramos (RA-1) was obtained from the American Type Culture Collection (ATCC; Manassas, VA) and cultured using standard methods. Cells were cultured in suspension with RPMI-1640 with HEPES medium (Sigma-Aldrich, St. Louis, MO) containing 10% heat inactivated fetal bovine serum (Invitrogen, Carlsbad, CA) and 100 U/ml penicillin and 100 mg/ml streptomycin (Invitrogen, Carlsbad, CA) at 37°C in 5% CO_2.

The human B cell line HL-60 was obtained from the American Type Culture Collection (ATCC; Manassas, VA) and cultured using standard methods. Cells were cultured in suspension with Iscove's Modified Dulbecco's Medium (IMDM; Sigma-Aldrich, St. Louis, MO) containing 20% fetal bovine serum (Invitrogen, Carlsbad, CA) and 100 U/ml penicillin and 100 mg/ml streptomycin (Invitrogen, Carlsbad, CA) at 37°C in 5% CO_2.

5.4.1.3 Intracellular Delivery of TAT Coated Magnetic Nanoparticles

RA-1 or HL-60 cells were washed in serum free RPMI-1640 or IMDM, respectively, counted and suspended in the same media at various cell concentrations between 5,000-100,000 cells per 10µl and kept at 37°C. Conjugated MNP solutions were then added the cell solutions at a ratio of 1:2 and incubated in microcentrifuge tubes for various times prior to measurement in the SQUID system. 15µl of the samples were then pipetted into individual BSA blocked microtiter wells (Greiner Bio-One, Monroe, NC).

Magnetic Detection by SQUID Magnetometer: Each microwell was cut out and sealed before measurement in the SQUID system. The samples were analyzed individually in quadruplicate in the SQUID system, where, after various incubation times, they were briefly magnetized in a 20G field and immediately brought into close proximity to the SQUID sensor via pneumatically controlled actuator, as shown in Figure 1-10. The SQUID sensor recorded the magnetic field strength in picotesla due to the remanent magnetization of each sample.

5.4.1.4 Confocal Microscopy

50nm Miltenyi or 140nm Molecular Probes fluorescent, TAT-anti-tubulin conjugated MNPs were added to a cell suspension, as described in the previous section and incubated for at least 2 hours. The samples containing the fluorescent, TAT/anti-tubulin conjugated MNPs and cells were dispensed into the chamber slides (Nalge Nunc Intl., Rochester, NY), mounted and sealed. Fluorescent microscopy was performed with a MRC 1024UV laser scanning confocal (Bio-Rad, United Kingdom) equipped with a UV argon and Kr/Ar laser attached to a Diaphot 300 inverted microscope (Nikon, Melville, NY). Images were obtained and analyzed using Lasersharp software (Bio-Rad, United Kingdom).

5.4.2 Results and Discussion

5.4.2.1 Magnetic Nanoparticle Conjugation

The use of magnetorelaxometry for intracellular assays is critically dependent upon the ability of the magnetic probes to transverse the plasma membrane and immobilize themselves within the cell. Toward these ends a conjugation scheme for the attachment of TAT and anti-tubulin antibodies to MNPs was developed and performed. First, TAT peptides were sequentially synthesized and biotinylated with exactly one biotin per peptide, thus precluding the aforementioned possibility of specifically crosslinking streptavidin coated MNPs with multibiotinylated ligands. Similarly, anti-tubulin antibodies were also biotinylated at a ratio of 0.5 to 0.75 biotin per antibody molecule. Various numbers of TAT were then attached to streptavidin coated MNPs and allowed to bind prior to the addition of various amounts of biotinylated anti-tubulin antibody. In order to optically visualize the conjugated MNPs and confirm their entry into the cells, in some cases a fluorescein conjugated anti-streptavidin antibody was added prior to the TAT and anti-tubulin modifications. A schematic of the conjugation process, including fluorescent derivitization is shown in Figure 5-8.

5.4.2.2 Empirical Optimization of Nanoparticle Stability and Delivery

Ideally, for magnetorelaxometric applications, the coordination of a given ligand to the magnetic labels should not affect the colloidal stability of the MNP solution nor should it lead to increased nonspecific binding. The use and attachment of highly positively charged species such as TAT to the negatively charged MNPs, however, poses and intensifies many undesirable ionic interactions, lowering or even reversing the electrostatic repulsion energy U_{el}, which leads to increased nonspecific binding, particle agglomeration, background levels and thus results in lower signal to noise levels. The ionic interactions which are responsible

for the binding of TAT to the negatively charged surface proteoglycans and temporary immobilization of the conjugated MNPs on the cells can also lead to increases in the background signal making detection and discernment of specific binding to intracellular proteins difficult. Additionally, once inside the cell, the highly positive charges on the TAT conjugated MNPs will intrinsically bind nonspecifically to the negatively charged proteinaceous intracellular structures. Indeed this binding, being proportional to the number of MNPs in the intracellular space, can be and is used in the present work as a metric of delivery efficiency into the intracellular space of the cells. In Figure 5-9, the potential sources of magnetic signal, both undesirable and desirable, in an intracellular magnetorelaxometric assay are shown: (a) MNP aggregation and/or NSB to the well surface, (b) nonspecific binding to the outside of the cells, (c) nonspecific binding within the cell, and (d) the desired specific binding and immobilization via anti-tubulin to microtubules within the cells. Due to the potential sources of nonspecific signal, it becomes necessary to run a variety of appropriate controls in each intracellular magnetorelaxometric assay in order to accurately distinguish the true signal due to specific binding. A matrix of the desired binding/magnetic signal versus various conjugation scenarios is shown in Table 5-1.

5.4.2.3 Intracellular Magnetorelaxometry Using Modified 50nm Magnetic Nanoparticles

Previously published studies of TAT mediated intracellular delivery of nanoparticles have almost exclusively been limited to the delivery of structures of 50nm or less (Zhao and Weissleder 2004). In light of this, initial intracellular magnetorelaxometric assays were performed using MNPs on a similar size scale. These 50nm MNPs also presumably offer the additional advantage of more rapid diffusion based release into the cytoplasm from leaky macropinosomes following entry into the cells via macropinocytosis. As stated previously,

however, these smaller MNPs produce a significantly smaller remanent magnetic signal per binding event than the typically used 140nm MNPs.

While it has been previously reported that conjugation of increasing amounts of TAT results in an increased intracellular delivery efficiency (Zhao, Kircher et al. 2002), initial conjugation attempts showed that the coordination of large numbers of TAT to the MNP surface resulted in visibly observable losses in colloidal stability and very large background signal levels of the type depicted in Figure 5-9a. An example of this is shown in Figure 5-10, which shows a typical plot of magnetic signal versus time for MNPs conjugated with 100 TAT per nanoparticle. It was subsequently observed that lowering the number of TAT per 50nm MNP to 10 or less seemingly circumvented this problem and lowered the background signal to within control levels. The effect of the coordination of larger amounts of TAT is clearly demonstrated in Figure 5-11, where confocal images of two different live cells incubated with MNPs conjugated to 4 versus 20 TAT per MNP are shown. Figure 5-11a shows an image of the former case, taken from a center section of the cell, where the MNPs are more or less evenly dispersed throughout the interior of the cell. Conversely, Figure 5-11b shows an image taken at an optical plane on the surface of a cell incubated with MNPs coordinated to 20 TAT per nanoparticle, showing the resulting large discrete aggregates of MNPs stuck on the plasma membrane, unable or impeded from entering the intracellular space via macropinocytosis, presumably due to steric hindrances.

In order to optimize conditions for the delivery of MNPs into the cells, initial experiments were performed with only TAT coordinated to the MNPs and their nonspecific binding to the interior of the cells, such as depicted in Figure 5-9c, was monitored. In one such experiment, using assay conditions of $1x10^{11}$ MNPs, 4 TAT per MNP and 100,000 cells per sample, the magnetic signal was monitored in real time, as shown in Figure 5-12a. The results show the delivery of roughly at least 4,000 MNPs per cell and a nonspecific "signal" to noise of over 10

after 100 minutes of incubation with the conjugated MNPs and the delivery of over 20,000 MNPs per cell after 18 hours of incubation. In this case, the delivery of the MNPs is most likely reagent limited, as subsequent assays performed on fewer cells, such as 2700 cells per sample as plotted in Figure 5-12b, show binding of upwards of 200,000 MNPs per cell, a 50 fold increase, after 100 minutes of incubation time.

While the delivery of TAT conjugated MNPs into living cells was successfully confirmed both magnetically and optically, magnetorelaxometric assays performed using 50nm MNPs further conjugated with anti-tubulin antibodies proved somewhat problematic, yielding lower signal to noise ratios than desired. The data from one of the successful assays using 50nm MNPs conjugated with 10 TAT and 6 antibody per particle, shown in Figure 5-13(A), reveals a signal to noise of roughly 3 when compared to the no cell case, but shows a less efficient MNP delivery efficiency than the 4 TAT case in Figures 5-11 and 5-12, possibly due to TAT induced increases in MNP aggregation. Figure 5-13(B) shows a confocal image taken from a focal plane at the center of the cell, showing binding to the microtubule cytoskeletal structure, confirming entry of the MNPs into the cytoplasm.

5.4.2.4 Intracellular Magnetorelaxometry Using Modified 140nm Magnetic Nanoparticles

The limited success and low signal of the initial assays utilizing TAT/anti-tubulin conjugated 50nm MNPs indicates poor delivery into the cytoplasm of the cells and binding to tubulin cytoskeletal structures. Because of the multiple requirements for entry into the cytoplasm: binding of the MNP complex to the plasma membrane, successful passage across the membrane via macropinocytosis, leakage from macropinosomes into the cytoplasm and binding to microtubules, diagnosis of problems in cytoplasmic delivery proves somewhat problematic. As it has been shown in previous reports, TAT mediated delivery, at least to the

plasma membrane, is directly dependent upon the number of TAT conjugated to the cargo. While many previous studies have shown successful delivery of MNPs into the intracellular space, these studies are not only less concerned with the slow escape of the MNPs from macropinosomes into the cytoplasm, which would severely be affected by any MNP aggregation, additionally there currently does not exist a method of quantifying such release, present methods excluded. Quantitative differentiation between delivery to the plasma membrane versus inside macropinosomes versus the cytoplasmic space has proved difficult or impossible with traditional methods. Nonetheless, delivery to at least the membrane of the cell is dependent upon the number of TAT conjugated to the MNPs. Unfortunately, as previously demonstrated, the addition of large numbers of TAT to the surface of the MNPs significantly undermines the ferrofluid colloidal stability. While this problem was somewhat evident in the conjugation of 50nm MNPs, the coordination of TAT to 140nm MNPs resulted in even more severe agglomeration issues. In this case, lower numbers of TAT per MNP resulted in little to no delivery into the cells, while raising the number of TAT simply elevated the background signal due to agglomeration, resulting in little to no signal to noise. In order to circumvent this seeming paradox, a method of allowing the conjugation of high numbers of TAT to the MNPs while preventing their charge induced aggregation would prove useful. Toward this end, a high density of nonmetallic and nonmagnetic polystyrene spheres was added to the MNP solutions prior to TAT conjugation to act as physical barriers to MNP aggregation. A schematic depicting conjugation processes with or without the polystyrene spheres is shown in Figure 5-14. This technique proved quite successful for the conjugation of 140nm MNPs, with conjugations of up to 1000 TAT per 140nm MNP while lowering the background signal to levels near the no TAT controls.

The use of the larger moment 140nm MNPs conjugated to TAT and anti-tubulin antibodies in the presence of polystyrene spacers was considerably more successful for intracellular

protein detection than the 50nm experiments. As shown in Figure 5-15, intracellular assays performed on 50, 000 B-cells using $1x10^8$ 140nm MNPs conjugated to 1000 TAT and 100 anti-tubulin antibodies per MNP per sample resulted in signals to noise of nearly 6 at 100 minutes and 15 overnight compared to the no TAT control (and a S/N of roughly 3.5 and 2, respectively compared to the TAT alone control), a significant improvement over assays performed with 50nm MNPs. A typical overnight assay with various timepoints is shown in Figure 5-15a, while in Figure 5-15b the data from an identical, but separate 40 minute assay is shown, where the cells are transferred from the incubation vials to the wells at an earlier timepoint than the former assay to show the rapid initial increase from background levels at the beginning of the assays. In order to confirm the delivery of the 140nm MNPs into the intracellular space, confocal microscopy was also performed on the 1000 TAT conjugated MNPs, as can be seen in the micrograph of the mid-cell focal plane shown in Figure 5-15(C), the 140nm MNPs successfully traverse the plasma membrane and enter the cytoplasm. Figure 5-16 shows the results of another assay, using similarly conjugated 140nm MNPs, but with only 5,000 B cells per sample. Similar to the 50,000 cell cases, this assay also shows a signal to noise of over 5 at 100 minutes incubation time. While the signal does not directly scale to the 50,000 cell experiments, this is most likely due to a global or local reagent limitation in the experiments with larger numbers of cells. Since the cells rapidly settle to the bottom of the microplate wells, larger numbers locally deplete the MNP concentration, significantly slowing the overall kinetics. This is somewhat offset, as the initial incubation occurs in microcentrifuge tubes placed on a rocker, but does become a factor once the cells are pipetted into the measurement wells. Lastly, it should be noted, that as shown in Chapter 2, the 140nm MNPs give a remanent magnetic moment of roughly 1000 times that of the 50nm MNPs, implying that significantly fewer MNPs (less than 100 per cell) are delivered into the cells and the

cytoplasmic space in the larger MNP case than in the 50nm cases. This tradeoff is discussed in further detail below.

5.5 Intracellular Assay Summary and Conclusions

In this section, the first intracellular magnetorelaxometric assay for the detection of an intracellular protein, namely tubulin within microtubules, was developed and demonstrated. A conjugation scheme for the attachment of the CPP TAT along with anti-tubulin antibodies was developed and further optimized for delivery of the MNPs into the intracellular space. The intracellular delivery of both 50nm and 140nm conjugated MNPs into live cells was demonstrated through magnetorelaxometry and additionally confirmed through confocal microscopy. The highly charged nature of TAT posed several technical challenges in maintaining the colloidal stability of the conjugated MNPs and initially resulted in high background signals. This problem was remedied through the use of nonmagnetic polystyrene nanoparticle spacers, which acted to physically prevent MNP aggregation. The assays performed, particularly with 140nm MNPs, showed moderate, but statistically significant differences in binding between MNPs conjugated with both TAT and anti-tubulin antibodies and those conjugated to TAT alone, successfully demonstrating the ability to detect the presence of an intracellular protein. The techniques employed in this assay are readily amenable to the detection of almost any immobile intracellular target, and, as such, act as an archetype for such experiments.

While both 50nm and 140nm MNPs were successfully delivered across the plasma membrane via TAT, specific protein detection was more successful in assays performed using the 140nm MNPs, due to their higher remanent magnetization levels. In terms of numbers, however, the delivery of these MNPs into the cell was much less efficient (by a factor of roughly 1000) than with the 50nm MNPs. This is most likely simply due to the fact that only

$1x10^8$ MNPs were used per sample in the 140nm case (larger numbers significantly increased background levels) versus the $1x10^{11}$ MNPs used in the 50nm experiments. It should be noted, however that TAT mediated intracellular delivery and release from the macropinosomes is also expected to be somewhat size dependent, with larger cargoes exhibiting slower entry into the cell and/or release from macropinosomes. Distinguishing between these two potential issues, however, currently proves difficult and highlights the need for better MNP alternatives, as the use of smaller numbers of the 50nm MNPs do not produce a detectable signal and the use of larger numbers of the 140nm MNPs significantly increases background signal levels.

5.6 Considerations for Further Development

Overall, the magnetorelaxometric assay developed successfully demonstrated the ability to *detect* the presence of an intracellular protein, but most likely requires further development for *quantification* of such proteins. Several improvements to the current intracellular assay are readily feasible, the most obvious of which is the development of smaller (<140nm) MNPs with high remanent magnetization levels. Such an improvement would allow for the intracellular delivery of more MNPs than in the 140nm case and more signal than in the 50nm case. The use of smaller MNPs should also increase the rate of release from the macropinosomes, leading to additional gains in specific signal to noise.

The magnitude and sensitivity of the assay are critically dependent upon the release of the MNPs from the macropinosomes following macropinocytosis by the cells. The process of escape from the macropinosomes is not only important in the present case, but also in the delivery of any cargo via TAT. Consequently, methods for enhancing the inefficient release of cargo from the macropinosomes are currently under active development and have been reported. The most notable of these methods is the creation of a fusogenic peptide between

TAT and HA2, a peptide sequence derived from the influenza virus which enhances endosomal escape by destabilizing lipid membranes following the pH drop in mature endosomes. The use of TAT-HA2 fusogenic peptides has been reported to markedly increase the delivery of both a TAT-Cre protein (the Cre protein excises a stop DNA sequence for EGFP expression once inside the cytoplasm) (Wadia, Stan et al. 2004) and, more recently, 50nm MNPs (Won, Kim et al. 2005).

5.7 Acknowledgements

The consistent hard work of Jennifer Blackwell was invaluable in carrying out the cytotoxicological studies; they could not have been done without her. The help and advice of Veronica Shubayev was also greatly appreciated. A great thanks to Rita Fiñones and Chiara Daraio for the TEM work. The intracellular magnetorelaxometric assay work was supported by DARPA grant HR0011-05-C-0047 "Next Generation Cell-Based Magnetic Assays for Bio-Magnetic Interfacing Concepts". The collaborative work of Leslie LaConte and the Bao group in this project was appreciated and proved helpful.

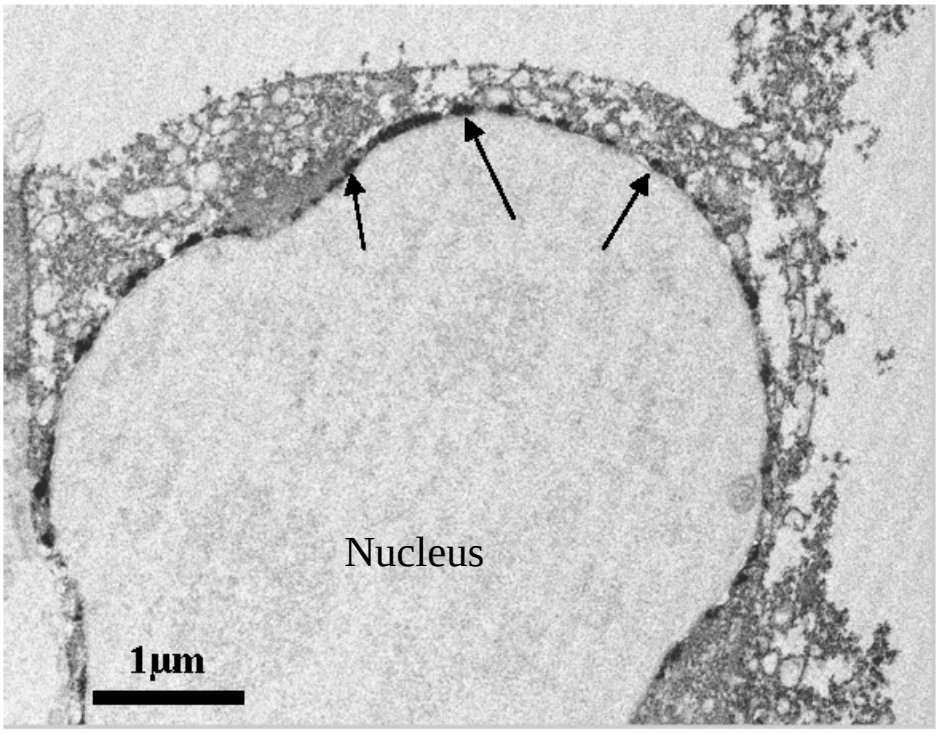

Figure 5-1. TEM micrograph of a PC12 cell following 24 hour exposure to AMNPs at an Fe concentration of 1.5 mM; arrows indicate typical endosomes containing the magnetic nanoparticles.

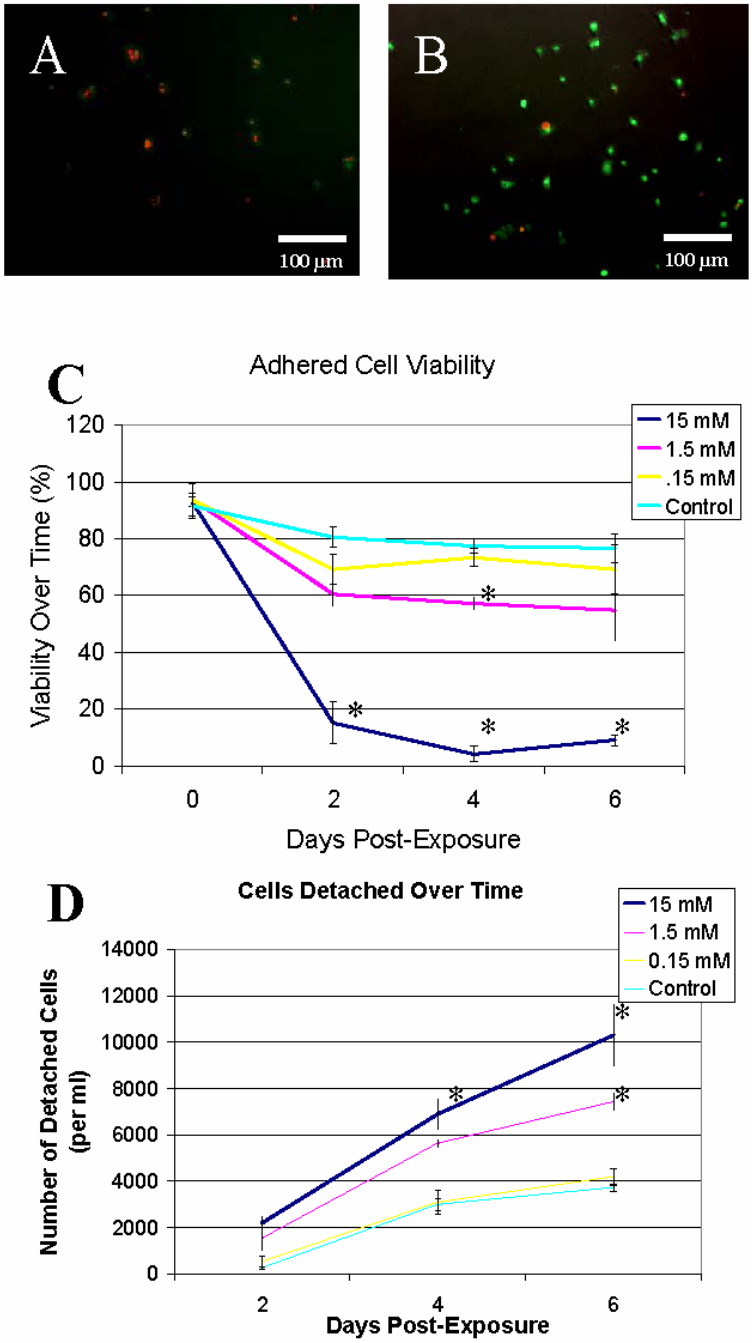

Figure 5-2. Live (Green)/Dead (Red) stain of NGF induced PC12 cells 4 days after AMNP exposure at Fe concentrations of (A) 15mM and (B, control) 0mM. (C) Note reduced cell viability and (D) attachment following AMNP exposure at different Fe concentrations. (Statistics: ANOVA with Tukey's *post-hoc*, expressed as mean ± standard error, *, $p<0.05$, **, $p<0.01$)

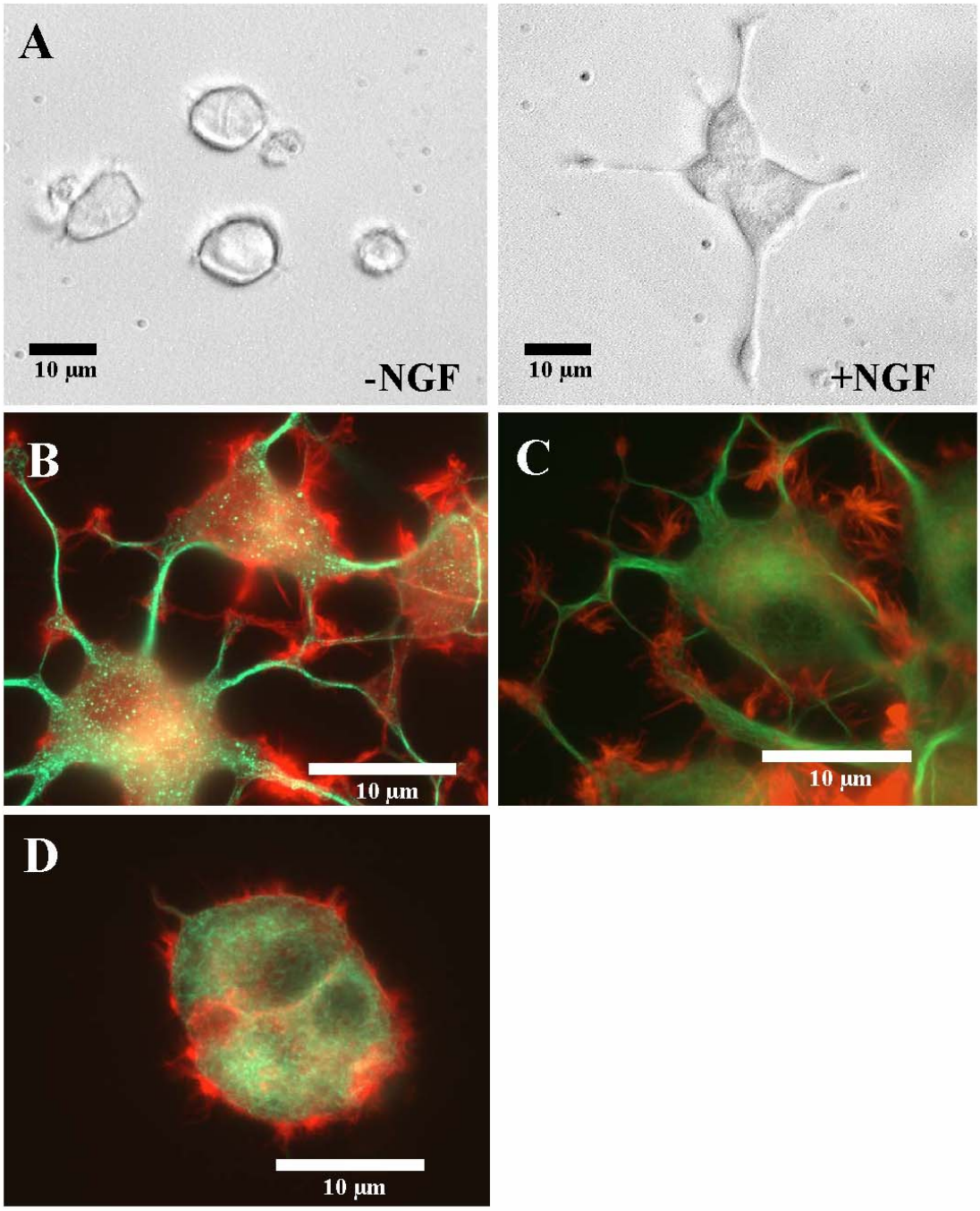

Figure 5-3. (A)Phase contrast images of PC12 cells, 48 hours in culture without NGF (-NGF) and with NGF (+NGF). PC12 immunofluorescence for tubulin (green) and actin (red), 6 days post AMNP exposure and 5 days post NGF exposure at Fe concentrations of (B, control cells) 0 mM, (C) 0.15 mM and (D) 15mM.

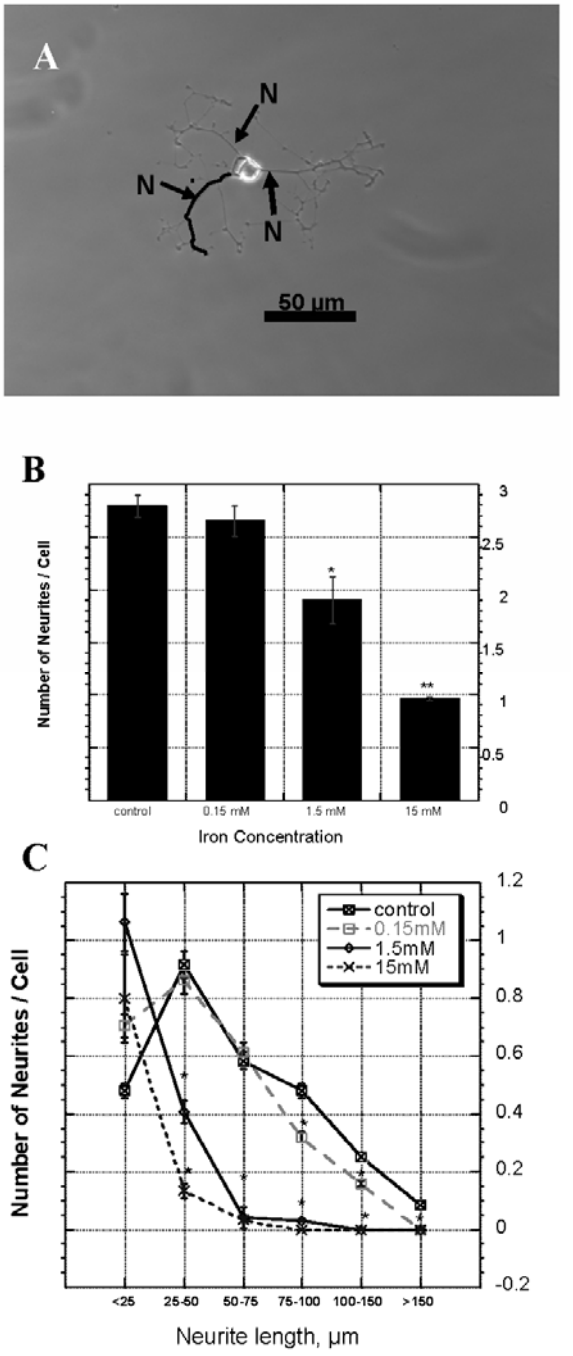

Figure 5-4. Effect of AMNP exposure on neurite outgrowth of NGF induced PC12 cells at different Fe concentrations. (A) Phase-contrast micrograph of a typical PC12 cell showing a trace along the extension of the lower neurite (N) used for length calculation. Note reduced number of neurites (B, C), and reduced length of extended neuritis (C) with increased AMNP Fe concentration 6 days post-exposure. (Statistics: ANOVA with Tukey's *post-hoc*, expressed as mean ± standard error, *, $p<0.05$, **, $p<0.01$).

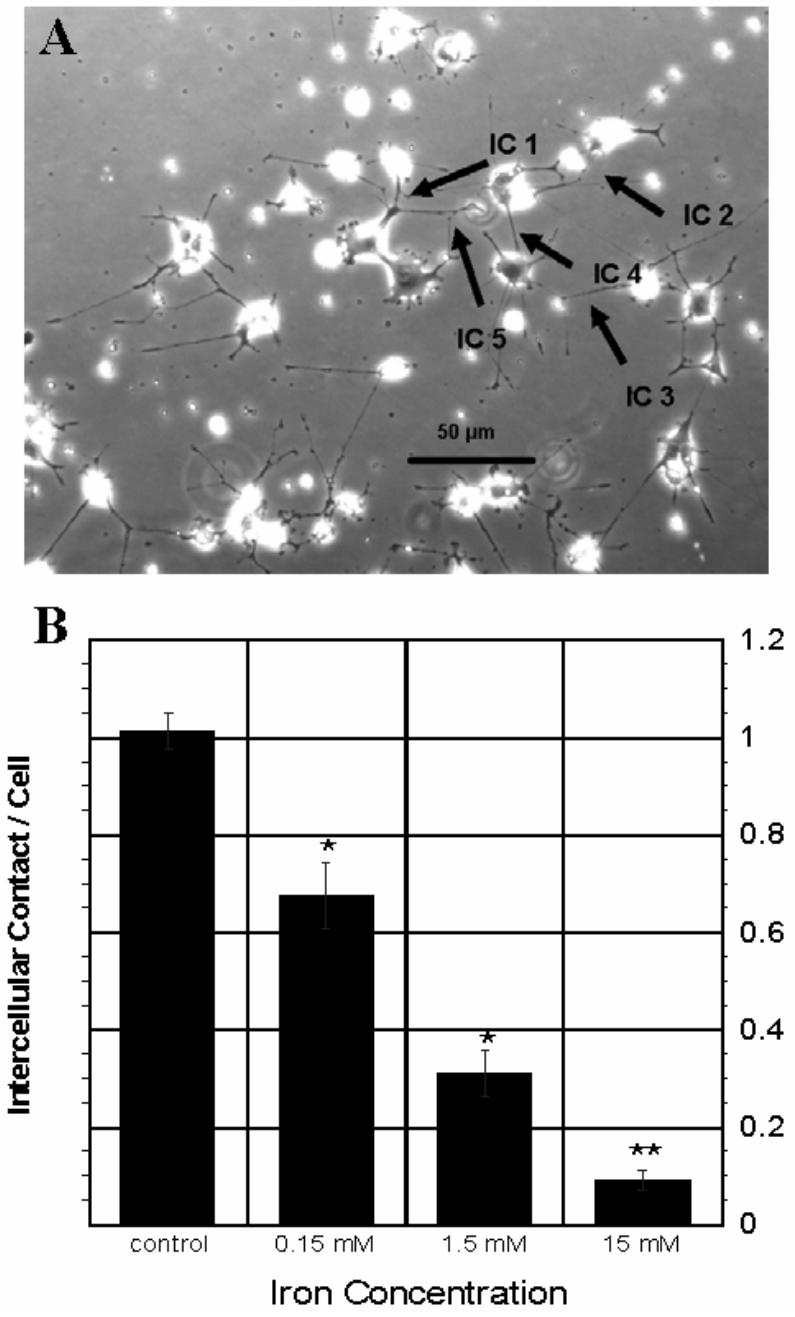

Figure 5-5. Effect of AMNP exposure upon intercellular contacts. (A) Phase-contrast micrograph of a typical NGF induced PC12 cell showing intercellular contacts (IC) 6 days after AMNP exposure. Note reduced number of intercellular contacts per cell with increased AMNP Fe concentration 6 days post-exposure in (B). (Statistics: ANOVA with Tukey's *post-hoc*, expressed as mean ± standard error, *, $p<0.05$, **, $p<0.01$)

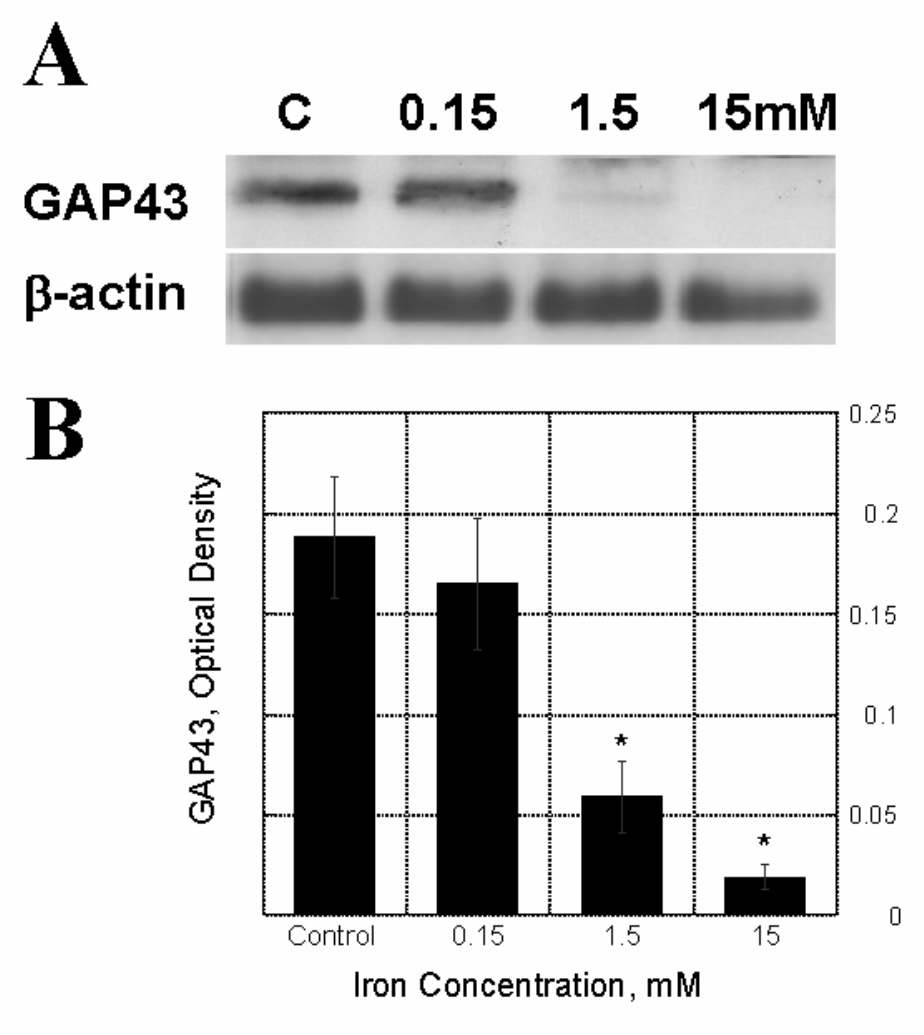

Figure 5-6. (A) Western blot for growth associated protein, GAP-43 in NGF induced PC12 cells (normalized to β-actin, protein loading control) 6 days post AMNP exposure at [Fe] = 0, 0.15, 1.5 and 15 mM. (B) Relative optical densities of GAP-43 bands shown in (A) (n= 3/group, *, $p<0.05$)

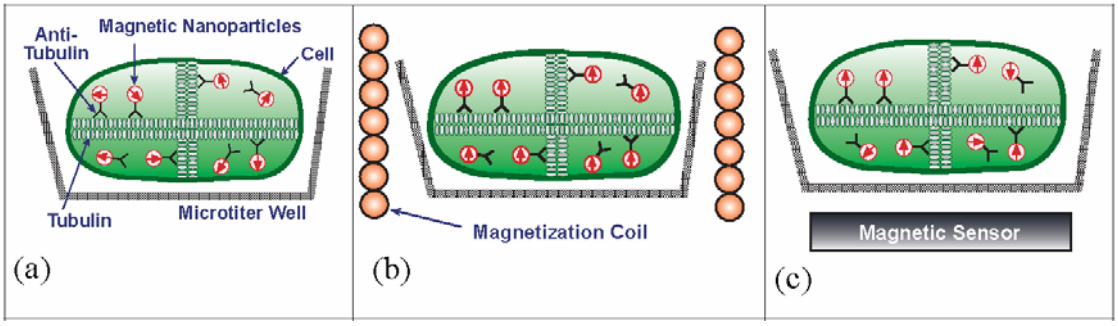

Figure 5-7. Intracellular *in situ* magnetorelaxometric assay on live cells. (a) TAT and anti-tubulin conjugated MNPs are delivered into the cytoplasm of live cells, resulting in binding of the labels to intracellular microtubules. (b) Apply a magnetic field to align the MNP moments of the labels. (c) Remove field and measure sample in SQUID system. Unbound MNPs randomize and contribute no net signal. Bound MNPs are not free to rotate and produce a net magnetic moment that is detected by the SQUID.

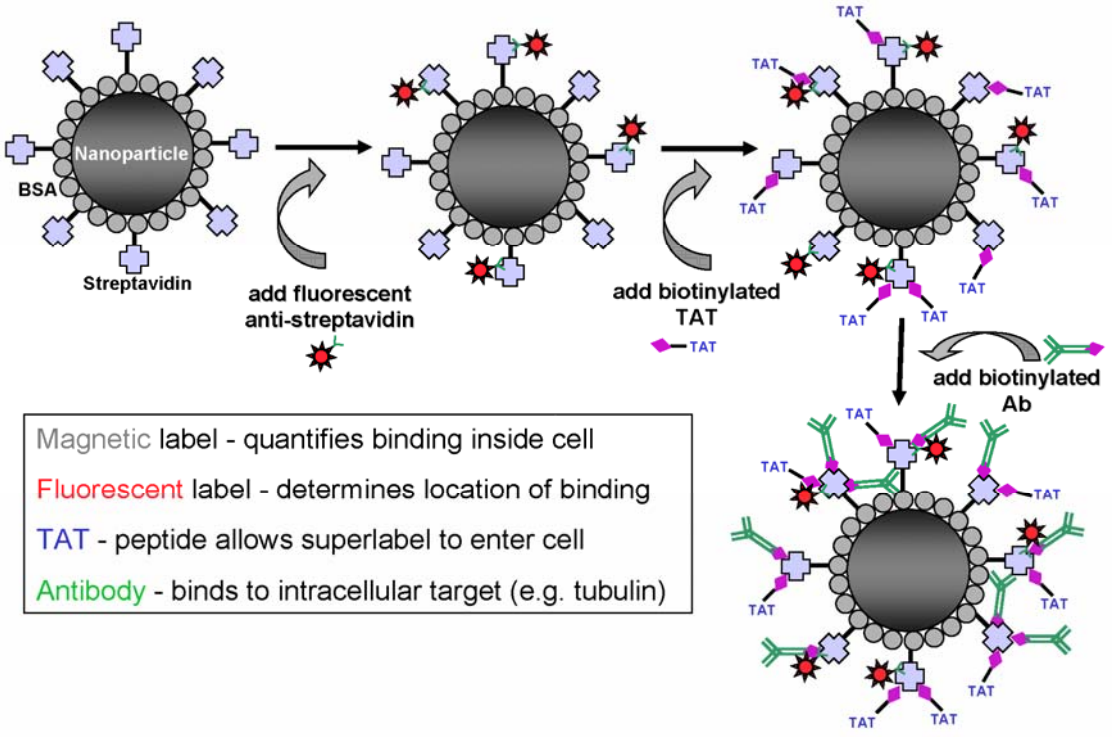

Figure 5-8. Reaction scheme for the conjugation of TAT and anti-tubulin to MNPs. The first step of attaching fluorescent anti-streptavidin is optional and is used in confocal experiments to confirm delivery of the MNPs into the cells.

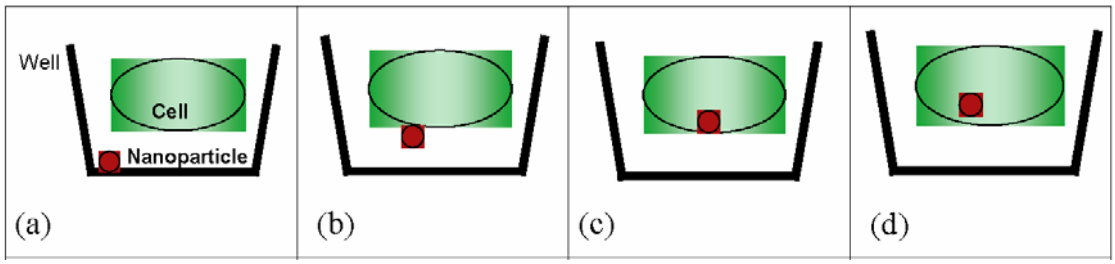

Figure 5-9. Potential sources of signal in an intracellular magnetorelaxometric assay. (a) Undesirable aggregation and/or immobilization of MNPs to the microtiter well surface. (b) Undesirable nonspecific binding of the MNPs to the cell surface. (c) Nonspecific binding of MNPs to intracellular structures. (d) Desired specific binding of MNPs to microtubules within the cytoplasm.

Table 5-1. Matrix of various controls used in the assays, showing desired binding levels.

	Cells	TAT	Ab	Desired Outcome	Implication
SIGNAL	X	X	X	High	specific binding
CONTROL A	X	X		Low **	shows no NSB to well or to cell surface; unbound if inside cell (** only want if using to determine delivery inside cell using TAT)
CONTROL B	X			Low	shows no aggregation of unconjugated magnetic nanoparticles; no NSB to well or cell surface
CONTROL C		X	X	Low	shows no aggregation due to TAT and Ab; no NSB to well
CONTROL D		X		Low	shows no aggregation due to TAT; no NSB to well
CONTROL E			X	Low	shows no aggregation due to Ab; no NSB to well
CONTROL F				Low	shows no aggregation due to unconjugated nanoparticles

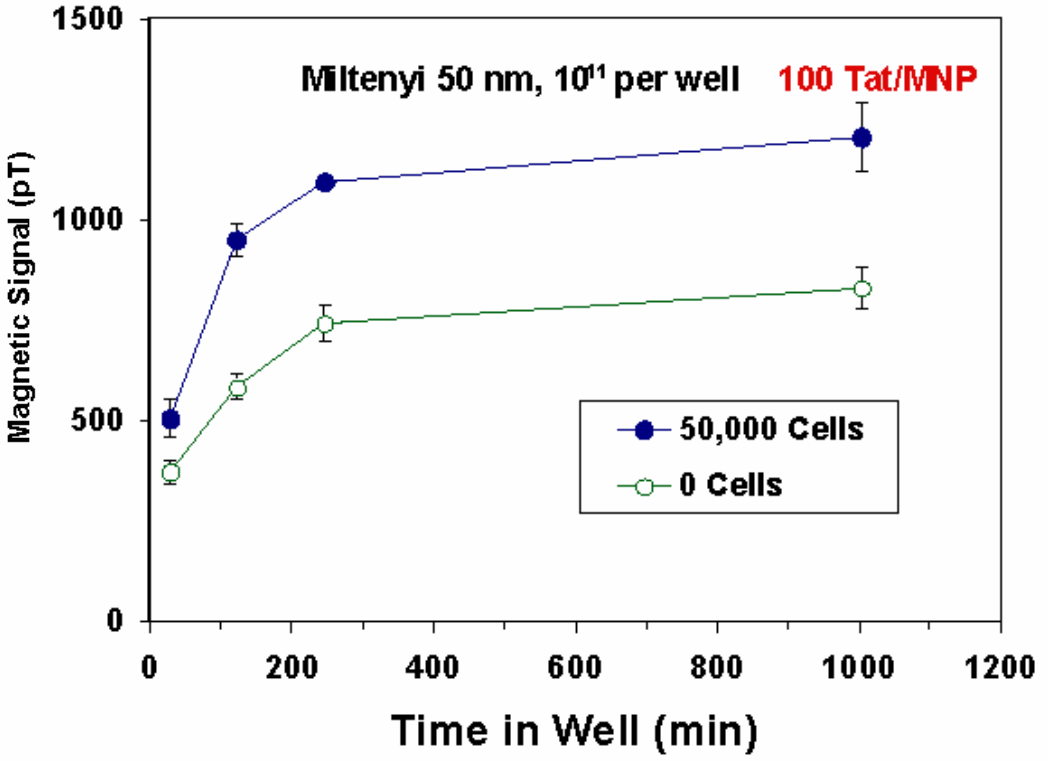

Figure 5-10. Intracellular magnetorelaxometric assay using 50nm MNPs coated with 100 TAT per MNP, showing high degree of background signal in the absence of cells due to particle aggregation.

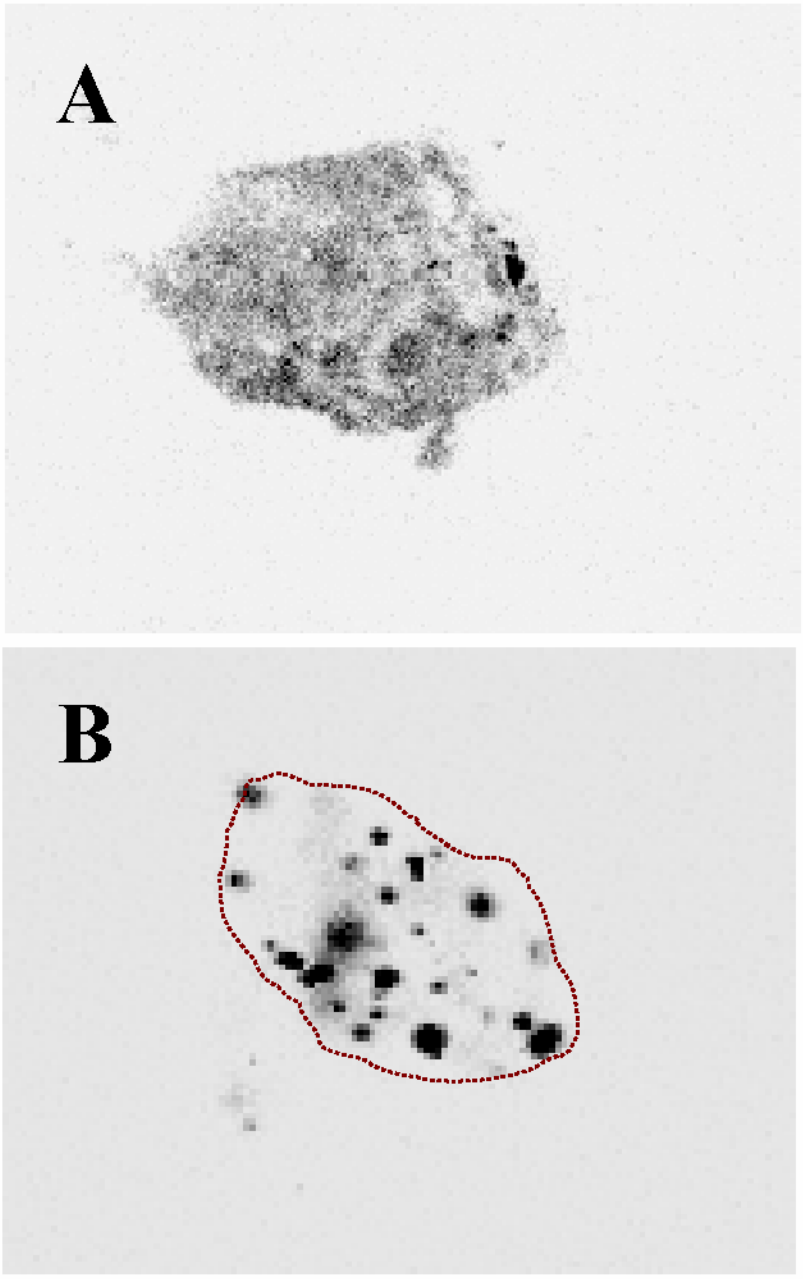

Figure 5-11. Confocal images (inverted for clarity) of MNPs with cells. (A) Focal plane of the center of a cell showing intracellular delivery of MNPs conjugated with a lower TAT (4) per MNP ratio, preventing MNP aggregation allowing entry into the cell. (B) Surface of cell focal plane from separate sample showing unsuccessful entry of MNPs conjugated with five times as many TAT (20) per MNP, resulting in optically observable MNP aggregation and failure to traverse the plasma membrane.

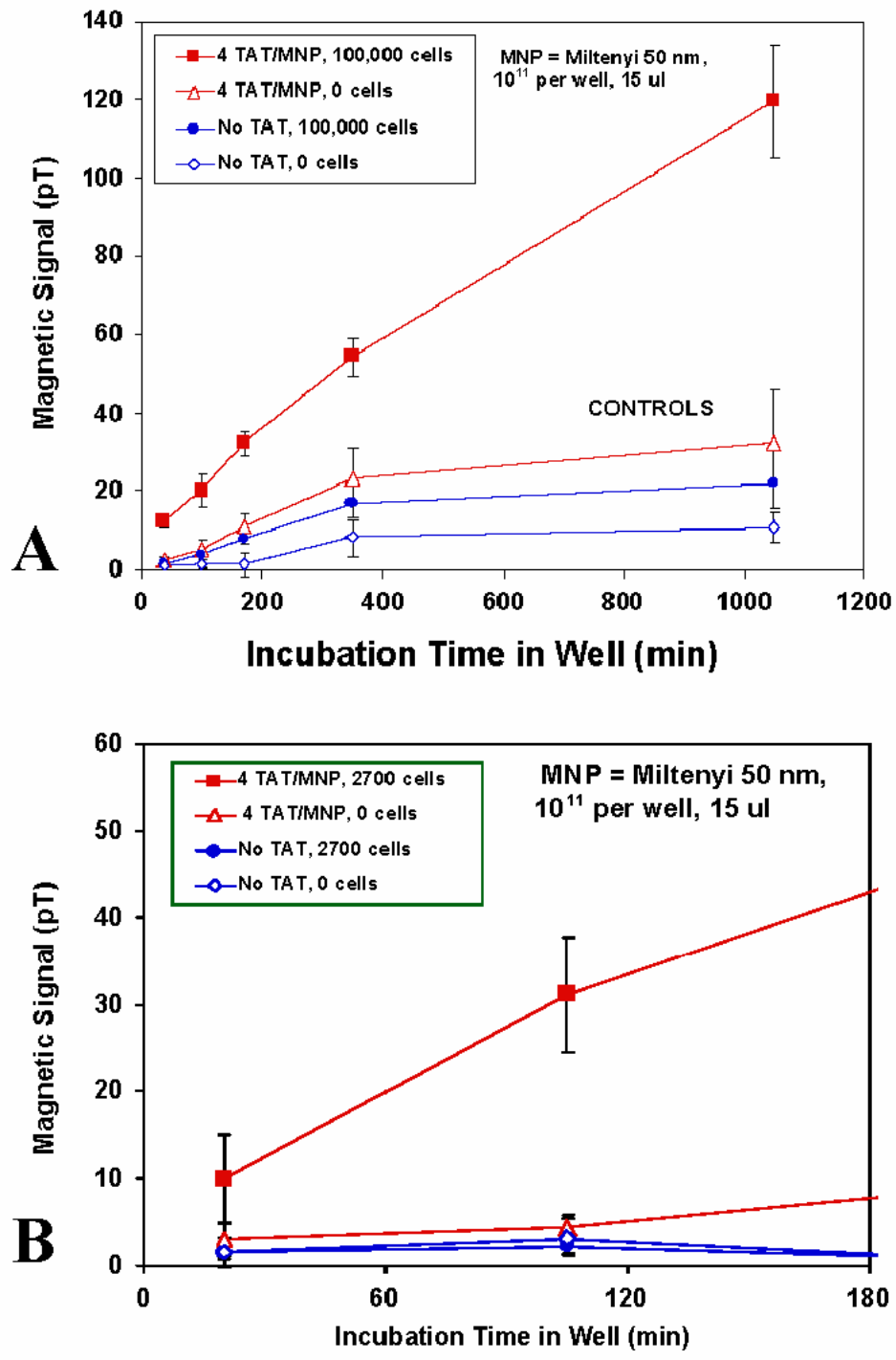

Figure 5-12. (A) Nonspecific intracellular magnetorelaxometric assay, showing delivery of 50nm MNPs conjugated with 4 TAT/MNP into 100,000 cells. "Signal" is produced from intentional nonspecific bindings (intracellular and extracellular). Data shows 4,000 MNP/cell at 100 min. and 20,000/cell at 18 hours. (B) Similar assay performed on fewer cells, exhibiting reagent limitation in (A), showing greater binding of 200,000 MNP/cell at 100 minutes.

A

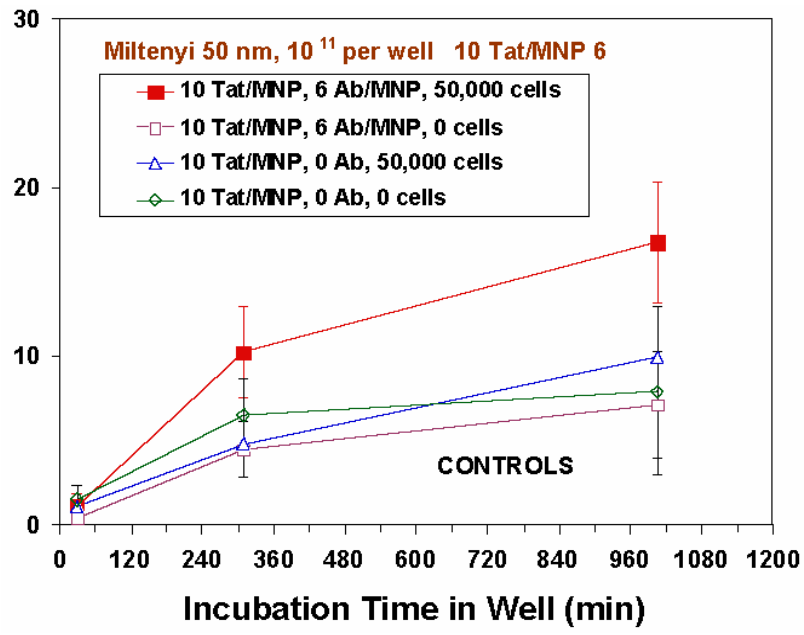

B

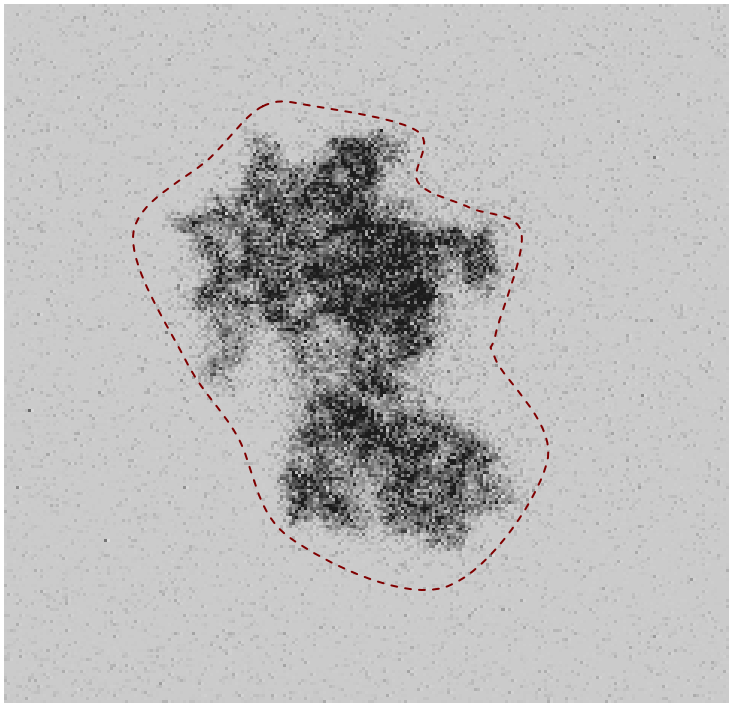

Figure 5-13. Intracellular magnetorelaxometric assay. (A) 50nm MNPs conjugated to 10 TAT and 6 anti-tubulin antibodies show larger signal than without antibody or without cells due to antibody mediated binding within the cells. (B) Confocal image at focal plane in center of cell treated with 50nm MNPs conjugated to 10 TAT and 6 anti-tubulin antibodies, showing cytoskeletal structure (Image inverted for clarity).

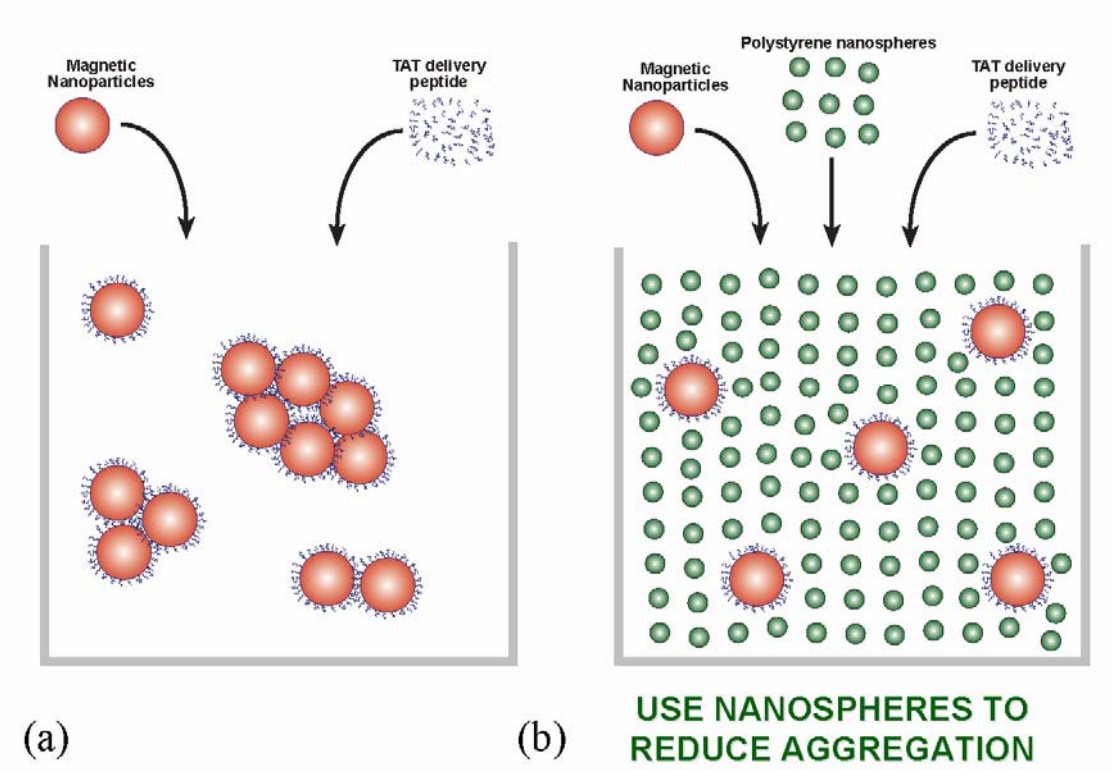

Figure 5-14. Technique used to reduce TAT mediated aggregation of 140nm MNPs. (a) Large numbers of TAT per MNP are required for binding to the cell, but result in optically observable aggregation and prohibitively large background magnetorelaxometric signal. (b) Through addition of 50nm nonmagnetic polystyrene sphere, the MNPs are physically isolated from one another, preventing aggregation.

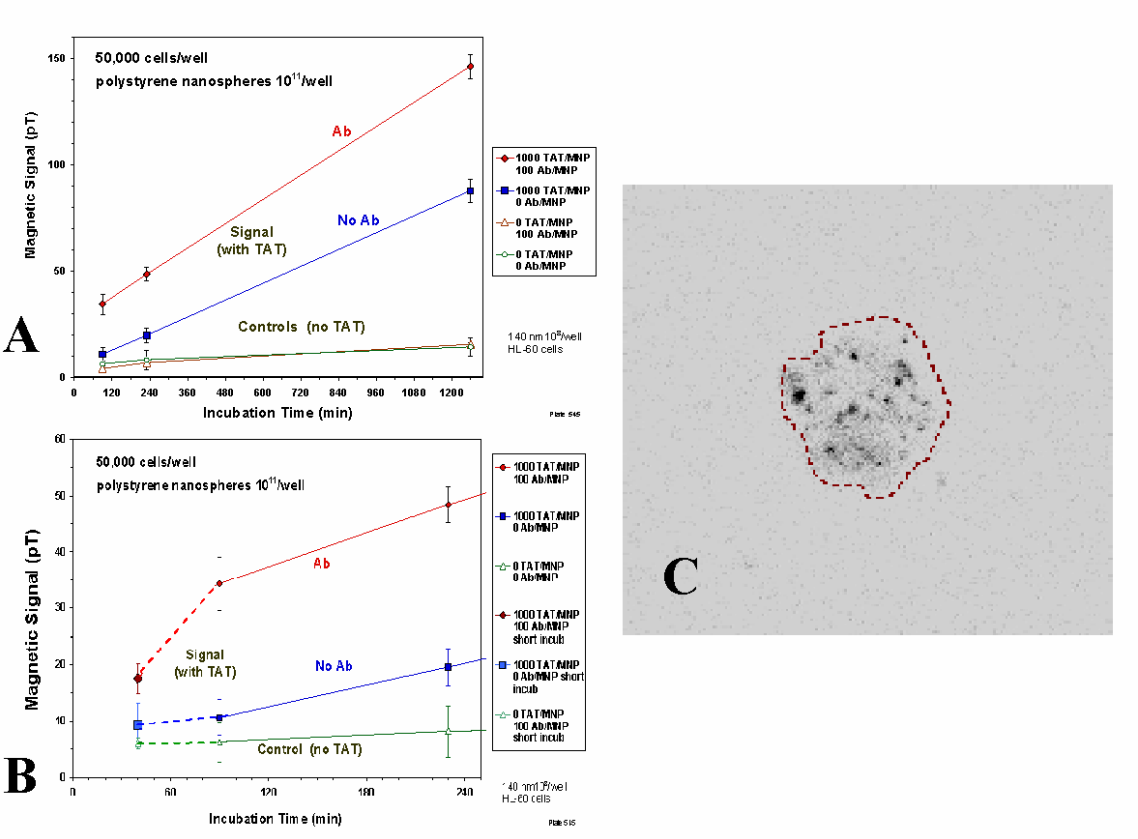

Figure 5-15. Intracellular magnetorelaxometric assay using 140nm MNPs and polystyrene sphere conjugation procedure. (A) Magnetic signal versus time for delivery of 1000 TAT and 100 anti-tubulin antibody conjugated 140nm MNPs into 50,000 cells/sample. Controls are no anti-tubulin and no TAT. (B) Addition of earlier timepoints from similar assay, modified to permit earlier magnetorelaxometric evaluation. (C) Inverted confocal image taken from center focal plane of a cell, showing delivery of 1000 TAT conjugated 140nm MNPs into the intracellular space.

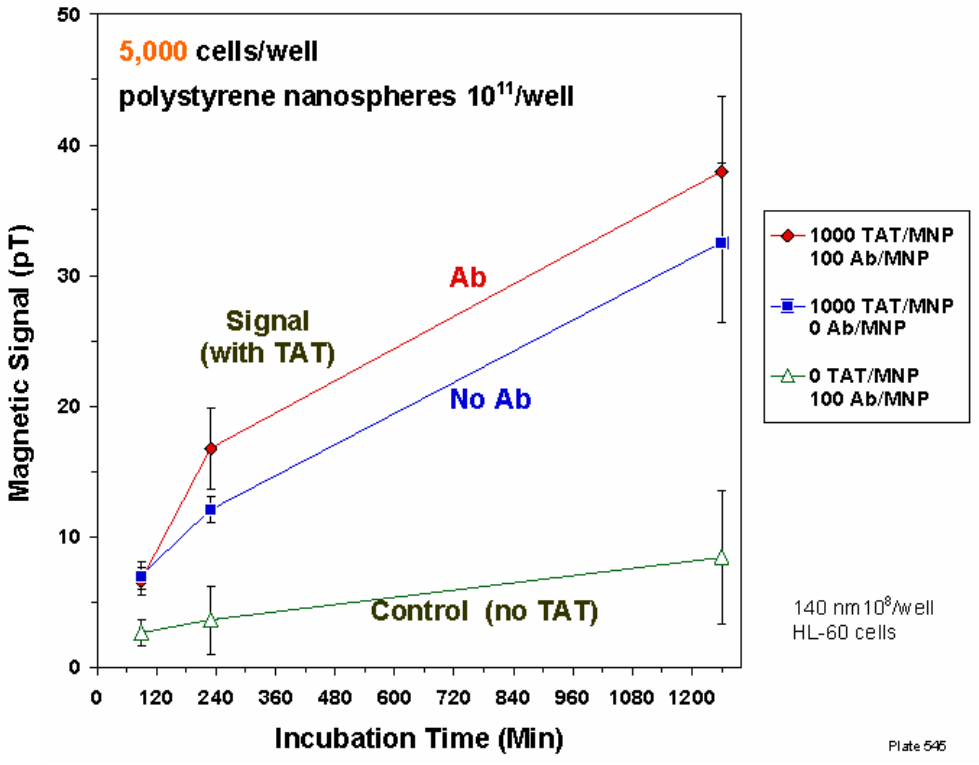

Figure 5-16. Intracellular magnetorelaxometric assay on fewer cells. Magnetic signal versus time for delivery of 1000 TAT and 100 anti-tubulin antibody conjugated 140nm MNPs into 5,000 cells/sample. Controls are no anti-tubulin and no TAT.

CHAPTER 6

CONCLUSIONS

6.1 Contribution to Nanotechnology

Nanotechnology is the science and application of submicroscopic materials, whose dimensions range from one to hundreds of nanometers. Materials on this scale can be seen both as very large molecules, allowing access to extended quantum behaviors, and as materials so small that they exhibit characteristics and attributes not available to larger structures. Recent advances in chemistry, biology, physics and materials science in this size regime have endowed researchers with the ability to not only create a plethora of nanometer scale materials, but also to precisely tailor their properties for many novel and exciting applications. Magnetic materials on this size scale, such as magnetic nanoparticles, also exhibit unique properties not available in larger structures and have likewise become of chief interest in the field of nanotechnology. Through exploitation of various synthesis techniques and parameters, the physicochemical and magnetic properties of magnetic nanoparticles can be precisely and exquisitely controlled.

The primary objective of this work is the development and optimization of MNPs for magnetorelaxometric assays. In light of this, the exclusive physicochemical, magnetic and colloidal characteristics required for use in biomedical magnetorelaxometry necessitated the

experimental evaluation of the magnetic characteristics of a large number of MNP preparations; as such an analysis has previously never been reported. In fact, the results of this analysis indicate a very large variation in magnetic properties among MNPs, even those of nearly identical chemical composition. This variability additionally underscores the extraordinary influence that synthesis parameters can exert upon these properties, as was also demonstrated through the differential syntheses of MNPs in Chapter 2. The analysis of these commercially available MNP preparations is of *prima facie* importance to the field of magnetorelaxometry, as it provides a fundamental basis for the use of these preparations in all such assays.

The initial screening of the MNP preparations assessed the *potential* for their use in magnetorelaxometry and included an evaluation of the colloidal stability of the base solutions. While this stability is critical in determination of the ferrofluid's possible magnetorelaxometric utility, it can be drastically affected through chemical modifications, such as those required for homogeneous assay development. The particular conjugation chemistry of attaching biomolecules to the surface of the MNPs, can, ironically, often specifically and/or nonspecifically destabilize the MNP suspensions, rendering them all but useless for the desired magnetorelaxometric application. This was highlighted in the present work through use of the chosen streptavidin biotin binding paradigm, where indiscriminate biotinylation of the desired bioconjugate, e.g., anti-*E.coli* antibody or Cry5B toxin, readily resulted in rapid aggregation of the streptavidin coated MNPs. To address this issue, novel specific and discrete biotinylation, conjugation and magnetic separation procedures were developed and employed, producing colloidally stable and highly functional MNP suspensions with minimal aggregation or background signals. The methods employed are readily amenable for use in innumerable protein based binding paradigms, particularly in the field of magnetorelaxometry.

The already stringent magnetic and colloidal requirements for the magnetorelaxometric use of MNP preparations in physiological saline solutions became all the more exacerbated in assays involving the use of biological samples such as blood and serum. Only a few MNP preparations were stable or marginally stable in such fluids, and those that were were much more weakly magnetic than the preferred MNP preparations. While the utility of one such weakly magnetic yet stable MNP solution was demonstrated for use in sepsis diagnostic assays, it became immediately clear that alternative means of biological sample preparation were necessary in order to achieve high levels of sensitivity in clinical specimens. Such preparation methods were developed and utilized to achieve the development of a highly sensitive and specific assay for *E. coli* O157:H7. These preparation methods, while not ideal, are applicable to the use of magnetorelaxometry for the much broader fields of pathogen detection and sepsis diagnostics in clinical specimens. These methods additionally highlight the need for the development of MNP preparations of superior biostability.

In many biomedical applications it may be desirable to attach highly charged or somewhat hydrophobic biomolecules to nanostructures. Nonspecific interactions between such molecules, however, can readily undermine the colloidal stability of the nanostructures, as was evidenced in the present work in the use of TAT for intracellular delivery of MNPs. The highly positive charge on the TAT molecules caused severe aggregation between MNPs following conjugation, resulting in high background levels and failure of the aggregates to traverse the plasma membrane. While this issue was initially circumvented through the conjugation of lower numbers of TAT per MNP, this solution was not amenable to larger MNPs, which required the conjugation of high numbers of TAT for pinocytotic entry into the cells. Through the use of alternative methods, namely the use of nonmagnetic polystyrene spheres as physical barriers, large numbers of the highly charged TAT molecules were conjugated to the larger MNPs while preventing their aggregation and maintaining their

colloidal stability. These colloidally stable, TAT conjugated MNP solutions were successfully delivered into the cells and resulted in the development and demonstration of the first intracellular magnetorelaxometric assay. The employment of aggregation preventing physical barriers such as polystyrene spheres should be useful for conjugation of many destabilizing agents to MNPs or other nanostructures.

6.2 Contribution to Biomedicine

In the present work, MNPs were tailored to permit the development of three quantitative biomedical assays: an *in vitro* assay for sepsis diagnostics; an *in vivo* assay for the detection of binding events in living organisms; and an *in situ* assay for the detection of intracellular protein expression in live cells. Many of the methods employed towards these ends were previously undeveloped for magnetorelaxometry or simply undeveloped altogether. Each of these assays provides specific advantages over current methodologies and demonstrates the intrinsic utility of magnetorelaxometry for biomedical diagnostics.

Sepsis is the second leading cause of death in non-coronary ICUs, the 10th leading cause of death overall in the U.S. and the number one cause of death in neonatal intensive care units for low birth-weight children (NIH 2004). Sepsis mortality rates are estimated to be 18-29% and sepsis results in annual health care costs in excess of $17 billion. Autopsies have revealed that failure to accurately diagnose and provide efficient and specific antimicrobial therapies is the most common avoidable error in sepsis mortalities (Hotchkiss and Karl 2003). Most clinical microbiological diagnostics are performed through culture of the etiologic agent using appropriate substrates and analysis of the resulting amplified bacteria. This process, while typically considered the "gold standard" of microbial analysis normally requires days or weeks to complete and can often be inaccurate due to sample contamination. This often results, not only in significant delays in treatment, but also in suboptimal treatments with

reduced efficacy, unnecessary side effects or even death. While there are *no* adequately rapid and sensitive methods for sepsis diagnostics currently being clinically utilized, these issues have prompted the proposal and demonstration of several novel methods of bacterial pathogen detection. These methodologies, however, typically suffer from insensitivity, extended prep and/or measurement times, interference from other biochemicals and biological entities or lack of physical robustness. The concept of using magnetorelaxometry for the detection of bacteria was also recently introduced and demonstrated on *Listeria monocytogenes* (Grossman, Myers et al. 2004). The authors, however, reported only the detection of unrealistically high concentrations of bacteria and failed to demonstrate the use of the assay in clinically relevant biological fluids such as blood and serum. In this work, a prototype magnetorelaxometric assay for *E. coli* O157:H7 sepsis diagnostics was proposed, developed and demonstrated. The homogeneous assay proved to be significantly more rapid and sensitive than most current sepsis diagnostic methodologies, with a detection limit below 2000 CFU per ml in PBS. Furthermore, this detection limit was also demonstrated in a clinically relevant biofluid, viz. human serum. The developed assay provides a sensitivity improvement of over 5 orders of magnitude compared with the previously published magnetorelaxometric assay data on *L. monocytogenes* ($2.8x10^8$ compared to $2x10^3$ CFU/ml) and one order of magnitude better than the pseudo homogeneous assay ($26x10^3$ CFU/ml). A clinical sensitivity of 90% and a clinical specificity of 100% were also each demonstrated on pools of 20 samples. Additionally, a pseudo-homogeneous assay, with reduced sensitivity of 50,000 total bacteria, was successfully performed in human blood, as was a homogeneous version that detected 20,000 *E. coli* O157:H7 CFU per ml of blood.

The use and evaluation of living subjects is critical to almost every area of biomedical research. As such, analysis techniques which can provide scientific advantages and significantly increase the welfare of laboratory animals are of valuable interest to the scientific

community. In this work, an *in vivo* magnetorelaxometric assay was proposed, developed and demonstrated using Cry5B toxin binding to the gut cells of wild type *C. elegans* as a model system. This is the first time an *in vivo* magnetorelaxometric assay has been successfully demonstrated. The demonstration of this technique, while still in its infancy, acts as a fundamental archetype for the noninvasive magnetorelaxometric analysis of binding interactions in living subjects. The further development of these and similar techniques could provide untold benefits for live animal based biomedical research.

The delivery of magnetic nanoparticles to or into various cell types has become an area of increasing interest in the biomedical sciences. Targeted drug/gene delivery is used to deliver drugs or genes regio-specifically by attaching them to magnetic nanoparticles and locally concentrating the resulting complexes *in vivo* to the desired locale. Similarly, magnetic hyperthermia, the local concentration of magnetic nanoparticles and subsequent heating via AC magnetic fields, has shown promise as a potentially viable cancer therapy. And it has additionally been shown that if cells are labeled with large enough numbers of magnetic nanoparticles, that these cells can be located, tracked and recovered using high resolution imaging techniques, such as high-resolution magnetic resonance imaging (MRI). The "action at a distance" properties of MNPs and the lack of interference of biological entities make the use of MNPs an attractive option for the manipulation of and interaction with living cells. The delivery of MNPs into and interaction with living cells, however, poses several technical challenges and naturally raises concern over the effects of their intimate contact with cellular machinery. This work addressed both the long term *in vitro* cytotoxicity of intracellular delivery of iron oxide MNPs and its use as a means of intracellular protein detection. The results of the former indicate that even temporary exposure to iron oxide/AMNPs results in a dose dependent reduced ability of PC12 cells to appropriately respond to nerve growth factor. This may have significant implications for *in vivo* and phenotypic dependent *in vitro*

uses of AMNPs and iron oxide magnetic nanoparticles in general. In particular it was shown that the exposure of cells to locally high concentrations of magnetic nanoparticles can adversely affect cell function, phenotype and viability.

The capability of detecting intracellular binding in live cells can benefit a wide range of applications, including therapeutics, clinical diagnostics and basic science. As an example, in drug delivery, a tool that can accurately determine the rate of release of a therapeutic delivered inside a cell would be especially valuable, as the delivery kinetics play a major role in the effectiveness and time course of the therapeutic. Similarly, for drug development, intracellular assays that quantitatively measure protein expression in response to a drug would also be very useful. Ultimately, the ability to quantify the expression and dynamics of proteins in live cells on a time scale of seconds could improve understanding of protein and second messenger pathways, leading to the elucidation of key cellular processes in biomedicine and disease. In this work, the initial steps toward such an assay, the first magnetorelaxometric assay for the detection of an intracellular protein, namely tubulin, were developed and demonstrated. The methods employed in the development of this assay are readily amenable to the magnetorelaxometric detection of any accessible cytoskeletal protein and act as a fundamental basis for similar and more quantitative future work in this area.

6.3 Further Considerations for Magnetorelaxometry

Still in its infancy, the burgeoning field of magnetorelaxometry offers several key advantages over currently existing diagnostic and detection methodologies in biomedicine. At the core of the technology are the development, tailoring and use of MNPs for detection of specific biochemical interactions. This work acts to underscore the drastic effect that both the MNP core synthesis and surface modification of these particles can have upon the outcome of magnetorelaxometric evaluations. In particular, the large variance in magnetic properties

from different synthesis schemes and the technical difficulties, such as low signal and colloidal instability, encountered when working with particular MNP products engenders substantial impetus for the future development of methods of synthesis of smaller, highly magnetic, colloidally stable MNPs. An ideal MNP preparation would incorporate a solid magnetic core of dimensions near or above the 26nm SPM limit thereby yielding higher values of both M_r and τ_N *without* sacrificing loss in binding area upon immobilization due to large hydrodynamic radii. While some of the paradoxical hurdles to this development were outlined in this text, the rapidly growing fields of nanotechnology and nanochemistry offer reason for hope toward the accomplishment of these ends.

While MNP probes permit magnetorelaxometric evaluation of biological samples, it is the exquisite sensitivity of the SQUID system which is the workhorse responsible for the detection of these probes. There are specific improvements that can be made in this or any SQUID detection platform intended for magnetorelaxometry such as methods of higher throughput, optimization of sensor geometry, the incorporation of gradiometers and signal processing algorithms for background subtraction and, most notably, shorter sample magnetization to detection times. The quicker the sample can be brought into proximity with the sensor following magnetization, the less Néel relaxation that will have occurred and the larger the magnetizing field, the larger the moment that will be induced in the sample, both resulting in a greater value of B sensed by the SQUID system and its overall sensitivity.

With many of these improvements looming on the horizon, the future of the field of magnetorelaxometry looks bright.

6.4 General Acknowledgements

This work and its results would not have been possible without the excellent guidance of my two advisors, Sungho Jin and Xiaohua Huang, who provided me with the encouragement, provisions, and license to freely pursue my research interests that ultimately led to my work at Magnesensors. It was there that I was given the tremendous privilege of working with my colleagues and superiors, Mark DiIorio and Kai Yang, without whom I may very well have never completed my doctoral degree; the work, advice and help of these two men were invaluable in producing this work and getting me to this point. I would also like to thank Eduardo Macagno for providing me with opportunities to pursue research with him and for taking some time to work side by side with me to broaden my scientific experiences. Finally, I thank Gabriel Silva for his proffer of help and understanding in my times of personal crisis and Shu Chien for his good nature and who, despite his truly tremendous accomplishments, provides a continuous example of scientific humility.

REFERENCES

Albornoz, C., E. E. Sileo, et al. (2004). "Magnetic polymers of maghemite (gamma-Fe2O3) and polyvinyl alcohol." Physica B-Condensed Matter **354**(1-4): 149-153.

Alexiou, C., W. Arnold, et al. (2000). "Locoregional cancer treatment with magnetic drug targeting." Cancer Res **60**(23): 6641-8.

Anonymous (1998). "Genome sequence of the nematode C-elegans: A platform for investigating biology." Science **282**(5396): 2012-2018.

Aposhian, H. V. and M. M. Aposhian (1990). "meso-2,3-Dimercaptosuccinic acid: chemical, pharmacological and toxicological properties of an orally effective metal chelating agent." Annu Rev Pharmacol Toxicol **30**: 279-306.

Baumans, V. (2004). "Use of animals in experimental research: an ethical dilemma?" Gene Therapy **11**: S64-S66.

Berkov, D. V. and R. Kotitz (1996). "Irreversible relaxation behaviour of a general class of magnetic systems." Journal of Physics-Condensed Matter **8**(9): 1257-1266.

Berkovsky, B., Ed. (1978). Thermomechanics of magnetic fluids : theory and applications International Advanced Course and Workshop on Thermomechanics of Magnetic Fluids, Udine, Italy, 1977. Washington, Hemisphere Pub. Corp.

Berry, C. C. and A. S. G. Curtis (2003). "Functionalisation of magnetic nanoparticles for applications in biomedicine." Journal of Physics D-Applied Physics **36**(13): R198-206.

Berry, C. C., S. Wells, et al. (2004). "Cell response to dextran-derivatised iron oxide nanoparticles post internalisation." Biomaterials **25**(23): 5405-13.

Berry, C. C., S. Wells, et al. (2003). "Dextran and albumin derivatised iron oxide nanoparticles: influence on fibroblasts in vitro." Biomaterials **24**(25): 4551-4557.

Billotey, C., C. Wilhelm, et al. (2003). "Cell internalization of anionic maghemite nanoparticles: Quantitative effect on magnetic resonance imaging." Magnetic Resonance in Medicine **49**(4): 646-654.

Blesa, M. A., E. B. Borghi, et al. (1984). "Adsorption of Edta and Iron-Edta Complexes on Magnetite and the Mechanism of Dissolution of Magnetite by Edta." Journal of Colloid and Interface Science **98**(2): 295-305.

Bogardus, E. H., R. Scranton, et al. (1975). "Pulse Magnetization Measurements in Ferrofluids." Ieee Transactions on Magnetics **11**(5): 1364-1366.

Bokken, G., R. J. Corbee, et al. (2003). "Immunochemical detection of Salmonella group B, D and E using an optical surface plasmon resonance biosensor." Fems Microbiology Letters **222**(1): 75-82.

Bonnemain, B. (1998). "Superparamagnetic agents in magnetic resonance imaging: physicochemical characteristics and clinical applications. A review." J Drug Target **6**(3): 167-74.

Borrelli, N. F., A. A. Luderer, et al. (1984). "Hysteresis heating for the treatment of tumours." Phys Med Biol **29**(5): 487-94.

Brenner, S. (1974). "Genetics of Caenorhabditis-Elegans." Genetics **77**(1): 71-94.

Bulte, J. W., T. Douglas, et al. (2001). "Magnetodendrimers allow endosomal magnetic labeling and in vivo tracking of stem cells." Nat Biotechnol **19**(12): 1141-7.

Bulte, J. W., I. D. Duncan, et al. (2002). "In vivo magnetic resonance tracking of magnetically labeled cells after transplantation." J Cereb Blood Flow Metab **22**(8): 899-907.

Bulte, J. W., L. D. Ma, et al. (1993). "Selective MR imaging of labeled human peripheral blood mononuclear cells by liposome mediated incorporation of dextran-magnetite particles." Magn Reson Med **29**(1): 32-7.

Butterworth, M. D., L. Illum, et al. (2001). "Preparation of ultrafine silica- and PEG-coated magnetite particles." Colloids and Surfaces a-Physicochemical and Engineering Aspects **179**(1): 93-102.

Carrigan, S. D., G. Scott, et al. (2004). "Toward resolving the challenges of sepsis diagnosis." Clinical Chemistry **50**(8): 1301-1314.

Cartmell, S. H., J. Dobson, et al. (2002). "Development of magnetic particle techniques for long-term culture of bone cells with intermittent mechanical activation." IEEE Trans Nanobioscience **1**(2): 92-7.

Chan, D. Y. C., D. Henderson, et al. (1985). "The stability of a colloidal suspension of coated magnetic particles in an aqueous solution." IBM Journal of Research & Development **29**(1): 11-17.

Chemla, Y. R., H. L. Crossman, et al. (2000). "Ultrasensitive magnetic biosensor for homogeneous immunoassay." Proceedings of the National Academy of Sciences of the United States of America **97**(26): 14268-14272.

Chen, Z. X., S. Y. Chen, et al., Eds. (2004). Nematology Advances and Perspectives, Volume 1 Nematode Morphology, Physiology and Ecology. Beijing, Tsinghua University Press.

Choi, H., S. R. Choi, et al. (2004). "Iron oxide nanoparticles as magnetic resonance contrast agent for tumor imaging via folate receptor-targeted delivery." Acad Radiol **11**(9): 996-1004.

Chung, S. H., A. Hoffmann, et al. (2005). "Biological sensing with magnetic nanoparticles using Brownian relaxation (invited)." Journal of Applied Physics **97**(10).

Clarke, J. (1966). "A Superconducting Galvanometer Employing Josephson Tunnelling." Philosophical Magazine **13**(121): 115-&.

Cora, L. A., F. G. Romeiro, et al. (2006). "Gastrointestinal transit and disintegration of enteric coated magnetic tablets assessed by ac biosusceptometry." European Journal of Pharmaceutical Sciences **27**(1): 1-8.

Cora, L. A., F. G. Romeiro, et al. (2005). "AC biosusceptometry in the study of drug delivery." Advanced Drug Delivery Reviews **57**(8): 1223-1241.

Cozensroberts, C., J. A. Quinn, et al. (1990). "Receptor-Mediated Adhesion Phenomena - Model Studies with the Radial-Flow Detachment Assay." Biophysical Journal **58**(1): 107-125.

Cranfield, C. G., A. Dawe, et al. (2004). "Biogenic magnetite in the nematode Caenorhabditis elegans." Proceedings of the Royal Society of London Series B-Biological Sciences **271**: S436-S439.

Cullity, B. D. (1972). Introduction to Magnetic Materials. Philippines, Addison-Wesley.

Dailey, J. P., C. Li, et al. (1997). "Magnetic fluids in vitreoretinal surgery." Investigative Ophthalmology & Visual Science **38**(4): 3110-3110.

Debye, P. (1929). Polar Molecules. New York, over.

Deng, L., L. L. Bao, et al. (1996). "In situ continuous detection of bacteria on the surface of solid medium with a bulk acoustic wave-impedance sensor." Journal of Microbiological Methods **26**(1-2): 197-203.

Derfus, A. M., W. C. W. Chan, et al. (2004). "Probing the cytotoxicity of semiconductor quantum dots." Nano Letters **4**(1): 11-18.

Dilorio, M. S., S. Yoshizumi, et al. (1991). "Manufacturable low-noise SQUIDs operating in liquid nitrogen." Nature **354**(6354): 513-515.

Dobson, J. (2006). "Gene therapy progress and prospects: magnetic nanoparticle-based gene delivery." Gene Ther **13**(4): 283-7.

Dodd, S. J., M. Williams, et al. (1999). "Detection of single mammalian cells by high-resolution magnetic resonance imaging." Biophys J **76**(1 Pt 1): 103-9.

Dousset, V., C. Delalande, et al. (1999). "In vivo macrophage activity imaging in the central nervous system detected by magnetic resonance." Magnetic Resonance in Medicine **41**(2): 329-333.

Elson, E. L. (2004). "Quick tour of fluorescence correlation spectroscopy from its inception." J Biomed Opt **9**(5): 857-64.

Ennas, G., A. Musinu, et al. (1998). "Characterization of iron oxide nanoparticles in an Fe2O3-SiO2 composite prepared by a sol-gel method." Chemistry of Materials **10**(2): 495-502.

Enpuku, K., M. Hotta, et al. (2001). "High-T-c SQUID system for biological immunoassays." Physica C **357**: 1462-1465.

Enpuku, K., D. Kuroda, et al. (2003). "High Tc SQUID system and magnetic marker for biological immunoassays." Ieee Transactions on Applied Superconductivity **13**(2): 371-376.

Fahlvik, A. K., E. Holtz, et al. (1990). "Relaxation efficacy of paramagnetic and superparamagnetic microspheres in liver and spleen." Magn Reson Imaging **8**(4): 363-9.

Fauconnier, N., J. N. Pons, et al. (1997). "Thiolation of maghemite nanoparticles by dimercaptosuccinic acid." Journal of Colloid and Interface Science **194**(2): 427-433.

Ferreira, A. P., M. M. Werneck, et al. (2001). "Development of an evanescent-field fibre optic sensor for Escherichia coli O157 : H7." Biosensors & Bioelectronics **16**(6): 399-408.

Frankel, A. D. and C. O. Pabo (1988). "Cellular uptake of the tat protein from human immunodeficiency virus." Cell **55**(6): 1189-93.

Gallo, J. M. and U. Hafeli (1997). "A.S. Lubbe et al., Preclinical experiences with magnetic drug targeting: tolerance and efficacy. Cancer Res., 56: 4694-4701, 1996; and Clinical experiences with magnetic drug targeting: a phase I study with 4'-epidoxorubicin in 14 patients with advanced solid tumors. Cancer Res., 56: 4686-4693, 1996." Cancer Res **57**(14): 3063-5.

Gee, S. H., Y. K. Hong, et al. (2003). "Synthesis and aging effect of spherical magnetite (Fe3O4) nanoparticles for biosensor applications." Journal of Applied Physics **93**(10): 7560-7562.

Gilbert, R. J. C. (2002). "Pore-forming toxins." Cellular and Molecular Life Sciences **59**(5): 832-844.

Gilchrist, R. K., R. Medal, et al. (1957). "Selective inductive heating of lymph nodes." Ann Surg **146**(4): 596-606.

Goodwin, S. C., C. A. Bittner, et al. (2001). "Single-dose toxicity study of hepatic intra-arterial infusion of doxorubicin coupled to a novel magnetically targeted drug carrier." Toxicol Sci **60**(1): 177-83.

Gordon, R. T., J. R. Hines, et al. (1979). "Intracellular hyperthermia. A biophysical approach to cancer treatment via intracellular temperature and biophysical alterations." Med Hypotheses **5**(1): 83-102.

Gould, F. (1998). "Sustainability of transgenic insecticidal cultivars: Integrating pest genetics and ecology." Annual Review of Entomology **43**: 701-726.

Goya, G. F., T. S. Berquo, et al. (2003). "Static and dynamic magnetic properties of spherical magnetite nanoparticles." Journal of Applied Physics **94**(5): 3520-8.

Green, M. and P. M. Loewenstein (1988). "Autonomous functional domains of chemically synthesized human immunodeficiency virus tat trans-activator protein." Cell **55**(6): 1179-88.

Griffitts, J. S., J. L. Whitacre, et al. (2001). "Bt toxin resistance from loss of a putative carbohydrate-modifying enzyme." Science **293**(5531): 860-864.

Grossman, H. L., W. R. Myers, et al. (2004). "Detection of bacteria in suspension by using a superconducting quantum interference device." Proceedings of the National Academy of Sciences of the United States of America **101**(1): 129-134.

Gupta, A. K. and A. S. Curtis (2004). "Surface modified superparamagnetic nanoparticles for drug delivery: interaction studies with human fibroblasts in culture." J Mater Sci Mater Med **15**(4): 493-6.

Halavaara, J., P. Tervahartiala, et al. (2002). "Efficacy of sequential use of superparamagnetic iron oxide and gadolinium in liver MR imaging." Acta Radiol **43**(2): 180-5.

Halbreich, A., D. Sabolovic, et al. (2000). Magnetic nanoparticles coupled to annexine and utilization thereof. US.

Harbarth, S., J. Garbino, et al. (2003). "Inappropriate initial antimicrobial therapy and its effect on survival in a clinical trial of immunomodulating therapy for severe sepsis." American Journal of Medicine **115**(7): 529-535.

Harris, L. A., J. D. Goff, et al. (2003). "Magnetite nanoparticle dispersions stabilized with triblock copolymers." Chemistry of Materials **15**(6): 1367-1377.

Hilger, I., S. Fruhauf, et al. (2003). "Cytotoxicity of selected magnetic fluids on human adenocarcinoma cells." Journal of Magnetism and Magnetic Materials **261**(1-2): 7-12.

Hobson, N. S., I. Tothill, et al. (1996). "Microbial detection." Biosensors & Bioelectronics **11**(5): 455-477.

Hong, C. Y., C. C. Wu, et al. (2006). "Magnetic susceptibility reduction method for magnetically labeled immunoassay." Applied Physics Letters **88**(21).

Horng, H. E., S. Y. Yang, et al. (2005). "Nanomagnetic particles for SQUID-based magnetically labeled immunoassay." Ieee Transactions on Applied Superconductivity **15**(2): 668-671.

Horvath, R., H. C. Pedersen, et al. (2003). "Optical waveguide sensor for on-line monitoring of bacteria." Optics Letters **28**(14): 1233-1235.

Hoshino, A., K. Fujioka, et al. (2004). "Physicochemical properties and cellular toxicity of nanocrystal quantum dots depend on their surface modification." Nano Letters **4**(11): 2163-9.

Hotchkiss, R. S. and I. E. Karl (2003). "Medical progress: The pathophysiology and treatment of sepsis." New England Journal of Medicine **348**(2): 138-150.

Hsu, H. C., C. Dodd, et al. (2000). "Novel method for in vivo magnetic resonance imaging of activated T cells labeled with Tat-derived magnetic nanoparticles." Arthritis and Rheumatism **43**(9): S371-S371.

Huang, X. H. and Z. H. Chen (2005). "gamma-Fe2O3/SiO2 nanocomposites obtained by sol-gel synthesis." Journal of Inorganic Materials **20**(3): 685-691.

Hussain, S. M., K. L. Hess, et al. (2005). "In vitro toxicity of nanoparticles in BRL 3A rat liver cells." Toxicol In Vitro **19**(7): 975-83.

Hyeon, T. (2003). "Chemical synthesis of magnetic nanoparticles." Chemical Communications(8): 927-934.

Ito, A., M. Shinkai, et al. (2005). "Medical application of functionalized magnetic nanoparticles." J Biosci Bioeng **100**(1): 1-11.

Ito, A., Y. Takizawa, et al. (2004). "Tissue engineering using magnetite nanoparticles and magnetic force: heterotypic layers of cocultured hepatocytes and endothelial cells." Tissue Eng **10**(5-6): 833-40.

Ivnitski, D., I. Abdel-Hamid, et al. (1999). "Biosensors for detection of pathogenic bacteria." Biosensors & Bioelectronics **14**(7): 599-624.

Jacobs, R. E. and S. E. Fraser (1994). "Imaging neuronal development with magnetic resonance imaging (NMR) microscopy." J Neurosci Methods **54**(2): 189-96.

Jenks, W. G., I. M. Thomas, et al. (1997). SQUIDS. Encyclopedia of Applied Physics. G. L. Trigg, E. S. Vera and W. Greulich. New York, VCH**:** 457-468.

Johnston, D. L., P. Liu, et al. (1987). "Use of gadolinium-DTPA as a myocardial perfusion agent: potential applications and limitations for magnetic resonance imaging." J Nucl Med **28**(5): 871-7.

Jones, S. K., J. G. Winter, et al. (2002). "Treatment of experimental rabbit liver tumours by selectively targeted hyperthermia." Int J Hyperthermia **18**(2): 117-28.

Jordan, A., R. Scholz, et al. (1997). "Effects of magnetic fluid hyperthermia (MFH) on C3H mammary carcinoma in vivo." Int J Hyperthermia **13**(6): 587-605.

Jordan, A., R. Scholz, et al. (1999). "Magnetic fluid hyperthermia (MFH): Cancer treatment with AC magnetic field induced excitation of biocompatible superparamagnetic nanoparticles." Journal of Magnetism and Magnetic Materials **201**(1-3): 413-419.

Jordan, A., P. Wust, et al. "Inductive heating of ferrimagnetic particles and magnetic fluids: physical evaluation of their potential for hyperthermia." International Journal Of Hyperthermia: The Official Journal Of European Society For Hyperthermic Oncology, North American Hyperthermia Group **9**(1): 51-68.

Josephson, L., M. F. Kircher, et al. (2002). "Near-infrared fluorescent nanoparticles as combined MR/optical imaging probes." Bioconjugate Chemistry **13**(3): 554-560.

Josephson, L., C. H. Tung, et al. (1999). "High-efficiency intracellular magnetic labeling with novel superparamagnetic-tat peptide conjugates." Bioconjugate Chemistry **10**(2): 186-191.

Kaplan, I. M., J. S. Wadia, et al. (2005). "Cationic TAT peptide transduction domain enters cells by macropinocytosis." J Control Release **102**(1): 247-53.

Khalafalla, S. E. and G. W. Reimers (1973). Preparation of aqueous magnetic liquids in alkaline and acidic media. U.S.

Kim, D. K., M. Mikhaylova, et al. (2003). "Starch-coated superparamagnetic nanoparticles as MR contrast agents." Chemistry of Materials **15**(23): 4343-4351.

Kim, J. S., T.-J. Yoon, et al. (2006). "Toxicity and Tissue Distribution of Magnetic Nanoparticles in Mice." Toxicol. Sci. **89**(1): 338-347.

Kircher, M. F., J. R. Allport, et al. (2002). "Intracellular magnetic labeling with CLIO-Tat for efficient in vivo tracking of cytotoxic T cells by MR imaging." Radiology **225**: 453-453.

Kirchner, C., T. Liedl, et al. (2005). "Cytotoxicity of colloidal CdSe and CdSe/ZnS nanoparticles." Nano Letters **5**(2): 331-8.

Klein, S., J. Stein, et al. (2005). "Site-specific delivery of anti-inflammatory drugs in the gastrointestinal tract: an in-vitro release model." Journal of Pharmacy and Pharmacology **57**(6): 709-719.

Kohler, N., C. Sun, et al. (2005). "Methotrexate-modified superparamagnetic nanoparticles and their intracellular uptake into human cancer cells." Langmuir **21**(19): 8858-64.

Kotitz, R., T. Bunte, et al. (1997). "Superconducting quantum interference device-based magnetic nanoparticle relaxation measurement as a novel tool for the binding specific detection of biological binding reactions." Journal of Applied Physics **81**(8): 4317-4317.

Kotitz, R., P. C. Fannin, et al. (1995). "Time domain study of Brownian and Neel relaxation in ferrofluids." Journal of Magnetism and Magnetic Materials **149**(1-2): 42-46.

Kotitz, R., H. Matz, et al. (1997). "SQUID based remanence measurements for immunoassays." Ieee Transactions on Applied Superconductivity **7**(2): 3678-3681.

Krotz, F., H. Y. Sohn, et al. (2003). "Magnetofection potentiates gene delivery to cultured endothelial cells." J Vasc Res **40**(5): 425-34.

Kubaska, S., D. V. Sahani, et al. (2001). "Dual contrast enhanced magnetic resonance imaging of the liver with superparamagnetic iron oxide followed by gadolinium for lesion detection and characterization." Clin Radiol **56**(5): 410-5.

Kumar, R. V., Y. Koltypin, et al. (2001). "Fabrication of magnetite nanorods by ultrasound irradiation." Journal of Applied Physics **89**(11): 6324-8.

Lacava, Z. G. M., R. B. Azevedo, et al. (1999). "Biological effects of magnetic fluids: toxicity studies." Journal of Magnetism and Magnetic Materials **201**(1-3): 431-434.

Lange, J., R. Kotitz, et al. (2002). "Magnetorelaxometry - a new binding specific detection method based on magnetic nanoparticles." Journal of Magnetism and Magnetic Materials **252**(1-3): 381-383.

Lauenstein, T. C. M. D. and R. C. M. D. Semelka (2005). "Whole-Body Magnetic Resonance Imaging." Topics in Magnetic Resonance Imaging **16**(1): 15-20.

Lazarou, J., B. H. Pomeranz, et al. (1998). "Incidence of adverse drug reactions in hospitalized patients: a meta-analysis of prospective studies." Jama **279**(15): 1200-5.

Lee, J., T. Isobe, et al. (1996). "Preparation of ultrafine Fe3O4 particles by precipitation in the presence of PVA at high pH." Journal of Colloid and Interface Science **177**(2): 490-494.

Leslie-Pelecky, D. L. and R. D. Rieke (1996). "Magnetic Properties of Nanostructured Materials." Chemistry of Materials **8**(8): 1770.

Lewin, M., N. Carlesso, et al. (2000). "Tat peptide-derivatized magnetic nanoparticles allow in vivo tracking and recovery of progenitor cells." Nature Biotechnology **18**(4): 410-414.

Liberti, P. A. and M. A. Pino (1997). Resuspendable coated magnetic particles and stable magnetic particle suspensions. U.S.

Lin, H., Y. Watanabe, et al. (2003). "Preparation of magnetic poly(vinyl alcohol) (PVA) materials by in situ synthesis of magnetite in a PVA matrix." Journal of Applied Polymer Science **87**(8): 1239-1247.

Lippincott-Schwartz, J. and G. H. Patterson (2003). "Development and use of fluorescent protein markers in living cells." Science **300**(5616): 87-91.

Lok, C. (2001). "Picture perfect." Nature **412**(6845): 372-374.

Lubbe, A. S., C. Alexiou, et al. (2001). "Clinical applications of magnetic drug targeting." J Surg Res **95**(2): 200-6.

Lubbe, A. S., C. Bergemann, et al. (1996). "Clinical experiences with magnetic drug targeting: a phase I study with 4'-epidoxorubicin in 14 patients with advanced solid tumors." Cancer Res **56**(20): 4686-93.

Ludwig, F. (2006). "Magnetorelaxometry of magnetic nanoparticles for the quantitative and specific analysis of biomolecules." Tm-Technisches Messen **73**(4): 217-222.

Malins, C., P. R. Fielden, et al. (2004). "Imaging of unlabelled bacteria at a sensor surface using aluminium-clad integrated waveguide chips." Measurement Science & Technology **15**(5): 948-954.

Marroquin, L. D., D. Elyassnia, et al. (2000). "Bacillus thuringiensis (Bt) toxin susceptibility and isolation of resistance mutants in the nematode Caenorhabditis elegans." Genetics **155**(4): 1693-1699.

Massart, R. (1981). "Preparation of Aqueous Magnetic Liquids in Alkaline and Acidic Media." Ieee Transactions on Magnetics **17**(2): 1247-1248.

Massart, R. (1982). Magnetic fluids and process for obtaining them. USPTO. USA, Agence Nationale de Valorisation de la Recherche (ANVAR)**:** 14.

Massart, R. and V. Cabuil (1987). "Effect of Some Parameters on the Formation of Colloidal Magnetite in Alkaline-Medium - Yield and Particle-Size Control." Journal De Chimie Physique Et De Physico-Chimie Biologique **84**(7-8): 967-973.

Mikhaylova, M., D. K. Kim, et al. (2004). "BSA immobilization on amine-functionalized superparamagnetic iron oxide nanoparticles." Chemistry of Materials **16**(12): 2344-2354.

Mitsumori, M., M. Hiraoka, et al. (1994). "Development of intra-arterial hyperthermia using a dextran-magnetite complex." Int J Hyperthermia **10**(6): 785-93.

Miyoshi, H., K. A. Smith, et al. (1999). Transduction of Human CD34+ Cells That Mediate Long-Term Engraftment of NOD/SCID Mice by HIV Vectors. **283:** 682-686.

Molday, R. S. and D. MacKenzie (1982). "Immunospecific ferromagnetic iron-dextran reagents for the labeling and magnetic separation of cells." J Immunol Methods **52**(3): 353-67.

Molday, R. S. and L. L. Molday (1984). "Separation of Cells Labeled with Immunospecific Iron Dextran Microspheres Using High-Gradient Magnetic Chromatography." Febs Letters **170**(2): 232-238.

Molday, R. S., S. P. Yen, et al. (1977). "Application of magnetic microspheres in labelling and separation of cells." Nature **268**(5619): 437-8.

Moritz, B. and H. E. Meyer (2003). "Approaches for the quantification of protein concentration ratios." Proteomics **3**(11): 2208-20.

Moroz, P., S. K. Jones, et al. (2002). "Magnetically mediated hyperthermia: current status and future directions." Int J Hyperthermia **18**(4): 267-84.

Moroz, P., S. K. Jones, et al. (2002). "Tumor response to arterial embolization hyperthermia and direct injection hyperthermia in a rabbit liver tumor model." J Surg Oncol **80**(3): 149-56.

Muldoon, L. L., M. Sandor, et al. (2005). "Imaging, distribution, and toxicity of superparamagnetic iron oxide magnetic resonance nanoparticles in the rat brain and intracerebral tumor." Neurosurgery **57**(4): 785-96; discussion 785-96.

Nataro, J. P. and J. B. Kaper (1998). "Diarrheagenic Escherichia coli." Clinical Microbiology Reviews **11**(1): 142-+.

Neel, L. (1949). Annales de Geophysicae **5**: 99.

Neel, L. (1951). "Le Trainage Magnetique." Journal de Physique et le Radium **12**.

Neidhardt, F. C., Ed. (1996). Escherichia coli and Salmonella Cellular and Molecular Biology. Washington D.C., ASM Press.

Nel, A., T. Xia, et al. (2006). "Toxic potential of materials at the nanolevel." Science **311**(5761): 622-7.

NIH (2004). RFA-AI-04-043, "Sepsis and CAP: Partnerships for Diagnostics Development". N. I. o. Health.

Odenbach, S. (2002). Magnetoviscous effects in ferrofluids. New York, Springer.

Olsvik, O., T. Popovic, et al. (1994). "Magnetic separation techniques in diagnostic microbiology." Clin Microbiol Rev **7**(1): 43-54.

Ong, S. E. and M. Mann (2005). "Mass spectrometry-based proteomics turns quantitative." Nat Chem Biol **1**(5): 252-62.

Palmacci, S. and L. Josephson (1993). Synthesis of polysaccharide covered superparamagnetic oxide colloids. U.S.

Pankhurst, Q. A., J. Connolly, et al. (2003). "Applications of magnetic nanoparticles in biomedicine." Journal of Physics D-Applied Physics **36**(13): R167-81.

Papell, S. S. (1965). Low viscosity magnetic fluid obtained by te colloidal suspension of magnetic particles. U.S.

Pardoe, H., W. Chua-anusorn, et al. (2001). "Structural and magnetic properties of nanoscale iron oxide particles synthesized in the presence of dextran or polyvinyl alcohol." Journal of Magnetism and Magnetic Materials **225**(1-2): 41-46.

Phillips, C. A. (1999). "The epidemiology, detection and control of Escherichia coli O157." Journal of the Science of Food and Agriculture **79**(11): 1367-1381.

Pickering, L. K., T. G. Obrig, et al. (1994). "Hemolytic-Uremic Syndrome and Enterohemorrhagic Escherichia-Coli." Pediatric Infectious Disease Journal **13**(6): 459-475.

Plank, C., F. Scherer, et al. (2003). "Magnetofection: enhancing and targeting gene delivery with superparamagnetic nanoparticles and magnetic fields." J Liposome Res **13**(1): 29-32.

Plank, C., U. Schillinger, et al. (2003). "The magnetofection method: using magnetic force to enhance gene delivery." Biol Chem **384**(5): 737-47.

Pulfer, S. K. and J. M. Gallo (1998). "Enhanced brain tumor selectivity of cationic magnetic polysaccharide microspheres." J Drug Target **6**(3): 215-27.

Radbruch, A., B. Mechtold, et al. (1994). High-Gradient Magnetic Cell Sorting. Methods in Cell Biology, Vol 42. **42:** 387-403.

Rand, R. W., H. D. Snow, et al. (1982). "Thermomagnetic surgery for cancer." J Surg Res **33**(3): 177-83.

Rheinlander, T., R. Kotitz, et al. (2000). "Magnetic fractionation of magnetic fluids." Journal of Magnetism and Magnetic Materials **219**(2): 219-28.

Sangregorio, C., J. K. Wiemann, et al. (1999). "A new method for the synthesis of magnetoliposomes." Journal of Applied Physics **85**(8): 5699-5701.

Sarda, S., D. Pointu, et al. (2004). "Specific recognition of macroscopic objects by the cell surface: Evidence for a receptor density threshold revealed by micrometric particle binding characteristics." Biophysical Journal **86**(5): 3291-3303.

Scherer, F., M. Anton, et al. (2002). "Magnetofection: enhancing and targeting gene delivery by magnetic force in vitro and in vivo." Gene Ther **9**(2): 102-9.

Schneider, B. H., J. G. Edwards, et al. (1997). "Hartman interferometer: versatile integrated optic sensor for label-free, real-time quantification of nucleic acids, proteins, and pathogens." Clinical Chemistry **43**(9): 1757-1763.

Schoepf, U., E. M. Marecos, et al. (1998). "Intracellular magnetic labeling of lymphocytes for in vivo trafficking studies." Biotechniques **24**(4): 642-6, 648-51.

Schwarze, S. R., A. Ho, et al. (1999). "In vivo protein transduction: delivery of a biologically active protein into the mouse." Science **285**(5433): 1569-72.

Service, R. F. (2005). "Nanotechnology. Calls rise for more research on toxicology of nanomaterials." Science **310**(5754): 1609.

Shah, J. and E. Wilkins (2003). "Electrochemical biosensors for detection of biological warfare agents." Electroanalysis **15**(3): 157-167.

Shen, T., R. Weissleder, et al. (1993). "Monocrystalline Iron-Oxide Nanocompounds (Mion) - Physicochemical Properties." Magnetic Resonance in Medicine **29**(5): 599-604.

Shubayev, V. I. and R. R. Myers (2004). "Matrix metalloproteinase-9 promotes nerve growth factor-induced neurite elongation but not new sprout formation in vitro." J Neurosci Res **77**(2): 229-39.

Sonvico, F., S. Mornet, et al. (2005). "Folate-conjugated iron oxide nanoparticles for solid tumor targeting as potential specific magnetic hyperthermia mediators: synthesis, physicochemical characterization, and in vitro experiments." Bioconjug Chem **16**(5): 1181-8.

Steinberg, B. A., A. Roguin, et al. (2005). Magnetocardiogram Recordings in a Nonshielded Environment—Reproducibility and Ischemia Detection. **10:** 152-160.

Strable, E., J. W. M. Bulte, et al. (2001). "Synthesis and characterization of soluble iron oxide-dendrimer composites." Chemistry of Materials **13**(6): 2201-2209.

Stutz, H. (2005). "Advances in the analysis of proteins and peptides by capillary electrophoresis with matrix-assisted laser desorption/ionization and electrospray-mass spectrometry detection." Electrophoresis **26**(7-8): 1254-90.

Su, X. L. and Y. B. Li (2004). "A self-assembled monolayer-based piezoelectric immunosensor for rapid detection of Escherichia coli O157 : H7." Biosensors & Bioelectronics **19**(6): 563-574.

Suehiro, J., R. Hamada, et al. (2003). "Selective detection of viable bacteria using dielectrophoretic impedance measurement method." Journal of Electrostatics **57**(2): 157-168.

Sugimoto, T. and E. Matijevic (1980). "Formation of Uniform Spherical Magnetite Particles by Crystallization from Ferrous Hydroxide Gels." Journal of Colloid and Interface Science **74**(1): 227-243.

Sulston, J. E., E. Schierenberg, et al. (1983). "The Embryonic-Cell Lineage of the Nematode Caenorhabditis-Elegans." Developmental Biology **100**(1): 64-119.

Suslick, K. S., Ed. (1988). Ultrasound: Its Chemical, Physical and Biological Effect. London, Weinheim.

Suslick, K. S. and G. J. Price (1999). APPLICATIONS OF ULTRASOUND TO MATERIALS CHEMISTRY. **29:** 295-326.

Tartaj, P., M. del Puerto Morales, et al. (2003). "The preparation of magnetic nanoparticles for applications in biomedicine." Journal of Physics D-Applied Physics **36**(13): R182-97.

Tischler, A. S. and L. A. Greene (1975). "Nerve growth factor-induced process formation by cultured rat pheochromocytoma cells." Nature **258**(5533): 341-2.

Vasir, J. K. and V. Labhasetwar (2005). "Targeted drug delivery in cancer therapy." Technol Cancer Res Treat **4**(4): 363-74.

Vaughan, R. D., R. M. Carter, et al. (2003). "A quartz crystal microbalance (QCM) sensor for the detection of Bacillus cereus." Analytical Letters **36**(4): 731-747.

Vayssieres, L., C. Chaneac, et al. (1998). "Size tailoring of magnetite particles formed by aqueous precipitation: An example of thermodynamic stability of nanometric oxide particles." Journal of Colloid and Interface Science **205**(2): 205-212.

Wacker, F. K., K. Reither, et al. (2003). "MR image-guided endovascular procedures with the ultrasmall superparamagnetic iron oxide SH U 555 C as an intravascular contrast agent: study in pigs." Radiology **226**(2): 459-64.

Wacker, F. K., M. Wendt, et al. (2002). "Use of a blood-pool contrast agent for MR-guided vascular procedures: feasibility of ultrasmall superparamagnetic iron oxide particles." Acad Radiol **9**(11): 1251-4.

Wadia, J. S., R. V. Stan, et al. (2004). "Transducible TAT-HA fusogenic peptide enhances escape of TAT-fusion proteins after lipid raft macropinocytosis." Nat Med **10**(3): 310-5.

Wang, N., J. P. Butler, et al. (1993). "Mechanotransduction across the Cell-Surface and through the Cytoskeleton." Science **260**(5111): 1124-1127.

Wang, Y. X., S. M. Hussain, et al. (2001). "Superparamagnetic iron oxide contrast agents: physicochemical characteristics and applications in MR imaging." Eur Radiol **11**(11): 2319-31.

Washburn, M. P., D. Wolters, et al. (2001). "Large-scale analysis of the yeast proteome by multidimensional protein identification technology." Nat Biotechnol **19**(3): 242-7.

Weissleder, R., G. Elizondo, et al. (1990). "Ultrasmall Superparamagnetic Iron-Oxide - an Intravenous Contrast Agent for Assessing Lymph-Nodes with Mr Imaging." Radiology **175**(2): 494-498.

Weissleder, R., G. Elizondo, et al. (1990). "Ultrasmall Superparamagnetic Iron-Oxide - Characterization of a New Class of Contrast Agents for Mr Imaging." Radiology **175**(2): 489-493.

Weissleder, R., A. S. Lee, et al. (1991). "Polyclonal Human Immunoglobulin-G Labeled with Polymeric Iron-Oxide - Antibody Mr Imaging." Radiology **181**(1): 245-249.

Weissleder, R., A. Moore, et al. (2000). "In vivo magnetic resonance imaging of transgene expression." Nat Med **6**(3): 351-354.

Wheless, J. W. M. D., E. P. Castillo, et al. (2004). "Magnetoencephalography (MEG) and Magnetic Source Imaging (MSI)." Neurologist **10**(3): 138-153.

Widder, K. J., R. M. Morris, et al. (1983). "Selective targeting of magnetic albumin microspheres containing low-dose doxorubicin: total remission in Yoshida sarcoma-bearing rats." Eur J Cancer Clin Oncol **19**(1): 135-9.

Wilhelm, C., C. Billotey, et al. (2003). "Intracellular uptake of anionic superparamagnetic nanoparticles as a function of their surface coating." Biomaterials **24**(6): 1001-1011.

Wilhelm, C., F. Gazeau, et al. (2003). "Rotational magnetic endosome microrheology: Viscoelastic architecture inside living cells." Physical Review E **67**(6).

Wilhelm, C., F. Gazeau, et al. (2002). "Interaction of anionic superparamagnetic nanoparticles with cells: Kinetic analyses of membrane adsorption and subsequent internalization." Langmuir **18**(21): 8148-8155.

Won, J., M. Kim, et al. (2005). "A magnetic nanoprobe technology for detecting molecular interactions in live cells." Science **309**(5731): 121-5.

Wormuth, K. (2001). "Superparamagnetic Latex via Inverse Emulsion Polymerization." Journal of Colloid and Interface Science **241**(2): 366-377.

Xenariou, S., U. Griesenbach, et al. (2006). "Using magnetic forces to enhance non-viral gene transfer to airway epithelium in vivo." Gene Ther.

Yeh, T. C., W. Zhang, et al. (1995). "In vivo dynamic MRI tracking of rat T-cells labeled with superparamagnetic iron-oxide particles." Magn Reson Med **33**(2): 200-8.

Zhang, Y., N. Kohler, et al. (2002). "Surface modification of superparamagnetic magnetite nanoparticles and their intracellular uptake." Biomaterials **23**(7): 1553-61.

Zhang, Y., C. Sun, et al. (2004). "Self-assembled coatings on individual monodisperse magnetite nanoparticles for efficient intracellular uptake." Biomed Microdevices **6**(1): 33-40.

Zhao, M., M. F. Kircher, et al. (2002). "Differential conjugation of tat peptide to superparamagnetic nanoparticles and its effect on cellular uptake." Bioconjugate Chemistry **13**(4): 840-844.

Zhao, M. and R. Weissleder (2004). "Intracellular cargo delivery using tat peptide and derivatives." Medicinal Research Reviews **24**(1): 1-12.

Zhao, X. J., L. R. Hilliard, et al. (2004). "A rapid bioassay for single bacterial cell quantitation using bioconjugated nanoparticles." Proceedings of the National Academy of Sciences of the United States of America **101**(42): 15027-15032.